IRRADIATED SINGLE CRYSTALS

Thosts for the Degree of Ph. D.
MICHIGAN STATE UNIVERSITY

James Clyde Watson
1970



#### This is to certify that the

#### thesis entitled

## AN ESR STUDY OF RADICALS IN SOME IRRADIATED SINGLE CRYSTALS

presented by

James Clyde Watson

has been accepted towards fulfillment of the requirements for

Ph.D. degree in Chemistry

Major professor

Date Dec. 22, 1969.

ESR spect ndiation in s fration of te tals and the t ere: Cl<sub>2</sub> (77 acetamidine hy CH<sub>2</sub> O C-NH<sub>2</sub> CH<sub>3</sub>

3660K, from tr

from isobutyr:

inirradiata

1130K) in 7-i

Eydrogen atom

(770<sub>K</sub>-1930<sub>K</sub>)

Marazinium d

#### **ABSTRACT**

## AN ESR STUDY OF RADICALS IN SOME IRRADIATED SINGLE CRYSTALS

Ву

#### James Clyde Watson

ESR spectra of radicals produced by electron and  $\gamma$ -ir-radiation in six single crystals were investigated as a function of temperature. The radicals produced in the crystals and the temperature range over which they are stable,

are:  $\text{Cl}_2^-$  (770K-1230K) and  $\text{CH}_2$ -C-NH<sub>2</sub> (1230K-1930K) from acetamidine hydrochloride  $\gamma$ -irradiated at 770K;

$$\dot{C}H_2$$
 0  $CH_3-\dot{C}-\ddot{C}-NH_2$  (770K-1930K) and  $\underline{t}$ -butyl radical (770K- $\dot{C}H_3$ 

3000K) from trimethylacetamide  $\gamma$ -irradiated at 770K;

$$\overset{\mathring{\text{CH}}_2}{\underset{\text{CH}_3}{\smile}} \overset{\overset{O}{\underset{\text{CH}_2}{\smile}}} \underbrace{\overset{O}{\underset{\text{CH}_3}{\smile}} \overset{O}{\underset{\text{CH}_3}{\smile}} \overset{O}{\underset{\text{$$

from isobutyramide  $\gamma$ -irradiated at  $77^0 \text{K}$ ;  $\text{Cl}_2^-$  ( $77^0 \text{K}$ -193°K) in  $\gamma$ -irradiated hydrazinium dichloride at  $77^0 \text{K}$ ;  $\text{Br}_2^-$  ( $77^0 \text{K}$ -113°K) in  $\gamma$ -irradiated hydrazinium dibromide at  $77^0 \text{K}$ ; and hydrogen atoms ( $77^0 \text{K}$ -193°K), an unidentified radical pair ( $77^0 \text{K}$ -193°K) and a radical, possibly  $N_2 \text{H}_6^+$ , (193°K-300°K) in hydrazinium difluoride  $\gamma$ -irradiated at  $77^0 \text{K}$ .

In the cas hydrochloride tensor and g a V center in stable at inte byperfine spli and -7.5 gauss ad -5.8 gauss reasonable agr of --electron protons was de tangs of -6.4 In 'i-irra ioth t-butyl r atter irradia. thenting fast Sperfine spli it was possib 123 (92 gaus ised to s

Con-planar wif

arerage radic

James Clyde Watson

In the case of the  ${\rm Cl_2}^-$  radical anion in acetamidine hydrochloride it was found that the hyperfine splitting tensor and g tensor exhibited the anisotropy expected for a V center in a monoclinic crystal. The radical  ${\rm CH_2-C-NH_2}$ ,  ${\rm NH_2}$ 

stable at intermediate temperatures, exhibited principal hyperfine splitting values of -35.9 gauss, -23.1 gauss, and -7.5 gauss for one proton and -36.2 gauss, -19.0 gauss, and -5.8 gauss for the second proton. These values are in reasonable agreement with predicted splittings for  $\alpha$ -protons of  $\pi$ -electron radicals. A further interaction with the -NH<sub>2</sub> protons was detected giving principal proton hyperfine splittings of -6.4 gauss, -4.1 gauss and -1.7 gauss.

In y-irradiated trimethylacetamide single crystal

after irradiation at  $77^0 \rm K$ . Both radicals appear to be reorienting faster than  $10^7~\rm sec^{-1}$  since only the isotropic hyperfine splittings were observed in each case. The

 $$^{\text{CH}_2}$$  O  $$^{\text{CH}_3}$$  -C -C-NH $_2$  radical was stable only from  $77^0\text{K}\text{--}\ 193^0\text{K}$  .  $$^{\text{CH}_3}$$ 

It was possible to obtain the maximum  $^{13}$ C hyperfine splitting (92 gauss) for <u>t</u>-butyl radical at  $77^{0}$ K. This value was used to show that the <u>t</u>-butyl radical is probably slightly non-planar with the C-C bonds tipped about  $3-4^{0}$  from the average radical plane.

-20.3 gauss, ar.

morienting slo

fine splittings

daracteristic

madicals. The

shows that the

mining the two

arbon. The

mopic & protor

teing 23.0 gaus

sistent with n

7-Irradia

intoxide crys

mase of hydraz

found to be or

In hydrazinium

of the hyperfi

sistent with t

In v-irra

Resence of the

illes at g ≥

ta over a ran

Isobutyramide single crystal gave two radicals upon irradiation at  $77^{\circ}K$ . In  $\begin{array}{c} \text{CH}_2 & \text{O} \\ \text{CH}_2 & \text{CH-C-NH}_2 \end{array}$  radical the equivalent

 $\alpha\text{-proton principal hyperfine splittings of -24.2 gauss,}$  -20.3 gauss, and -17.8 gauss show that the -CH<sub>2</sub> group is reorienting slowly at 77°K. The  $\beta\text{-proton principal hyper-fine splittings of 22.8 gauss, 18.9 gauss and 12.2 gauss are characteristic of <math display="inline">\beta\text{-hyperfine splittings in -C-CH-XY type}$  radicals. The isotropic  $\beta\text{-hyperfine splitting of 18.0 gauss}$  shows that the  $\beta$  proton is oriented 93° from the plane containing the two carbon atoms and the  $p_{\pi}$  orbital of the  $\alpha$ 

carbon. The CH<sub>3</sub> C-C-NH<sub>2</sub> radical exhibited essentially iso-CH<sub>3</sub>

tropic  $\beta$ -proton hyperfine splittings, the principal values being 23.0 gauss, 21.7 gauss, and 21.7 gauss. This is consistent with nearly free rotation of the CH<sub>2</sub>- groups at  $77^{0}\mathrm{K}$ .

 $\gamma$ -Irradiated hydrazinium dichloride and hydrazinium dibromide crystals contained V centers at  $77^0 K$ . In the case of hydrazinium dichloride  $Cl_2^-$  radical anions were found to be oriented along (110) directions in the crystal. In hydrazinium dibromide  $Br_2^-$  exhibited principal values of the hyperfine splitting and g tensors which were consistent with the monoclinic symmetry of the crystal.

In  $\gamma$ -irradiated hydrazinium difluoride hydrogen atoms were detected at  $77^{\circ}K$ , along with a radical pair. The presence of the pair was verified by the observation of lines at  $g \cong 4$ . Because of insufficiently resolved spectra over a range of orientations in the magnetic field it

 was not possible to identify the radical pair. Upon warming to  $-70^{\circ}$  a spectrum was observed which indicated a radical in which the odd electron interacts with six equivalent protons and two equivalent nitrogen nuclei. Three possiblities which could explain the spectra observed were postulated; a) formation of  $N_2H_6^{3+}$  radical cation, b) addition of an electron to  $N_2H_6^{++}$  cation to form the radical  $N_2H_6^{+-}$  with a three electron bond between the nitrogen atoms, or c) formation of an F center by trapping an electron in a fluoride ion vacancy. Further work will be required to distinguish among these possiblities.

# AN ESR STUDY OF RADICALS IN SOME IRRADIATED SINGLE CRYSTALS

Ву

James Clyde Watson

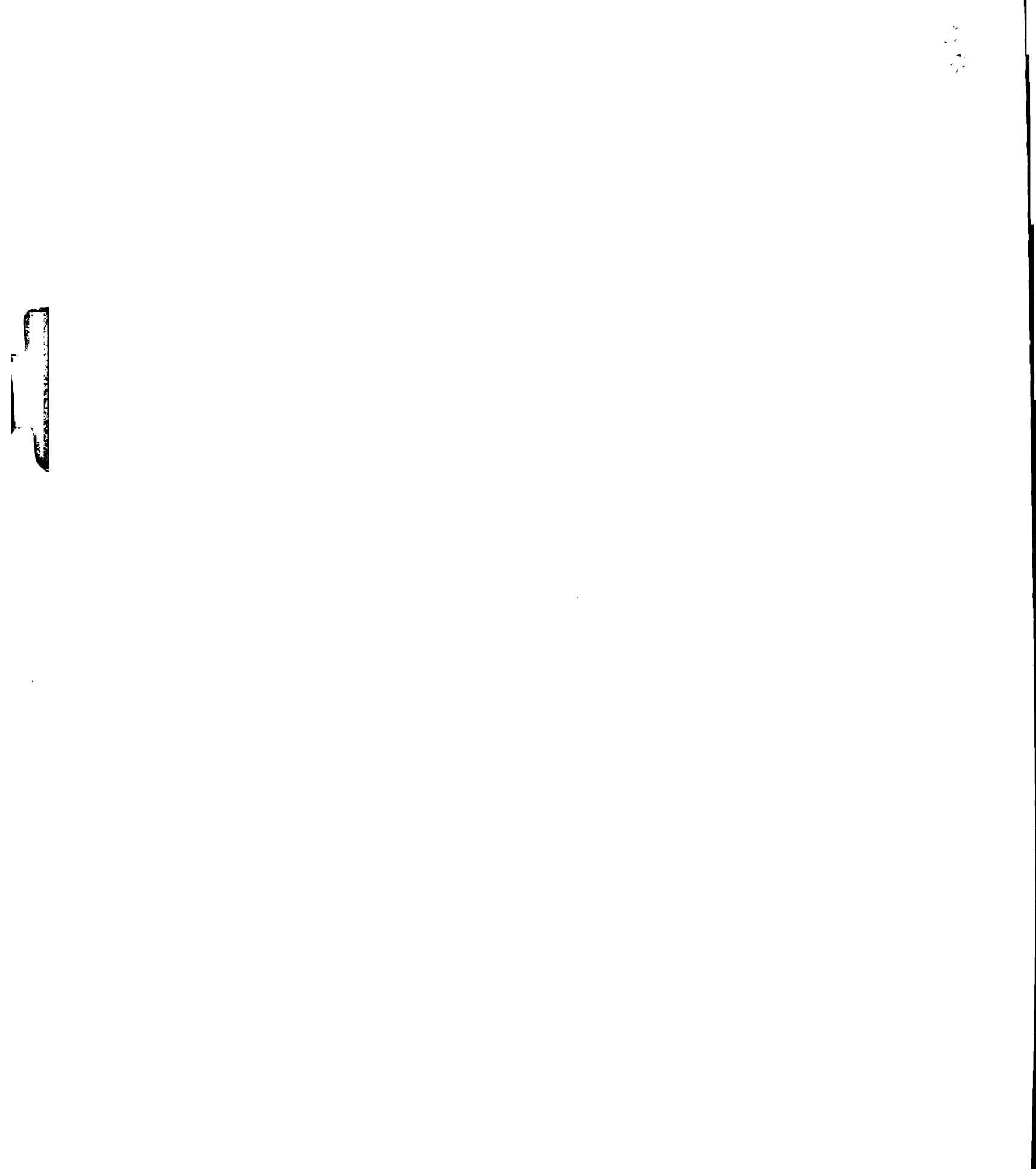
#### A THESIS

Submitted to
Michigan State University
in partial fulfillment of the requirements
for the degree of

DOCTOR OF PHILOSOPHY

Department of Chemistry

1970



G62850 7-1-70

To Sandy

#### **ACKNOWLEDGMENTS**

The author would like to take this opportunity to express his appreciation to Professor M. T. Rogers for his helpful suggestions and encouragement during this research.

The author is also indebted to Mr. George Giddings and Mr. Gary Blair for performing the  $\gamma$ -irradiations, Mr. Pat Hock for performing the electron irradiations, Mr. Norman Fishel for aiding with the X-ray analyses, Dr. H. A. Eick for the use of the X-ray equipment, and Mr. Tom Krigas for helping with the computer simulation program.

Finally thanks are extended to the Atomic Energy Commission for a research assistantship and to Michigan State University for a teaching assistantship.

#### TABLE OF CONTENTS

		Page
INTRODUC	TION	1
HISTORIC	AL BACKGROUND	4
ı.	Proton Splittings in $\pi ext{-Electron Radicals}$ .	4
	A. $\alpha$ -Proton Hyperfine Splittings	4
	B. $\beta$ -Proton Hyperfine Splittings	9
	C. $\gamma$ -Proton Hyperfine Splittings	14
	D. 14N-H Proton Splittings	16
II.	14N Splittings	19
III.	13C Hyperfine Splittings	20
IV.	V Centers	28
v.	Free Atom Hyperfine Splittings and g Values	32
THEORETI	CAL	34
ı.	Basic Theory of Electron Spin Resonance	34
	A. Classical Treatment	34
	B. Electron Dipole-Nuclear Dipole (Hyperfine) Interactions	35
	C. First-Order Quantum Mechanical Perturbation Theory	39
	D. Spin-Orbit Coupling	41
	E. Second-Order Perturbation Theory	43
II.	Evaluation and Interpretation of Spectral Parameters	47
	A. Experimental Determination of Hyperfine Splitting and g Values	47

### EGERIMENTAL .

- I. Analy Cryst
- II. Spect
- III. X-Ray Cryst
- IV. Mater
  - A.
  - В. C.
  - D.
  - E.
  - P.
- V. Proce
  - A.
  - В. c.
  - D.
  - E.
- WI. Stand ESUITS ...

- I. Irrac
  - A.
  - В.

### TABLE OF CONTENTS (Continued)

		Page
	B. Interpretation of Hyperfine Splittings and Their Signs	51
	<ul><li>1) Isotropic Splittings</li><li>2) Anisotropic Splittings</li></ul>	51 58
III.	Planarity of Radicals	62
EXPERIMEN	NTAL	65
ı.	Analysis of ESR Data for Irradiated Single Crystals	65
II.	Spectrometer System	67
III.	X-Ray Structure Determination and Optical Crystallography	68
IV.	Materials	71
	A. Acetamidine Hydrochloride	71
	B. Isobutyramide	72
	C. Trimethylacetamide	72
	D. Hydrazinium Dichloride	· <b>72</b>
	E. Hydrazinium Difluoride	72
	F. Hydrazinium Dibromide	73
v.	Procedure	73
	A. Crystal Growing	73
	B. Radiation Procedure	74
	C. Mounting Crystals	76
	D. Rotation Spectra	82
	E. Temperature Studies	83
VI.	Standard Samples and Conversion Factors	83
RESULTS		85
I.	Irradiated Acetamidine Hydrochloride	85
	A. Crystal Structure	85
	B. Identification of Radicals Produced in Irradiated Acetamidine Hydrochloride	86
	1) Low-Temperature Radical Cl <sub>2</sub> 2) High-Temperature Radical ·CH <sub>2</sub> -C-NH <sub>2</sub> +NH <sub>2</sub>	86 99

В.

c.

D.

III. Irrad

Α.

В.

c.

IV. Irrad Dichl

A.

В.

V. Irrad Dibro

A.

В.

c.

WI. Irrad

A.

В.

С.

D.

### TABLE OF CONTENTS (Continued)

			Page
II.	Irra	diated Trimethylacetamide Single Crystal	116
	Α.	Crystal Structure	116
		ĊH <sub>2</sub> O	
	В.	t-Butyl Radical and CH3-C - C-NH2 Radical	
		at 770K	118
	c.	Temperature Studies	123
	D.	<sup>13</sup> C Splitting for $\underline{t}$ -Butyl Radical	126
III.	Irra	diated Isobutyramide Single Crystal	129
	Α.	Crystal Structure	129
		сн <sub>2</sub> О	
	в.	Low-Temperature Radical CH-C-NH <sub>2</sub>	129
		CH <sub>3</sub>	
	c.	Radical Stable at Higher Temperatures	
		$CH_3$ $C-C-NH_2$ $C-C-NH_2$	146
		CH3	140
IV.		diated Single Crystals of Hydrazinium	
	Dich	loride	153
	Α.	Crystal Structure	153
	В.	Presence of $Cl_2$ at $77^0K$	153
V.		diated Single Crystals of Hydrazinium omide	159
	_		159
	Α.	Crystal Structure	109
	В.	at 770K	159
	c.	Temperature Studies	171
VI.	Irra	diated Hydrazinium Difluoride	173
	<b>A</b> .	Crystal Structure	173
	в.	Hydrogen Atoms Formed at 770K	173
	c.	Radical Pairs at 77°K	176
		The Radical at -70°	178

TABLE OF CONTEN

EXELUSIONS

I. Radica

A.

В.

II. Radica

A.

В.

С. н

III. Radica

A.

В.

IV. V Cent Dihali

A.

В.

V. Radica Diflua

A.

В.

c.

M. Summa:

### TABLE OF CONTENTS (Continued)

		Page
CONCLUSI	ions	193
I.	Radicals in Irradiated Acetamidine	
	Hydrochloride	193
	A. Cl <sub>2</sub> Radical	193
	B. $CH_2-C-NH_2$ Radical	196
II.	Radicals in Irradiated Trimethylacetamide	199
	A. $\underline{t}$ -Butyl Radical	199
	CH <sub>3</sub>	
	B. $^{13}$ C Splitting in $H_3C-^{13}$ C	201
	ĊH <sub>2</sub> О СН <sub>3</sub>	
	C. $H_3C-C$ - $C-NH_2$ Radical	202
	Сн <sub>з</sub>	
III.	Radicals in $\gamma$ -Irradiated Isobutyramide	203
	CH <sub>2</sub> O A. CH-C-NH <sub>2</sub> Radical at 77°K	203
	B. CH <sub>3</sub> C-C-NH <sub>2</sub> Radical	206
IV.	V Centers in γ-Irradiated Hydrazinium Dihalides	207
	A. $Cl_2$ Radical Anion in $\gamma$ -Irradiated Hydrazinium Dichloride	207
	B. Br <sub>2</sub> Radical Anion in γ-Irradiated Hydrazinium Dibromide	208
v.	Radicals in γ-Irradiated Hydrazinium Difluoride	210
	A. Trapped Hydrogen Atoms	210
	B. Radical Pairs at 770K	211
	C. The Radical at -70°	211
VT.	Summary	216

TABLE OF CONTI

REFERENCES .

APPENDIX . .

### TABLE OF CONTENTS (Continued)

																						Page
REFERENCES	•	•	•	•	•	•	•	•	•	•	•	•	•	•	•	•	•	•	•	•	•	218
APPENDIX .																						227

II. f-Prot carbon

III. 7-Prot

IV. Hyperf bound

V. 14N hy

M. 14% hy the od nitrog

MI. 130 hy

Hyperf for V

IX. Free à

X. Repres

M. Deviat

MI. Princ: and the irrad:

EII. Princ: tenso: • CH<sub>2</sub>-(

+!

#### LIST OF TABLES

TABLE		Page
I.	lpha-Proton hyperfine interactions in hydrocarbon radicals	5
II.	$\beta$ -Proton hyperfine splittings in hydrocarbon radicals	10
III.	γ-Proton hyperfine splittings in hydrocarbon radicals	15
IV.	Hyperfine splitting constants for protons bound to 14N	17
v.	14N hyperfine splitting tensors	21
VI.	14N hyperfine splitting tensors in radicals whe the odd electron is delocalized over two nitrogen atoms	re (
VII.	13C hyperfine splittings	26
VIII.	Hyperfine splitting constants and g values for V centers	30
IX.	Free atom hyperfine splittings and g values	33
х.	Representative <sup>13</sup> C and <sup>14</sup> N isotropic splittings	55
XI.	Deviation from planarity for some substituted methyl radicals	64
XII.	Principal hyperfine splitting and g values and their orientations for $Cl_2$ radical in irradiated acetamidine hydrochloride	98
XIII.	Principal values of the hyperfine splitting tensor for the two nonequivalent $\alpha$ -protons in $\cdot \text{CH}_2$ -C-NH $_2$ radical	113

MV. Hyperfin ·C:

XV. Hyperfitrimet

MI. Hyperf

H<sub>2</sub>C

III. Hyperf

in the

MMI. Princis tensor hydraz

MIX. Hyperf: hydrog:

M. Radica;

## LIST OF TABLES (continued)

PABLE	I	?age
XIV.	Hyperfine splitting values for -NH <sub>2</sub> protons in ·CH <sub>2</sub> -C-NH <sub>2</sub> radical	117
xv.	Hyperfine splittings for radicals in irradiated trimethylacetamide	
XVI.	Hyperfine splitting tensors for protons of the $H_2\dot{C}$ CH-C-NH <sub>2</sub> radical	149
XVII.	Hyperfine splitting tensor for methyl protons in the $CH_3$ " $C-C-NH_2$ radical	153
KVIII.	Principal values of the hyperfine splitting tensor and g tensor for $\text{Br}_2$ in $\gamma$ -irradiated hydrazinium dibromide	163
XIX.	Hyperfine splitting tensors for nitrogen and hydrogen in the $-70^{\circ}$ radical	190
XX.	Radical pairs	212

- ESR enermand sin
- 2. Spin pc radical
- 3. Relation to the dis shown dotted delectron
- 4. Principatensor
- 5. Signs a values proton
- 6. Single
- 7. Single transfe
- 8. Dewar (
- magnet
- Crysta;
- II. ESR sp. chlori.
  a in
- ESR sp chlori c'in

#### LIST OF FIGURES

FIGURE		Page
1.	ESR energy level diagram for a single electron and single nucleus	40
2.	Spin polarization for $\alpha$ hydrogens in $\pi$ -electron radicals	52
3.	Relationship of nucleus at $\beta$ -position relative to the odd electron orbital. A ·C-CH fragment is shown looking along the C-C bond with the dotted line outlining the $p_{\pi}$ orbital of the odd	
	electron	57
4.	Principal directions of the hyperfine splitting tensor or g tensor for an $\alpha$ proton	60
5.	Signs and relative magnitudes of the principal values of the dipolar coupling tensor for an $\alpha$ proton illustrated for a -C-H fragment	61
6.	Single crystal holder	77
7.	Single crystal mounted in crystal holder for transfer to ESR cavity	79
8.	Dewar container for ESR single crystal studies	80
9.	Apparatus for rotating single crystals in the magnetic field	81
10.	Crystallographic axes for acetamidine hydrochloride	87
11.	ESR spectrum of irradiated acetamidine hydrochloride showing $\text{Cl}_2$ at $77^0\text{K}$ . $\overline{\text{H}}^{>}$ is $50^0$ from a in the ac* plane	88
12.	ESR spectrum of irradiated acetamidine hydrochloride showing $Cl_2$ at $77^0K$ . H is $40^0$ from c* in the ac* plane	90

- 13. ESR spec chloride a in th
- 14. ESR spec
- 15. ESR spec
- 16. Hyperfir in the
- 17. Hyperfin in the
- 18. Hyperfining the
- 19. Plot of the bo
- 20. Plot of the ac
- N. Plot of the ab
- 22. ESR Spe
  - from ;
- 23. ESR sp from
- 24. ESR SP
- 25. ESR SF 1400 F

### LIST OF FIGURES (Continued)

FIGURE	F	age
	ESR spectrum of irradiated acetamidine hydrochloride showing $Cl_2$ at $77^0K$ . $\overline{H}^{>}$ is $60^0$ from a in the ac* plane	91
14.	ESR spectrum of $Cl_2$ with $\overline{H}^>     b$ in the ab plane	92
15.	ESR spectrum of $Cl_2$ with $\overline{H}^>    a$ in the ab plane	93
16.	Hyperfine splitting of $Cl_2$ vs angle of rotation in the bc* plane	95
17.	Hyperfine splitting of $Cl_2$ vs angle of rotation in the ac* plane	96
18.	Hyperfine splitting of $Cl_2$ vs angle of rotation in the ab plane	97
19.	Plot of g vs angle of rotation for Cl <sub>2</sub> in the bc* plane	100
20.	Plot of g vs angle of rotation for Cl <sub>2</sub> in the ac* plane	101
21.	Plot of g vs angle of rotation for Cl <sub>2</sub> in the ab plane	102
22.	ESR spectrum of $CH_2-C-NH_2$ radical with $\overline{H}^>$ 60° +NH <sub>2</sub>	
	from b in the ab plane	103
23.	ESR spectrum of $CH_2-C-NH_2$ radical with $\overline{H}^> 50^0$ from b in the ab plane	105
24.	$\stackrel{+}{\rm NH_2}$ ESR spectrum of $\stackrel{-}{\rm CH_2-C-NH_2}$ radical with $\stackrel{-}{\rm H}^{>}$ 1000 from b in the ab plane	106
	, NH₂	
25.	ESR spectrum of $\dot{C}H_2 - \ddot{C} - NH_2$ radical with $\overline{H}^>$ 1400 from b in the ab plane	107

splitti

27. Angular

fine sp radical

28. Angular

fine sp

29. ESR spe with  $\frac{1}{H}$ 

30. ESR sp<u>e</u> with H

31. Crystal

32. ESR spec crystal a'b pl

33. ESR sper crystal a\*c pl

34. ESR spec crystal plane .

35. ESR spectorystal the as

36. ESR firs methylac H is 10

### LIST OF FIGURES (Continued)

FIGURE		Page
26.	Angular variation in the ab plane of hyperfine +NH2	
	splittings for $\alpha$ protons in $CH_2-C-NH_2$ radical	110
27.	Angular variation in the bc* plane of hyper- +NH <sub>2</sub>	
	fine splittings for $\alpha$ protons in $\dot{C}H_2 - \ddot{C} - NH_2$ radical	111
28.	Angular variation in the ac* plane of hyper- $+NH_2$	
	fine splittings for $\alpha$ protons in $\dot{C}H_2-\ddot{C}-NH_2$ radical	112
	+NH <sub>2</sub>	
29.	ESR spectrum of deuterated $CH_2-C-NH_2$ radical with $H$   a in the ac* plane	114
	+NH <sub>2</sub>	
30.	ESR spectrum of deuterated $CH_2-C-NH_2$ radical with $H^> \mid \mid C^*$ in the ac* plane	115
31.	Crystallographic axes for trimethylacetamide .	119
<b>32.</b>	ESR spectrum of ir radiated trimethylacetamide crystal at $77^{\circ}$ K. H is $60^{\circ}$ from b in the	
	a*b plane	121
33.	ESR spectrum of irradiated trimethylacetamide crystal at $77^{\circ}$ K. $\overline{\text{H}}^{>}$ is $60^{\circ}$ from c in the	
	a*c plane	122
34.	ESR spectrum of an irradiated trimethylacetamide crystal warmed to $-80^{\circ}$ . $\overline{\text{H}}^{>}  $ c in the a*c	•
	plane	125
35.	ESR spectrum of an irradiated trimethylacetamide crystal warmed to $-80^{\circ}$ . $\overline{\text{H}}^{>}$ is $40^{\circ}$ from c in	•
	the a*c plane	127
36.	ESR first derivative spectrum of irradiated tri-	
	methylacetamide crystal at $77^{0}$ K showing $^{13}$ C line H is $10^{0}$ from b in the a*b plane	128

- 37. Crysta
- 38. ESR spe at 770;
- 39. ESR spa amide o ab pla
- $^{40}$ . ESR spear at  $77^{ ilde{0}}\mathrm{K}$
- 41. Angular CH<sub>2</sub> CH−
- 42. Variabl
- Variable
  CH2
  CH2
  CH3
- Variabl CH<sub>2</sub> CH<sub>3</sub>
- 45. Plot of
  - as a fur plane .
- 46. Plot of
  - as a fur plane

### LIST OF FIGURES (Continued)

FIGURE	Page
37.	Crystallographic axes for isobutyramide 130
38.	ESR spectrum of irradiated isobutyramide crystal at $77^{\circ}K$ . $\overrightarrow{H}$ is $10^{\circ}$ from b in the ab plane. 131
39.	ESR spectrum of irradiated deuterated isobutyramide crystal at $77^0K$ . $\overline{H}^>$ is $10^0$ from b in the ab plane
40.	ESR spectrum of irradiated isobutyramide crystal at $77^{\circ}K$ . $\overrightarrow{H}$ $\downarrow$ $\downarrow$ c* in the bc* plane 134
41.	Angular plot of line positions for the CH <sub>2</sub> OCH <sub>2</sub> CH-C-NH <sub>2</sub> radical in the ab plane 136
42.	Variable temperature study of the spectrum of the $\dot{C}H_2$ $\ddot{C}H_2$ $\ddot{C}H_2$ $\ddot{C}H_3$ $\ddot{H}^>   a$
43.	Variable temperature study of the spectrum of the $CH_2$ $CH_2$ $CH-C-NH_2$ radical with $\overline{H}^>  $ b 141
44.	Variable temperature study of the spectrum of the $\dot{C}H_2$ $\ddot{C}H_2$ $\ddot{C}H_2$ $\ddot{C}H_2$ radical with $\ddot{H}^>  $ $c^*$
45.	Plot of line positions for CH-C-NH <sub>2</sub> radical CH <sub>3</sub> as a function of field orientation in the bc* plane
46.	Plot of line positions for CH <sub>2</sub> CH-C-NH <sub>2</sub> radical CH <sub>3</sub> as a function of field orientation in the ac* plane

- 47. ESR sp
  - H | L
- 48. ESR sp
  - H | c
- 49. ESR spachloric aa' pl
- 50. ESR spa chlorit aa' p:
- 51. ESR spa chloric aa' p:
- 52. ESR spe chlorid from a
- 53. Crystal
- 54. ESR spe bromide bc pla
- 55. ESR spe bromide a\*c pl
- Nyperfinitatio
- Nyperf. rotatic
- 38. Hyperfi rotatio
- in the

### LIST OF FIGURES (Continued)

FIGURE	CH <sub>2</sub> 0	Page
47.	ESR spectrum of the C-C-NH <sub>2</sub> radical with	
	ESR spectrum of the $CH_3$ $C-C-NH_2$ radical with $\overline{H}^{>}  $ b in the ab plane	151
48.	ESR spectrum of the $CH_3$ $C-C-NH_2$ radical with $\overline{H}^{>}  $ c* in the ac* plane	
	H   c* in the ac* plane	152
49.	ESR spectrum of irradiated hydrazinium dichloride at $77^{0}K$ . $\overrightarrow{H}^{>}$ is $45^{0}$ from a in the aa' plane	154
50.	ESR spectrum of irradiated hydrazinium dichloride at $77^{0}$ K. H is $135^{0}$ from a in the aa' plane	156
51.	ESR spectrum of irradiated hydrazinium dichloride at $77^0K$ . $\overline{H}^{>}$ is $90^0$ from a in the aa' plane	157
52.	ESR spectrum of irradiated hydrazinium dichloride after warming to $-80^{\circ}$ . $\overline{\text{H}}^{>}$ is $45^{\circ}$ from a in the aa' plane	158
53.	Crystal axes for hydrazinium dibromide	160
54.	ESR spectrum of irradiated hydrazinium dibromide at $77^0K$ . $\overline{H}^>$ is $30^0$ from b in the bc plane	162
55.	ESR spectrum of irradiated hydrazinium dibromide at $77^{0}$ K. $\overline{\text{H}}^{>}$ is $30^{0}$ from c in the a*c plane	164
56.	Hyperfine splitting of Br <sub>2</sub> versus angle of rotation in the a*b plane	165
57.	Hyperfine splitting of Br <sub>2</sub> versus angle of rotation in the bc plane	166
58.	Hyperfine splitting of Br <sub>2</sub> versus angle of rotation in the a*c plane	167
59.	Plot of g versus angle of rotation for Br <sub>2</sub> in the a*b plane	168

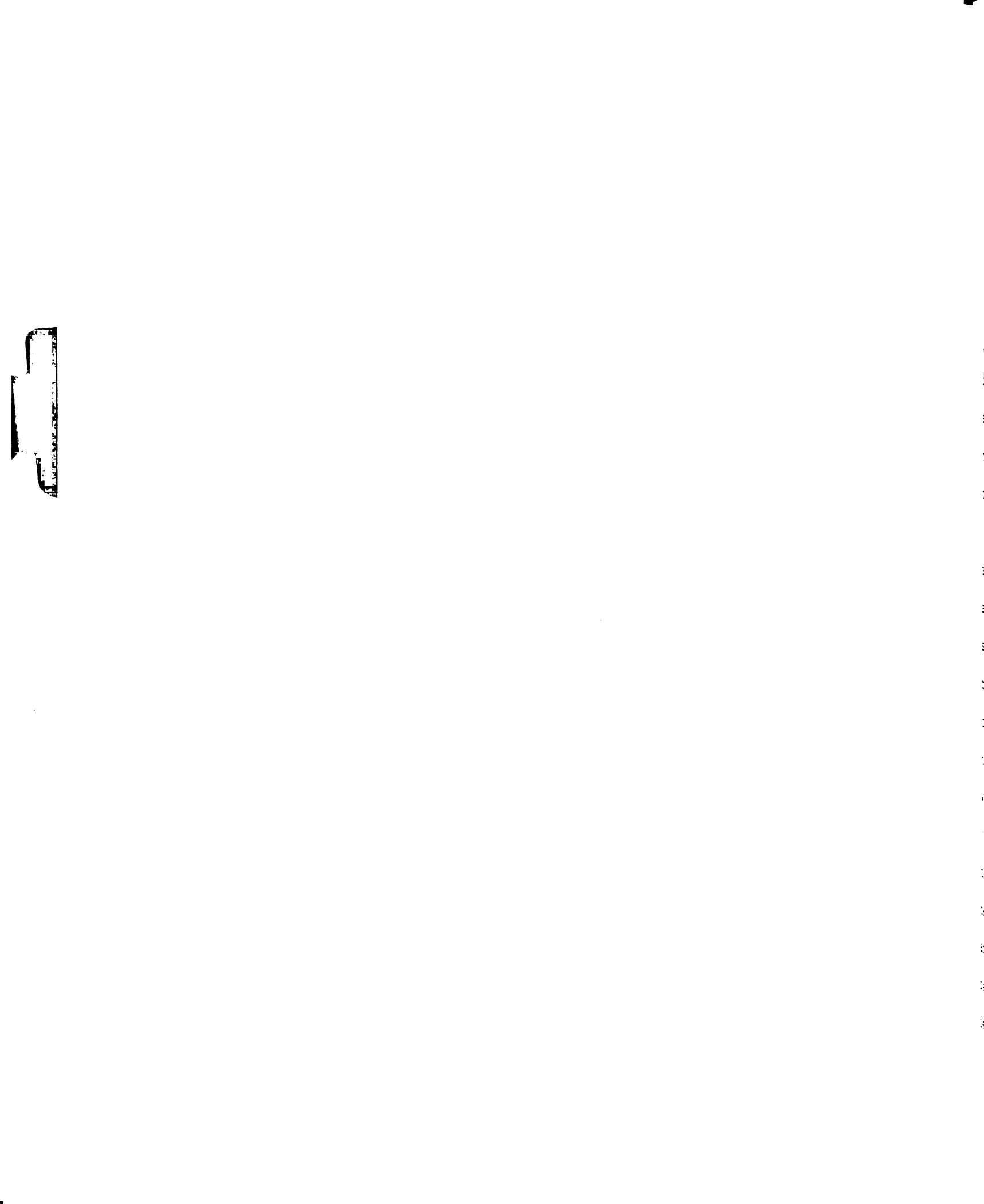
- 60. Plot coin the
- 61. Plot of in the
- 62. First hydraz in the
- 63. Crysta fluori
- 64. ESR sy ium d the h the
- 65. ESR s ium d D<sub>2</sub>O.
- 66. ESR s fluor plane are a
- 67. Firshydra, pthe with
- 68. ESR fluo plan
- 69. ESR fluc in t
  - 70. ESR fluc a ax

## LIST OF FIGURES (Continued)

FIGURE		Page
60.	Plot of g versus angle of rotation for Br <sub>2</sub> in the bc plane	169
61.	Plot of g versus angle of rotation for Br <sub>2</sub> in the a*c plane	170
62.	First derivative ESR spectrum of irradiated hydrazinium dibromide warmed to -1600; H   c in the a*c plane	172
63.	Crystal reference axes for hydrazinium di- fluoride; c is the threefold axis	174
64.	ESR spectrum of electron irradiated hydrazin- ium difluoride at $77^{0}K$ showing the spectrum of the hydrogen atom (outer doublet). $H^{>}     c$ in the bc plane	175
65.	ESR spectrum at $77^0 \text{K}$ of $\gamma$ -irradiated hydrazinium difluoride which has been exchanged with D <sub>2</sub> O. H     c in the bc plane	177
66.	ESR spectrum of $\gamma$ -irradiated hydrazinium difluoride at $77^0K$ with $ H\rangle$   c in the bc plane. The outer seven lines on each side are attributed to a radical pair	179
67.	First derivative ESR spectrum of $\gamma$ -irradiated hydrazinium difluoride at $77^{0}$ K with $\frac{1}{H}$   c; a) position of the $g=4$ lines relative to the resonance at $g=2$ , b) the $g=4$ lines with better resolution	180
68.	ESR spectrum of $\gamma$ -irradiated hydrazinium difluoride warmed to $-70^{\circ}$ . H   c in the bc plane	181
69.	ESR spectrum of $\gamma$ -irradiated hydrazinium difluoride warmed to $-70^{\circ}$ . H is $40^{\circ}$ from c in the bc plane	183
70.	ESR spectrum of $\gamma$ -irradiated hydrazinium diffuoride warmed to $-70^{\circ}$ . H is $30^{\circ}$ from the a axis in the ab plane (plane $\perp$ to c-axis).	184

## LIST OF FIGURES (Continued)

FIGURE	P	age
71.	ESR spectrum of $\gamma$ -irradiated hydrazinium diffuoride warmed to $-70^{\circ}$ . H is $120^{\circ}$ from the a axis in the ab plane	186
72.	Angular variation of the hydrogen hyperfine splitting in the $$ ab $$ plane for the $-70^{\circ}$ radical	187
73.	Angular variation of the nitrogen and hydrogen hyperfine splitting in the bc plane for the -70° radical	188
74.	Angular variation of the nitrogen and hydrogen hyperfine splitting in the ac plane for the $-70^{\circ}$ radical	189
75.	ESR spectrum of $\gamma$ -irradiated deuterated hydrazinium difluoride at $77^0 K$ . H is $-10^0$ from the caxis in the ac plane	
76.	ESR spectrum of $\gamma$ -irradiated acetamidine hydrochloride powder at $77^{\circ}K$ . a) Observed spectrum b) Computed spectrum	195



#### INTRODUCTION

Irradiation of organic compounds by X-rays or  $\gamma$ -rays produces free radicals by adding or removing electrons or by breaking chemical bonds. If single crystals are irradiated well below their melting points the radicals may be trapped in the crystal and may be partially or completely oriented.

The molecular and electronic structures of the radicals are determined from ESR studies. If the odd electron interacts with nuclei which have magnetic moments hyperfine structure is observed and usually serves, along with the measured g values, to identify the radical. If the radical is oriented the hyperfine splitting constant for each nucleus, as well as the g factor, are second-rank tensors whose elements are determined by obtaining ESR spectra for various orientations of the magnetic field with respect to the crystal (or radical) axes. The hyperfine splitting tensors thus obtained have both an isotropic part and an anisotropic part; the former is related to the odd electron density in s orbitals and the latter to the odd electron density in p orbitals.

The relative s tensor are fou

at asually of gereor (d<sup>xx</sup>, c

The most

impounds is ( the three ;

the cdd e

\*\*pendicular menty calle

In typica

Claract With

est with hydro Stogen, etc.

detailly remo

The ESR spectra of the radicals may then be characterized by giving the principal components of the hyperfine splitting tensor for each nuclear interaction  $A_{xx}$ ,  $A_{yy}$ ,  $A_{zz}$  or by giving separately the isotropic portion  $A_{iso}$  and the anisotropic portion  $B_{xx}$ ,  $B_{yy}$ ,  $B_{zz}$ . These are related by the equations

$$B_{xx} + B_{yy} + B_{zz} = 0$$

$$1/3(A_{xx} + A_{yy} + A_{zz}) = A_{iso}$$

$$A_{xx} = B_{xx} + A_{iso}$$

$$A_{yy} = B_{yy} + A_{iso}$$

$$A_{zz} = B_{zz} + A_{iso}$$

The relative signs of the principal components of the A tensor are found experimentally but the absolute signs are not usually obtained. The principal components of the g tensor  $(g_{xx}, g_{yy}, g_{zz})$  are also found from the spectra.

The most common type of radical from irradiated organic compounds is of the type  $\cdot$ CRR'R" or  $\cdot$ NRR'R" where the bonds to the three groups R, R', R" lie approximately in a plane and the odd electron is largely in a p orbital directed perpendicular to the radical plane; such radicals are commonly called  $\pi$ -electron radicals.

In typical  $\pi$ -electron radicals the odd electron may interact with the nucleus of the atom on which it is centered and with hydrogen (or other) atoms on adjacent carbon (or nitrogen, etc.) atoms ( $\alpha$ -hydrogens) or on carbon atoms more distantly removed ( $\beta$ ,  $\gamma$ -hydrogens, etc.). The convention

Irradiate radical R

the sec-butyl

SR studies has rimethylacetal Few studice radiated sall radiated sall radiation has richard and radiation decrease and the radiate radiate radiation of radiation and the radiate radiate

tistal ESR s

for designating these is illustrated by the radical

Irradiated amides RCONH<sub>2</sub> usually give the trapped radical 'R; it would be of interest to know whether the <u>sec</u>-butyl and <u>t</u>-butyl radicals are planar or not, hence ESR studies have been made of irradiated <u>sec</u>-butyramide and trimethylacetamide.

Few studies have been made of the radicals produced in irradiated salts such as acetamidine hydrochloride or the hydrazinium halides. Single crystals of acetamidine hydrochloride, hydrazinium dichloride, hydrazinium dibromide and hydrazinium difluoride have therefore been irradiated with  $\gamma$ -rays and the radicals produced identified from single crystal ESR studies.

tensors for a

the splittings

itta. Data fr

iction will be

A. <u>2-Pro</u>

Isctropic is of a numi

The

te results w

It has b 'electron in

Mital of an

Militings in

We I it ca

Se fall in

Sticks. Th

shown to

#### HISTORICAL BACKGROUND

### I. Proton Splittings in $\pi$ -Electron Radicals

There are now available ESR data for a large number of organic radicals which have been studied in single crystal matrices. It is found that the hyperfine splitting tensors for  $\alpha$  protons tend to be similar as do those for the splittings by the  $\beta$  or  $\gamma$  protons or by the central atom. Data from the literature for each class of interaction will be collected and discussed below.

#### A. $\alpha$ -Proton Hyperfine Splittings

Isotropic and anisotropic splittings for the  $\alpha$  hydrogens of a number of hydrocarbon radicals are listed in Table I. The list is not complete but is representative of the results which have been obtained.

It has been shown theoretically (113) that a single  $\pi$  electron induces a spin density of about -0.05 in the 1s orbital of an  $\alpha$  hydrogen atom corresponding to predicted  $\alpha$  splittings in the range -20 gauss  $\leq A_{iso} \leq -25$  gauss. From Table I it can be seen that most of the isotropic splittings fall in the range predicted by theory with some exceptions. The negative sign for the isotropic splitting has been shown to be correct (1).

Radical

Irradiated Crystal

Toole 1. . . - Profon byserfine interactions in hydrocarbon radicals.

Hyperfine Splittings

Anisotropic

Anisotropic

Asso Bxx By Bzz

(gauss)

Refer-ence

 $\alpha\text{--Proton}$  hyperfine interactions in hydrocarbon radicals. Table I.

Irradiated Crystal	Radical	Hyp Isotropic Aiso (qauss)	erfine Ar Bxx	e Splittings Anisotropic Byy B	ngs ic Bzz (qauss)	Refer- ence
HOOC-(CH <sub>2</sub> ) <sub>2</sub> -COOH	ноос-сн <sub>2</sub> -сн-соон	-21.4	+10.7	-0.4	-11.4	2,3
CH <sub>2</sub> (COOH) <sub>2</sub>	н2с-соон	-21.1	+10.3	1. 1. 4. 1.	- 9.3 -10.3	4
CH2 (COOH)2	нċ(соон) <sub>2</sub>	-21.4	+11.1	-0.4	-11.1	ည
HOOC-CH <sub>2</sub> -CH(NH <sub>2</sub> )-COOH	ноос-сн2-сн-соон	-22.5	+ 8.6	+1.1	9.6 -	9
ноос-(сн <sub>2</sub> ) <sub>3</sub> -соон	ноос-(сн <sub>2</sub> ) <sub>2</sub> -сн-соон	-20.0 -18.2	+10.7	+1.1	-11.4	7
HOOC-(CH <sub>2</sub> ) <sub>4</sub> -COOH	ноос-(сн <sub>2</sub> ) <sub>3</sub> -сн-соон	-20.3	+10.3	+2.5	-13.2	œ
HO-CH <sub>2</sub> -COOH	но-сн-соон	-20.3	9.6 +	+0.7	-10.3	6
HO-CH2-COO K	но-сн-соо_	-18.2	+10.0	+0.4	-10.3	10
HO-CH2-COO Li	но-сн-соо_	-17.8	9.6 + +	+1.1 +1.1	-10.3	11
$\alpha$ -CH $_3$ -CH $(NH_2)$ -COOH	нэс-сн-соон	-19.6	+10.7	+1.8	-12.1	12,13
H <sub>2</sub> N-CH <sub>2</sub> -COOH	H <sub>3</sub> N-co-coo_	-22.1	+12.5	-1.4	-10.7	14,15
O " H <sub>3</sub> C-C-NH-CH <sub>2</sub> -COOH	о Н <sub>3</sub> С-С-NH-СН-СООН	-18.2	+ 8.2	+1.1	တ် အ ၊	16

Radical

Irradiated Crystal

Hyperfine Splittings Isotropic Anisotropic

Refer-ence

Byy Bzz (ganss)

Aiso (gauss)

Table I. (Cont.)

Trradiated Gruetal	[בי : מבס	Hype Isotropic	rfine	Splittings Anisotropic	js oic	Refer-
iiadiated Ciystai	Nadical	$f{A}_{f iso}$	Bxx	$^{\mathrm{B}}_{YY}$	B <sub>ZZ</sub> gauss)	ש ב ש
CH3-CH2-C-NH2	O CH3-CH-C-NH2	-23.0	+12.4	-1.3	-11.1	17
$_{\text{CH}_3}^{\text{O}} - (_{\text{CH}_2}^{\text{CH}_2})_{_2}{\text{C}}^{\text{-NH}_2}$	O CH3-CH2-CH-C-NH2	-23.0	+13.6	9.	-12.0	17
CH <sub>2</sub> =CH-C00H	HOOC-CH-CH3	-21.5	+13.0	-2.7	-10.3	18
$^{\rm O}_{\rm NH_2-C-CH_2F}$	O NH2-C-CHF	-22.5	+11.4	<b>∑</b> i	-11.8	19
CH3-0-CH2-C00 K	сн3-0-сн-соо к	-17.8	+11.7	8.0-	-11.5	20
H00C-CH2-O-CH2-C00H	HOOC-CH2-0-CH-COOH	-17.5	9.8+	-1.0	- 9.5	21
O " H <sub>2</sub> N-C-NH-CH <sub>2</sub> -COOH	O " H <sub>2</sub> N-C-NH-CH-COOH	-19.3	+ 9.3	-2.7	- 6.7	22
$\begin{array}{cccccccccccccccccccccccccccccccccccc$	O O " " " H2N-C-CH-C-NH2	-21.2	+11.0	+0.1	-10.7	23
${ m CH_3COONa\cdot 3H_2O}$	·CH3	-22.3	- 0.2	+0.4	- 0.2	24
Na 00C-H	_оос-о-сн-о_	-14.4	+ 7.5	+0.3	6.7 -	25
$HOSO_2 - CH_2 - CH(NH_2) - COOH$	HOSO <sub>2</sub> -CH <sub>2</sub> -CH-COOH	-20.9	0.6 +	6.0+	-10.0	26

Irradiated Crystal

( come - )

Traffic 1 . .

Radical

Hyperfine Splittings

Isotropic Anisotropic
Aiso Bxx By Bzz

Refer-ence

BZZ

Table I. (Cont.)

ביייל בסורי בבייוד	ר מל יר יר מל יר	Hype Isotropic	rfine S	plittings Anisotropic	ıs pic	Refer-
iiiadia ced Cifstai		Aiso (gauss)	Bxx	$^{\mathrm{B}}_{\mathrm{YY}}$ (	B <sub>ZZ</sub> (gauss)	ence
$\operatorname{Zn}(\operatorname{CH_3COO})_2 \cdot \operatorname{2H_2O}$	·CH3	-23.0±1.0		Isotropic	<b>a</b> .	27
$z_{n}(c_{H_{3}}c_{00})_{2}\cdot 2_{H_{2}}o$	-CH2 COO -	-21.9	+10.1	+1.3	-11.4	27
		-21.2	+12.1	+0.2	-12.2	
0:	0:					
$H_2N-C-(CH_2)_2-C-NH_2$	$H_2N-C-CH_2-\dot{C}H-C-NH_2$	-20.3	+10.3	+1.2	-11.6	28
$CH_3CH_2OSO_3^-$ K	CH <sub>3</sub> -cH-OSO <sub>3</sub> -	-18.9	+10.9	-2.0	- 9.1	29
ноос-сн=сн-соон	H00C-CH-CH2-C00H	-20.3	+10.3	+0.7	-10.7	30
NH3 + C1 - H2N-(CH2) - CH-COOH · 2H2O	H <sub>2</sub> N-(CH <sub>2</sub> ) <sub>4</sub> -CH <sub>2</sub> -ĊH-COO	-20.0	+10.4	+1.3	-11.8	31
$CH_3 - S - (CH_2)_2 - CH - COOH$	$_{2}^{CH_{3}}$ -S -CH- $_{2}^{CH_{2}}$ (NH <sub>3</sub> $^{+}$ ) CO $_{2}^{-}$	-14.3	+ 7.5	+1.5	8.9	32

cal NH2 (22)

Reference

Radical

Irradiated Crystal

Terror 1 . (Come - )

Refer-33 34 -10.7 gauss Anisotropic Hyperfine Splittings В УУ +1.3 +1.7 6.6 BXX Isotropic -21.5 Aiso (gauss) -21.2- p, Radical O CH2-C-NH2 HO-C-H Irradiated Crystal Table I. (Cont.) CH2F-C-NH2

for an a-pro:

B. <u>2-P</u>:

Por §

are in fair a

2) that the Connell (2) we mentally in ly that the

expression

relating the serveen the

carbon and position.

ineoretica

Whittings

itom Tabl

either ve

Por alculat Moton.

Witte

ge zel

The anistropic splitting tensor has been calculated for an  $\alpha$ -proton and the values +14, -2.9 and -15 G obtained for  $B_{XX}$ ,  $B_{YY}$ ,  $B_{ZZ}$  (170). The observed values (Table I) are in fair agreement with the theoretical prediction.

### B. $\beta$ -Proton Hyperfine Splittings

For  $\beta$  and  $\gamma$  protons it has been shown by McConnell (2) that the splittings should be nearly isotropic. Mc-Connell (2) was the first to observe  $\beta$  splittings experimentally in irradiated succinic acid. It was found empirically that the isotropic splittings could be described by an expression

$$A_{\beta} = B_0 + B_2 \cos^2 \theta$$

relating the isotropic  $\beta$  splitting to  $\theta$ , the dihedral angle between the axis of the odd electron  $\pi$  orbital on the  $\alpha$  carbon and the plane containing the NH or CH bond in the  $\beta$  position. This expression is discussed further in the theoretical section. Because of the dependence on  $\theta$ , the splittings observed experimentally for  $\beta$  protons can be quite different from one radical to the next as can be seen from Table II. It should be noted that the anisotropy is either very small or was not detected.

For a radical with two  $\beta$  protons, it is necessary to calculate two angles,  $\theta_1$  and  $\theta_2$ , with an angle  $\theta$  for each proton. The relationship of  $B_0$  and  $B_2$  to the observed splittings is given in the theoretical section in Equation 59. The relationships above for  $\theta$  are valid assuming that the  $\beta$  carbon is sp<sup>3</sup> hybridized.

Radical

A proton hypertine aplittings in hydrocarbon radicals.

Reference

Isotropic Anisotropic Aiso Bxx Byy Bzz (gauss)

Radi

Irradiated Crystal

The same of the same

 $\beta$ -Proton hyperfine splittings in hydrocarbon radicals. Table II.

		Tuno	Tuncy fine Galitting	1:++:	0	
			de auti.	11111111111111111111111111111111111111		200
Trradiated Crystal	Radical	Isorropic	١	Anisotropic	opic	Kerer-
		Aiso	жх хх	$_{YY}^{B}$	B <sub>ZZ</sub>	ence
					Sanak	
HOOC-(CH <sub>2</sub> ) <sub>2</sub> -COOH	ур- 2нр- 2нр- 200н	8.7	+3.8	6.0-	-2.0	35
	но	27.9	+2.1	-1.1	-1.1	
. O. J.	° 2°H					
H <sub>2</sub> C CH-C-NH <sub>2</sub>	H <sub>2</sub> C-C-NH <sub>2</sub>	21.7	+1.0	-0.1	6.0-	17
0	0					
$CH_3-CH_2-C-NH_2$	$CH_3 - \dot{C}H - \ddot{C} - NH_2$	21.0-25.0	OSI	ISOTROPIC		17
$CH_3-CH(NH_2)-COOH$	сн3-сн-соон	42.8				
		27.1	ISO	ISOTROPIC		36
AN		5.0				
H <sub>3</sub> C -C00H	н <sub>з</sub> с г-соон	23.4	+1.3	-0.4	6.0-	37
к-сн(он)-сн(он)-сн(он)-к	R-CH(OH)-сн-СН(OH)-R	5.0	OSI	ISOTROPIC		38
CH <sub>2</sub> = CH - COOH NH <sub>2</sub> + Cl -	сн <sub>з</sub> -сн-соон	22.3-28.1	OSI	ISOTROPIC		18
HOOO- "HO- DOOH	ноос-сн-сн-соон	24.3	6	6		U
		41.5	Teo	ISOTROFIC		Þ

Radical Hyperfine Splittings

Radical Anisotropic

Aiso

Axx

Bxx

By

Bzz

(ganes)

Reference

Bag

Irradiated Crystal

· Fr .....

41

42

43

Refer-ence Anisotropic

Byy Bzz Hyperfine Splittings 8.0-ISOTROPIC +2.2 +2.7 +1.7 +2.8  $_{\text{HOOC-CH}_2\text{-C}}^{\text{CH}_3}$  (from CH<sub>2</sub>)  $\left\{21.8 + 2.8 \atop \text{CH}_3 + 3.2 \atop \text{CH}_3 + 3.2 \right\}$ 23.8(CH<sub>3</sub>) +0.8 16.6 + 4  $^{2H_2O}$   $^{2B.7}$   $^{-OOC-CH-CH_2-(CH_2)_3-NH_3^+C1^-}$   $^{-37.3}$ Isotropic 25.0 38.1 Aiso (gauss) 20.0 o "C-NH-ĊH-CH27 ноос-сн-сн-соон '  $\mathsf{L}_{\mathsf{CH_2}}\mathsf{-}_{\mathsf{CH_2}}\mathsf{-}_{\mathsf{CH_2}}\mathsf{J}$ CH3 HOOC-CH2-C Radical ноос-с-соон  $HOOC-CH(NH_2)-(CH_2)_4-NH_3C1-2H_2O$ Irradiated Crystal СН3 НООС – СН2 – С – СООН СН3 O "C-NH-CH2-CH27 HOOC-CH=CH-COOH Lсн<sub>2</sub> -сн<sub>2</sub> -сң<sub>2</sub> -HOOC-СН2-С-СООН CH2-CH3 ноос-сн-соон

(cont.) Table II.

Hyperfine Splittings

Isotropic Anisotropic
Aiso Bxx Byy Bzz (gauss) Radical

Reference

Irradiated Crystal

( - , , , , , , , ,

Table II. (Cont.)

	1 - 56 - 8	Hyperfine Isotropic	Hyperfine Splittings opic Anisotropic	Refer-
irradiated Crystai	Kadıcal	Aiso Bxx	Byy	ence
		(dauss)	(danss)	
$(HO_2C-CH_2-CH_2-S)_2$	$HO_2C-CH_2-CH_2-\dot{S}$	12.4	•	
		5.3	ISOTROPIC	45
$HOSO_2 - CH_2 - CH(NH_2) - COOH$	HOSO <sub>2</sub> -CH <sub>2</sub> -CH-COOH	12.3		
		12.3	ISOTROPIC	<b>5</b> 6
0:	0:			
$H_2N-C-(CH_2)_2-C-NH_2$	$H_2N-C-CH_2-CH-C-NH_2$	31.0		
		34.0	ISOTROPIC	88
$(CH_3)_2$ CH-CH $(NH_2)$ -COOH	$(CH_3)_2\dot{c}-CH(NH_3^+)-COO^-$	23.3(CH <sub>3</sub> ) <sub>2</sub> +1.1	-0.1 -0.9	46
$CH_3-CH_2-OSO_3-K^+$	сн3-сн-0803	$23.0\pm0.5$	ISOTROPIC	59
ноос-сн=сн-соон	HOOC-CH-CH2-COOH	28.9	ISOTROPIC	30
NH2	-			
$CH-S-(CH_2)_2-CH-COOH$	$CH_3 - S - \dot{C}H - CH_2 - CH(NH_3)CO_2 18.2$	$0_{2}^{-}$ 18.2	1	(
		31.1	ISOTROPIC	89 17

Refer-ence Hyperfine Splittings

Isotropic Anisotropic
Aiso Bxx By Bzz

(gauss) Radical Irradiated Crystal

Table II. (Cont.)

Irradiated Crystal	Radical	Hype Isotropic	ertine S	Hypertine Splittings Opic Anisotropic	ys copic	Refer-
1		Aiso (qauss)	XX B	$\mathbf{B}_{\mathbf{Y}\mathbf{Y}}$	Bzz gauss)	ence
	HO-C-H HO-C-H C-C HO-P-C HO-P-	29.5	H	ISOTROPIC		33
ноос-сн (он )-сн (он )-соон	ноос-сн-с-соон он он	10.0	7.8	0.3	-2.1	151
DOCH <sub>2</sub> -CH (NH <sub>2</sub> )-COOD	$(DO)_2 - C - CH - CH_2OD$ $NH_2$	40.4	1.6	6.0-	8.0-	152
	C Output					

Bailey a couplings at Ty consider:

at the carb $\varepsilon$ 

lings for  $\gamma$ 

Tather small

and S-proton

for a-proton.

mained for a

splittings

ain of the

Recentl

tecry to pre

#### C. y-Proton Hyperfine Splittings

For protons further removed than the  $\beta$  position from the atom on which the unpaired electron is centered, the splittings become quite small in aliphatic radicals. In fact, Whiffen (47) postulated that these splittings would be less than 1.8 gauss and so would usually be lost in the line width. However, these small splittings were detected in aliphatic radicals by Fessenden and Schuler (48) in electron irradiated liquid hydrocarbons where the line widths are smaller. These results are given in Table III.

Bailey and Golding (49) have calculated proton hyperfine couplings at various positions in aliphatic radical fragments by considering a second-order expansion of the spin density at the carbon nucleus. Using this approach isotropic couplings for  $\gamma$  protons were predicted to be only 0.05 gauss, rather smaller than observed. Agreement was better for  $\alpha$ -and  $\beta$ -proton splittings; a value of -23.2 gauss was obtained for  $\alpha$ -proton splittings and a value of -1.6 gauss was obtained for  $\beta$  splittings. The peculiar value obtained for  $\gamma$  splittings was due to a lack of available values for certain of the exchange intergals used in the calculation.

Recently Underwood and Givens (50) used extended Hückel theory to predict the  $\gamma$  splittings in aliphatic semidiones.





Table III.  $\gamma$ -Proton hyperfine splittings in hydrocarbon radicals.

Irradiated Host	Radical	A Refe iso ence (gauss)
CH <sub>3</sub> -CH <sub>2</sub> -CH <sub>3</sub> (liquid)	CH <sub>3</sub> -CH <sub>2</sub> -CH <sub>2</sub>	0.38 48
$CH_3 - (CH_2)_3 - CH_3$ (liquid)	CH <sub>3</sub> -CH <sub>2</sub> -CH-CH <sub>2</sub> -CH <sub>3</sub>	0.45-0.50 48
CH <sub>2</sub> CH <sub>2</sub> (liquid)	CH <sub>2</sub> ĊH	1.12 48
CH <sub>2</sub> — CH <sub>2</sub> CH <sub>2</sub> (liquid)	$CH_2$ $CH_2$ $CH_2$ $CH_2$	0.53 48
CH <sub>2</sub> ——CH <sub>2</sub> CH <sub>2</sub> (liquident)	CH <sub>2</sub> —CH <sub>2</sub> CH CH <sub>2</sub> —CH <sub>2</sub>	0.71 48

mese result

ported by Fe

ENDOR

sible to det

coming increa

The treatme:

# D. 14<sub>N</sub>

te discussed

Protons

incompagnet in the codd electory and the codd electory and the value ob interest in the compagnet in the codd electory in the codd elector

Se or y p

is project

Sediated h

The treatment was also tested with propyl radical in which different conformations and  $\beta$  substitutions were considered. These results predicted the temperature dependence of the  $\gamma$  splitting for propyl radical within 12% of the values reported by Fessenden and Schuler (48).

ENDOR (Electron Nuclear Double Resonance) makes it possible to detect small hyperfine splittings and so is becoming increasingly useful for studying long-range proton interactions. The ENDOR technique is quite different from the normal ESR technique used in this thesis and will not be discussed further.

#### D. <sup>14</sup>N - H Proton Splittings

Protons attached to nitrogen can give hyperfine splittings also; the hyperfine components are similar to those obtained in the case of  $\alpha$  protons bound to carbon. When the odd electron is centered on nitrogen the isotropic component for an  $\alpha$  proton is slightly greater than 23 gauss, the value obtained in the case of protons bound to carbon. Radicals showing this type of coupling are quite commonly found in irradiated amino acids and in some irradiated inorganic compounds. Examples of the magnitude of these couplings are given in Table IV. The anisotropic components for  $\alpha$  protons are about the same as in hydrocarbon radicals and for  $\beta$  or  $\gamma$  protons are small. Of particular interest in this project are N-H couplings in radicals resulting from irradiated hydrazine compounds.

rants IV. Hyperfilm mplitting constants for protons bound to 14N. Radical

Irradiated Host

Hyperfine Splittings
Isotropic Anisotropic
Aiso Bxx Byy Bzz

Refer-ence

Hyperfine splitting constants for protons bound to 14N. Table IV.

		HVD	Hynerfine C	71:++:		
Irradiated Host	רמטינים מינים מינים	Isotropic	2117	Anisotropic	ys ropic	Refer-
		Aiso (gauss)	Bxx	$^{\rm B}_{\rm YY}$	Bzz (gauss)	ence
O H <sub>+</sub> c1-	O H+(1)					
= U	့ - = ပ	(1)-7,7	+ 8.7	-1.3	- 7.3	1
H-N C H-2H-2H-0	H-N O N-H	(2)-2.9	+ 2.0	0 €	- 2.1	51
$H_2N-C$	H <sub>2</sub> N-C					
(crystal)	N - (2)					
$ ext{N}_2 ext{H}_5 ext{HC}_2 ext{O}_4$ (crystal)	N2H4	-10.4	+12.4	-2.6	-10.2	52
NH <sub>3</sub> +	NH3 +	+ 1.2	+ 8.3	7.0-	- 2.6	
CH2-CO2 (crystal)	_ch-co_	+22.1	+ 3.4	-1.1	- 2.1	53
		+29.3	+ 3.6	-1.5	- 2.2	
NH2-CONHNH2-C1-(crystal)	(1) (2) +	(1)-24.9	+14.4	-2.7	-11.8	ì
	8	$(2)15.0\pm0.5$		( 0 ≅ )		<b>5</b> 4
CO CH2 (crystal)	CO CH <sub>2</sub> )4	+ <b>7.7</b> (β)	က က +	7.0-	- 2.7	41

Refer-ence Isotropic Splittings Anisotropic Aiso Bxx By Bzz (gauss) Radical + II-N · (NH4 )2HPO4 (CTYStal) Irradiated Host

Refer-55 56 59 139 57 58 - 2.7 gauss Anisotropic Hyperfine Splittings -0.7 +0.3 +10.6 +13.9 +12.0 + 2.3 X M X 0 Isotropic -23.3 Aiso (gauss) +25.9 -22.8 -3.3(y)Radical SO3 -NH2+ O "-" NH-C-NH  $\cdot$ NH(SO<sub>3</sub>) + <sup>8</sup>HN. + N-H HO-NH-C-NH<sub>2</sub> (crystal) (NH4)2HPO4 (crystal) SO<sub>3</sub> - NH<sub>3</sub> (crystal) Irradiated Host NH4ClO4 (crystal) KH2NSO<sub>3</sub> (crystal)

Table IV. (Cont.)

The 14: ∷ radicals The largest

for 14N mos.

mbital.

te directio

d electron

Derpendi ate of c

## II. 14N Splittings

For irradiated crystals where splittings due to 14N (I = 1) are present, it is possible to analyze the resulting spectra in much the same manner as was done for  $\alpha$ -proton splittings. When the odd electron is centered on nitrogen the isotorpic coupling for <sup>14</sup>N is usually about 8-20 gauss and the anisotropic coupling shows nearly axial symmetry. The theoretical spin density for  $\Psi_{2S}$  for  $^{14}N$  has been calculated using Hartree-Fock wavefunctions (60,61) and is equal to 550 gauss. So if  $A_{iso}$  (14N) < 23 gauss this implies that only a small amount offs character exists in the odd electron molecular orbital. Calculations with Hartree-Fock (60, 61) functions also yield the theoretical 2p spin density and this value equals 17.1 gauss. If the anisotropic splitting corresponding to the direction parallel to the p orbital is compared with the theoretical 2p spin density then the fractional p character can be measured. Generally for 14N most of the unpaired spin density is in a 2p orbital.

The <sup>14</sup>N hyperfine splitting tensor shows axial symmetry for radicals with the odd electron centered on nitrogen. The largest principal value of the tensor corresponds to the direction parallel to the p orbital containing the odd electron. The smaller values are associated with the two perpendicular directions and are usually nearly equal but are of opposite sign to the parallel value. This may

be seen if

Since the a

if  $\theta = 0$ orbital the

perpendicul

The 14

are present

some specie

equivalentl

radicals ob

species, X

in irradiat

Hyperf

Hyperf

idd electron
served if the relative to tope. Since it is usual?

s capable c

tat from an

Ceraction |

be seen if the form of the anisotropic splitting is examined, Since the anistropic part of A,  $A_{aniso} = B \langle (3\cos^2 \theta - 1)/r^3 \rangle$ ; if  $\theta = 0$  corresponds to the splitting parallel to the p orbital then  $A_{aniso} = 2B$ ; if  $\theta = \pi/2$  then  $A_{aniso} = -B$  perpendicular to the 2p orbital.

The  $^{14}N$  hyperfine couplings for a variety of radicals are presented in Table V. Listed in Table VI are data for some species containing two nitrogen nuclei which couple equivalently to the odd electron. Of special interest are radicals obtained from hydrazine compounds and the diatomic species,  $N_2$ , which is similar to the V centers observed in irradiated alkali halides.

### III. <sup>13</sup>C Hyperfine Splittings

Hyperfine splittings can result from interaction of the odd electron with <sup>13</sup>C (I = 1/2) in a radical and will be observed if there is a high enough concentration of <sup>13</sup>C present relative to <sup>12</sup>C, the most abundant naturally occurring isotope. Since <sup>13</sup>C is present in only 1.1% natural abundance it is usually very difficult to detect any ESR signal from <sup>13</sup>C in natural abundance. It is usually necessary to substitute <sup>13</sup>C by synthesizing the required compound starting from Ba<sup>13</sup>CO<sub>3</sub> or some other appropriate available reagent. The radicals formed are the same but now the carbon nucleus is capable of giving hyperfine interaction in addition to that from any attached protons, nitrogen, etc. Hyperfine interaction with the <sup>13</sup>C nucleus of the atom on which the

 $Table \ V.$  14N hyperfine splitting tensors.

דיים מיים דיים דיים דיים דיים דיים דיים	רים: אַרָּים	Hype Isotropic	rfine S	Hyperfine Splittings opic	gs ropic	Refer-
	אמנוכמו	Aiso (qauss)	XX XX	Вуу	Bzz (gauss)	ence
0 " " 'H <sup>+</sup> C1-	+H, Z					
H-N C -H - 2H <sub>2</sub> O	H-N CH <sub>2</sub>	0.8+	+13.0	-6.5	6.5	51
H2N-C C-N (crystal)	H <sub>2</sub> N-C C N					
$H_2N-CH_2-COOH\left(crystal\right)$	$\dot{\text{CH}} - \left( \text{NH}_3^+ \right) - \text{CO}_2^-$	±3.2(β)	+ 0.4	+0.3	T.0 ±	ი ც
CH <sub>3</sub> 0 CH <sub>3</sub> CH-C-NH <sub>2</sub> (crystal)	CH <sub>3</sub> 0 c-C-NH <sub>2</sub>	+1.3(7)	+ 1.9	6.0-	- 1.0	17
NH4ClO4 (crystal)	+ + + NH3	+19.5	+ 2.6	-0.5	- 2.1	56
KH2NSO3 (crystal)	.NHSO3	+13.5	+21.3	8.6-	-11.5	28
NH2 6+0 NH2 O. H2O		+ 4.0	+ 5.0	-2.0	. 3.0	62
(crystal)	N - H					

Refer-ence Radical + 1110 - 03 Irradiated Host SO2 NII, +

. . . . . . . . . . .

(crystal)

Table V. (Cont.)

Irradiated Host	ויסיהאמ	Hype Isotropic	rfine S	Hyperfine Splittings opic Anisotropic	gs ropic	Refer-
		Aiso (gauss)	Bxx	Byy	B <sub>ZZ</sub> (gauss)	ence
SO <sub>3</sub> NH <sub>3</sub> (crystal)	SO3 -NH2	+18.2	+18.8	-6.4	-12.1	57
CH2 CH2 (glass)	CH <sub>2</sub> —CH <sub>2</sub>	+14.3	+18.7	9	e. 6	63
(803)2	·N(SO <sub>3</sub> ) <sub>2</sub> -2	+ 13.3	+24.5	-11.2	-13.3	64
$C_6H_5$ -NH-NH- $CNH_2$ (crystal)	C <sub>6</sub> H <sub>5</sub> -NH-n-CSNH <sub>2</sub>	+11.7	+17.3	7.8-	- 8.7	65
(NH4) <sub>2</sub> HPO <sub>4</sub> (crystal)	+ H-N•	+16.0	+20.1	6.7-	-12.3	55
CO CH <sub>2</sub> (crystal)	CO CH CH2 )4	-1.8(β)	+ 1.7	-0.3	1.3	41
$\begin{array}{ccc} & \text{O} & \text{O} \\ \text{"} & \text{"} & \text{"} \\ \text{A_2N-C-}(\text{CH}_2)_2 & \text{"} \\ \text{(crystal)} \end{array}$	0 0 " "-C-CH <sub>2</sub> -CH-C-NH <sub>2</sub>	+2.0(y)	+ +	-1.6	1.8	28

Hyperfine Splittings

Aiso Bx By Bzz (gauss) Radical Irradiated Host

Reference

Table V. (Cont.)

Reference 59 99 46 -10.0 8.0 gauss Anisotropic Hyperfine Splittings 8.9--0.4  $\mathbf{B}_{\mathbf{Y}\mathbf{Y}}$ -10.0 +20.0 +13.9 + 1.3 χ m Isotropic + 8.3 Aiso (gauss) +7.7(y) +28 R-N Or R-N CH<sub>3</sub> C-CH-COO CH<sub>3</sub> NH<sub>3</sub> Radical O "NH2 -C-NH H O HO-N-C-NH<sub>2</sub> (crystal) Irradiated Host (crystal)  $R-NO_2$  R = alkylCH<sub>3</sub> CH-CH-COO CH<sub>3</sub> (crysta (glasses) NH<sup>3</sup>

Table V. (Cont.)

Table VI. 14N hyperfine applitting tensors in radicals where the odd electron is delocalized over two nitrogen atoms.

Refer-ence

Hyperfine Splittings
Isotropic Anisotropic

Radical

 $^{14}\mathrm{N}$  hyperfine splitting tensors in radicals where the odd electron is delocalized over two nitrogen atoms. Table VI.

	100.000	Hype Isotropic	Hyperfine Splittings opic Anisotro	Anisotropic	s	Refer-
Illaulateu nost	Kadicai	Aiso (gauss)	B XX	$\mathbf{P}_{\mathbf{YY}}$	Bzz (gauss)	ence
NH2-CONHNH3 <sup>+</sup> Cl <sup>-</sup> (crystal)	$\alpha \beta + \alpha$	α + <b>16.9</b>	-17.3 ±1.0	-12.1 ±4.0	-5.1 ±4.0	54
		β - 4.0				
LiN2H5SO4 (crystal)	N2H4	+14	. 8 +	!	!	29
		+12	+ 7.	1	!	
$N_2H_5HC_2O_4$ (crystal)	°2H4+	+10.9	+16.7	-8.4	- 8.4	52
OH doped KCl(crystal)	N <sub>2</sub> -	+10.8	+10.5	-4.7	- 5.8	89
OH doped KBr (crystal)	N <sub>2</sub> -	+10.1	+11.3	-4.7	- 6.5	89
OH doped KI (crystal)	N <sub>2</sub> -	+11.4	+10.2	-4.3	0.9 -	89
$\mathtt{NaN_3}$ (crystal)	$^{-}$ N <sub>2</sub>	+12.8	+10.7	-1.8	6. 80 1	69
Ba(N <sub>3</sub> ) <sub>2</sub> (crystal)	N <sub>2</sub> -	+ 9.2	+10.8	-5.1	- 5.6	02
						1

odd electron is centered are similar to those found for <sup>14</sup>N interactions in radicals with the odd electron centered on nitrogen.

Hartree-Fock calculations (60,61) have been performed to calculate the theoretical isotropic hyperfine splitting for an odd electron in a carbon 2s or 2p orbital. It was found that the theoretical isotropic splitting for a 2s electron was 1190 gauss while that for a 2p electron was 32.5 gauss. It is possible to obtain an estimate of the amount of s or p character in the odd electron orbital in exactly the same manner as was done for 14N. The amount of s character in the case of <sup>13</sup>C is small, as it was for <sup>14</sup>N. The odd electron is therefore primarily localized in the 2p orbital and so the anisotropic hyperfine tensor should be axially symmetric. The anisotropic splittings are therefore equal to + 2B parallel to the p-orbital containing the odd electron and -B perpendicular to this direction for interaction of the odd electron with the  $^{13}$ C nucleus of the atom on which it is centered.

Some examples of the magnitudes of <sup>13</sup>C hyperfine splittings are given in Table VII. It is obvious that the anisotropic components show axial symmetry. Where deviations from cylindrical symmetry occur it is usually a result of delocalization of some of the spin density from the <sup>13</sup>C nucleus to one of the other nuclei in the radical.

Refer-ence Isotropic Anisotropic Anisotropic Anisotropic Anisotropic Anisotropic Anisotropic Associated Associ 0 0 7 6 66+ Radical Irradiated Crystal  $CH_2$  ( $CO_2H$ )2

, 13CH(CO2H),

Table VII. 13C hyperfine splittings

Irradiated Crystal	Radical	Hype Isotropic Aiso (gauss)	rfine B <sub>XX</sub>	Splittings Anisotropic By Bzz	s Opic B <sub>Z</sub> z gauss)	Refer- ence
$\operatorname{CH}_{2}\left(\operatorname{CO}_{2}\operatorname{H}\right)_{2}$	* 13 CH (CO <sub>2</sub> H)2	+33.2	+42.8	-17.8	-25.0	71,72
$NH_3$ $^+$ $CH_2$ $(CO_2$ $^-)$	18 CH2 (CO2H)	+44.3	+34.6	+ 3.2	-37.8	73
$\mathrm{NH_3}^+\mathrm{CH_2}(\mathrm{CO_2}^-)$	13 CNH3 + (CO2 -)	+45.3	+45.3	-13.2	-21.4	73
$\mathrm{CH_2}\left(\mathrm{SO_3K}\right)_{2}$	$^{13}$ CH $(\mathrm{SO_3}^-)_2$	+45.0	+47.8	-22.8	-25.0	64
CH3COONa · 3H2O	$^{13}^{\mathrm{CH}_3}$	+37.5	+45.	-22.5	-22.5	24
CF3 CONH2	13 CF3	+271	+47.0	-14.0	-33.0	74
CF3 CONH2	13 CF2CONH2	+88.2	+41.8	-20.6	-22.1	74
$HOOC - (CH_2)_2 - COOH$	ноос-сн <sub>2</sub> -сн- <sup>13</sup> соон	+33.2	+47.8	-21.8	-26.1	35
H-COONa	CO2 -0-CHO	+ 7.1	+ 3.6	+ 3.6	- 7.1	25
CFH2-C-NH2	O " " NH2 -C-13 CH-F	+85 gau	gauss maximum splitting	num spli	tting	19
$\mathtt{CS_2}(\mathtt{matrix})$	$^{13}\mathrm{CS}_{2}^{-}$	+87.2	+34.4	-14.1	-20.2	75
ин₄ -оос -сн <sub>2</sub> -сн (он ) -соон •	·H <sub>2</sub> O HOOC-CH <sub>2</sub> - <sup>13</sup> C(OH)COOH	+82.8	gauss maximum splitting	Kimum sp	litting	92

Hyperfine Splittings

Aiso

Aiso

Ax

Bx

By

Bzz

(gauss) Radical Irradiated Crystal

Reference

Table VII. (Cont.)

Trradiated Crustal	[ פין: הפס	Hype: Isotropic	Hyperfine Splittings	olittings Anisotropic	s opic	Refer-
iradiaced crystar	hadical	$egin{align*} \mathbf{A_{iso}} \ (\mathtt{gauss}) \end{aligned}$	B XX	$^{\mathrm{B}}_{\mathrm{YY}}$	B <sub>ZZ</sub> gauss)	ence
CD3COOD (matrix)	CD <sub>3</sub> -13C OD	+113.7	+50.3	-25.2	-25.2	7.7
HCOONa	13CO2 -	+167.1	+27.9	-11.4 -16.4	-16.4	78
NH2 - CH3 – CH – COOH	NH3 0 CH3-CH-13C	7.68+	+45.8	-27.6	-18.2	62

# IV. V Centers

Irradiati centers in the ine to an elec center may be new centers (V in the otherwi In a later par V centers in s with the radio seem to be mor then be shared Since the the hyperfine molear spin o and 5 for F2 emplication t Resence of mo T and Br. Ch

<sup>24 37</sup>Cl in 24 :50.6% abund

A problem

i tensor. The the free s

estin-orbit c Ster's bock

#### IV. V Centers

Irradiation of alkali halides produces paramagnetic centers in these materials. Besides the F center, which is due to an electron trapped near an alkali vacancy, another center may be formed. Känzig (80) was first to detect these new centers (V centers) and attributed them to holes trapped in the otherwise filled electron shells of the halogen ions. In a later paper (81) Castner and Känzig investigated these V centers in some detail and were able to identify them with the radicals  $F_2$ ,  $Cl_2$ , and  $Br_2$ . The diatomic species seem to be more stable since the electron deficiency can then be shared with a neighboring halide ion.

Since the electron is shared equally by both nuclei the hyperfine splitting pattern will depend on the total nuclear spin of the diatomic species. This means I=1,3,3 and 5 for  $F_2$ ,  $Cl_2$ ,  $Br_2$ , and  $I_2$ , respectively. Another complication to the hyperfine splitting arises from the presence of more than one naturally occurring isotope for Cl and Br. Chlorine has two isotopes,  $^{35}Cl$  in 75.4% abundance and  $^{37}Cl$  in 24.6% abundance. Bromine has two isotopes,  $^{79}Br$  in 50.6% abundance and  $^{81}Br$  in 49.4% abundance.

A problem also arises in evaluating components of the g tensor. The principal g values are quite different from the free spin value g = 2.0023 primarily as a result of spin-orbit coupling. An explanation is given in Slichter's book (82) where it is shown that the g anisotropy

is primarily g ground st g principa g unchange The alka should show a and the g v  $g_{zz} = g_{||}$  as tion of Table case. When i as in the cas hydroxylamine three differ glycine hydr tals are mon are expected C. in irra sent in the ciroxylamin tecently bee

The dia ther V cent : irradiate

In addi

Eligen nucl eger A Ce

90), FBr

is primarily due to a mixing of a  $\pi_g$  excited state with the  $\sigma_g$  ground state. The net effect is to change the  $g_{xx}$  and  $g_{yy}$  principal values from the free-spin value and to leave  $g_{zz}$  unchanged.

The alkali halides are all cubic in structure and so should show axial symmetry in both the hyperfine splitting and the g values. This means that  $g_{xx} = g_{yy} = g_{\downarrow}$ ,  $g_{zz} = g_{||}$  and  $A_{xx} = A_{yy} = A_{\downarrow}$ ,  $A_{zz} = A_{||}$ . From an examination of Table VIII it can be seen that this is indeed the case. When the internal symmetry is not as high as cubic, as in the case of irradiated glycine hydrochloride (86) and hydroxylamine hydrochloride (85), it is possible to get three different principal values for either g or A. Both glycine hydrochloride and hydroxylamine hydrochloride crystals are monoclinic. The greater g and A anisotropies are expected since the environment about the bond axis of  $Cl_2^-$  in irradiated KCl is more symmetrical than the environment in the case of irradiated glycine hydrochloride or hydroxylamine hydrochloride.

The diatomic V center I<sub>2</sub> was detected later than the other V centers. Boesman and Schoemaker (87) first found it in irradiated KCl doped with KI. This species has also recently been detected in irradiated PH<sub>4</sub>I single crystal (88).

In addition to the V centers formed from two identical halogen nuclei there have also been cases where heteronuclear V centers have been detected. These include FCl (89,90), FBr (90), FI (90), and ICl (91). The analysis

Refer-ence Principal 9 Values Hyperfine Splitting Principal Values (gauss) Radical (Isotope)

V centers.

Values for

7

mental and application commensure and

rrradiated Crystal (1

g values for V centers. Table VIII. Hyperfine splitting constants and

Irradi- ated Crystal	Radical (Isotope)	Hyperfine Splitting Principal Values (gauss)	ing (gauss)	Principal g Values	Refer- ence
LiF	F2 (19-19)	A <sub>ZZ</sub> =887	$A_{xx} = A_{yy} = 59$	$egin{align*} g_{\mathbf{xx}} = 2.0227 \ g_{\mathbf{yy}} = 2.0234 \ g_{\mathbf{zz}} = 2.0031 \ \end{array}$	81
KC1	cl <sub>2</sub> <sup>-</sup> (35-35)	$A_{ZZ} = 101$	$^{A}_{XX}$ $=$ $^{A}_{YY}$ $=$ $^{9}$	$g_{xx} = 2.0428$ $g_{yy} = 2.0447$ $g_{zz} = 2.0010$	81
NaCl	cl <sub>2</sub> <sup>-</sup> (35-35)	A <sub>ZZ</sub> =98	$^{\mathrm{A}_{\mathbf{x}\mathbf{x}}=^{\mathrm{A}_{\mathbf{y}\mathbf{y}}}=9}$	$g_{xx} = 2.0489$ $g_{yy} = 2.0425$ $g_{zz} = 2.0010$	81
KBr	Br <sub>2</sub> <sup>-</sup> (81-81)	A <sub>22</sub> =455	$A_{xx} = A_{yy} = 80$	$g_{xx} = 2.179$ $g_{yy} = 2.175$ $g_{zz} = 1.980$	81
NH4C1	c1 <sub>2</sub> <sup>-</sup> (35-35)	Azz=97.6	$A_{XX}=A_{YY}=10$	$g_{xx} = g_{yy} = 2.0437$ $g_{zz} = 2.0011$	& &
NH4Br	Br <sub>2</sub> <sup>-</sup> (81-81)	$A_{ZZ} = 431$	$A_{XX} = A_{YY} = 81$	$g_{xx}^{=g_{yy}} = 2.181$ $g_{zz}^{=1.980}$	84

Refer-ence 85 Principal g Values  $g_{11} = 2.0557$ Hyperfine Splittings Principal Values (gauss)  $A_{11} = 12.1$ Acc=32.1 ringdi-Radical Crystal (Isotope) Cl<sub>2</sub> <sup>-</sup>(35-35)  $NH_3OHC1$ 

Table VIII. (Cont.)

Irradi- ated Crystal	Radical (Isotope)	Hyperfine Splittings Principal Values (gauss)	Principal g Values	Refer- ence
NH30HC1	c12 (35-35)	A <sub>11</sub> =12.1	g <sub>11</sub> =2.0557	82
+		A33=103.9	933=1.9982	
NH3 CI CH2-COOH	cl <sub>2</sub> <sup>-</sup> (35-35)	A <sub>11</sub> =110.7	g <sub>11</sub> =1.999	86
		A33=24.3	932=2.037 933≈2.037	
KC1-KI	I <sub>2</sub> (127-127)	$A_{xx} = A_{yy} = 110.0$ $A_{zz} = 400.0$	gaverage=1.992	87
PH₄I	I <sub>2</sub> (127-127)	$A_{xx} = A_{yy} = 73.0 \pm 15.0$ $A_{zz} = 363.6 \pm 0.4$	$g_{xx} = g_{yy} = 2.28 \pm 0.01$ $g_{zz} = 1.901 \pm 0.001$	88
NaF	F <sub>2</sub> (19-19)	$A_{xx} = A_{yy} = 47.0$ $A_{zz} = 897.1$	$g_{xx} = g_{yy} = 2.0220$ $g_{zz} = 2.0014$	92
KF	F <sub>2</sub> (19-19)	$A_{xx} = A_{yy} = 30.0$ $A_{zz} = 908.0$	$g_{xx} = g_{yy} = 2.0214$ $g_{zz} = 2.0020$	92
RbF	F <sub>2</sub> <sup>-</sup> (19-19)	$A_{zz} = 908.4$	$g_{xx}^{=g_{yy}^{=}2.0160}$ $g_{zz}^{=2.0034}$	92
CaF <sub>2</sub>	F <sub>2</sub> <sup>-</sup> (19-19)	$A_{xx} = A_{yy} = 45 \pm 10$ $A_{zz} = 916 \pm 1$	$g_{xx} = g_{yy} = 2.019 \pm 0.002$ $g_{zz} = 2.002 \pm 0.002$	93

of these heterocle interactions type

# V. Free Ato

not be treat

In some ated material not criterate as a result.

Table IX give ferent atoms are some result irradiated series.

in irradiate
in Gardner
to be in eri
if low inte

tings agree

ally in the

It has

I. is thate orbital

Elsotropy .

94 . Howe.

Phase b

te included

of these heteronuclear V centers is complicated due to quadrupole interactions and second-order effects. Since none of this type of center was detected in this work, they will not be treated further.

#### V. Free Atom Hyperfine Splittings and g Values

In some cases free atoms have been detected in irradiated materials. Since these are small particles and are not oritented, they exhibit essentially isotropic splittings as a result of their random distribution in the matrix. Table IX gives a summary of the ESR data obtained for different atoms in various matrices. Also included in Table IX are some results for free atoms which have been detected in irradiated single crystals. The observed hyperfine splittings agree quite well with theoretical predictions especially in the case of hydrogen atoms where  $A_{iso} = 508$  gauss.

It has not been possible (94) to detect halogen atoms in irradiated crystals or matrices by ESR. A recent article by Gardner (102) which reported Cl. has been shown (103) to be in error; the radical is  $\text{Cl}_2^-$  with the outermost lines of low intensity. The reason for the failure to observe Cl. is that the interaction between the matrix field and the orbital angular momentum produces a large enough magnetic anisotropy to broaden the resonance lines beyond recognition (94). However, these fragments have been observed in the gas phase by Vanderkooi and McKenzie (104) and the results are included in Table IX.

Table IX. Free atom hyperfine splittings and g values.

Irradiated Host	Radical	Hyperfine Splitting A <sub>iso</sub> (gauss)	g	Refer- ence
CH <sub>4</sub> (solid)	н.	504.0 + 0.01	2.0021	94
NH <sub>3</sub> (solid)	н.	508.9		95
$H_2$ (solid)	н.	506.1 ± 0.01	2.0023	<b>&lt;94,96</b>
CaF <sub>2</sub> (crystal)	н.	522.9	2.0023	97
HClO <sub>4</sub> (solid)	н.	502.5	2.0022	98
H <sub>2</sub> SO <sub>4</sub> (solid)	н.	505.6	2.0024	98
H <sub>3</sub> PO <sub>4</sub> (solid)	н.	508.3	2.0024	98
N <sub>2</sub> H <sub>4</sub> ·HCl (crystal)	н.	510.0		99
D <sub>2</sub> (solid)	D.	77.7 ± 0.01	2.0023	94
CD <sub>4</sub> (liquid)	D.	77.5	2.0022	48
CaF <sub>2</sub> (solid)	D.	$80.3 \pm 0.01$	2.0025	97
$N_2$ (solid)	и.	4.3	2.0020	100
H <sub>2</sub> (solid)	и.	4.1	2.0020	100
NH <sub>3</sub> (solid)	и.	4.0	2.0020	95
O <sub>2</sub> (gas)	0.	Single line	1.5009	101
$F_2$ (gas)	F.		1.3333	104
Br <sub>2</sub> (gas)	Br•		1.3333	104
Cl <sub>2</sub> (gas)	c1·		1.3333	104

#### THEORETICAL

#### I. Basic Theory of Electron Spin Resonance

#### A. Classical Treatment

In electron spin resonance (ESR) spectroscopy, as in other types of spectroscopy, the spectra obtained are related to the allowed transitions between energy states. These transitions follow certain selection rules to be mentioned later. ESR is concerned with interactions between free or unpaired electrons and magnetic fields which may be internal or external in nature. The type of interaction is expressed in Equation (1)

$$E = -\overline{\mu_J} \cdot \overline{H}^{>} \tag{1}$$

where  $\overline{\mu}_J^>$  is the magnetic moment of the jth electron,  $\overline{H}^>$  is the magnetic field, and E is the resultant interaction energy.

The basic ESR experiment is concerned with interactions of electron magnetic moments with magnetic fields arising from two sources. In one case a large external magnetic field is applied resulting in a coupling known as the Zeeman coupling. The other coupling results from the fact that the nuclei are spinning charged masses and as such generate their

where  $\overline{H}_{\mathbf{I}}^{>}$  i with magneti is being mea and abla is th of interacti

> where E<sub>D</sub> is The tota

dipole intera

contribution

and can be de

Rere now He <sup>% defined</sup> ab ed over a

> B. Elec <u>acti</u>

Some furn ission for t

et of an e

own magnetic field of the form given in Equation (2)

$$\overline{H}_{I}^{>} = -\nabla \times [\overline{\mu}_{I}^{>} \times (\frac{1}{r})]$$
 (2)

where  $\overline{H}_{\mathbf{I}}^{\flat}$  is the magnetic field created by the I<sup>th</sup> nucleus with magnetic moment  $\overline{\mu}_{\mathbf{I}}^{\flat}$ , r is the distance at which  $\overline{H}_{\mathbf{I}}^{\flat}$  is being measured relative to the position of the nucleus and  $\nabla$  is the familiar gradient operator. The second type of interaction called the hyperfine interaction, or dipoledipole interaction, has the form given in Equation (3)

$$E_{D} = -\overline{\mu}_{J} \cdot \overline{H}_{I}^{>} \tag{3}$$

where  $E_n$  is the dipolar energy.

The total interaction energy is the sum of the energy contribution of the Zeeman type and the dipolar interaction and can be denoted by Equation (4)

$$\mathbf{E}_{\mathbf{T}} = -\overline{\mu}_{\mathbf{J}}^{\rightarrow} \cdot (\overline{\mathbf{H}}_{\mathbf{ext}}^{\rightarrow} + \Sigma \overline{\mathbf{H}}_{\mathbf{I}}^{\rightarrow})$$
 (4)

where now  $\overline{H}^{>}_{ext}$  is the external magnetic field and  $\overline{H}^{>}_{I}$  is as defined above. Notice that this field,  $\underline{\underline{t}}.\underline{e}$ .  $\overline{H}^{>}_{I}$ , is summed over all nuclei I.

# B. <u>Electron Dipole-Nuclear Dipole (Hyperfine) Inter-</u> actions

Some further rearrangements need to be made in the expression for the hyperfine interaction. The spin magnetic moment of an electron is defined by Equation (5)

$$\overline{\mu}_{\mathbf{J}}^{>} = -g \beta \overline{\mathbf{S}}_{\mathbf{J}}^{>} \tag{5}$$

texts (105),
associated wi
angular moment
accent arising
disregarded.
in a similar r
accear g fact
is the spin v

At this sion for the forms given i

 $\overrightarrow{\mathbb{H}_{N}}$ 

in it is ned

Ration (8)

: 0, ho

where g is the spectroscopic g factor defined in several texts (105),  $\beta$  is the Bohr magneton and  $\overline{S}_J^{>}$  is the vector associated with the direction and magnitude of the spin angular momentum. For the present the contribution to the moment arising from orbital angular momentum  $\overline{L}^{>}$  will be disregarded. The nuclear magnetic moment  $\overline{\mu}_I^{>}$  can be defined in a similar manner (Equation 6) where  $g_N$  and  $\beta_N$  are now the nuclear g factor and nuclear magneton, respectively, and  $\overline{I}^{>}$  is the spin vector associated with the nucleus of interest:

$$\overline{\mu}_{\mathbf{I}}^{>} = g_{\mathbf{N}} \beta_{\mathbf{N}} \overline{\mathbf{I}}_{\mathbf{I}}^{>} \tag{6}$$

At this point it is convenient to rearrange the expression for the magnetic field created by the nuclei to the forms given in Equations (7) and (8)

$$\overrightarrow{H}_{N} = -\sum_{\mathbf{I}} \{\overrightarrow{\mu}_{\mathbf{I}} \left[ \nabla \cdot (\nabla \frac{1}{r}) - (\nabla \frac{1}{r}) \nabla \cdot \overrightarrow{\mu}_{\mathbf{I}} \right] + \left[ (\nabla \frac{1}{r}) \nabla^{2} \frac{1}{r} - (\overrightarrow{\mu}_{\mathbf{I}} \cdot \nabla) (\nabla \frac{1}{r}) \right] \qquad (7)$$

$$= -\sum_{\mathbf{I}} \left[ \overrightarrow{\mu}_{\mathbf{I}} \nabla^{2} \frac{1}{r} - (\overrightarrow{\mu}_{\mathbf{I}} \cdot \nabla) (\nabla \frac{1}{r}) \right] \qquad (8)$$

Now it is necessary to examine Equation (8) to consider what happens as  $r \longrightarrow 0$  and  $r \ne 0$ . It is found that for  $r \ne 0$  Equation (8) adequately describes the interaction. For  $r \longrightarrow 0$ , however, the following expressions are obtained

 $\overline{H}_{N}^{>} = 1$ 

= .

where & (T The to

of two part

E<sub>D</sub> = .

If the in Equation

then one ob

 $E_{D} = \frac{8}{3}$ 

imations (

â<sup>7</sup>5<sup>8</sup>85

$$\overline{H}_{N}^{>} = \lim_{r \to 0} \sum_{I} \left( \overline{\mu}_{1}^{>} \cdot \nabla \right) \left( \nabla \frac{1}{r} \right) - \overline{\mu}_{I}^{>} \nabla^{2} \frac{1}{r}$$

$$\tag{9}$$

$$= - \sum_{\mathbf{T}} \left[ \frac{4\pi}{3} \overline{\mu}_{\mathbf{I}}^{\flat} \delta (\overline{\mathbf{r}}^{\flat}) - 4\pi \overline{\mu}_{\mathbf{I}}^{\flat} \delta (\overline{\mathbf{r}}^{\flat}) \right]$$
 (10)

$$= \frac{8\pi}{3} \sum_{\mathbf{I}} \overline{\mu}_{\mathbf{I}} \delta (\overline{\mathbf{r}})$$
 (11)

where  $\delta$  ( $\overline{r}$ ) is the Dirac delta function.

The total hyperfine energy,  $\mathbf{E}_{\mathbf{D}}$ , is therefore composed of two parts and can be written

$$\mathbf{E}_{\mathbf{D}} = -\frac{8\pi}{3} \sum_{\mathbf{I}} \overline{\mu}_{\mathbf{I}}^{\flat} \cdot \overline{\mu}_{\mathbf{J}}^{\flat} \delta (\overline{\mathbf{r}}^{\flat}) + \sum_{\mathbf{I}} \frac{\overline{\mu}_{\mathbf{I}}^{\flat} \cdot \overline{\mu}_{\mathbf{J}}^{\flat} \mathbf{r}^{2} - 3(\overline{\mu}_{\mathbf{J}}^{\flat} \cdot \overline{\mathbf{r}}^{\flat})(\overline{\mu}_{\mathbf{I}}^{\flat} \cdot \overline{\mathbf{r}}^{\flat})}{\mathbf{r}^{5}}$$
(12)

If the expressions for the spin magnetic moments given in Equations (5) and (6) are substituted in Equation (12) then one obtains the relation

$$\mathbf{E}_{\mathbf{D}} = \frac{\mathbf{g}\pi}{\mathbf{3}} \mathbf{g}_{\mathbf{N}} \mathbf{g}_{\mathbf{N}}$$

A more convenient rearrangement can be made resulting in Equations (14) and (15):

$$\mathbf{E_{D}} = \frac{8\pi}{3} \mathbf{g_{N}} \beta_{N} \mathbf{g} \beta \delta(\mathbf{r}^{-}) \sum_{\mathbf{I}} \mathbf{I_{I}^{+}} \cdot \mathbf{S_{J}^{+}}$$

$$-\mathbf{g_{N}} \beta_{N} \mathbf{g} \beta \sum_{\mathbf{I}} (\mathbf{S_{XJ}}, \mathbf{S_{YJ}}, \mathbf{S_{ZJ}}) \begin{bmatrix} (\mathbf{r^{2}} - 3\mathbf{x^{2}})/\mathbf{r^{5}} & -3\mathbf{xy}/\mathbf{r^{5}} & -3\mathbf{xz}/\mathbf{r^{5}} \\ -3\mathbf{xy}/\mathbf{r^{5}} & (\mathbf{r^{2}} - 3\mathbf{y^{2}})/\mathbf{r^{5}} & -3\mathbf{yz}/\mathbf{r^{5}} \end{bmatrix} \mathbf{I_{XI}} \mathbf{I_{YI}} =$$

$$-3\mathbf{xz}/\mathbf{r^{5}} \quad -3\mathbf{yz}/\mathbf{r^{5}} (\mathbf{r^{2}} - 3\mathbf{z^{2}})/\mathbf{r^{5}} \mathbf{I_{ZI}}$$

 $=\frac{8}{3}$ 

where  $\overset{=}{A}$  is ther thing to  $3 \times 3$  matrix then be writ

where the fi

element of

The significant the independent

:= 0 , and

the dipolar

adirection

lation. It

the matr

ine is to t

Tobtain th

er the is

e tete

inesis.

$$= \frac{8\pi}{3} g_{\mathbf{N}} \beta_{\mathbf{N}} g_{\beta} \delta(\overline{\mathbf{r}}) \sum_{\mathbf{I}} \overline{\mathbf{I}}_{\mathbf{I}} \cdot \overline{\mathbf{S}}_{\mathbf{J}} - g_{\mathbf{N}} \beta_{\mathbf{N}} g_{\beta} \sum_{\mathbf{I}} \overline{\mathbf{S}}_{\mathbf{J}} \cdot \overline{\mathbf{A}} \cdot \overline{\mathbf{I}}_{\mathbf{I}}$$
(15)

where  $\bar{A}$  is the matrix defined by Equation (14). One further thing to note at this point is that the trace of the  $3\times 3$  matrix is zero. The total dipolar interaction can then be written in the following simplified form

$$E_{D} = \sum_{\mathbf{I}} S_{\mathbf{J}} \cdot \overline{A}_{\mathbf{I}} \cdot \overline{\mathbf{I}}_{\mathbf{I}}$$
 (16)

where the first term and the constants g, g,  $\beta$  and  $\beta$  have been included in  $\bar{A}$  as constants multiplying each element of the matrix.

The significance of the separation in Equations 9-12 is that the term containing the Dirac delta function is independent of direction, <u>i.e.</u> it vanishes except where r=0, and is referred to as the isotropic contribution to the dipolar coupling, whereas the second term is dependent on direction and is referred to as the anisotropic contribution. It is possible to separate the two contributions if the matrix  $\bar{A}$ ' can be determined. All that needs to be done is to take 1/3 the trace of  $\bar{A}$ ', as in Equation (17), to obtain the isotropic contribution

$$A_{iso} = \frac{T_R \bar{\bar{A}}'}{3} \tag{17}$$

The anisotropic terms are naturally the terms remaining after the isotropic contribution has been abstracted.  $\bar{\bar{A}}$  will be referred to as the hyperfine splitting matrix in this thesis.

where Y i te system The bracket ated to obt

Equation (1

lay be obta <sup>led</sup> as

In the

ie perturba

In the The stand if

#### C. First-Order Quantum Mechanical Perturbation Theory

Effects arising from electrons interacting with magnetic fields are considered perturbations of the total energy of the system and these effects can be treated by perturbation theory. For most cases to be dealt with in this thesis first-order perturbation theory is adequate to describe the interactions. The total energy of the system from the standpoint of first-order theory can be expressed by Equation (18)

$$E_{\text{total}} = E_{\text{unperturbed}} + \langle \Psi | \mathbf{W}' | \Psi \rangle$$
 (18)

where  $\Psi$  is the unperturbed ground-state wave function for the system and  $\bigstar'$  is the perturbing Hamiltonian operator. The brackets denote that a matrix element needs to be evaluated to obtain the perturbation energy.

In the case of ESR,  $\bowtie$  is the Hamiltonian operator which may be obtained from Equation (4). It can now be re-expressed as

$$\mathcal{H}' = g\beta \overline{S}_{J}^{\flat} \cdot \overline{H}_{ext}^{\flat} + \Sigma \overline{S}_{J}^{\flat} \cdot \overline{A}^{\flat} \cdot \overline{I}_{I}^{\flat}$$
(19)

The perturbation energy is therefore given by

$$E_{\text{pert}} = g\beta \langle \Psi | \overline{S}_{J}^{>} \cdot \overline{H}_{\text{ext}}^{>} | \Psi \rangle + \Sigma \langle \Psi | \overline{S}_{J}^{>} \cdot \overline{A}^{'} \cdot \overline{I}_{I}^{>} | \Psi \rangle (20)$$

In the case of first-order theory it is usually assumed that  $\overline{S}_J^{>}$  and  $\overline{I}_I^{>}$  are quantized along the direction of  $\overline{H}_{ext}^{>}$  and if we define this temporarily as the z direction,

tions betwe \_\_\_\_\_ = 0. T interacting

correspondi.

The selecti

Rigure 1.

Por the te electro iso, more to :12 sind

If the Station er

tid be pos in a

such that  $\overline{H}_{ext}^{>} = H_0 z$ , then we obtain

$$E_{pert} = g\beta H_0 m_s + \sum_{I} A_{zz} m_s m_I$$
 (21)

The selection rules for first-order theory allow for transitions between energy levels to occur only for  $\Delta m_g = \pm 1$ ,  $\Delta m_I = 0$ . Therefore for the simple case of one electron interacting with one proton (I = 1/2) the energy level scheme corresponding to the allowed transitions is given in Figure 1.

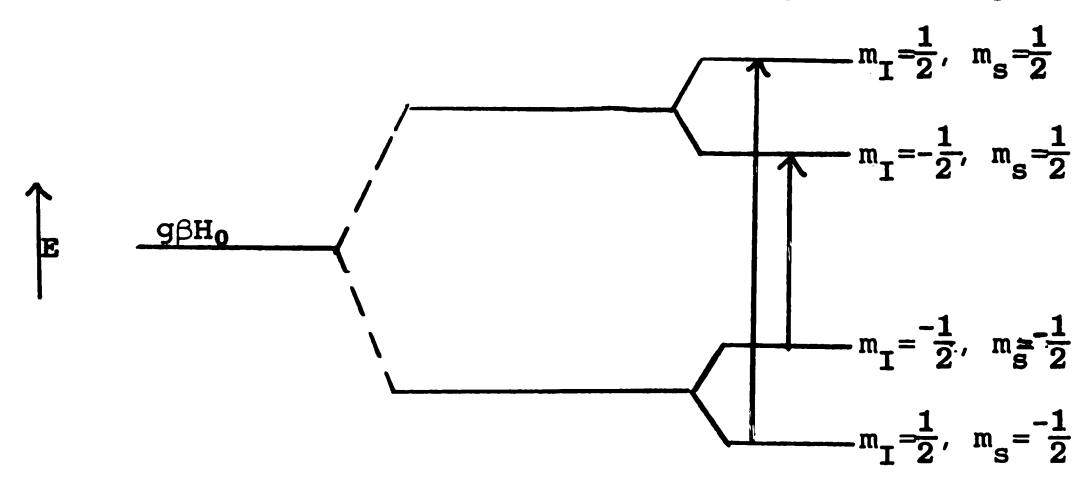


Figure 1. ESR energy level diagram for a single electron and single nucleus.

For the case of more than one nucleus coupling with the electron the scheme would naturally be more complicated. Also more transitions would be allowed for nuclei having  $I > 1/2 \text{ since } m_T \quad \text{can assume all values} \quad I \geq m_T \geq -I.$ 

If the hyperfine interaction contribution to the perturbation energy is examined it can be easily seen that it would be possible to determine completely the components of  $\bar{\bar{A}}$ , in a principal-axis system using only first-order

theory. In

 $\mathbf{E} = \sum_{i=1}^{n} \langle i \rangle$ 

= Σ < \;

Now if the

considered

ternal fiel

then it wou

simply by a direction c

components

D. <u>S</u>

In som

and the orb

The classic

H -

nere Z I

ie vector

intera

theory. In a principal-axis system the hyperfine interaction is of the type

$$\mathbf{E} = \sum_{\mathbf{I}} \langle \Psi | \overline{\mathbf{S}}_{\mathbf{J}}^{\mathbf{Y}} \cdot \overline{\mathbf{A}}^{\mathbf{I}} \cdot \overline{\mathbf{I}}_{\mathbf{I}}^{\mathbf{Y}} | \Psi \rangle$$

$$= \sum_{\mathbf{I}} \langle \Psi | (\mathbf{S}_{\mathbf{X}\mathbf{J}}^{\mathbf{A}} \mathbf{A}_{\mathbf{X}\mathbf{X}}^{\mathbf{I}} \mathbf{I}_{\mathbf{X}\mathbf{I}} + \mathbf{S}_{\mathbf{Y}\mathbf{J}}^{\mathbf{A}} \mathbf{A}_{\mathbf{Y}\mathbf{Y}}^{\mathbf{I}} \mathbf{I}_{\mathbf{Y}\mathbf{I}} + \mathbf{S}_{\mathbf{Z}\mathbf{J}}^{\mathbf{A}} \mathbf{Z}_{\mathbf{Z}}^{\mathbf{I}} \mathbf{I}_{\mathbf{Z}\mathbf{I}}) | \Psi \rangle \qquad (22)$$

Now if the spins of both the nuclei and the electron are considered to be quantized along the direction of the external field in some arbitrary direction,  $\overline{H}_{\text{ext}}^{>} = H_0 \overline{h}^{>}$ , then it would be possible to determine  $A_{xx}$ ,  $A_{yy}$ , and  $A_{zz}$  simply by appropriate alignment of the crystal along the direction of quantization  $\overline{h}^{>}$  to give each of the three components  $A_{xx}$ ,  $A_{yy}$ , and  $A_{zz}$ .

### D. Spin-Orbit Coupling

In some cases coupling of the spin angular momentum  $\overline{S}^{>}$  and the orbital angular momentum  $\overline{L}^{>}$  becomes important. The classical Hamiltonian which describes this type of interaction is of the form

$$\mathcal{H} = -\frac{|\underline{e}|}{c}|_{\overline{\mu}_{\mathbf{J}}}^{>} \cdot \sum_{\mathbf{I}} \left[ \frac{\mathbf{z}_{\mathbf{I}} \overline{\mathbf{r}}_{\mathbf{I}\mathbf{J}}^{>} \times (1/2 \overline{\mathbf{v}}_{\mathbf{J}}^{>} - \overline{\mathbf{v}}_{\mathbf{I}}^{>})}{\mathbf{r}_{\mathbf{I}\mathbf{J}}^{3}} \right]$$
(23)

where  $\mathbf{Z}_{\mathbf{I}}$  is the charge on nucleus I,  $\overline{\mathbf{r}}_{\mathbf{IJ}}^{>}$  is the distance between electron J and nucleus I, and  $\overline{\mathbf{V}}_{\mathbf{J}}^{>}$  and  $\overline{\mathbf{V}}_{\mathbf{I}}^{>}$  are the vector velocities of electron and nucleus, respectively. This interaction reduces to the form

 $\mathbf{k} = -\frac{1}{m}$ 

where the that  $\overline{V}_{\mathbf{I}}^{>}\cong$ 

where

......

Purther recordit coup

The ne excited state turbation to

eigenfuncti

the g fac

itee-spin v

tis subjec

 $^{106}$ , and  $_{
m w}$ 

The re

$$\mathcal{H} = -\frac{|\underline{e}|}{mc} \xrightarrow{\mu_J} \cdot \Sigma \left[ \frac{\mathbf{z_I} \overrightarrow{\mathbf{r_{IJ}}} \quad (1 \ 2 \ \overline{\mathbf{p_J}})}{\mathbf{r_{IJ}^3}} \right]$$
(24)

where the Born-Oppenheimer approximation has been used so that  $\overline{V}_I^> \cong 0$  relative to  $\overline{V}_J^>$ . A further reduction gives

$$\mathcal{H} = \frac{|\mathbf{e}|}{2mc} \stackrel{\longrightarrow}{\mu_{\mathbf{J}}} \stackrel{\Sigma}{\mathbf{I}} \mathbf{v_{\mathbf{I}}} \stackrel{\Sigma}{\mathbf{L}_{\mathbf{IJ}}}$$
 (25)

where

$$v_{I} = -\frac{z_{I}}{r_{I,I}^{3}}$$
 (26)

Further reduction gives the familiar form for the spinorbit coupling

$$\mathcal{H} = -\frac{g\beta |\mathbf{e}|}{2mc} \sum_{\mathbf{I}} V_{\mathbf{I}} \overline{\mathbf{L}}_{\mathbf{IJ}}^{\flat} \cdot \overline{\mathbf{S}}_{\mathbf{J}}^{\flat}$$

$$= \lambda \sum_{\mathbf{I}} \overline{\mathbf{L}}_{\mathbf{IJ}}^{\flat} \cdot \overline{\mathbf{S}}_{\mathbf{J}}^{\flat}$$
(27)

The net effect of spin-orbit coupling is to mix in excited states with the ground state by first-order perturbation theory. These modified states are no longer eigenfunctions of the true spin obtained previously and the g factor becomes significantly different from the free-spin value, g = 2.0023. An excellent treatment of this subject is given in Carrington and Mc Lachlan's book (106) and will not be repeated here.

The reason that spin-orbit coupling is of minor importance in organic free radicals is that the free electron

is usually If we cons

p<sub>z</sub> orbita

\*2pz

and the sp

E<sub>s.o.</sub>= λ

= 0

In cas

tet effect

the g fac to \$1', i.e

the total ;

E. <u>s</u>

When

Tied prev

is usually primarily localized in a  $p_z$  orbital on carbon. If we consider hydrogen-like wave functions the form of the  $p_z$  orbital is

$$\Psi_{2p_{z}} = \frac{1}{4(2\pi)^{1/2}} \left(\frac{z}{a_{0}}\right)^{3/2} \rho e^{-\rho/2} \cos \theta$$
 (28)

and the spin-orbit interaction energy is

$$E_{s.o.} = \lambda \langle \Psi_{2p_{Z}} | \Sigma [L_{IJ_{Z}} S_{J_{Z}} + \frac{1}{2} (L_{IJ}^{\dagger} S_{J}^{-} + L_{IJ}^{-} S_{J}^{\dagger})] | \Psi_{2p_{Z}} \rangle$$

$$= \lambda \langle \Psi_{2p_{Z}} | \Sigma (ih \frac{\partial}{\partial \phi})_{IJ} S_{J_{Z}} | \Psi_{2p_{Z}} \rangle$$

$$= 0 \quad (since \ \Psi_{2p_{Z}} \text{ does not depend on } \phi)$$

$$(29)$$

In cases where spin-orbit coupling is important the net effect is to change the form of the Hamiltonian so that the g factor becomes a matrix,  $\bar{g}$ , with properties similar to  $\bar{A}$ , i.e. with isotropic and anisotropic components, and the total Hamiltonian becomes

$$\mathcal{H} = \beta \ \overline{S}_{J}^{\flat} \cdot \overline{g}^{!} \cdot \overline{H}_{ext}^{\flat} + \sum_{T} \overline{S}_{J}^{\flat} \cdot \overline{A}^{!} \cdot \overline{I}_{I}^{\flat}$$
 (30)

### E. Second-Order Perturbation Theory

When the expressions for allowed transitions were derived previously it was assumed that the spin vectors,  $\overline{S}$  and  $\overline{I}$ , were quantized completely along some arbitrary

these vector hyperfine so the case as the directed then the continuous theory can:

Thus far to tems in what the tems in what the tems in what the tems in the temp.

The t

axial symm

derived the

**H** =

the nuclearly strains and the nuclearly strains and the nuclearly strains and the nuclear strains and

Mar inte

the abo

Tax in

Cirst-0

direction  $\overline{h}^{>}$  of the external field and that components of these vectors not along  $\overline{h}^{>}$  were neglected when calculating hyperfine splitting values. However, in reality this is not the case and if, for example, the field is considered to be directed along the z direction such that  $\overline{H}_{ext}^{>} = H_0 z$ , then the components  $S_x$ ,  $S_y$ ,  $I_x$  and  $I_y$  in second-order theory cannot be neglected.

The treatment of second-order effects is complicated in the case of radicals trapped in irradiated crystals. Thus far the theory has been successfully applied to systems in which there is axial symmetry, i.e. for cases in which  $A_{xx} = A_{yy} = A_{||}$  and  $A_{zz} = A_{\perp}$ . Bleaney (107) has derived the following Hamiltonian for a system possessing axial symmetry

$$\mathcal{H} = \beta[g] | H_z S_z + g_{\perp} (H_x S_x + H_y S_y)] + A_{\parallel} (S_z I_z)$$

$$+ A_{\parallel} (S_x I_x + S_y I_y) - \gamma \beta_N \overline{H}^{>} \cdot \overline{I}^{>} \qquad (31)$$

where the term involving  $\overline{H}^{>} \cdot \overline{I}^{>}$  includes the interaction of the nuclear spin  $\overline{I}^{>}$  with the external field. The Hamiltonian in the original paper also includes terms involving electron spin-electron spin interactions and quadrupolar interactions which will be neglected here. By use of the above Hamiltonian it can be seen that the result is to mix in states with different spins that were not allowed in first-order theory since by definition

where S<sub>+</sub> sperators  $\mathbf{I}_{\mathbf{y}}.$ 

Ultim

symmetric

hv = g3H +

Where K2g

ingle betw

responding iglae, a

Filse of

te quantu

is the nuc

Other <sup>∷de</sup>r effe

theo

$$S_{x} = \frac{S_{+} + S_{-}}{2}$$
 (32)

$$S_{y} = \frac{S_{+} - S_{-}}{2} \tag{33}$$

where  $S_+$  and  $S_-$  are the familiar raising and lowering operators and similar expressions are obtained for  $I_x$  and  $I_y$ .

Ultimately the expression for the energy in an axially symmetric system is given in Bleaney's paper (107) by

$$hv = g\beta H + Km + \frac{A^{2}}{4g\beta H_{0}} \left[ \frac{A^{2}_{||} + K^{2}}{K^{2}} \right] [I(I + 1) - m^{2}]$$

$$+ \frac{A^{2}_{||}}{2g\beta H_{0}} \left[ \frac{A_{||}}{K} \right] (2M-1)m + \frac{1}{2g\beta H_{0}} \left[ \frac{A^{2}_{||} - A^{2}_{||}}{K^{2}} \right] \times \left[ \frac{g || g ||}{g^{2}} \right]^{2}$$

$$\times \sin^{2} \theta \cos^{2} \theta m^{2} \qquad (34)$$

where  $K^2g^2 = A_1^2 |g^2| \cos^2 \theta + A_2^2 |g^2| \sin^2 \theta$  and  $\theta$  is the angle between the field direction and the direction z corresponding to the maximum hyperfine splitting and maximum g value,  $g_{\parallel}$ . The other parameters involved are the measured value of g for some value  $\theta$ , the field value  $H_0$  and the quantum numbers M, m; M = 1/2 for an electron, and m is the nuclear spin quantum number.

Other attempts have been made to incorporate secondorder effects to account for the discrepancy from firstorder theory. In an early paper by Breit and Rabi (108)

tings in t number, i defined by

where <u>LW</u>

Fessenden

Breit-Rabi

a power se

Precise va

ated radica

Eder expre

Tadio

ine specta

ions are c

Fin Hamilt

ti higher-

ed. T

the exact energy of an atom in a magnetic field is obtained as

$$W = \frac{-\Delta W}{2(2i+1)} \pm \frac{\Delta W}{2} (1 + \frac{2m}{i+1/2} \times + \times^2)^{1/2}$$
 (35)

where  $\Delta W$  is the separation between the two hyperfine splittings in the absence of a field, m is the magnetic quantum number, i is the nuclear spin and the other terms are defined by the expressions

$$x = \frac{g\omega}{\Delta W} \tag{36}$$

$$\omega = \frac{ehH}{4\pi mc} = \beta H \tag{37}$$

$$H = \mu_0 H \tag{38}$$

Fessenden (109) has treated second-order effects using the Breit-Rabi equation and expanding the square-root term in a power series. This treatment was used to obtain more precise values of the splitting constants for some fluorinated radicals. Maruani (110) has also derived a second-order expression for use in analyzing the splittings of the 'CF3 radical. The results are applicable to polycrystalline spectra. The assumption is made that the spin functions are constructed in the g' principal-axis system, the spin Hamiltonian matrix is constructed, evaluated, and thirdand higher-order terms in the secular equation are then ignored. The end result is the expression

where A

and Q a

Here the

3- axis sys

 $\tilde{z}^{'}$  matrix

the princip

I. Evalua

 $\lambda$ .  $\underline{\mathbf{E}_{\times}}$ 

Two met

inchents c

$$\Delta \epsilon = \nu = AQ \pm \frac{1\alpha}{2Q} + \frac{1\delta^2}{4AQ}$$
 (39)

where  $A = (g_0 \beta/h) H$ , H is the magnetic field and  $\alpha$ ,  $\delta$  and Q are defined by the equations

$$Q = \begin{bmatrix} \begin{pmatrix} g_{xx} & \mu_x \\ g_{yy} & \mu_y \\ g_{zz} & \mu_z \end{pmatrix}^2 \end{bmatrix}$$
(40)

$$\alpha = \begin{bmatrix} \begin{pmatrix} a_{xx} \\ a_{xy} \\ a_{xz} \end{pmatrix} g_{xx} \mu_x + \begin{pmatrix} a_{yx} \\ a_{yy} \\ a_{yz} \end{pmatrix} g_{yy} \mu_y + \begin{pmatrix} a_{zx} \\ a_{zy} \\ a_{zz} \end{pmatrix} g_{zz} \mu_z$$
(41)

$$\delta^{2} = \frac{1}{2} \begin{bmatrix} \begin{pmatrix} a_{xx} \\ a_{xy} \\ a_{xz} \end{pmatrix}^{2} + \begin{pmatrix} a_{yx} \\ a_{yy} \\ a_{yz} \end{pmatrix}^{2} + \begin{pmatrix} a_{zx} \\ a_{zy} \\ a_{zz} \end{pmatrix}^{2} - \frac{\alpha^{2}}{Q^{2}} \end{bmatrix}$$
(42)

Here the  $a_{ij}$  are the components of the  $\overline{A}$ ' matrix in the g-axis system, the  $g_{ii}$  are the principal values of the  $\overline{g}$ ' matrix and the  $\mu_i$  are the direction cosines of H in the principal-axis system of  $\overline{g}$ '. The equations are valid for one nucleus of spin 1/2 only.

#### II. Evaluation and Interpretation of Spectral Parameters

# A. Experimental Determination of Hyperfine Splitting and g Values

Two methods were used to determine experimentally the components of the hyperfine splitting matrix,  $\bar{\bar{A}}$ , and of

the matri
way to ob
external
However,
of refere
The matri
matrices
transform

 $ar{ar{A}}^{\dagger}$ . In a

Cons

relative

If a

order the

Typerfine

and the so

Te above

the mat

the matrix  $\overline{g}$ . As was mentioned previously the easiest way to obtain these values is by direct alignment of the external magnetic field along the principal directions. However, it is usually not possible to do this and a choice of reference axes in the crystal of interest must be made. The matrices obtained are therefore not diagonal as are the matrices containing the principal values but it is easy to transform them to a principal axis system.

Consider, for example, the hyperfine splitting matrix,  $\bar{\bar{A}}$ . In a non-principal-axis system the matrix will have the form

$$\bar{\bar{A}}^{i} = \begin{pmatrix} A_{xx}^{i} & A_{xy}^{i} & A_{xz}^{i} \\ A_{yx}^{i} & A_{yy}^{i} & A_{yz}^{i} \\ A_{zx}^{i} & A_{zy}^{i} & A_{zz}^{i} \end{pmatrix}$$
(43)

If a measurement is made of the hyperfine splitting relative to the axis of quantization h (assuming first-order theory) with  $\Delta m_s = \pm 1$  and  $\Delta m_I = 0$  then the hyperfine splitting is given by

$$A = (\overline{h}^{>} \cdot \overline{\overline{A}}^{"})$$
 (44)

and the square of the hyperfine splitting is

$$(\mathbf{A})^{2} = (\overline{\mathbf{h}}^{>} \cdot \overline{\overline{\mathbf{A}}}^{"}) \cdot (\overline{\overline{\mathbf{A}}}^{"} \cdot \overline{\mathbf{h}}^{>})$$

$$= \overline{\mathbf{h}}^{>} \cdot (\overline{\overline{\mathbf{A}}}^{"}) \cdot \overline{\mathbf{h}}^{>}$$

$$(45)$$

The above equation is in a convenient form for evaluation of the matrix. This may be seen if it is first assumed

that the v

 $\{h_{x}, h_{y}, h$ and heta is

the field

plane is d

(A)2 = (O,

= sin

Rotations

give simil

The e

or  $\bar{\bar{g}}$ ' in

an arbitra

the square

of the g

letween th

3 choosin

ill the ele

lan be seen

tat the ma

is poss:

Stary tra

Ty diagor

Equation :

that the vector  $\overline{h}^{>}$  has associated with it direction cosines  $(h_x, h_y, h_z)$ . Suppose a rotation is made in the yz plane and  $\theta$  is defined as the angle between the z axis and the field direction. The square of the splittings in this plane is defined by

$$(A)^{2} = (0, \sin \theta, \cos \theta) \begin{bmatrix} (A^{2})_{xx} & (A^{2})_{xy} & (A^{2})_{xz} \\ (A^{2})_{yx} & (A^{2})_{yy} & (A^{2})_{yz} \\ (A^{2})_{zx} & (A^{2})_{zy} & (A^{2})_{zz} \end{bmatrix} \begin{bmatrix} 0 \\ \sin \theta \\ \cos \theta \end{bmatrix}$$

= 
$$\sin^2\theta \left(A^{2}\right)_{yy}$$
 +  $2\sin\theta \cos\theta \left(A^{2}\right)_{yz}$  +  $\cos^2\theta \left(A^{2}\right)_{zz}$  (46)

Rotations in the other two planes, <u>i.e.</u> xz and xy, will give similar expressions.

The experimental procedure for determining either  $\bar{\mathbb{A}}^1$  or  $\bar{\mathbb{G}}^1$  in a non-principal axis system is simply to choose an arbitrary mutually orthogonal set of axes and measure the square of the hyperfine splitting,  $(A)^2$ , or the square of the g factor,  $(g)^2$ , as a function of  $\theta$ , the angle between the field direction,  $\overline{\mathbb{H}}^{>}_{\text{ext}}$ , and the axes chosen. By choosing three mutually orthogonal planes of rotation all the elements of the matrices may be evaluated. Now it can be seen that the above matrices are real, symmetric and that the matrices are therefore Hermitian (Equation 14). It is possible to diagonalize a Hermitian matrix by a unitary transformation with the resulting matrix containing only diagonal elements which are the eigenvalues. Therefore, in Equation 47 the transformation matrix  $\bar{\mathbb{S}}$  is the matrix

of eigenve reference the diagor of the  $\bar{\bar{A}}$ 

(A<sub>XX</sub>)<sup>2</sup> (A

of each el tion is th there is a

To obtain

isotropic

ones.

The a  $ar{ar{g}}^{'}$  and  $ar{ar{A}}$ 

gauss in a

iecause of

Schonland .

tis method

icrm

Cere a, e

Q

of eigenvectors relating the arbitrarily chosen orthogonal reference axes to the principal axes and the elements of the diagonal matrix are the squares of the principal values of the  $\bar{A}$ ' matrix:

$$\begin{pmatrix}
(A_{XX}^{1})^{2} & & & \\
(A_{YY}^{1})^{2} & & & \\
& & (A_{YY}^{1})^{2} & \\
& & & (A_{ZZ}^{1})^{2}
\end{pmatrix} = \overline{\overline{S}}^{-1} & \begin{pmatrix}
(A_{Z}^{12})_{XX} & (A_{Z}^{12})_{XY} & (A_{Z}^{12})_{XZ} \\
(A_{Z}^{12})_{YX} & (A_{Z}^{12})_{YY} & (A_{Z}^{12})_{YZ} \\
(A_{ZZ}^{12})_{ZX} & (A_{Z}^{12})_{ZY} & (A_{Z}^{12})_{ZZ}
\end{pmatrix} \overline{\overline{S}}$$
(47)

To obtain the principal values one must take the square root of each element. One property of this type of transformation is that the trace of the matrix is preserved so that there is an absolute guarantee that the anisotropic and isotropic components of the diagonal matrix are the correct ones.

The above procedure for obtaining principal values for  $\bar{g}$ ' and  $\bar{A}$ ' was generally used in this thesis. If A > 100 gauss in a field  $H_{\rm ext} \cong 3000$  gauss then complications arose because of second-order effects and another method, that of Schonland (111), was used to obtain principal values. By this method Equation (46) can be rewritten in the revised form

$$(A)^2 = \alpha + \beta \cos 2\theta + \gamma \sin 2\theta$$
 (48)

where  $\alpha$ ,  $\beta$ , and  $\gamma$  are defined by the equations

$$\alpha = \frac{A_{+}^{2} + A_{-}^{2}}{2} \tag{49}$$

A, and A fine splitt the angle f splitting i

The each tained sin

the usual

В.

ontribut

ie rewri

$$\beta = \frac{(A_+^2 - A_-^2) \cos 2\theta_+}{2} \tag{50}$$

$$\gamma = \frac{(A_{+}^{2} - A_{-}^{2}) \sin 2\theta_{+}}{2}$$
 (51)

 $A_{+}$  and  $A_{-}$  are respectively the maximum and minimum hyperfine splittings measured in a particular plane and  $\theta_{+}$  is the angle from the axis to the position of maximum hyperfine splitting in a particular reference plane. The elements of Equation (46) are related to  $\alpha$ ,  $\beta$ , and  $\gamma$  by the equations

$$A_{VV} = \alpha - \beta \tag{52}$$

$$\mathbf{A}_{\mathbf{Z}\mathbf{Z}} = \alpha + \beta \tag{53}$$

$$A_{yz} = \gamma \tag{54}$$

The elements, A<sub>ij</sub>, are generated by these equations and the corresponding ones in the other two planes are obtained similarly and the matrix is then diagonalized by the usual procedure (see Appendix).

# B. <u>Interpretation of Hyperfine Splittings and Their</u> <u>Signs</u>

1) Isotropic Splittings.

The Hamiltonian which gives rise to the isotropic contribution to the hyperfine splitting is derivable from the classical expression given in Equation (12) which may be rewritten

$$\mathcal{H}_{iso} = \frac{8\pi}{3} g_{N} \beta_{N} g \beta \delta(\overline{r}) \Sigma \overline{I}_{i} \cdot \overline{S}_{J}$$
 (55)

The first-order perturbation energy is then simply given by

$$E_{iso} = \langle \Psi | \mathcal{H}_{iso} | \Psi \rangle = c | \Psi(0) |^{2} m_{s}^{m_{I}}$$
 (56)

where c includes all the constants in the equation above, and  $|\Psi(0)|^2$  is the spin density at the nucleus, <u>i.e.</u> at r = 0. The isotropic splitting  $A_{iso}$  is then simply given by

$$A_{iso} = c |\Psi(0)|^2$$
 (57)

For organic radicals the most important types of isotropic splitting arise from interactions with nuclei  $\alpha$  and  $\beta$  to the carbon atom on which the odd electron is primarily localized. Because  $^{12}\text{C}$  has I = 0 it gives rise to no splittings but nuclei bonded to the central carbon having I > 0 can give splittings. The mechanism by which nuclei in the  $\alpha$  position give rise to hyperfine splitting is known as spin polarization.

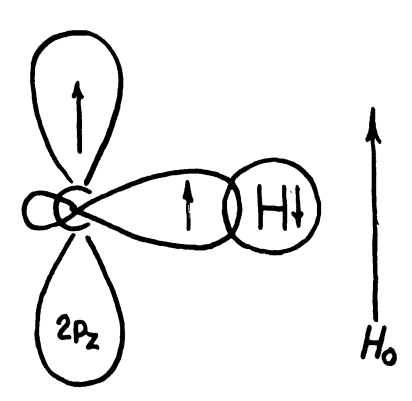


Figure 2. Spin polarization for  $\alpha$  hydrogens in  $\pi$ -electron radicals.

As can be seen (Figure 2) the electron in the  $\pi$  orbital and the one in the  $\sigma$  bond tend to align in the same direction resulting in the electron on the proton assuming the opposite direction. This effect can be explained by molecular orbital theory as resulting from a mixing of excited states with the ground state wave function resulting in a small amount of negative spin polarization at the hydrogen nucleus.

Now the largest spin density on an alpha hydrogen results if the electron is entirely localized in a 1s orbital on hydrogen. The hyperfine splitting has been measured for atomic hydrogen (112) and is  $A_{iso} \cong 506$  gauss, in good agreement with the value computed theoretically (106). From theoretical arguments it has been shown that a single  $\pi$  electron on a carbon induces a spin density of about -0.05 (113) in the hydrogen 1s orbital, corresponding to a splitting from  $\alpha$  protons of  $A_{iso} \cong -20$  to -25 gauss.

For isotropic splittings by the nucleus of the atom on which the odd electron is centered the isotropic splitting takes on more significance than previously. Remembering that  $A_{iso} \alpha |\Psi(0)|^2$ ,  $A_{iso}$  is a direct measure of the amount of s character in the odd electron molecular orbital. Two cases which are significant in this work are interactions with  $^{13}$ C, (I=1/2) and  $^{14}$ N, (I=1). However, a complication arises because now  $A_{iso} \alpha b |\Psi(0)|_{1s}^2 + c |\Psi(0)|_{2s}^2$ , where b and c are the respective weighting terms for the contributions from the 1s and 2s orbitals for  $^{13}$ C and  $^{14}$ N. For the present it will be assumed that the odd

electron contribution to the isotropic splitting on  $^{13}\text{C}$  or  $^{14}\text{N}$  arises primarily from the  $|\Psi(0)|^2_{2s}$  term. For a Hartree 2s atomic orbital it has been calculated that the isotropic splitting from  $\Psi_{2s}(^{13}\text{C})$  is  $A_{iso}_{2s}(^{13}\text{C}) = 1190$  gauss (60, 61), and for  $^{14}\text{N}$ ,  $A_{iso}_{2s}(^{14}\text{N}) = 550$  gauss (60,61). It is possible to calculate the fractional s character by simply dividing the observed isotropic splitting by the appropriate calculated Hartree splitting. This is justified recalling  $\frac{N}{total} = \sum_{i} c_{i} \phi_{i}$ , where the  $\phi_{i}$  are atomic orbitals, and if the coefficient of  $\phi_{1s}$  is assumed to be zero then  $\phi_{K}$  becomes  $\phi_{2s}$ , and the fractional s character for  $^{13}\text{C}$  will be given by

$$\% (2s)(^{13}C) = \frac{A_{iso}}{1190} \times 100$$
 (58)

An analogous expression holds for the fractional s character for <sup>14</sup>N.

In marked contrast to isotropic splittings from  $\alpha$  hydrogens which are nearly constant, isotropic splittings from  $^{13}\text{C}$  and  $^{14}\text{N}$  nuclei on which the odd electron is primarily localized have a wide range of different values as seen in Table X.

For the case of nuclei further removed than the  $\alpha$  position it has been shown by McConnell (2) that the total splittings are largely isotropic. Thus, the  $\beta$ -proton splittings are largely isotropic and are usually well described by an expression of the form (2)

$$A_{iso} = B_0 + B_2 \cos^2 \theta \tag{59}$$

Table X. Representative  $^{13}$ C and  $^{14}$ N isotropic splittings.

Radical	A <sub>iso</sub> (gauss)	Reference
13 <sub>CO2</sub> -	167	78,114
13 CH (COOH)2	33	71,72
13 <sub>CO3</sub> -	11.2	115
13 <sub>CH<sub>3</sub></sub>	37.7	24
14 NH(SO <sub>3</sub> -)	13.5	58
14NH3+	19.5	56,116
1.4 <sub>NH</sub> +	16.0	55
$(CH_3)_3^{14}$ N	27.5	117

where the values  $B_0$  and  $B_2$  are found by measuring the splitting for more than one nucleus  $\beta$  to the site of the odd electron. This can be done rather easily if the splittings arise from three different hydrogens in a non-rotating methyl group or  $NH_3$  group but must be done by comparative methods if this is not the case. In one radical,  $(CO_2H)CH_2-CH(CO_2H)$  (2), observed in irradiated succinic acid, a comparison with the splittings from  $(CH_3)_2COH$  radical was made. The angle  $\theta$  in Equation 59 is the angle between the axis of the orbital containing the odd electron and the plane containing the  $\beta$  C-H or N-H bond on the adjacent carbon or nitrogen (Figure 3). The isotropic splittings for nuclei, even from several protons in a methyl group or  $NH_3$  group, can be very different from one another if rotation of the group is not free.

In general it is quite difficult to determine the absolute signs of isotropic coupling constants. Recently Fessenden (118) proposed a method whereby the relative signs are determined by a detailed analysis of line positions. This involves an analysis of a system containing at least two nuclei which give separate isotropic splittings. Fessenden utilized the fact that hyperfine splittings are quite sensitive to changes in sign if second-order effects are included. The measurements were done mostly on fluorine-containing radicals although it was possible to make tentative determinations of the relative signs of  $\alpha$  vs  $\beta$  protons in isopropyl radical. By this

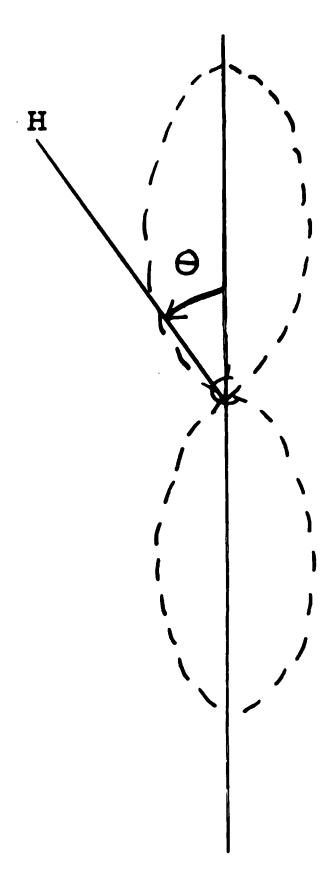


Figure 3. Relationship of nucleus at a  $\beta$  position relative to the odd electron orbital. A ·C-CH fragment is shown looking along the C-C bond with the dotted line outlining the  $p_{\pi}$  orbital of the odd electron.

method the Hamiltonian matrix is set up and the isotropic splittings calculated assuming various sign choices and the effect observed of the choices on the second-order corrections to the hyperfine splittings. Fessenden's calculations are an extension of the method of Heller (119), who used a similar procedure with a Hamiltonian including second-order terms, varying one isotropic splitting holding the second isotropic splitting constant. The computed spectra (119) were then compared with the experimental ones for the systems R<sub>2</sub>HC-CHR (substituted ethyl radical), R<sub>2</sub>C-CH-CHR (substituted allyl radical), and R<sub>2</sub><sup>13</sup>CH (substituted methyl radical) and the agreement was excellent.

#### 2) Anisotropic Splittings

The energy corresponding to the anisotropic contribution to the hyperfine coupling can be rewritten from Equation (14) if the substitutions to transform to polar coordinates are made as given in Equations 60-62:

$$x = R \sin \theta \cos \phi \tag{60}$$

$$y = R \sin \theta \sin \Phi \tag{61}$$

$$z = r \cos \theta$$
 (62)

where  $\theta$  is the angle between z and the direction R (in the reference axis system), and  $\phi$  is the angle from x to the projection of R in the x-y plane. Substituting these relationships in the matrix of Equation 14 and expanding, the following simplified forms are obtained to

first-order:

$$A_{xx} = -g\beta g_{N}^{\beta} \beta_{N} \left\langle \frac{R^{2} - 3x^{2}}{R^{5}} \right\rangle$$
 (63)

$$A_{yy} = -g\beta g_N \beta_N \left\langle \frac{R^2 - 3y^2}{R^5} \right\rangle$$
 (64)

$$A_{zz} = -g\beta g_{N}^{\beta} \beta_{N} \left\langle \frac{R^{2} - 3z^{2}}{R^{5}} \right\rangle$$
 (65)

or  $A_{ii} = c\langle 3 \cos^2 \theta_i - 1 \rangle / R^3 \rangle$ , where now  $\theta_i$  is the angle between the principal axis, i, and the direction of R in the principal-axis system.

It is possible to predict from this relationship the anisotropic splitting corresponding to a principal direction and the relative signs of the various splittings. If for the moment the anisotropic splittings are considered to arise from a hydrogen nucleus (I = 1/2) interacting with an odd electron localized primarily in a 2p orbital on carbon the principal directions are defined as 1) parallel to the C-H bond, 2) parallel to the p orbital occupied by the unpaired electron, and 3) perpendicular to the C-H bond in the plane of the radical, as illustrated in Figure 4.

Now from the above relationship the anisotropic splitting is proportional to  $(3\cos^2\theta - 1)/R^3$ . In Figures 5a-5c each plane is divided into regions in which the term  $(3\cos^2\theta - 1)$  is positive or negative. This is accomplished by setting  $(1 - 3\cos^2\theta) = 0$  from which is

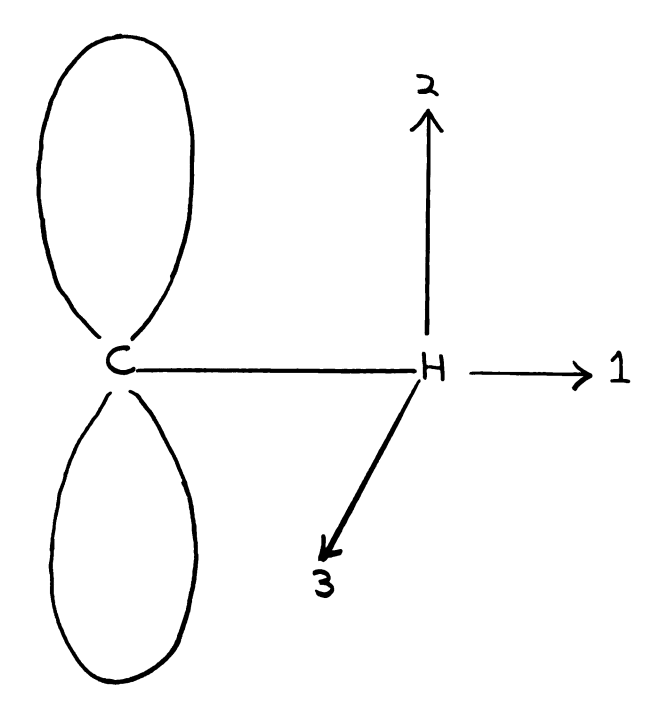
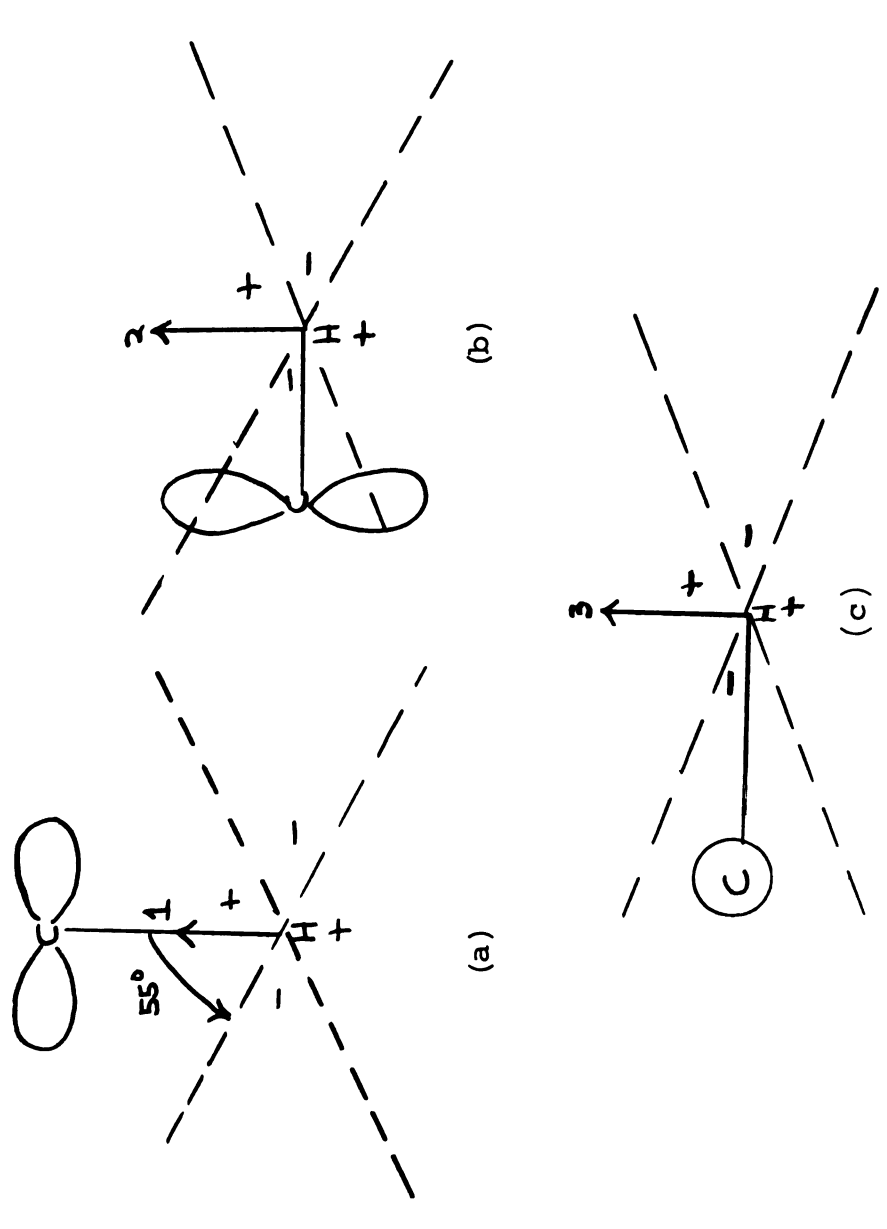


Figure 4. Principal directions of the hyperfine splitting tensor or g tensor for an  $\alpha$  proton.



Signs and relative magnitudes of the principal values of the dipolar coupling tensor for an  $\alpha$  proton illustrated for a -C-H fragment. Figure 5.

obtained  $\theta = 55^{\circ}$ . The values along the principal axis are determined by an examination of Figures 5a-5c.

It is assumed that the principal axis is always pointing in the positive direction. The largest positive principal value occurs in Figure 5a so that this direction corresponds to the largest positive splitting value (along the C-H bond). The largest negative splitting value corresponds to Figure 5c so that this is the direction perpendicular to the C-H bond in the plane of the radical. Therefore Figure 5b corresponds to a value intermediate between the other two coupling constants since the restriction still exists that the trace of the anisotropic splitting matrix,  $\bar{\bar{A}}$ , must vanish.

#### III. Planarity of Radicals

The  $^{13}$ C hyperfine splitting provides a good indication of the geometry of a  $\pi$ -electron radical. The deviation from planarity is easily calculated in the case of radicals with the odd electron centered on carbon if the components of the  $^{13}$ C tensor can be obtained. Karplus and Fraenkel (120) considered the case of a carbon atom with sp<sup>2</sup> hybridization. In the case of a planar radical the single unpaired electron is considered to be in a  $\pi$  orbital and all other electrons are paired in sigma atomic orbitals or bonds. The isotropic  $^{13}$ C splitting has a significant magnitude only if there is net unpaired spin density at the nucleus which in turn must arise from some s character in the odd-electron orbital. For a planar radical the odd

electron is in a  $\pi$  orbital and therefore the isotropic value would be expected to be small. However, if the radical is bent the amount of s character in the odd-electron orbital will increase through hybridization. The deviation of the  $^{13}$ C isotropic splitting in a bent radical from the  $^{13}$ C isotropic splitting in the case of planar methyl radical is the basis for determining the extent of bending of the radical out of the plane. For methyl radical the isotropic  $^{13}$ C splitting is described by

$$a_{c} = A_{iso}(^{13}C) = S^{C} + 3Q_{CH}^{C}$$
 (66)

where  $S^C$  is the contribution to the isotropic splitting  $a_C$  from 1s character on carbon and equals -12.7 gauss, and  $Q_{CH}^C$  is the contribution from spin polarization by the hydrogens attached to carbon and is equal to 18.85 gauss. The theoretical calculation by Karplus and Fraenkel (120) yields  $a_C = +43.8$  gauss in good agreement with the experimental value of 41 ± 3 gauss obtained by Cole et al. (106).

Karplus and Fraenkel (120) have also calculated the  $^{13}\text{C}$  isotropic splitting as a function of  $\theta$ , the angle between the direction of the  $\pi$  orbital and one of the CH bonds in methyl radical, and deduce the following relationship:

$$a_{C}(\theta) = a_{C}(0) + 1190 (2 \tan^{2} \theta)$$
 (67)

where  $a_c(0)$  is the measured isotropic <sup>13</sup>C splitting value for a given  $\theta$  and  $a_c(0)$  is the isotropic value for

planar methyl radical. This equation has been applied in a limited number of cases to determine  $\theta$  for substituted methyl radicals and some of the results are given in Table XI.

Table XI. Deviation from planarity for some substituted methyl radicals  $^{1}$ 

Radical	a <sub>C</sub> (gauss)	θ	Reference
·CH <sub>3</sub>	41 ± 3	<u> </u>	121,24
·CF <sub>3</sub>	271.6	17.8°	109
·CHF <sub>2</sub>	148.8	12.7°	109
·CH <sub>2</sub> F	54.8	<u>≺</u> 50	109
·CF <sub>3</sub>	270	17.8°	74
·CF <sub>2</sub> COO	145	12.5°	122
·CF2C00	73	80	122
·CF <sub>2</sub> COO	69	80	122
·CF2C00	70	80	122
·CCl <sub>3</sub>	90	80	122
·CFHCONH <sub>2</sub>	45	00	74
·C(CH <sub>3</sub> ) <sub>3</sub>	47	3.5°	+

Here a = A (13C) is the isotropic 13C hyperfine splitting.

<sup>+</sup>This work.

#### **EXPERIMENTAL**

## I. Analysis of ESR Data for Irradiated Single Crystals

There are now numerous references which provide the necessary background for carrying out ESR studies of irradiated single crystals. An introductory book has been written by Bersohn and Baird (123) which treats the subject fairly simply. A more advanced text which has good sections dealing with organic radicals, and magnetic resonance in general, has been written by Carrington and McLachlan (100). Carrington and Mc Lachlan's book also is excellent for a treatment of some of the experimental aspects involved when studying irradiated single crystals. A recent book by Ayscough (171) treats the theory and the experimental aspects of ESR. Books which treat the theory of resonance in some detail have been written by Slichter (82), Pake (124), and Low (125).

A good reference for the electronic aspects of ESR spectrometers as well as a short discussion of irradiation sources and dosages of irradiation is given in a recent book by Poole (126). Also useful in this respect are several Varian (127, 128) manuals which accompany the spectrometer systems. There are also numerous review articles which

provid organi

Whiffe

a summ

A

is not

magneti

align c

a good i

book by

should b

involved

writ cel

crystal

tion fro

X-ray d

introdu

optica:

A More

tte us

Sarts

ful if

if the

132 W

Ecryst:

provide an introduction to ESR. A very useful review of organic and inorganic radicals is given by Morton (61).

Whiffen (14) has a good introductory review which includes a summary of the relevant theory involved.

Although a knowledge of X-ray structure determination is not absolutely essential for aligning a crystal in the magnetic field, X-ray methods provide the best way to align crystals. The techniques involved are well known and a good treatment of structure analysis is given in a recent book by Stout and Jensen (129). Chapters 1-5 in this book should be sufficient to acquaint one with the techniques involved. A complete analysis is not required, only a unit cell and space group determination and the location of crystal axes. Although it is possible to get this information from other methods such as optical crystallography, X-ray diffraction is by far the best procedure. For an introduction to the general treatment of space groups and optical crystallography Phillips' (130) book is very good. A more complete discussion of optical crystallography and the use of a polarizing microscope is given in a book by Hartshorne and Stuart (131). Optical methods are very useful if the structure has already been determined, especially if the crystallographic data have been reported by Groth (132) who lists the interfacial angles for a large number of crystals.

## II. Spectrometer System

The spectrometer used operated in the X-band frequency range (\$\geq 9.0\ \text{GHz}\$) and was manufactured by Varian Associates, Palo Alto, California. The system (model V-4502-04) consisted of a 12-inch magnet which maintained a magnetic field approximately equal to 3000 gauss. The field was modulated with a 100 KHz crystal oscillator to improve the signal-to-noise ratio. An added circuit permitted switching from first to second-derivative presentation; the latter was normally used, since the positions of the lines could be followed more easily. The signal from the detector was fed into an oscilloscope or a Hewlett-Packard Model No.7000A XY-Recorder the x axis of which was driven as a function of magnetic field. The x axis (corresponding to the magnetic field) was regulated by a Hall probe device so that linearity was maintained when spectra were recorded.

The magnetic field was measured by means of a proton marginal oscillator (133). The frequency from this oscillator was measured by a Hewlett-Packard Electronic Counter, Model 524C. Provision was made so that a frequency mark could be put on all spectra.

The Klystron frequency was measured with a  $T_s$ -148/UP U.S. Navy spectrum analyzer. The analyzer was tunable over a range from 9.0-9.5 GHz, but most of the time was used at 9.2 GHz. The analyzer was usually accurate to 0.1 MHz and had been previously calibrated over the range 9.0-9.5 GHz so that the correction could easily be made.

# III. X-ray Structure Determination and Optical Crystal-lography

Since the alignment of crystals is very important in simplifying spectra, an explanation of the procedure used needs to be made. If no report of the structure was available, it was necessary to do an x-ray determination to obtain the space group, unit cell dimensions, and positions of the crystal axes. It is usually preferable to use a small crystal, 0.1 mm or less, for an X-ray analysis. However, it was found that it was possible to work with larger crystals, up to 0.5 mm maximum length, if the exposure time was increased. All determinations were done with unfiltered Cu ( $\lambda_{K\alpha} = 1.542 \ \text{Å}$ ) radiation. The crystals were chosen such that the crystal shape closely resembled those to be used for ESR analysis. In this way the faces corresponding to known directions of crystal axes could be used for alignment in the ESR cavity.

After a suitable crystal was found it was examined under a polarizing microscope to ascertain whether it was truly a single crystal. When a single crystal had been found, it was mounted on a glass fiber 2" long which was attached to a goniometer head. The fiber was held in place with Versene or some other type of putty-like material. The crystal was attached with Canada balsam or Duco cement. If the crystal was air sensitive or hygroscopic, it was necessary to seal off the crystal in a quartz capillary tube similar to the ones used in powder diffraction analyses.

The goniometer head was then attached to the Weissenberg camera and oscillation pictures were taken according to the procedures outlined in Stout and Jensen (129). The oscillation range was  $\pm 15^{\circ}$  and two pictures were taken  $90^{\circ}$  apart from one another on the scale of the Weissenberg camera. The alignment of the crystal was corrected with the arcs on the goniometer head and the correction was usually  $2^{\circ}$  or less. If more correction was needed, it was usually easier to realign the crystal on the head by moving the fiber slightly.

After the preliminary alignment axis had been measured, the beam stop was replaced with a layer screen and a zerolayer Weissenberg photo was taken. The range was usually  $200^{\circ}$  so that the complete reciprocal lattice could be taken on a single piece of film. The zero-layer film was allowed to expose for 5 or 6 hours. For most monoclinic organic crystals encountered in this work, it was possible to choose the b axis as the alignment axis. The zero-layer film, therefore, indicated the positions of the a and c\*, or and c, axes and the angle 6\* between them. The reflections on the zero-layer film were then indexed by plotting them on spherical coordinate graph paper using the scale 1 mm =  $2^{\circ}$  and the appropriate scale for zero-layer indexing which is given in Buerger's (134) book. The positions of the axes were usually quite evident if the plot on spherical coordinate paper was traced onto a plain sheet of white paper.

Once the positions of the axes were found the goniometer head was removed from the Weissenberg camera and mounted on the precession camera. The scale reading corresponding to the positions of the axes was set on the precession camera; the precession range was set at  $\mu=30^{\circ}$ . The film was allowed to expose for one hour. If the axes were indeed present at the respective scale positions on the camera, the resulting precession photograph showed the expected two-fold symmetry along the b-axis. By this procedure it was possible to identify positively the directions corresponding to the crystal axes. Buerger (135) also has a book dealing with the precession method which was quite useful.

The goniometer head was then remounted on the Weissenberg photos were taken. It was usually only necessary to take a zero-layer, a one-layer and a two-layer photo. The method for doing this is described in Stout and Jensen's (129) book. The first and second-layer photos were then indexed in the same manner as was used for the zero-layer photo with a change in the scale according to Buerger (134). In this way it was possible to make a space group determination with enough reflections along each axis. If the possibility arose of more than one space group corresponding to the observed reflections it was necessary to measure the number of molecules per unit cell by flotation methods. The crystal was floated in a mixture of carbon tetrachloride (d = 1.589) and heptane (d = 0.684). From the observed density and molecular weight it was possible to determine

the number of molecules per unit all by the method given in Stout and Jensen (129).

If the interfacial angles have been reported, in Groth's (132) book for example, it is possible to determine the positions of the crystal axes with an optical goniometer. However, determination of the space group still requires an X-ray analysis.

For the case of a hexagonal crystal it was possible to use the polarizing microscope to identify the position of the c-axis. Both of the prisms were inserted and the Bertrand lens was then put into position. The direction of the c crystallographic axis was easily identified by the interference fringes.

Although it is reported by Hartshorne and Stuart (131) that interference fringes are also seen for biaxial crystals it was not possible to detect these in the case of any of the monoclinic crystals used.

#### IV. Materials

#### A. Acetamidine Hydrochloride

Crystals were grown from a saturated aqueous solution of the reagent obtained from Eastman Organic Chemicals, Rochester, N.Y. The crystals were extremely hygroscopic and had to be kept in a desiccator when not in use. The crystals had to be sealed in quartz capillary tubes to do an X-ray analysis. The deuterated crystal was obtained by

recrystallizing acetamidine hydrochloride three times from 99.84% D<sub>2</sub>O (Stohler Isotope Chemicals, Montreal, Quebec, Canada).

# B. <u>Isobutyramide</u>

Crystals were grown from a saturated aqueous solution of the reagent obtained from Eastman Organic Chemicals, Rochester, N.Y. The crystals did not appear to be hygroscopic to any appreciable degree and could be easily handled while exposed to the air. Deuterated crystals were obtained by recrystallizing isobutyramide from D<sub>2</sub>O three times.

#### C. Trimethylacetamide

Trimethylacetamide was prepared by M. T. Rogers from pivalic acid. The crystals obtained were from a saturated aqueous solution. The amide did not appear to be hygroscopic and could be easily handled.

#### D. Hydrazinium Dichloride

Hydrazinium dichloride single crystals were obtained from a saturated aqueous solution of the reagent from Fisher Scientific Co., Fair Lawn, N.J. The crystals were hygroscopic and had to be stored in a desiccator.

#### E. Hydrazinium Difluoride

Hydrazinium difluoride was prepared by the method of Kronberg and Harker (136) by neutralizing 49% HF solution

(J.T. Baker Chemical Co., Phillipsburg, N.J.) with 95% hydrazine solution (Eastman Organic Chemicals, Rochester, N.Y.) in a 2:1 mole ratio. The crystals are hygroscopic according to Deeley and Richards (137) and were therefore kept in a desiccator. The deuterated crystals were obtained by recrystallizing hydrazinium difluoride three times from  $D_2O$ .

#### F. Hydrazinium Dibromide

Hydrazinium dibromide was prepared by neutralizing 48% HBr solution (Matheson, Coleman and Bell; Rutherford, N.J.) with 95% hydrazine solution (Eastman Organic Chemicals, Rochester, N.Y.) in a 2:1 mole ratio. The crystals were extremely hygroscopic and had to be kept in a desiccator when not in use.

#### V. Procedure

#### A. Crystal Growing

As was mentioned in the previous section all crystals were obtained from aqueous solution by slow evaporation.

The solutions were saturated by pumping carefully on them in a vacuum desiccator until a slight precipitate formed.

It was possible to obtain good seed crystals by this method.

These seeds were then used to obtain larger crystals from the saturated solutions.

The solutions were usually allowed to evaporate slowly by setting a beaker containing the solution on a shelf and

appeared to cator contour these method crystals of in about to pumping on a desiccat

covering t

В. <u>г</u>

Two to the most of the most of the most of the crystal caps and containing the center of the center of the containing the center of the contract of the contra

afficien

The

. Mer G.E

covering the beaker with a watch glass. If the solution appeared to evaporate very slowly it was placed in a desiccator containing CaSO<sub>4</sub> or some other desiccant. Using these methods it was usually possible to obtain single crystals of the required dimensions, about 3 mm on an edge, in about ten days. The crystals were then dried by either pumping on them in a vacuum desiccator or putting them in a desiccator containing CaSO<sub>4</sub>.

## B. Radiation Procedure

Two types of radiation were used to produce radicals. The most frequently used was the  $^{60}\text{Co}$   $\gamma\text{-ray}$  source which delivered a dose rate of 2  $\times$  10<sup>6</sup> rad/hr, or since 1 rad = 100 erg/gram the dose rate would be 2  $\times$  10<sup>8</sup> erg/gram-hr. The crystals were placed in 2-dram glass vials with screw caps and these vials were then placed in a glass dewar flask containing liquid nitrogen. The dewar flask was placed in the center well of the irradiation source and the samples irradiated for periods of from 3 to 10 hrs. It was usually possible to detect radicals after 3 hrs irradiation and the only effect of longer irradiations was to increase the concentration of radicals present. In some cases, however, it was necessary to irradiate longer than 3 hrs to obtain sufficient concentration of radicals, especially in the case of the hydrazinium compounds.

The other type of irradiation source available was a

1 Mev G.E. Resonant Transformer which produced accelerated

electron 2.97 x 1 of 47 cr insuffic It was p time, us than 8 m the crys tion and differin crystal ethylene of liqu the irra the crys in the : Eporta:

since th

if the

1 W110

ion as

Roof w

aally

<sup>lat</sup>iate

ied za

electrons. The dose rate available from the source was  $2.97 \times 10^6$  rad/min or  $2.97 \times 10^8$  erg/gram-min at a distance of 47 cm from the tube window. This source was used when insufficient radiation was obtained with the 60 co source. It was possible to irradiate for much shorter periods of time, usually from 3 to 8 minutes. Radiation periods longer than 8 minutes usually resulted in complete destruction of the crystal; sometimes this occurred with even less radiation and it was usually necessary to test the crystal with differing amounts of radiation to determine the limit. crystals to be irradiated were placed in small sealed polyethylene bags which were allowed to float on the surface of liquid nitrogen in a stainless steel dewar flask during the irradiation. If any difficulty was encountered keeping the crystals floating, a small piece of styrofoam was placed in the polyethylene bag to keep it afloat. It was very important to keep the crystals floating near the surface, since the crystals received very little radiation if they sank even 1 cm below the surface. The amount of heating of the crystal from the source while it was floating appeared neglibible. This was demonstrated in several instances in which the same radicals were present after y-irradiation as after electron irradiation. The most conclusive proof was with the V centers observed in this work. centers were stable over a very short temperature range, usually -1500 to -1960, and appeared in the electron irradiated material in higher concentration than in y-irradiated material.

## C. Mounting Crystals

It was necessary to keep the irradiated crystals at liquid nitrogen temperature  $(77^0\mathrm{K})$  in order to detect any radicals which had formed at this temperature. A procedure was devised for transferring the crystals to a crystal mount allowing as little warm-up as possible. When not in use the crystals were kept at  $77^0\mathrm{K}$ .

The irradiated crystals in glass vials or polyethylene bags were transferred to a  $100 \times 50$  crystallizing dish containing liquid nitrogen. This dish was insulated by a piece of Styrofoam which was hollowed out to accommodate the dish. The vials or bags were opened in this dish and the crystals allowed to float out into the liquid nitrogen. The crystals were handled with forceps which had been precooled with liquid nitrogen.

The crystals were transferred with these forceps into a small aluminum foil scoop containing liquid nitrogen.

The scoop containing the crystal under liquid nitrogen was then moved to the crystal mount. The crystal mount consisted of a 2 mm diameter glass rod 17 inches long. At one end was attached a brass clip held by Pliobond cement. The other end of the mount contained a circle of sponge rubber 1.5 inches in diameter and 3 inches thick. The mount is shown in Figure 6. The clip end of the mount was kept cooled to 770K by placing it in a small pool of liquid nitrogen. A piece of Styrofoam which had been hollowed out for this

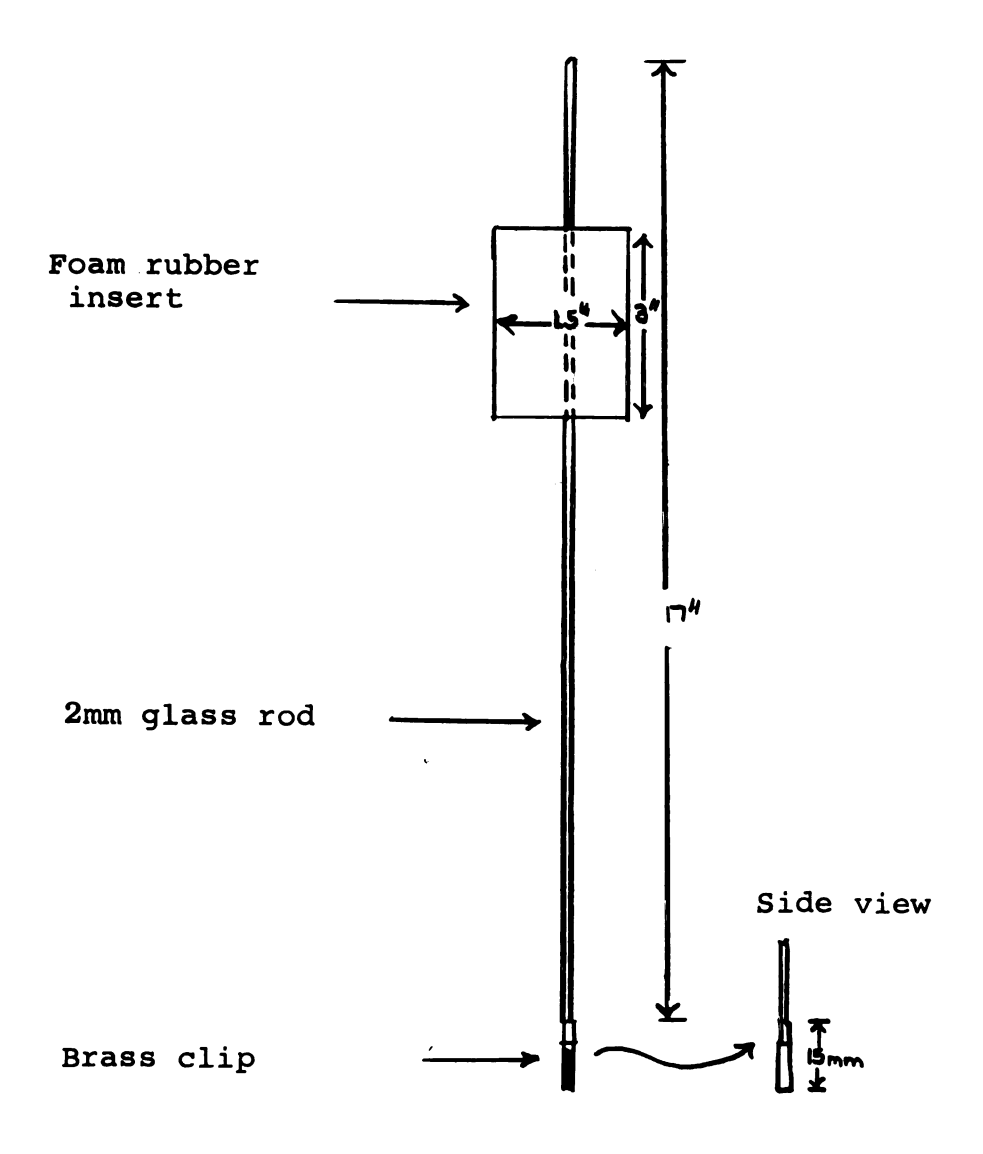


Figure 6. Single crystal holder.

purpose w and attac the dewar nitrogen as far d Cossible tagretic

transferr into posi forceps. of liquid Afte to a dewa TE<sub>102</sub> Var Palo Alto of glass

> quickly into the

the spon

in place

cT

glass pl

<sup>1800</sup>· T

ie dewa

 $n_{taine}$ ittached

ांe of

purpose was used. The scoop containing the crystal was transferred to this pool and the crystal was then moved into position under the brass clip with the aid of precooled forceps. Figure 7 shows the crystal mount lying in the pool of liquid nitrogen with the attached crystal.

After the crystal had been mounted it was transferred to a dewar flask which was designed to fit into the ESR TE<sub>102</sub> Varian Multipurpose Cavity. (Varian Associates, Palo Alto, California). The dewar container was constructed of glass with the tip constructed of optical grade quartz and attached to the glass by a graded seal. Figure 8 shows the dewar container used. It was filled first with liquid nitrogen and the crystal mount with crystal attached then quickly transferred to it and the sponge rubber top squeezed into the top of the dewar container. After several minutes the sponge rubber circle froze and kept the crystal mount in place. The brass clip containing the crystal was pushed as far down into the quartz tip of the dewar container as possible to prevent bumping from the liquid nitrogen.

To measure the angle of rotation of the crystal in the magnetic field, the dewar container was inserted in a plexiglass platform which had been scored in degrees from  $0^0$  to  $180^0$ . The platform rested on the top of the magnet with the dewar container inserted into the magnet pole gap which contained the rectangular  $TE_{102}$  cavity. A pointer was attached to the dewar flask to simplify the recording of angle of rotation. The system is shown in Figure 9.

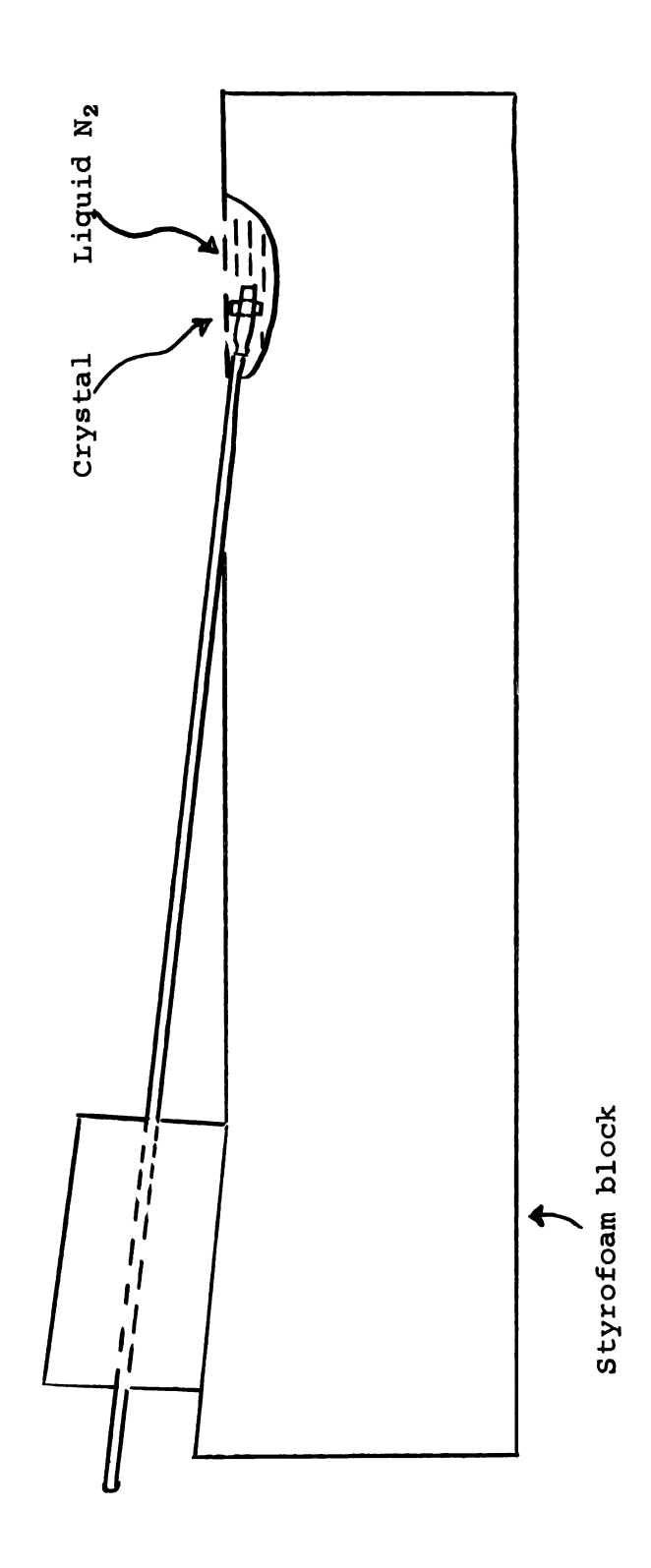


Figure 7. Single crystal mounted in crystal holder for transfer to ESR cavity.

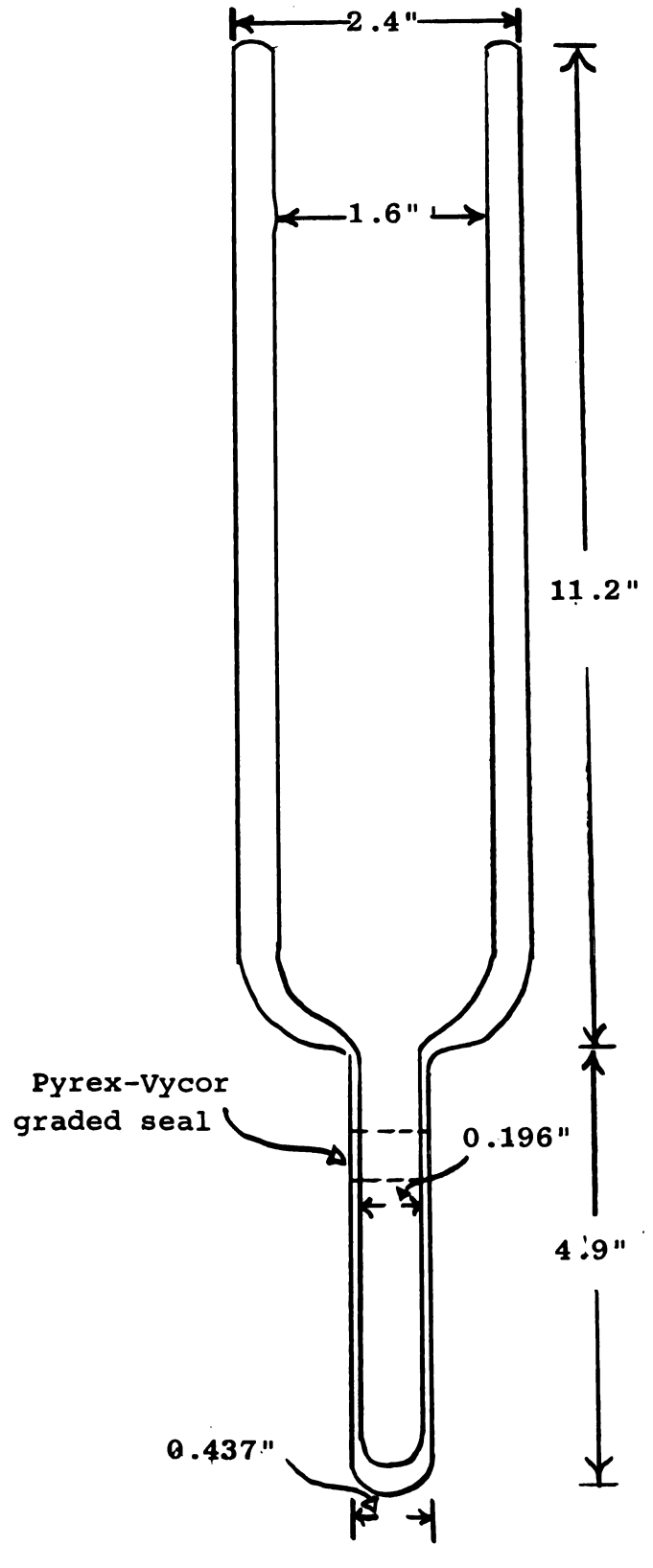


Figure 8. Dewar container for ESR single crystal studies.

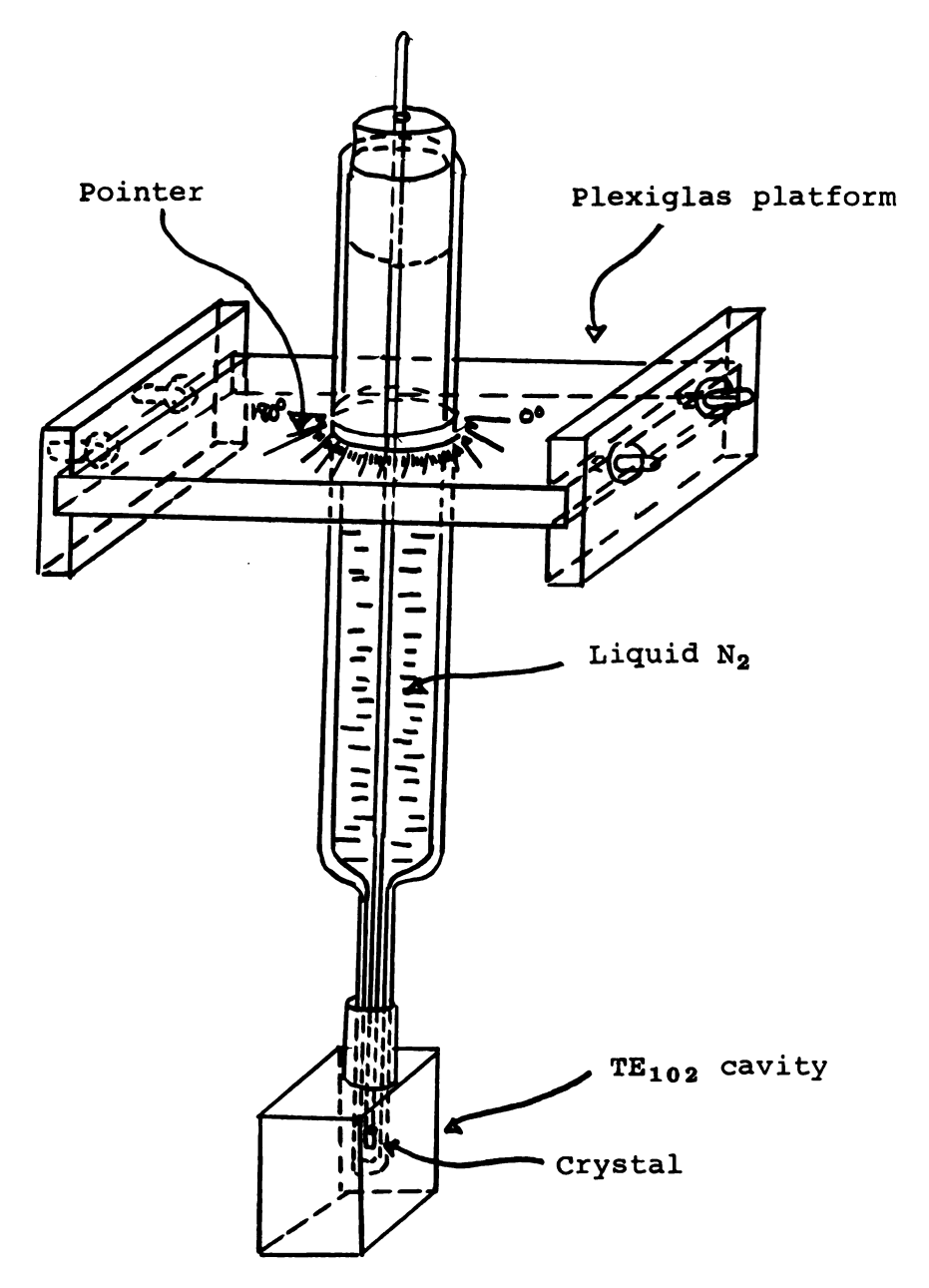


Figure 9. Apparatus for rotating single crystals in the magnetic field.

ery it

in

two

bra fe:

> o: to

> sp it

eχ

Mag

in Were

the :

of th

jian i

ised a

scald b

Spectra in one crystallographic plane could be taken in this manner. In order to obtain the spectra in the other two crystallographic planes, it was necessary to remove the crystal from the brass clip on the crystal mount and remount it repeating the above procedure.

There was no detectable background signal from the brass clip, Pliobond cement or quartz dewar tip which interferred with signals from the radicals.

#### D. Rotation Spectra

Spectra were recorded at intervals of  $10^{0}$ , or more often if the pattern was more complex. It was necessary to do a complete  $180^{0}$  rotation to obtain a complete set of spectra in one crystallographic plane. As stated above it was considered easier to rotate the crystal in the fixed external magnetic field,  $\overrightarrow{H}_{\text{ext}}^{>}$ , rather than to rotate the magnet.

After a complete set of rotation spectra were obtained in three mutually perpendicular planes, the line separations were measured as a function of  $\theta$ , the angle of rotation in the magnetic field. The hyperfine splittings were then fitted to either Equation 46 or 48 and the principal values of the tensor obtained by diagonalization. A computer program written by Lowell D. Kispert for this purpose was used and a listing of this program is given in the Appendix. The principal values of either the  $\bar{A}^{\dagger}$  or  $\bar{g}^{\dagger}$  tensor could be determined in this way.

#### E. Temperature Studies

If more than one type of radical was present after irradiation at 77°K, it was desirable to study each radical independently if possible. This could often be accomplished by warming the crystal slightly with different types of slush baths. This was found to be a better method than using the Varian V-4557 Variable Temperature Accessory (Varian Associates, Palo Alto, California). By a judicious choice of slush baths it was possible to heat the crystal enough to largely destroy one radical without allowing the other radical to decay appreciably. A good listing of slush baths providing a large range of temperatures has been given by Rondeau (138).

The crystal was placed in a 2-dram glass vial with screw cap and allowed to warm in the slush bath for periods of 15 seconds to 15 minutes. The crystals were then remounted at liquid nitrogen temperature  $(77^0 \, \text{K})$  using the procedure in Part D above.

#### VI. Standard Samples and Conversion Factors

Occasionally the spectrometer was checked with standard samples to determine if all systems were operating properly. The standard samples used were:

Varian Pitch in KCl: g = 2.0028Aqueous  $K_2Cr(CN)_5NO$ :  $g = 1.99454 \pm 0.00005$ 

 $A_{N} = 5.265 \pm 0.05$  gauss.

spec

wher

magn freq

quen

A list of conversion factors used in interpreting the spectra is given below:

$$g = \frac{0.714489 \, v_{e} \, (MHz/sec)}{H(gauss)} \tag{68}$$

$$H(gauss) = 2.3487465 \times 10^2 \times v_p \text{ (MHz/sec)}$$
 (69)

$$H(gauss) = \frac{0.714489 \times v_e \text{ (MHz) at free spin}}{2.0023}$$
 (70)

$$A(gauss) = A (MHz/sec)/2.8026 [for g = 2.0023] (71)$$

$$A(gauss) = (1.0697 \times 10^{4}) A (cm^{-1})$$
 (72)

where A is the measured hyperfine splitting, H is the magnitude of the external field,  $v_e$  is the klystron frequency in MHz and  $v_p$  is the proton oscillator frequency in MHz.

· I.

chlo

cord

Weight!

4.5

erice

grot

Teas

Dent

whic.

indic obser

ippeo

dewar

#### RESULTS

# I. <u>Irradiated Acetamidine Hydrochloride</u>

# A. Crystal Structure

No X-ray crystallographic study of acetamidine hydrochloride had been previously reported. The identification of the space group and unit cell dimensions was made according to the method described in the Experimental section and in Stout and Jensen's book (129). Oscillation and Weissenberg photos showed the crystal to be monoclinic with unit cell dimensions a = 7.25 Å, b = 8.18 Å, and c =4.54  $\stackrel{\circ}{A}$ ,  $\beta$  = 1040. The Weissenberg photos showed the presence of hkl reflections with no conditions; hk0, no conditions; 001, 1 = 2n. This is consistent with space groups  $P2_1$  or  $P2_1/m$ . The density of the crystal was measured with a mixture of carbon tetrachloride ( $\rho$  = 1.589 g/ml) and n-heptane ( $\rho = 0.684$  g/ml). The experimentally determined density was 1.210 g/ml in this mixture which gives 2.01 molecules per unit cell. This seems to indicate the space group  $P2_1$  rather than  $P2_1/m$ . The observation that a crystal of acetamidine hydrochloride dipped in liquid N2 was attracted to the walls of a silvered dewar flask (piezoelectric effect) means no center of

symm

to t

resu

the

flec

phot

axes

7-ir crys

the

tall

to t

crys

Tadi the

Pigu Lines

ines

ing :

Buss.

symmetry is present. This additional evidence lends support to the choice of  $P2_1$  as the correct space group and the resultant ESR spectra tend to confirm this assignment.

The crystals were easily aligned along the b axis and the a and c\* axes were chosen from the appearance of reflections along these axes from the zero-layer Weissenberg photos. A drawing of the crystal and crystallographic axes is shown in Figure 10.

## B. <u>Identification of Radicals Produced in Irradiated</u> Acetamidine Hydrochloride

1) Low-Temperature Radical - Cl<sub>2</sub>

Single crystals of acetamidine hydrochloride were  $\gamma$ -irradiated with the <sup>60</sup>Co source for 3 hours at  $77^{0}$ K. The crystals were then mounted, without warmup, according to the procedure in the Experimental section. The three crystallographic planes ab, bc\*, ac\* were chosen by reference to the crystallographic axes presented in Figure 10 and the crystals were rotated through  $10^{0}$  intervals in each plane.

Figure 11 shows the second-derivative spectrum of the radical stable at 77°K taken with the magnetic field in the ac\* plane at 50° from a. As can be seen from Figure 11 the spectrum consists of seven basic groups of lines. The measured intensity ratios for the most prominent lines (labeled 1 to 7) were 1:2:3:4.1:2.8:2:1. The splitting between these main peaks at this orientation was 95.5 gauss.



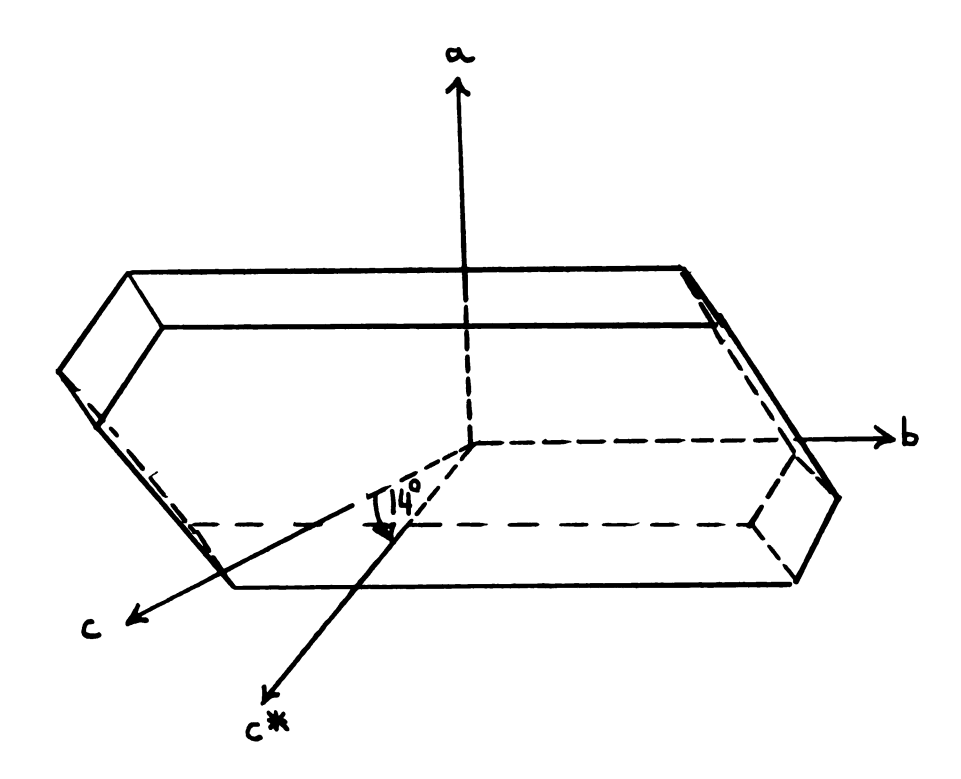


Figure 10. Crystallographic axes for acetamidine hydrochloride.

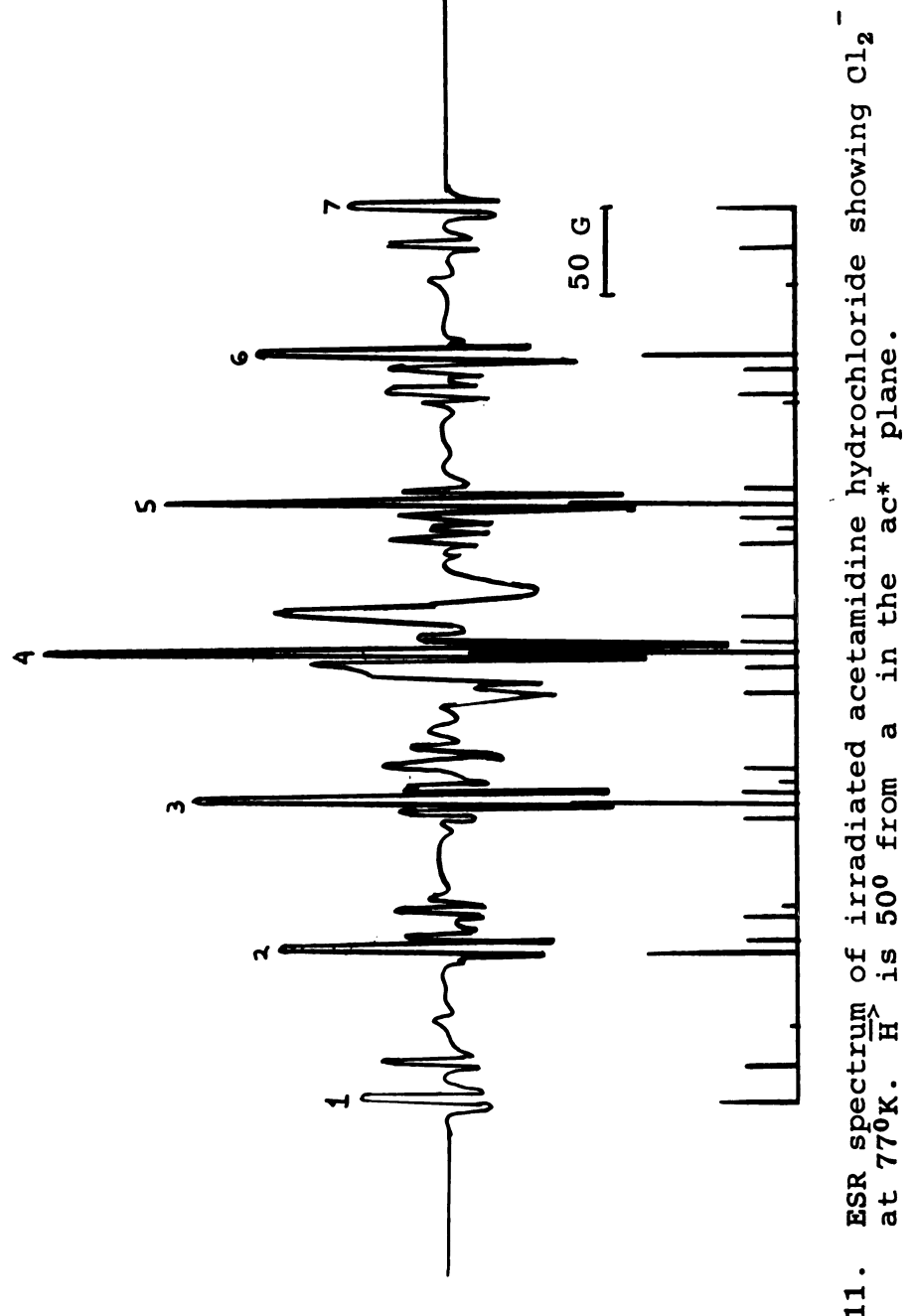
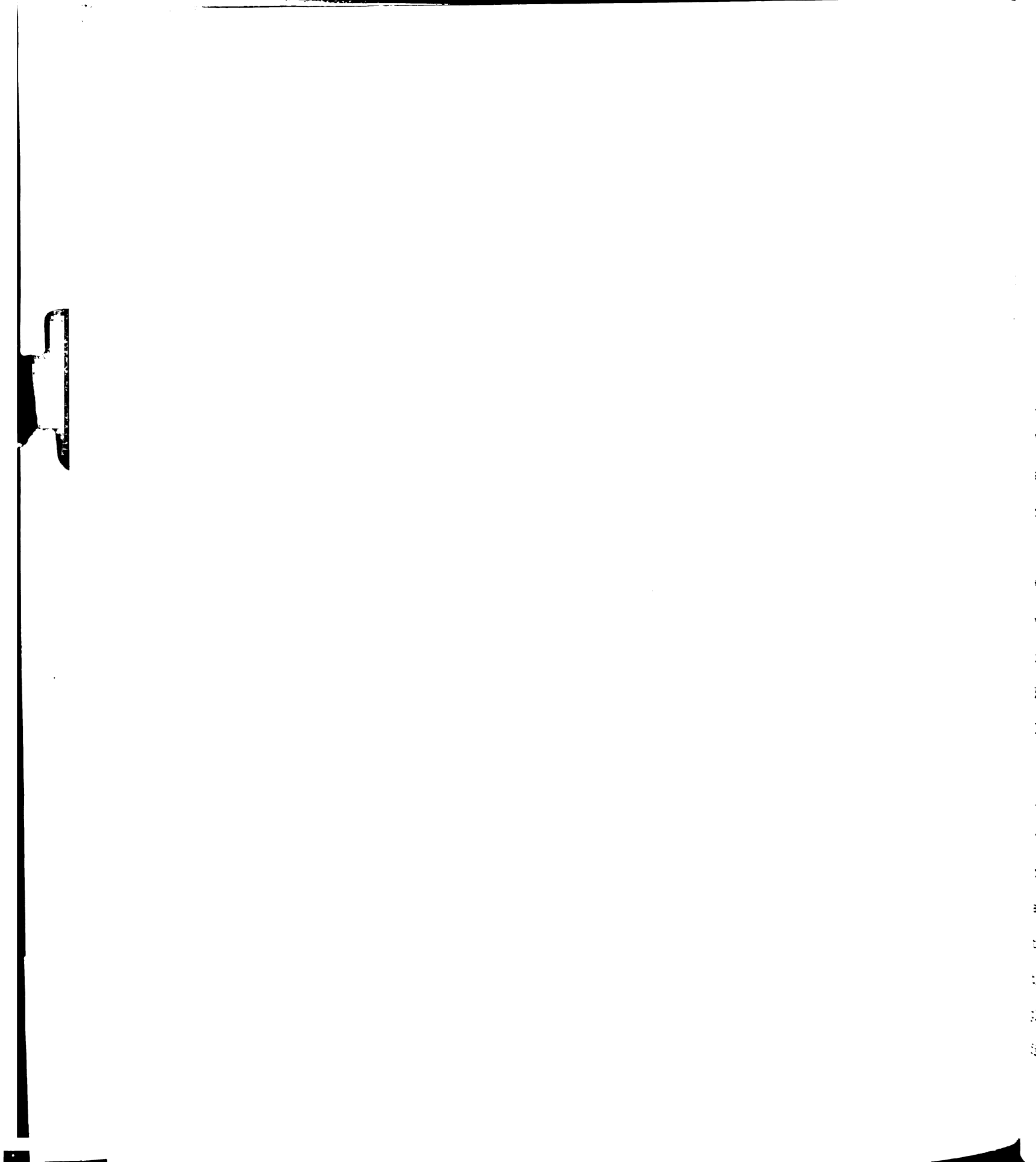
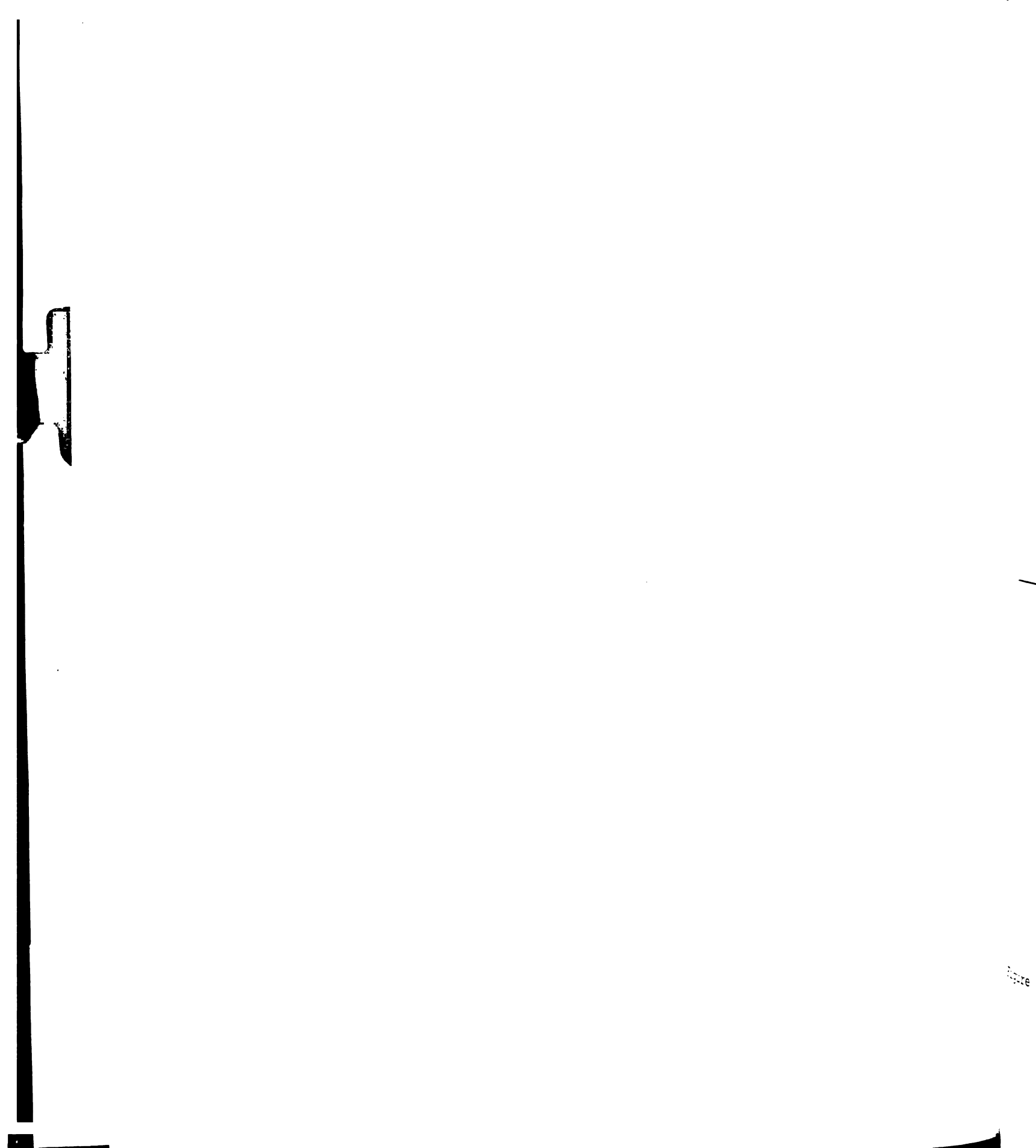


Figure 11.



When the crystal was rotated 90° from the position in Figure 11 a more complicated pattern resulted. Figure 12 shows the spectrum obtained with the magnetic field 40° from c\* in the ac\* plane. The spectrum has become considerably more compact, being only 285 gauss in total width compared with a 551 gauss total width in Figure 11. Seven main groups of lines are distinguishable but in this case there are two sets of seven lines each, resulting from the presence of two nonequivalent radicals at this position. This nonequivalence is also present if the crystal is examined at 60° from a in the ac\* plane as can be seen from Figure 13.

Rotations in the ab and bc\* planes similarly showed the presence of 7 basic groups of lines with two nonequivalent radicals present at most orientations. For rotations in both the ab and bc\* planes the two radicals present behaved differently than for the ac\* plane where, as can be seen from Figures 11 and 12, the angular dependence of the hyperfine splitting followed nearly the same pattern for both radicals. The spectrum shown in Figure 14 was obtained with the magnetic field parallel to the baxis in the ab plane and it can be seen that one radical exhibits a minimum hyperfine splitting at this position relative to the hyperfine splitting of the second radical. A 90° rotation to place a parallel to the magnetic field in the ab plane leads to the spectrum shown in Figure 15. The hyperfine splitting at H | | a in the ab plane is again at a



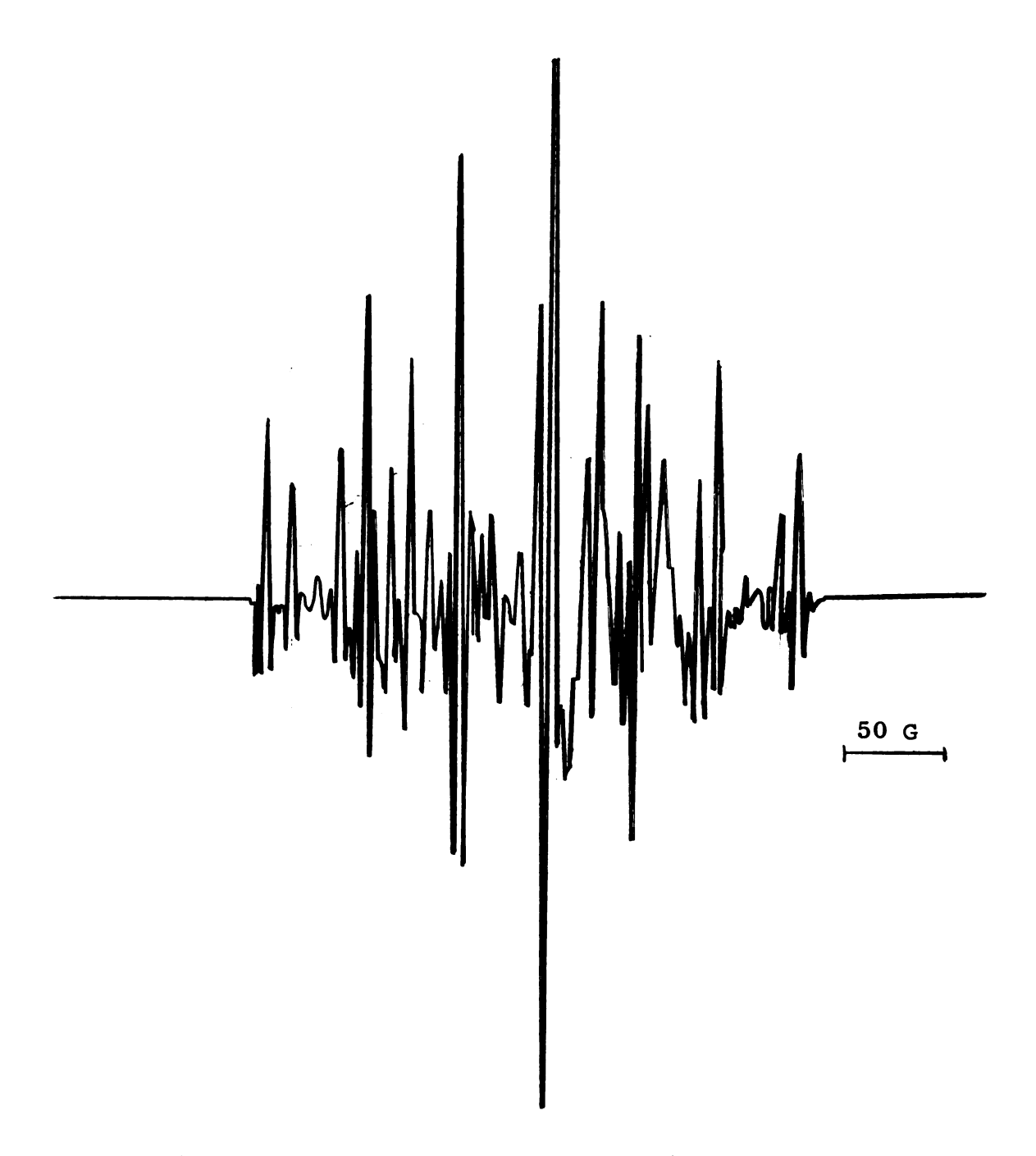
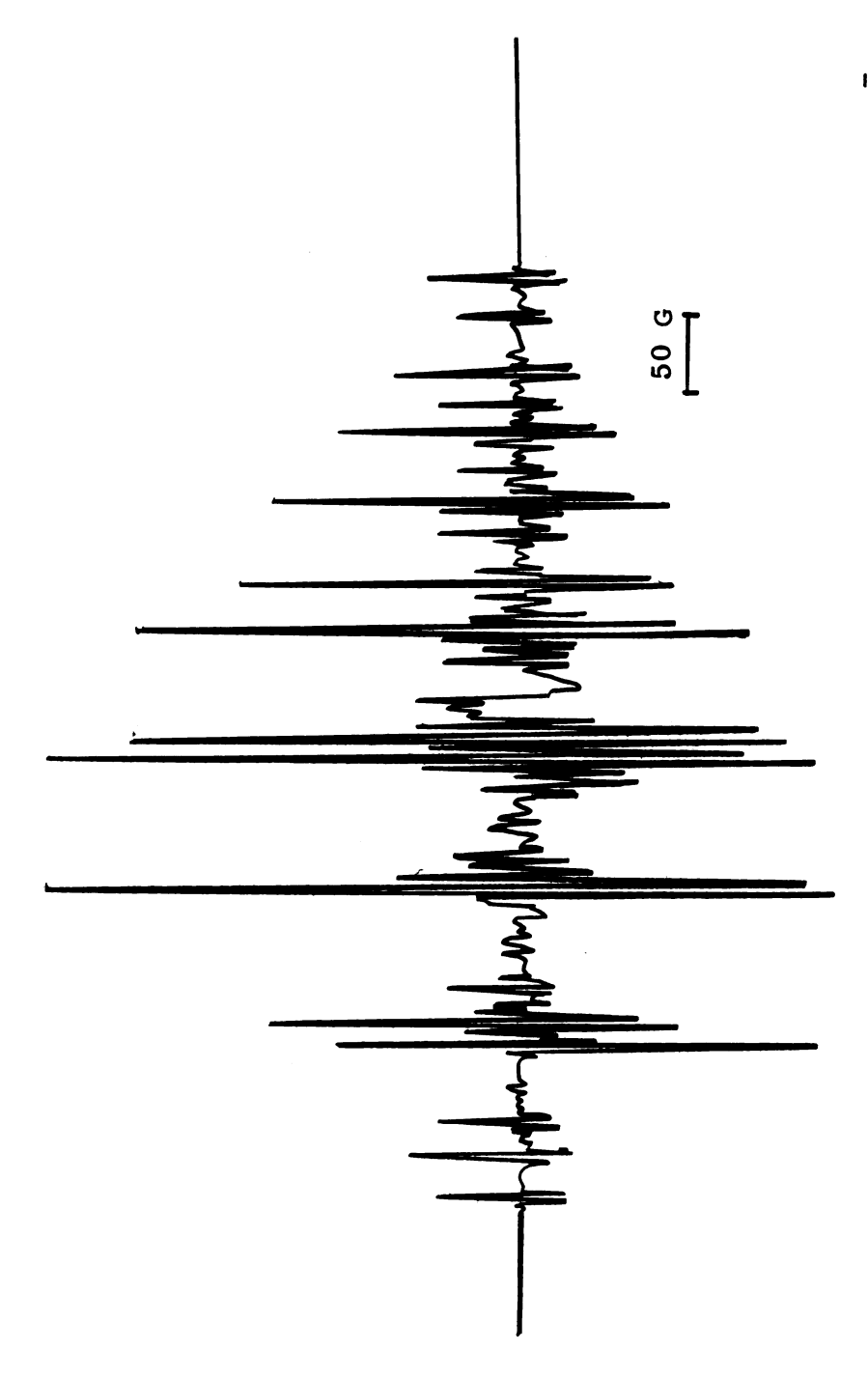


Figure 12. ESR spectrum of irradiated acetamidine hydrochloride showing Cl $_2$  at  $77^0 K$ .  $\overline{\rm H}^>$  is  $40^0$  from c\* in the ac\* plane.



 $cl_2^-$ ESR spectrum of irradiated acetamidine hydrochloride showing at  $770 {\rm K}$ . H is  $60^{\rm o}$  from a in the ac\* plane. Figure 13.

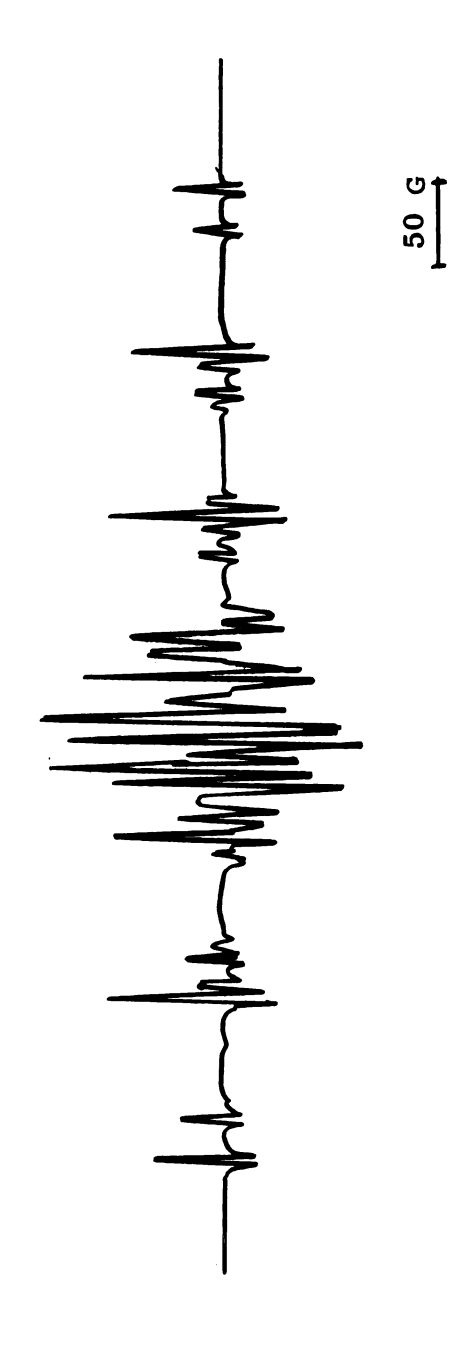
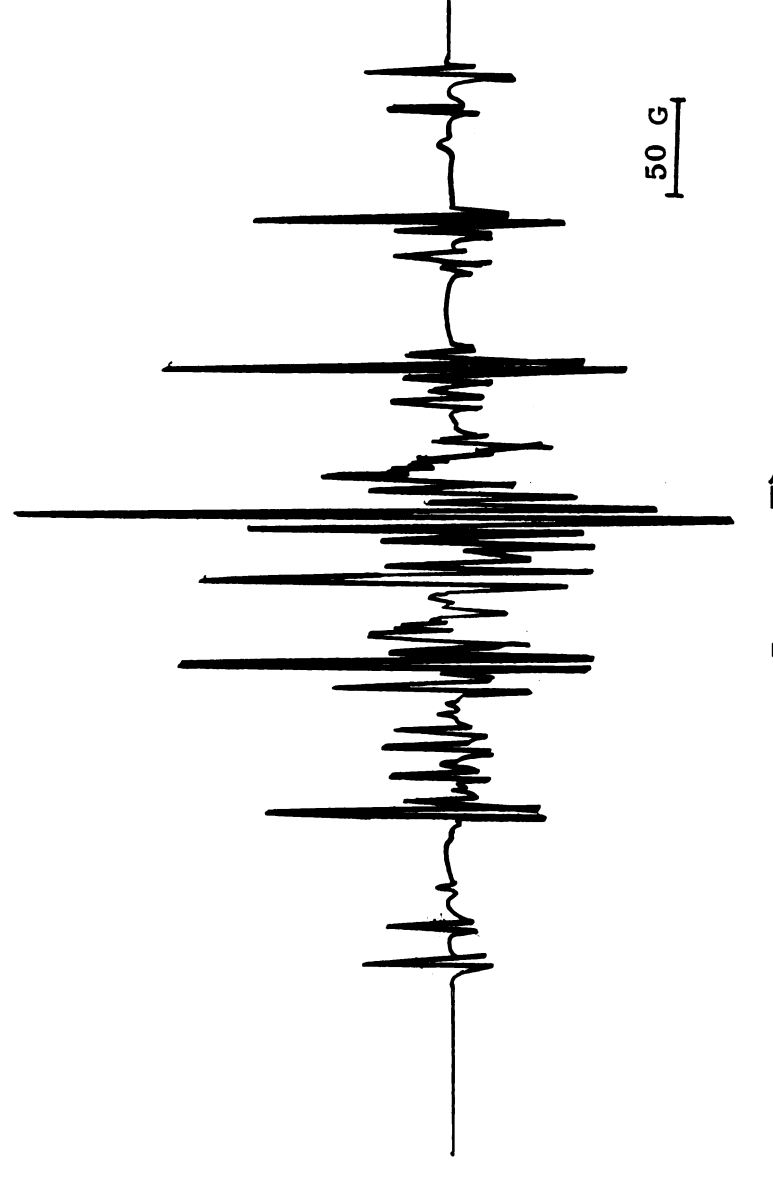


Figure 14. ESR spectrum of  ${\tt Cl}_2^-$  with  $\overline{{\tt H}}^>|\mid {\tt b}$  in the ab plane.



ESR spectrum of  $Cl_2$  with  $\overline{H}^> | |$  a in the ab Figure 15.

mini cal

plot

grap

twee axis

grou sul:

tin

the in

hyp cos:

the

Pigur

are theore

With th

the spe

tionship

is given

iere but :

all lines

minimum indicating that a maximum has occurred for the radical at a position somewhere between a and b.

In order to follow the hyperfine splitting in detail a plot of the splitting, A, was made in the three crystallographic reference planes as a function of  $\theta$ , the angle between the field direction and the respective crystallographic axis. The lines of maximum intensity for the seven basic groups of lines were followed in this manner and the results are given in Figures 16 to 18.

These plots were then used to fit the hyperfine splitting to Equation (46) and the principal values obtained by the diagonalization of the tensors according to the procedure in the Theoretical section. The principal values for the hyperfine tensor are given in Table XII with the direction cosines to the principal-axis system.

The experimentally determined hyperfine splittings and the measured intensities from Figure 11 are consistent with the presence of the radical anion  $Cl_2$ . The main lines in Figure 11 upon which the hyperfine splittings were based are the lines belonging to the  $\binom{35}{5}\text{Cl}^{-35}\text{Cl}$  species. The theoretical intensity ratios of 1:2:3:4:3:2:1 agree well with the experimentally measured ratios. The other lines in the spectrum of Figure 11 belong to the isotropic species  $\binom{35}{5}\text{Cl}^{-37}\text{Cl}$  and  $\binom{37}{5}\text{Cl}^{-37}\text{Cl}$ . A discussion of the relationship of these lines to those due to the  $\binom{35}{5}\text{Cl}^{-35}\text{Cl}$  species is given in Slichter's book  $\binom{82}{3}$  and will not be repeated here but it should be pointed out that using these arguments all lines can be accounted for.

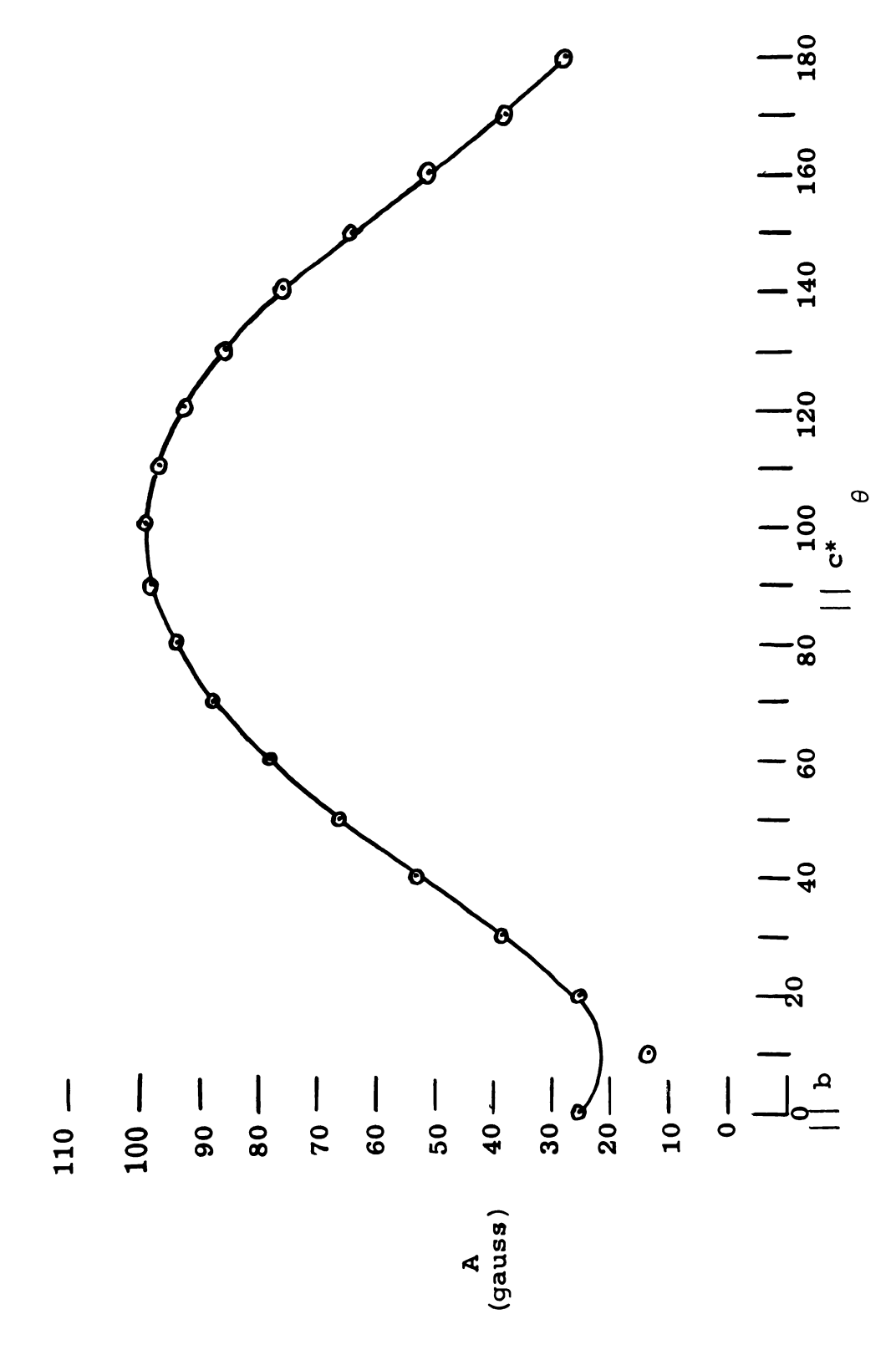


Figure 16. Hyperfine splitting of  $\mathrm{Cl_2}^-$  vs angle of rotation in the bc\* plane.

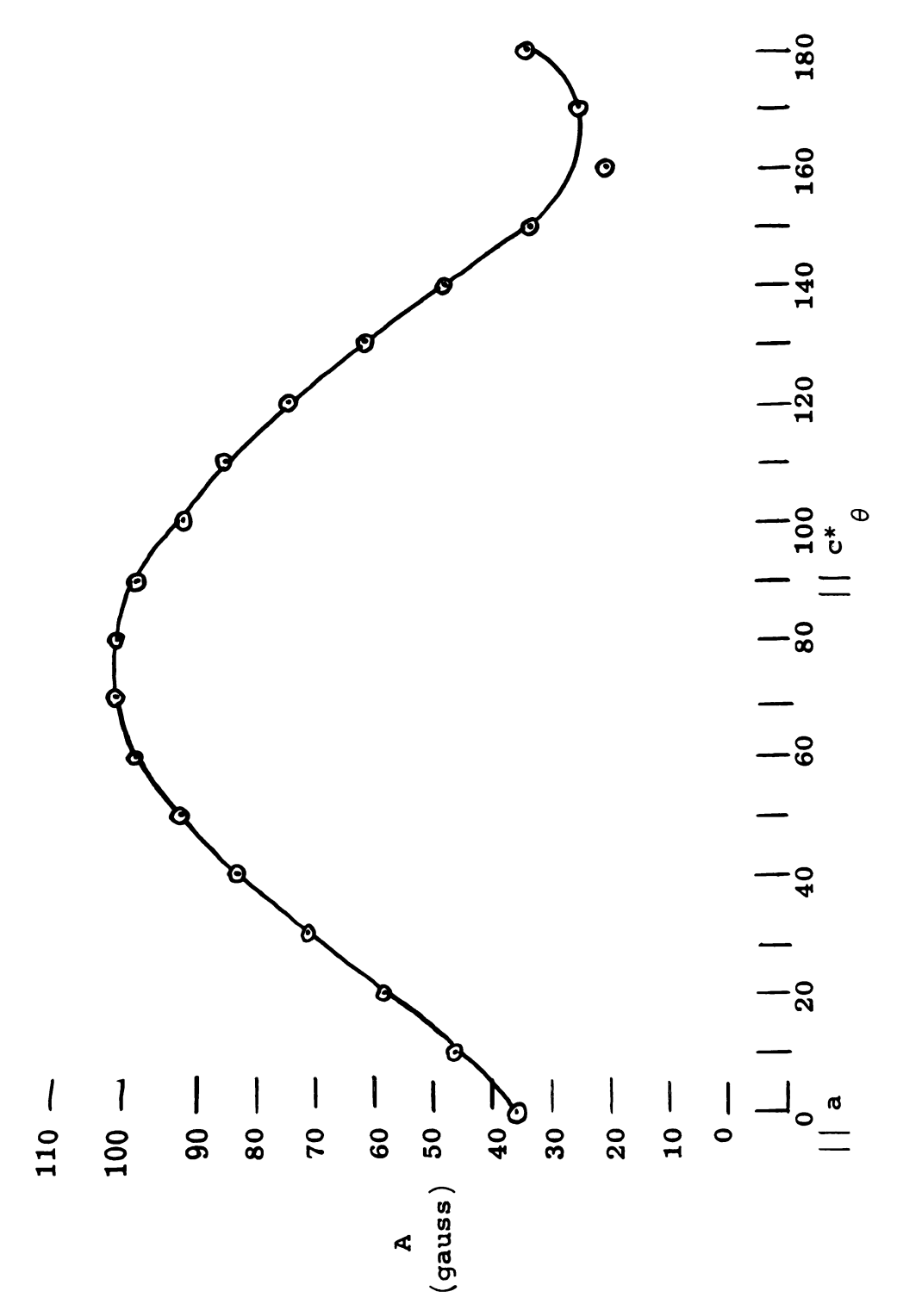


Figure 17. Hyperfine splitting of  ${
m Cl}_2^-$  vs angle of rotation in the ac\* plane.

- 00I

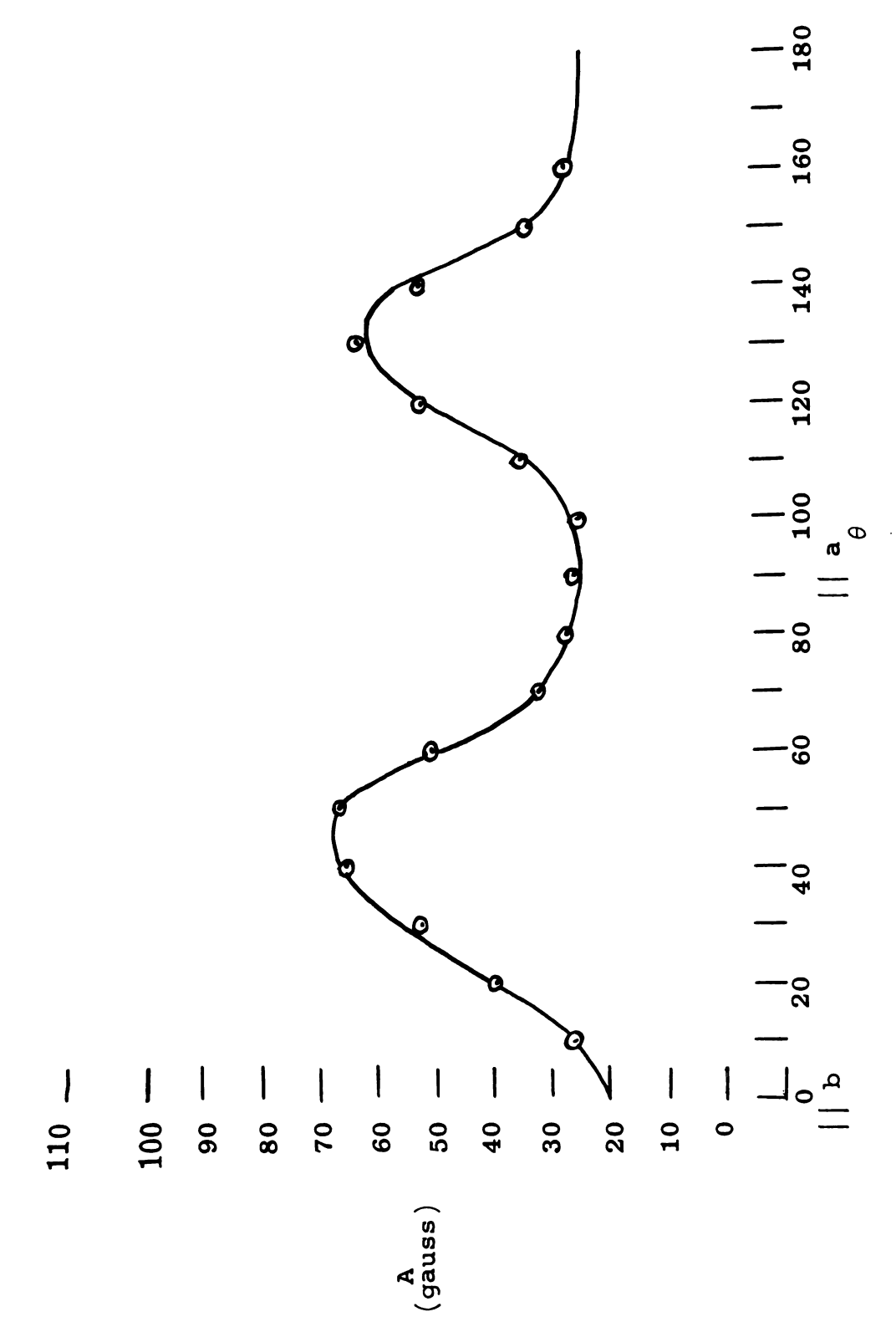


Figure 18. Hyperfine splitting of  $\mathrm{Cl}_2^-$  vs angle of rotation in the ab plane.

Table

Rad

С

Rad

C]

a Relat

Table XII. Principal hyperfine splitting and g values and their orientations for  $Cl_2$  radical in irradiated acetamidine hydrochloride.

Radical Cl <sub>2</sub>	Principal Values (gauss)		Direction Cosines		
	A <sub>C1</sub>	103.1	0.01	0.99	-0.07
		29.8	-0.52	0.07	0.85
		10.0	0.85	0.03	0.52

Radical	Principal Values g	Direction Cosines <sup>a</sup>		
	2.0437	0.08	0.18	0.98
	2.0317	-0.97	-0.18	0.12
	2.001	0.20	-0.96	0.16

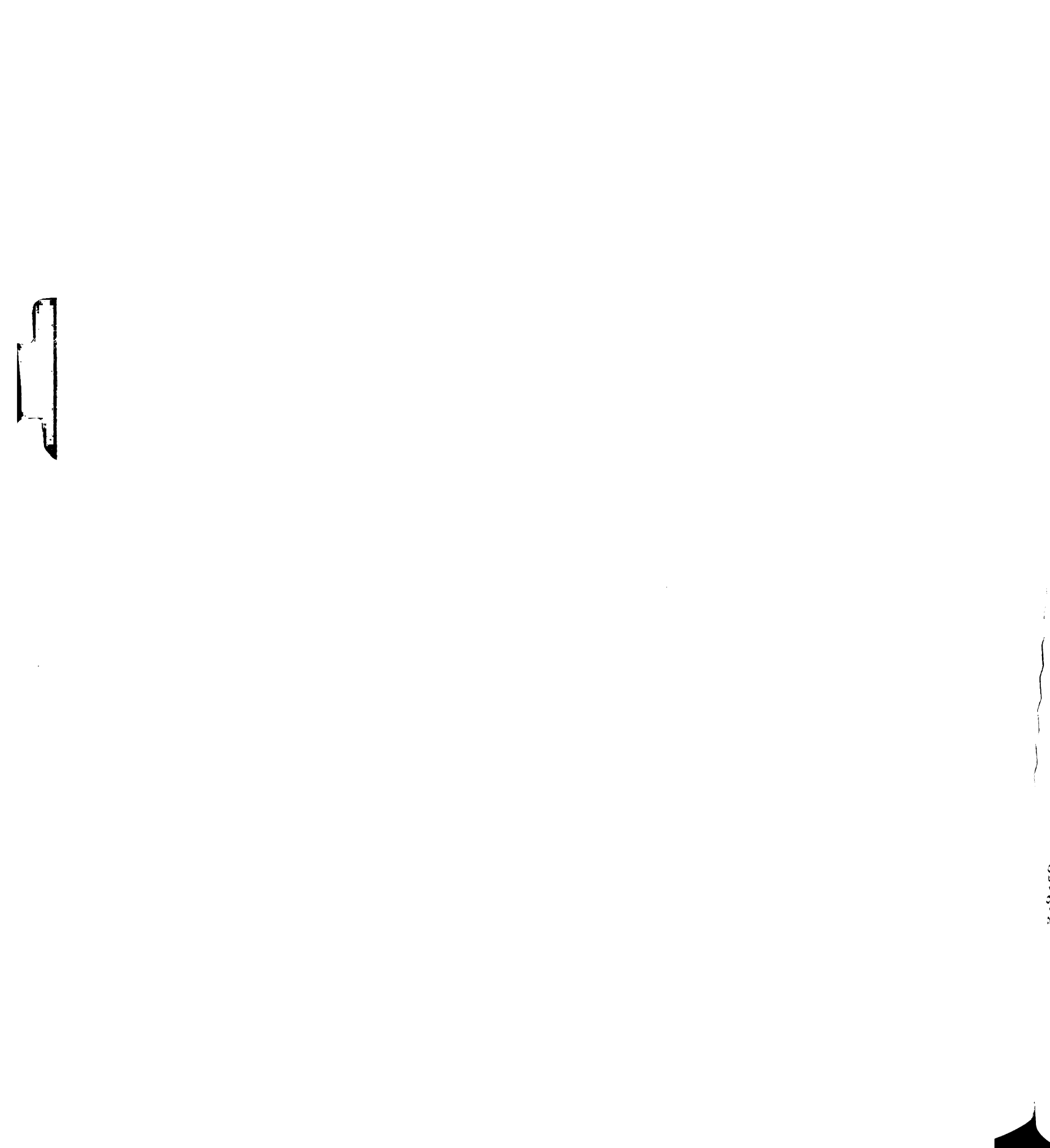
aRelative to a,b,c\* crystallographic axes.

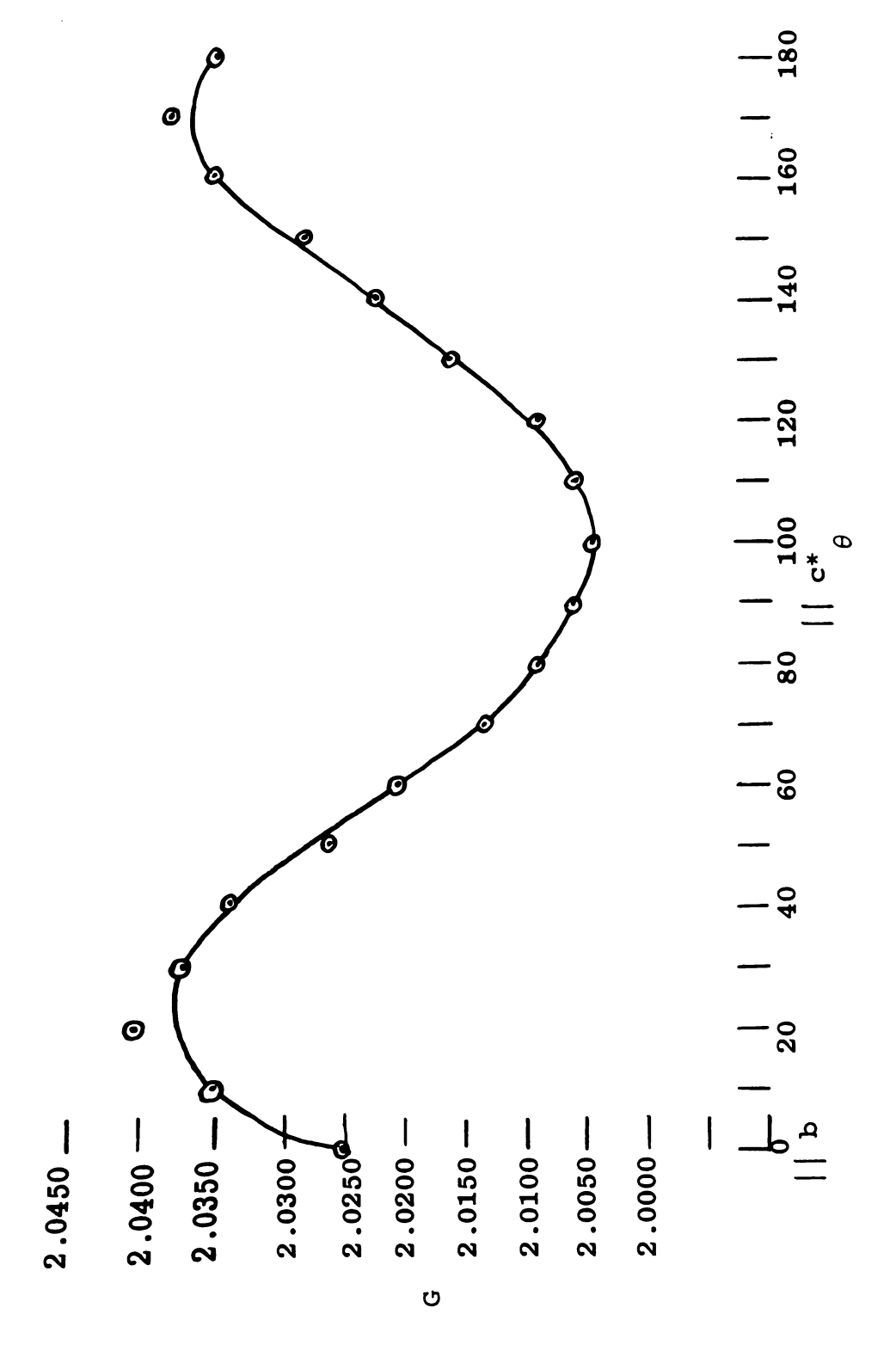
Since anisotropy of the  $\bar{g}'$  tensor exists for  $\mathrm{Cl}_2^-$  due to an admixture of the  $\pi_g$  excited state with the  $\sigma_g$  ground state (82), the principal values of the  $\bar{g}'$  tensor were also determined. This was accomplished by measuring the angular variation of g as a function of  $\theta$  and diagonalizing in the usual manner. The plots of angular variation for g are given in Figures 19-21. Principal values of the  $\bar{g}'$  tensor and the associated direction cosines are given in Table XII.

## 2) High-Temperature Radical ·CH<sub>2</sub>-C-NH<sub>2</sub>

It was felt that perhaps other radicals might be detected in addition to the radical  $\operatorname{Cl}_2^-$  observed at  $77^0\mathrm{K}$ . In order to determine whether this was the case, a single crystal of acetamidine hydrochloride was electron irradiated with the G.E. Resonant Transformer for 10 minutes at  $77^0\mathrm{K}$ . The single crystal was then allowed to warm up using a liquid nitrogen-isopentane slush bath maintained at  $-150^\circ$ . The crystal was mounted periodically and a spectrum recorded to detect whether  $\operatorname{Cl}_2^-$  was still present as the crystal was warmed. The presence of  $\operatorname{Cl}_2^-$  hampered the identification of any other radical due to the large number of lines.

After 1 hour at  $-150^{\circ}$  the crystal was removed from the slush bath and remounted in the crystal holder. It was found after 1 hour that all  $\text{Cl}_2^-$  had disappeared and a new radical was present. Figure 22 shows a spectrum of the new radical with the magnetic field  $60^{\circ}$  from b in the ab plane.





vs angle of rotation for Cl2 in the bc\* plane. ש Plot of Figure 19.



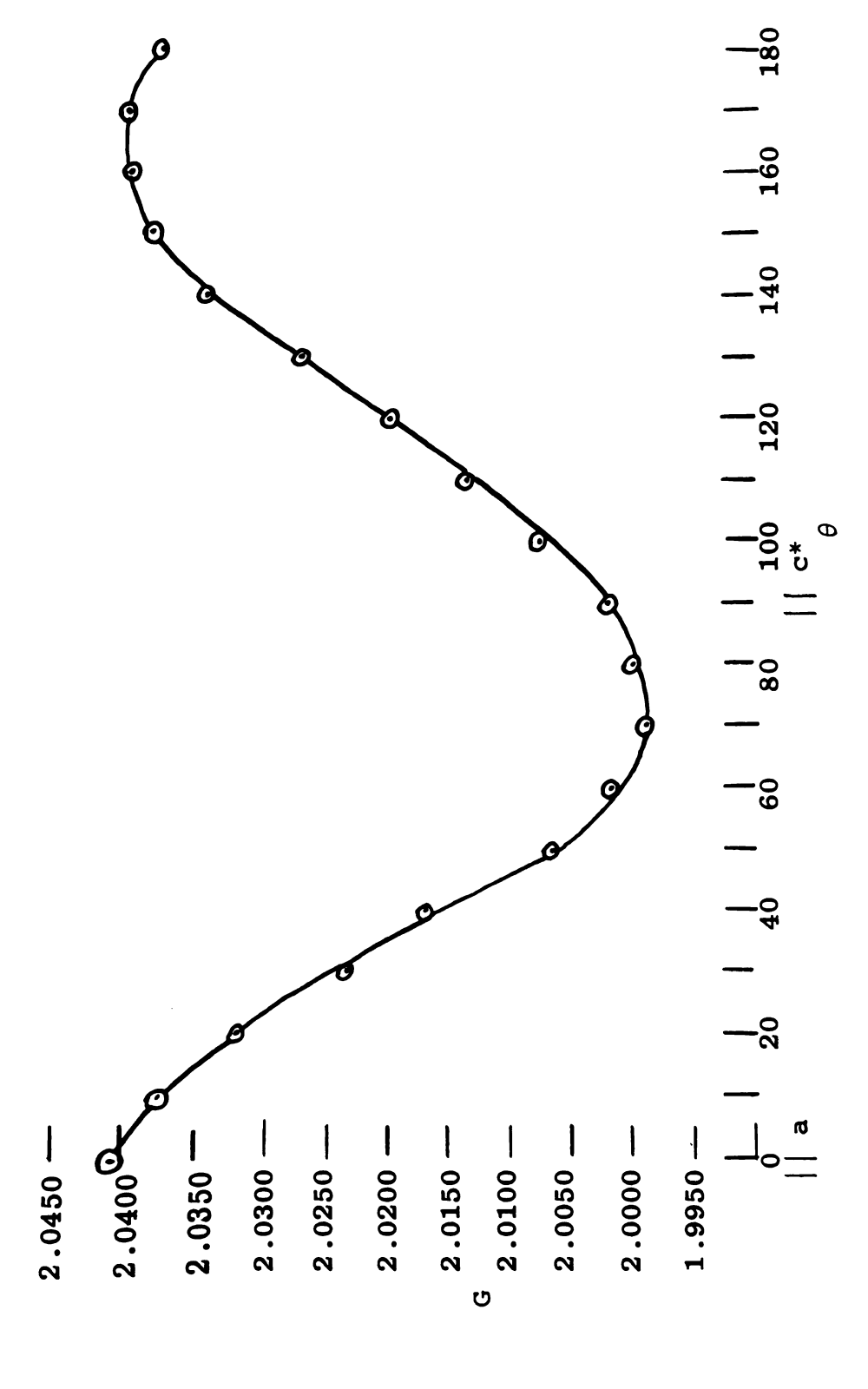
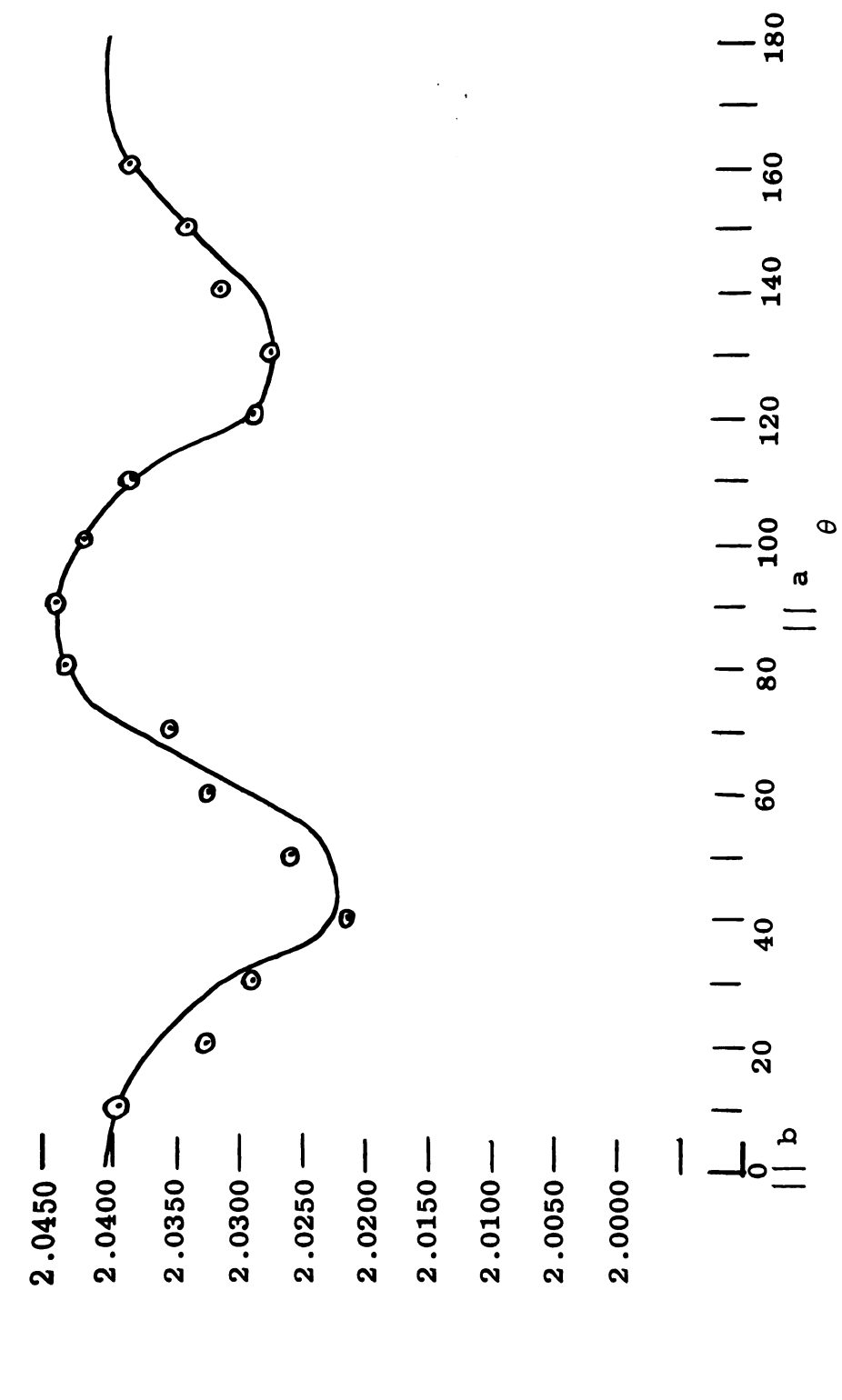


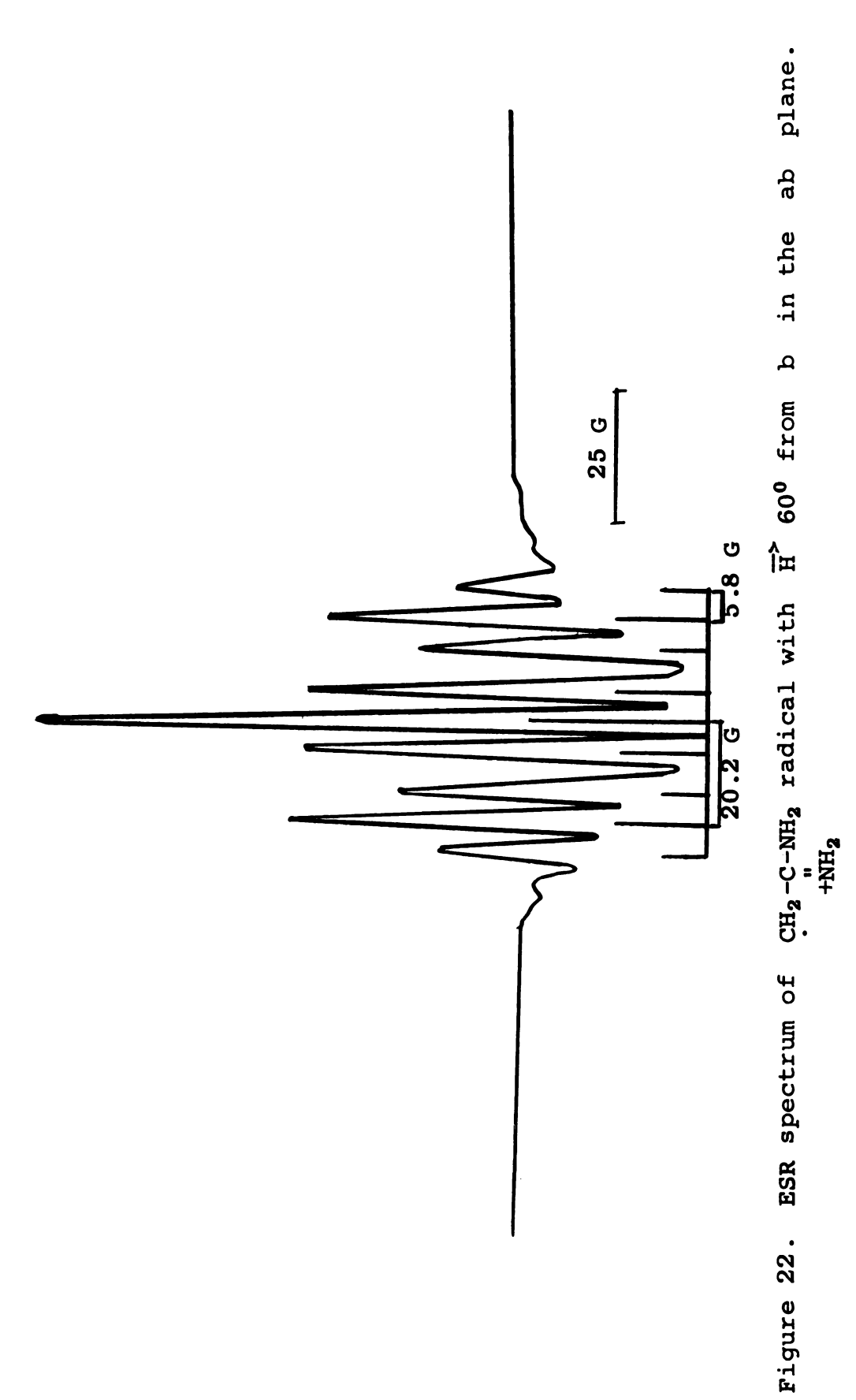
Figure 20. Plot of g  $\overline{\text{vs}}$  angle of rotation for  $\text{Cl}_2^-$  in the ac\* plane.

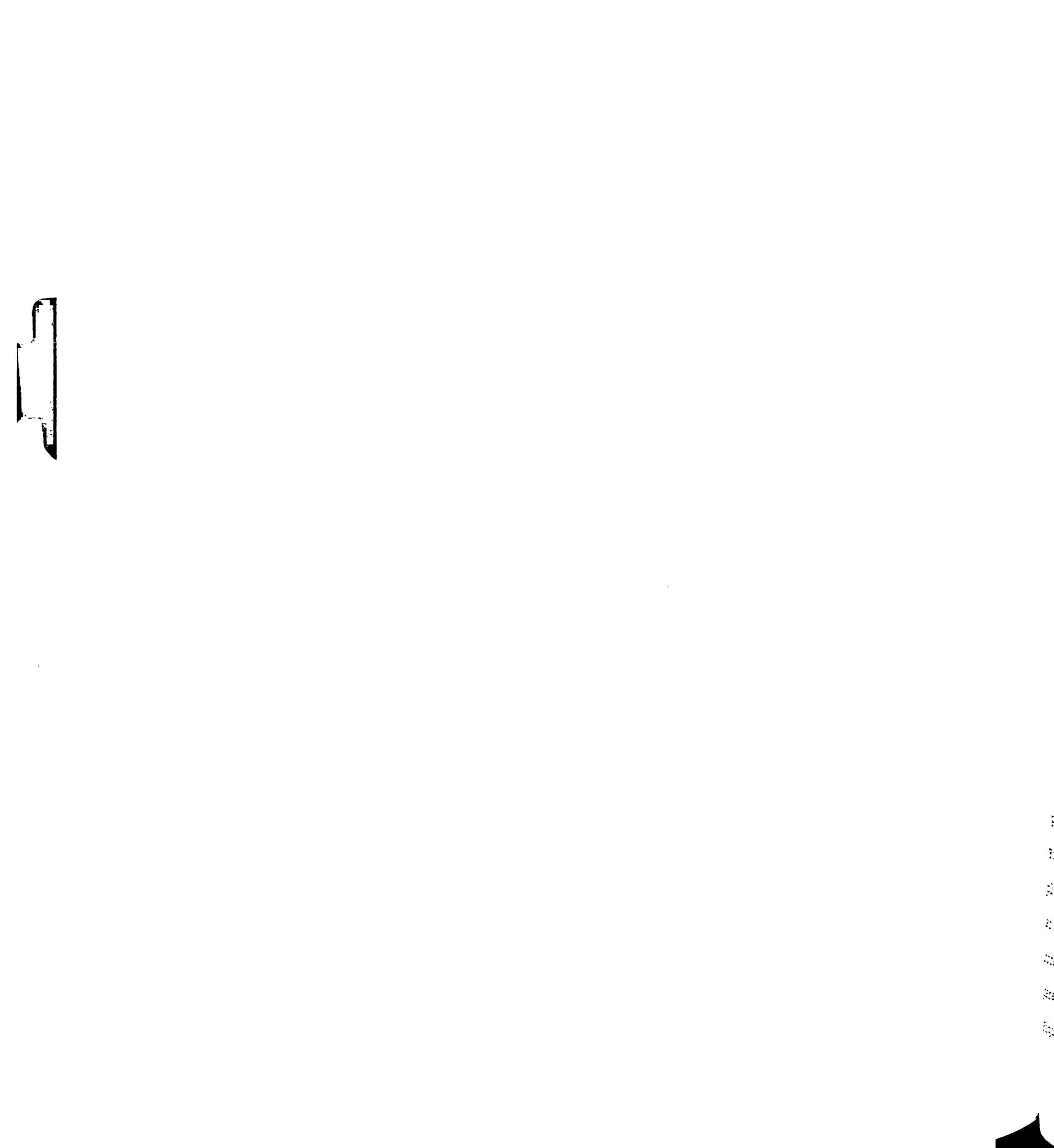


2.0550 —

2.0500 -

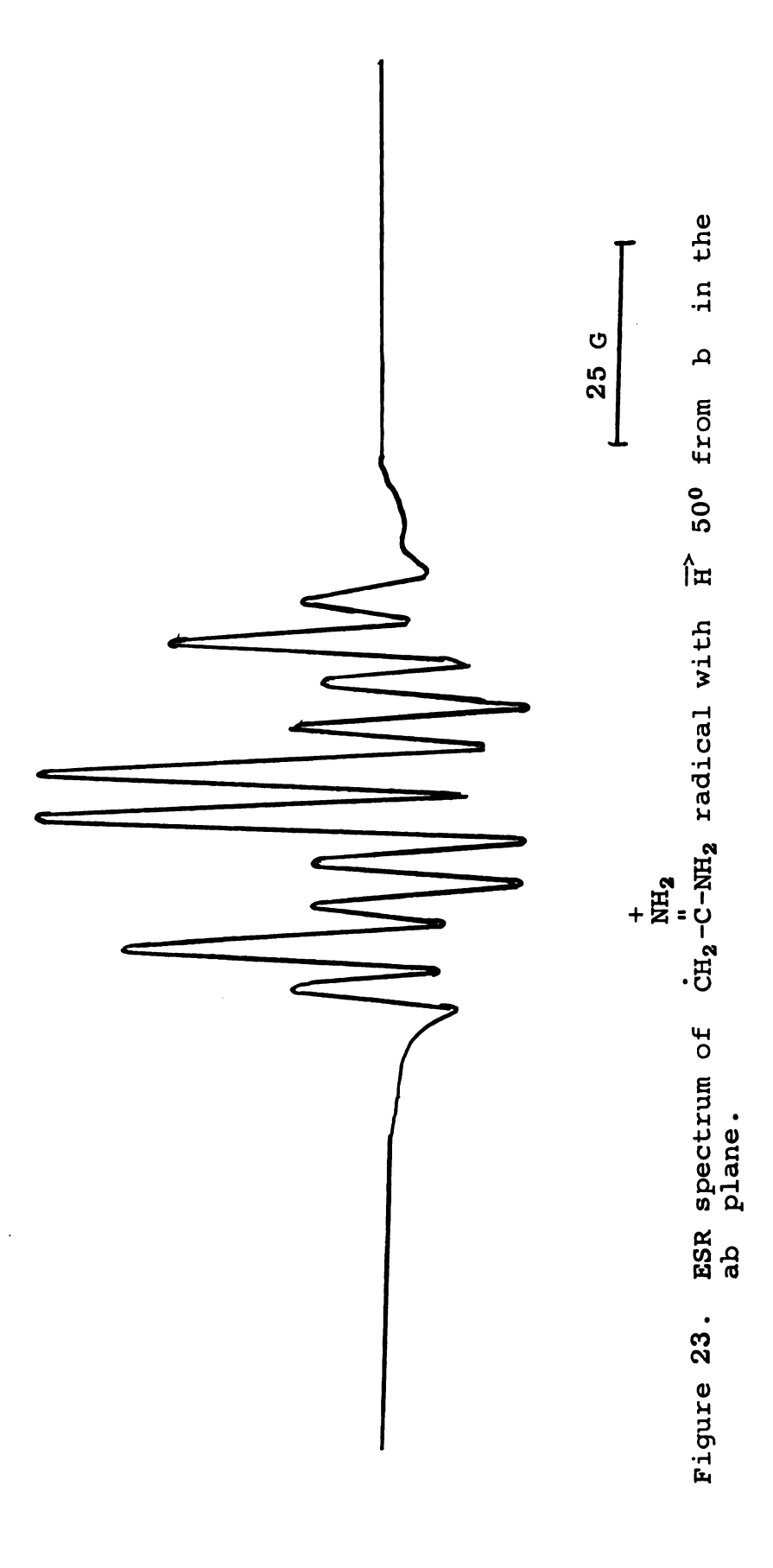
Figure 21. Plot of g  $\overline{\text{vs}}$  angle of rotation for  $\text{Cl}_2^-$  in the ab plane.

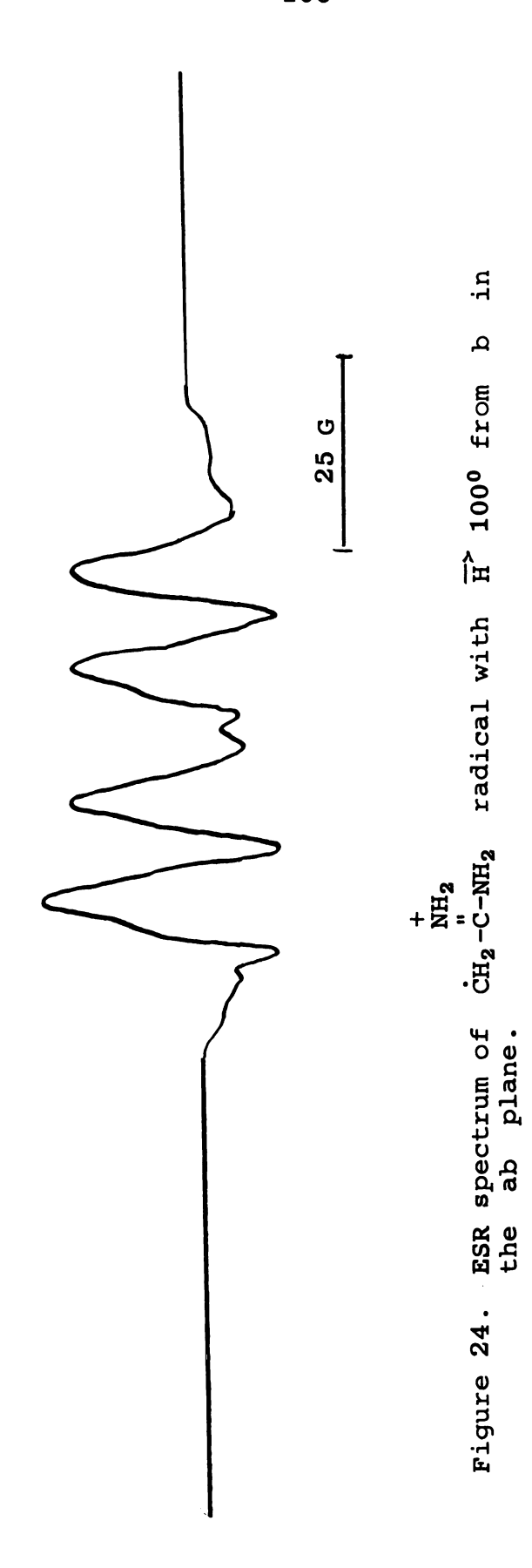


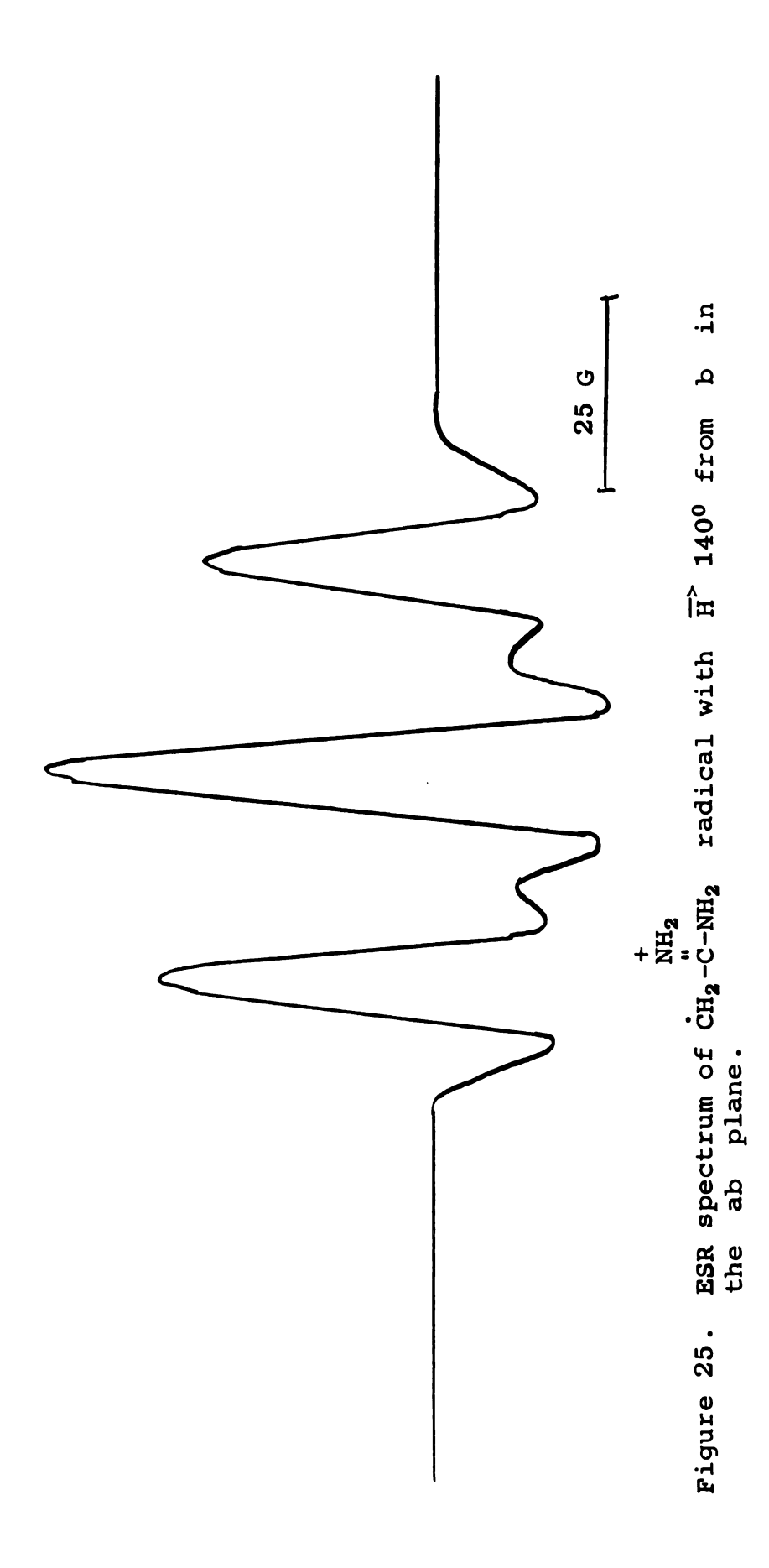


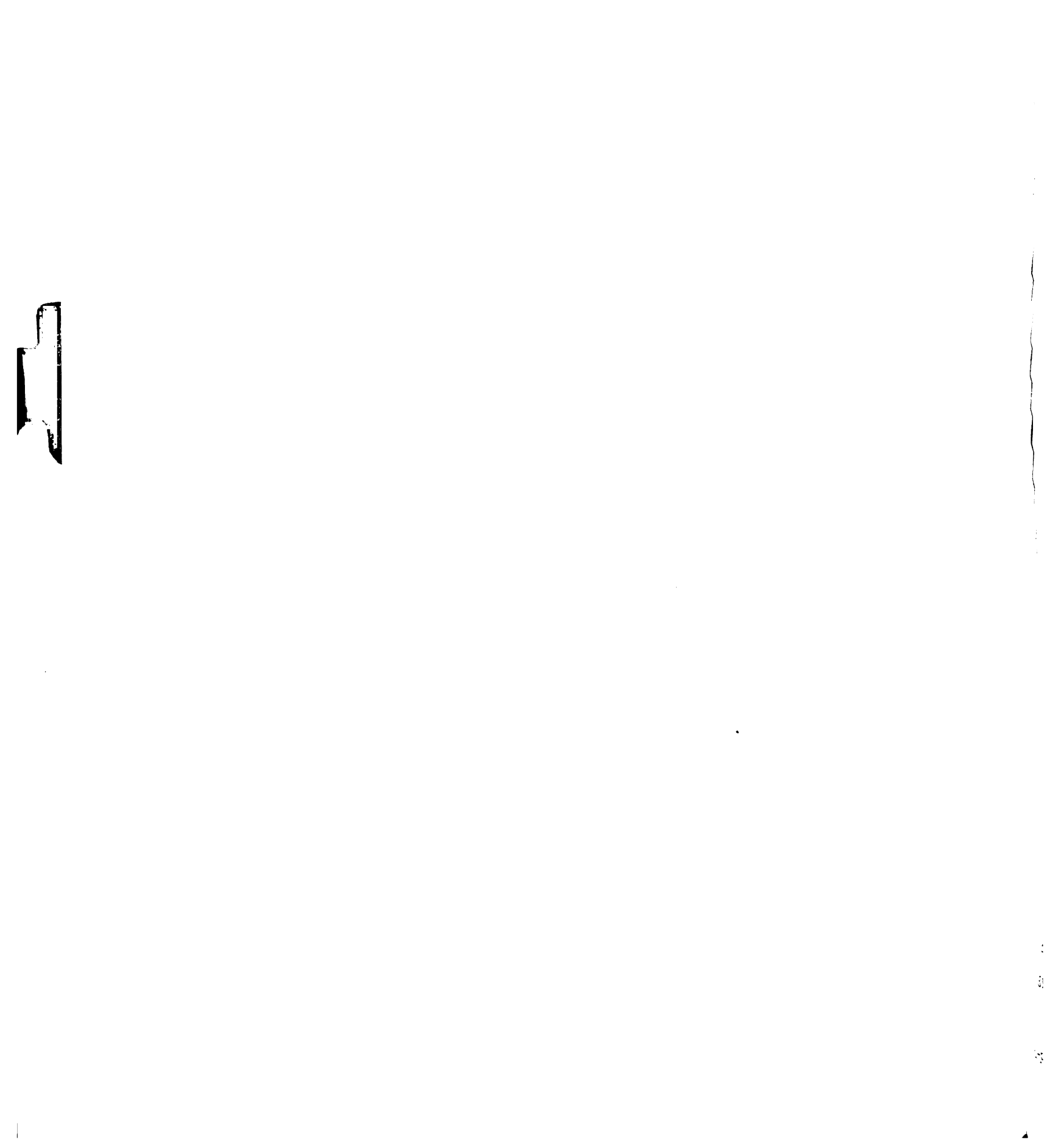
The appearance of the spectrum is a triplet of triplets with intensity ratios of 1:2:1:2:4:2:1:2:1. The larger triplet spacing is 20.2 gauss and the smaller 5.8 gauss as indicated in Figure 22. As the crystal is rotated in the ab plane a more complicated pattern appears at  $50^{\circ}$  and  $70^{\circ}$ from b in the ab plane. Figure 23 shows the pattern with the magnetic field at  $50^{\circ}$ , which is identical to that observed at  $70^{\circ}$ . This pattern consists of a quartet of approximately 1:1:1:1 intensity ratio with the smaller splitting of 5.8 gauss still present. Further rotation in the ab plane gives a quartet of 1:1:1:1 intensity ratio at 1000 from b as is seen in Figure 24. The smaller 5.8 gauss splitting has been lost in the line width at  $100^{\circ}$ . The spectrum simplifies further at  $140^{\circ}$  from b in the ab plane where a triplet is observed. Figure 25 shows this case with the splitting between these lines being 22.7 gauss. The measured intensity ratio at this orientation is 1:1.7:1.2.

Spectra in the ac\* and bc\* planes show similar patterns to those observed in the ab plane. In the ac\* plane with H || a an identical spectrum to that in Figure 23 results. As the crystal is rotated in the ac\* plane toward c\* the pattern simplifies to a triplet and at 90° (H || c\*) becomes similar to Figure 25. Continued rotation restores the spectrum of Figure 23 when H becomes parallel to a. In the bc\* plane a triplet similar to Figure 25 is observed when H || b , changing to the spectrum









of Figure 23 at  $80^{\circ}$  from b in the bc\* plane. The spectrum of Figure 22 is observed at H || c\* in the bc\* plane. Continuing the rotation in the bc\* plane gives a quartet similar to Figure 24 at  $160^{\circ}$  from b. This quartet reverts to the triplet of Figure 25 when the field becomes parallel to b in the bc\* plane.

The larger hyperfine splitting of 20.2 gauss for the triplet of triplets observed in Figure 22 can be interpreted as arising from the interaction of the odd electron with two equivalent protons, and smaller 5.8 gauss splitting could arise from interaction of the odd electron with a second set of two equivalent protons. This would result in a triplet of triplets with intensity ratios 1:2:1:2:4:2:1.2:1 as observed, so the interpretation of the spectra using these criteria was attempted. If the large 20.2 gauss proton splitting is attributed to two equivalent a protons the pattern should change to a quartet with two different splittings, one larger and one smaller, if the protons become nonequivalent. Such behavior is observed in Figure 23 where the quartet is attributed to two different  $\alpha$  proton hyperfine splittings, one of which has increased to 22.3 gauss and the second has decreased to 17.1 gauss. An even larger splitting occurs for the field at 1200 from b in the ab plane where one measured  $\alpha$  proton splitting becomes 31.5 gauss.

Using the above arguments the angular variation of the  $\alpha$ -proton lines was plotted in each of the ab, bc\*, and c\*a

planes. These plots are presented in Figures 26-28. The principal values for the  $\alpha$ -proton hyperfine coupling tensor were obtained using Equation (46). The values and direction cosines for the two  $\alpha$  protons are given in Table XIII. The isotropic values agree well with other  $\alpha$ -proton splittings reported in the literature (Table I). The principal values are somewhat different from the normal -10, -20, -30 gauss principal values expected for an  $\alpha$  proton but the values do appear reasonable for  $\alpha$  splittings.

In order to confirm that the 5.8 gauss splitting in Figure 22 belongs to the protons on the  $-\mathrm{NH}_2$  group, the ESR spectrum of a single crystal of acetamidine hydrochloride in which deuterium had replaced hydrogen was analyzed. The deuterated crystal was electron irradiated for 3 minutes at  $77^0\mathrm{K}$  and then warmed to  $-125^0$  for 1 hour to remove  $\mathrm{Cl}_2^{-1}$ .

It was found that  ${}^{\circ}CH_2 - {}^{\circ}C - NH_2$  radical was stable at  $-125^{\circ}$  and the higher temperature increased the rate of decay of  $Cl_2$ .

The deuterated crystals were not well formed but it was possible to identify the b axis with certainty and this allowed an analysis of spectra in the c\*a plane.

With H || a in the ac\* plane it was found that the spectrum of Figure 23 had changed so that now a quartet appeared with intensity ratios 1:1:1:1 as is seen in Figure 29. On rotation of the field in the c\*a plane to H || c a triplet with intensity ratios of 1:2:1 was obtained (Figure 30).

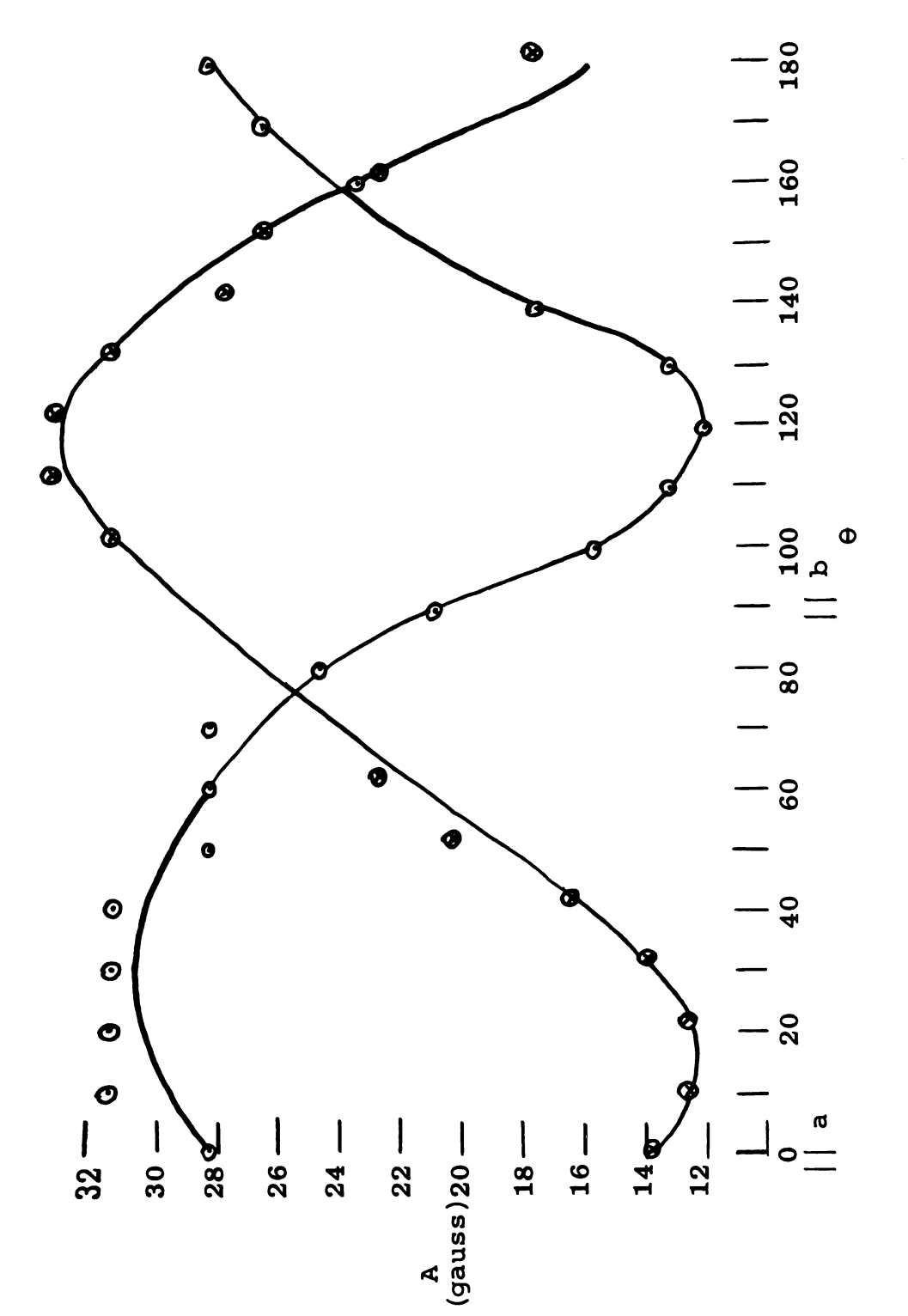


Figure 26. Angular variation in the ab plane of hyperfine splittings for  $\alpha$  protons +NH2 in  $\dot{c}_{H_2}-c_{-NH_2}$  radical.

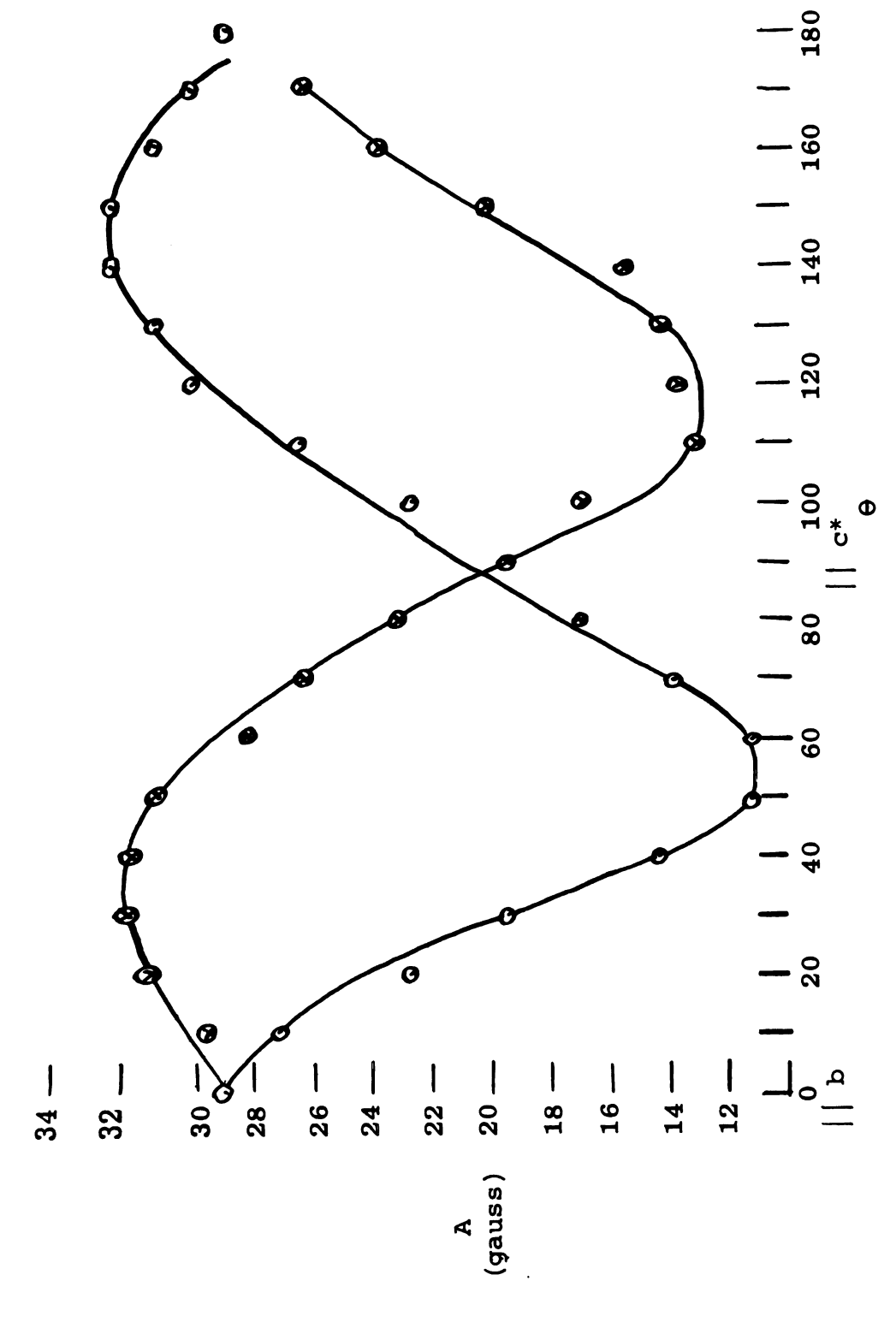
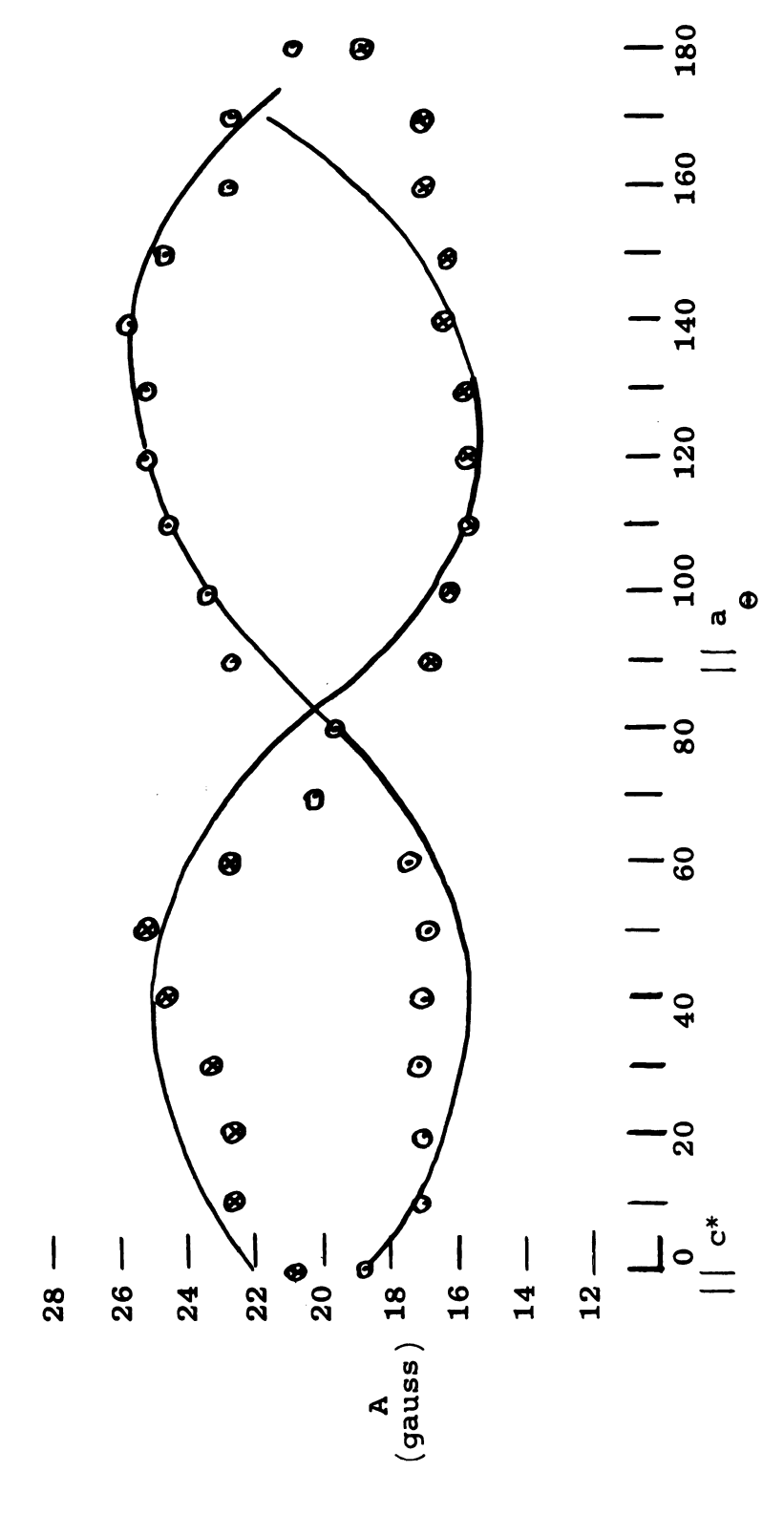


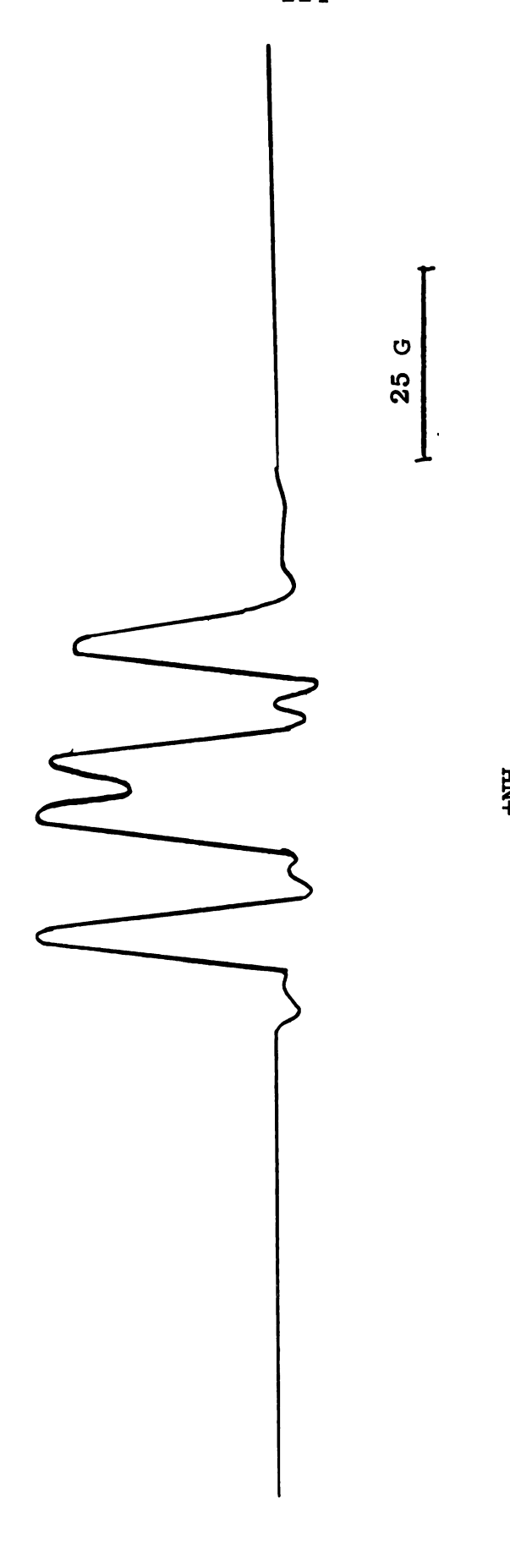
Figure 27. Angular variation in the bc\* plane of hyperfine splittings for  $\alpha$  protons +NH2 in  $\dot{c}_{H_2}$  radical.



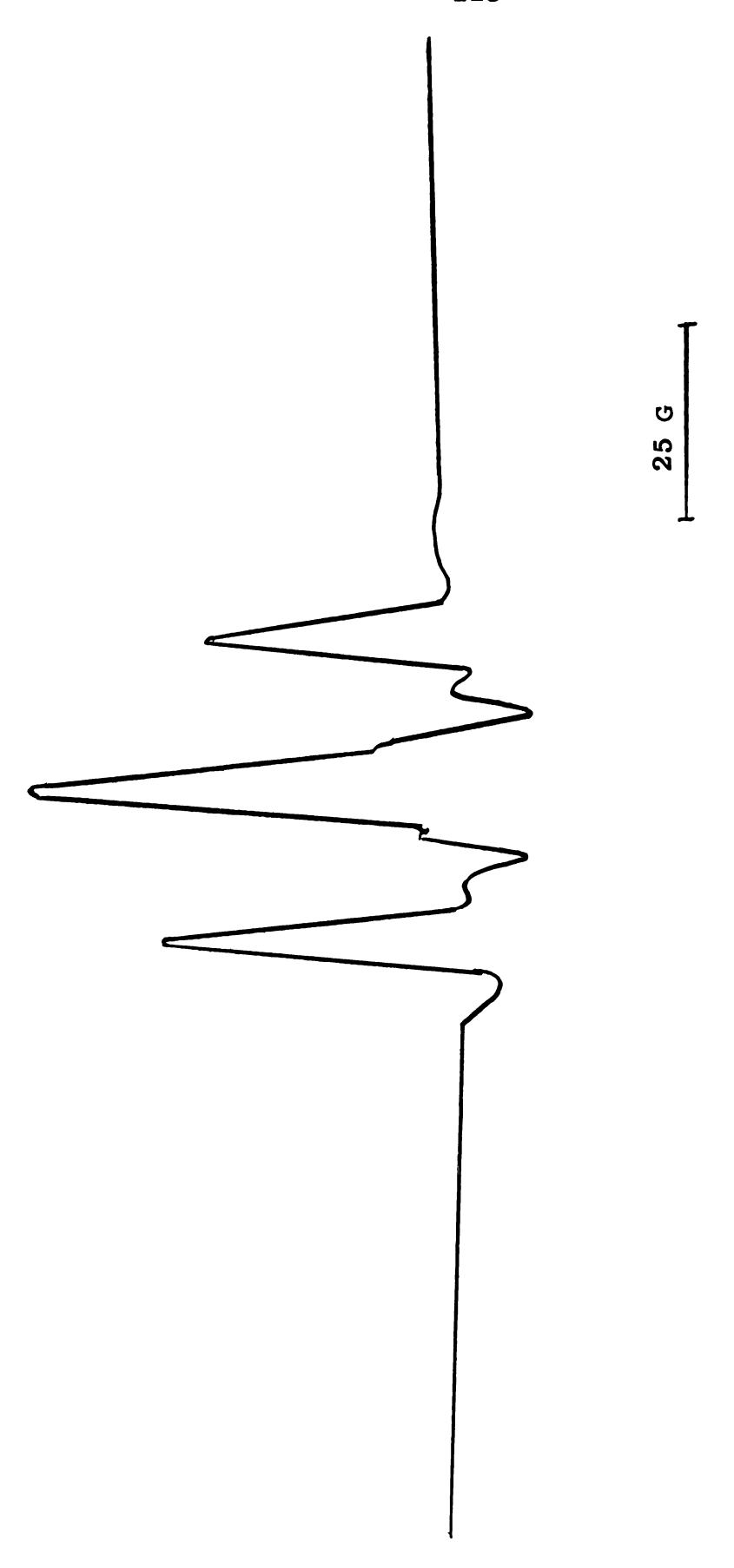
plane of hyperfine splittings for  $\alpha$  protons **a**G\* Figure 28. Angular variation in the +NH2  $$^{+}$  in  $\mathring{C}H_{2}-\mathring{C}-NH_{2}$  radical.

Table XIII. Principal values of the hyperfine splitting tensor for the two nonequivalent  $\alpha$  protons in  ${^{\circ}CH_2-C-NH_2}$  radical.  ${^{\circ}NH_2}$ 

Proton	Principal Values {( <b>g</b> auss)	Dire	ction Co	sines
1	-35.9	0.79	0.49	0.36
	-23.1	-0.58	0.44	-0.68
	- 7.5	-0.17	0.75	0.64
	$A_{iso} = -22.2$			
2	-36.2	0.06	0.92	0.38
	-19.0	-0.61	0.34	-0.72
	- 5.8	-0.79	-0.19	0.58
	$A_{iso} = -20.3$			



ESR spectrum of deuterated  $c_{H_2}$  \_ adical with  $\overline{H}^{>}\,|\,|\,|\,|\,|\,|\,|$  ac\* plane. Figure 29.



ESR spectrum of deuterated  $\dot{c}_{H_2}$ -C-NH2 radical with  $\overline{H}^>|\mid c^*$  in the ac\* plane. Figure 30.

At no orientation in the c\*a plane was any hyperfine structure detectable with a splitting value near 5.8 gauss. This provided conclusive proof that the smaller splitting results from protons on the -NH<sub>2</sub> group.

It was possible to obtain principal values of the tensor for the  $-\mathrm{NH_2}$  protons using Schonland's method (Equation 48). It was not possible to plot these lines as was done previously since at orientations where the splitting was small it was lost in the linewidth of the lines from the  $\alpha$  protons. The maximum and minimum hyperfine splitting and the angle at which the maximum splitting occurs, along with the principal values obtained, are given in Table XIV.

The hyperfine splitting values for the -NH<sub>2</sub> protons are in reasonable agreement with those reported recently (139) for X-irradiated succinamide. Kashiwagi reports principal values of -1, -3 and -6 gauss for the -NH<sub>2</sub> protons

in H<sub>2</sub>N-C-CH<sub>2</sub>-CH-C-NH<sub>2</sub> radical. This is reasonable agreement with the -1.7, -4.1, -6.4 gauss principal values reported in this case where the negative signs were selected to agree with those reported by Kashiwagi.

### II. Irradiated Trimethylacetamide Single Crystal

#### A. Crystal Structure

No previous report of the unit cell and space group of trimethylacetamide could be found so that it was necessary to determine these by the usual techniques. Weissenberg

Table XIV. Hyperfine splitting values for -NH $_2$  protons in  $^{\circ}\text{CH}_2$  -C-NH $_2$  radical  $^{"}_+\text{NH}_2$ 

Plane	A <sub>max</sub> (gauss)	A <sub>min</sub> (gauss)	$ heta_{ exttt{max}}$ (degrees)
ab	6.0	<b>≌ 0.0</b>	150
bc*	6.3	<b>≅ 0.0</b>	100
c*a	6.0	≅ 0.0	80

Radical	Principal Values (gauss)	Direction Cosines		
+NH <sub>2</sub> •CH <sub>2</sub> -C-NH <sub>2</sub>	-6.4	0.83	-0.42	0.37
(-NH <sub>2</sub> Protons)	-4.1	0.40	9.0≌	-0.91
	-1.7	0.39	0.91	0.17

layer photos and Precession photos showed the unit cell to be monoclinic with cell dimensions a = 12.84 Å, b = 10.27 Å, c = 5.18 Å, and  $\beta = 106^{\circ}$ . Restrictions for reflections were 001, l = 2n; 0k0, k = 2n; h01, l = 2n which is consistent with the spece group P2<sub>1</sub>/c. The density of the crystal was measured in a mixture of carbon tetrachloride ( $\rho = 1.589$  g/ml) and n-heptane ( $\rho = 0.684$ ) and the value found was 1.056 g/ml. The calculated number of molecules per unit cell using this density is 4.17 in good agreement with the theoretical number for the space group P2<sub>1</sub>/c, which is four.

The crystals grew as large hexagonal plates (Figure 31) with the large face perpendicular to the a\* axis. The crystal was easily mounted with the long edge along b.

Single crystals of trimethylacetamide were γ-irradiated for 3 hours at 77°K and were then mounted without warmup according to the usual procedure. According to previous ESR studies of irradiated trimethylacetamide (140) the radical observed at -140° is t-butyl radical. The spectrum from t-butyl radical would be expected to consist of ten lines with intensity ratios of 1:9:36:84:126:126:84:36:9:1 assuming that the nine protons were coupled equivalently to the odd electron.

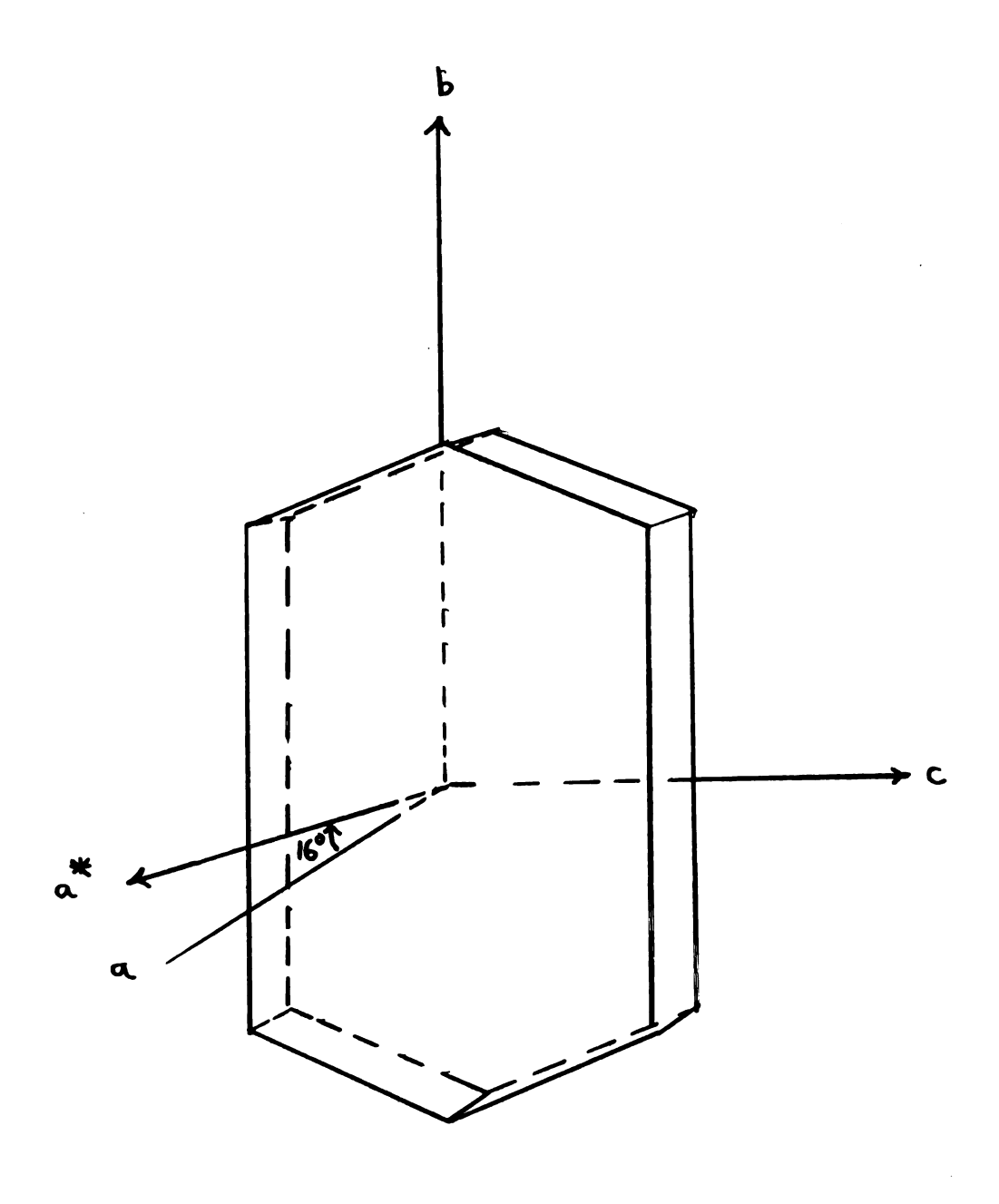


Figure 31. Crystallographic axes for trimethylacetamide.

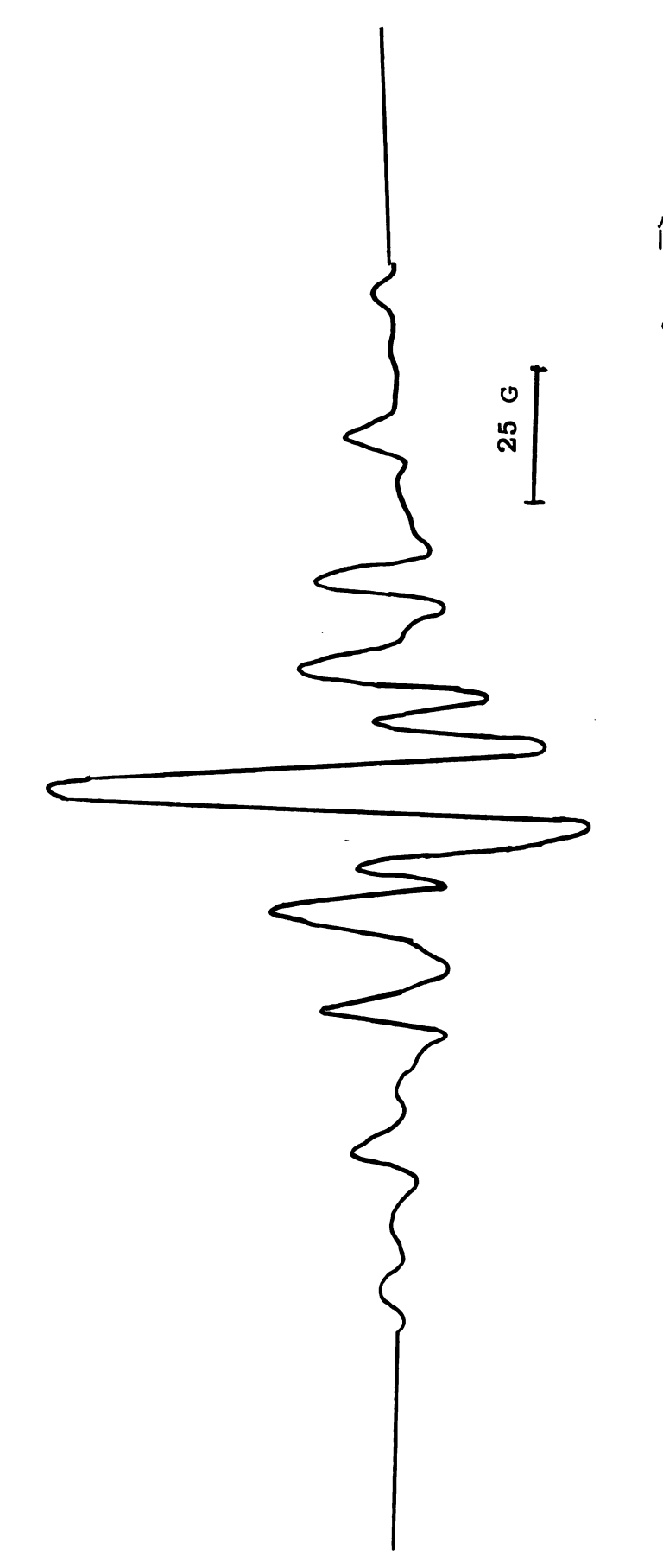
The type of spectrum observed at 77°K in γ-irradiated single crystals of trimethylacetamide is shown in Figure 32. The magnetic field in Figure 32 is 60° from the b axis in the a\*b plane. The presence of t-butyl radical is evident although only eight lines of the expected ten-line pattern are seen. If it is assumed that these eight lines are the central lines of a ten-line spectrum the experimentally observed intensity ratios (1:9:38:75:128:128:77:36:9:1) are in reasonably good agreement with the theoretical values. The hyperfine splitting at this orientation is 22.9 gauss.

In addition to the ten-line pattern attributed to the <u>t</u>-butyl radical a three-line pattern is also present.

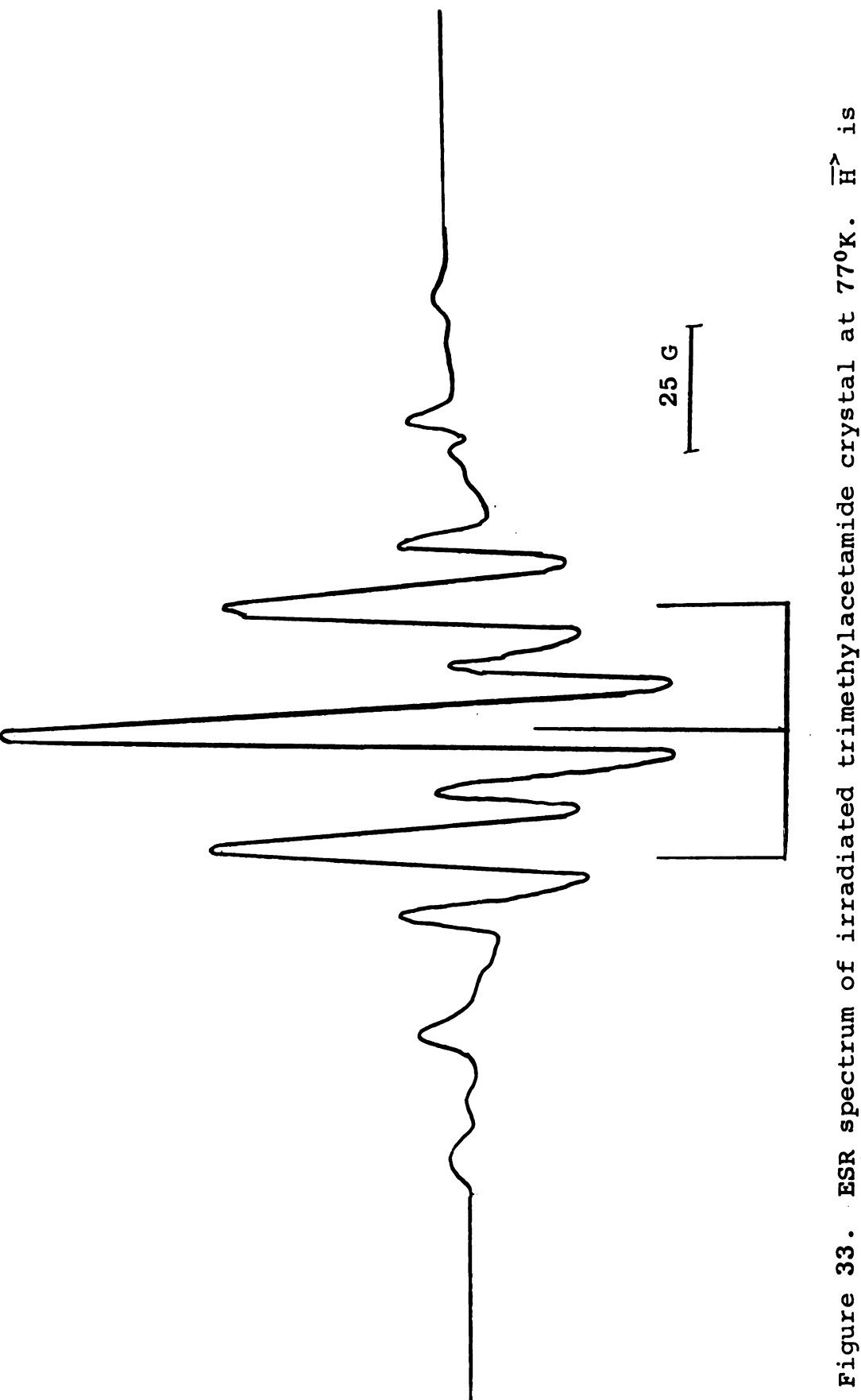
Figure 33 shows the spectrum obtained when the magnetic field is 30° from the axis c in the a\*c plane. The intensity ratios at this position for the three-line pattern are 1:1.9:1. The measured hyperfine splitting is 22.4 gauss. The same three-line pattern is also evident in Figure 32 although the intensities are not as easily measured. This

 $\mathring{\text{CH}}_2$  O three-line pattern is attributed to the  $\text{CH}_3$ - $\overset{\circ}{\text{C}}$ - $\overset{\circ}{\text{C}}$ - $\text{NH}_2$ 

radical for which coupling to two equivalent  $\alpha$ -protons would give rise to the triplet with 1:2:1 intensity ratios and -22.4 gauss hyperfine splitting. Deuteration showed this to be the correct assignment since the spectrum of  $\cdot$ CONH<sub>2</sub> would be lost upon deuteration. The same spectrum was observed after deuteration. The negative sign is selected to



is ľΞ ESR spectrum of irradiated trimethylacetamide crystal at  $77^0\mathrm{K}.$  60° from b in the a\*b plane. Figure 32.



is ESR spectrum of irradiated trimethylacetamide crystal at  $77^0 {\rm K}_{\odot}$ . 60° from c in the a\*c plane. Figure 33.

agree with previously reported  $\alpha$  proton splittings but is not determined in these experiments.

As the crystal was rotated in the a\*b, a\*c, and bc planes a negligible amount of anisotropy was noted in the spectrum of the <u>t</u>-butyl radical. At all positions in each of the three crystallographic planes the hyperfine splitting remained close to 22.9 gauss. Also in the case of the

detected indicating that this radical must be rapidly reorienting at 77°K.

The measured hyperfine splittings for both radicals are presented in Table XV.

# C. <u>Temperature Studies</u>

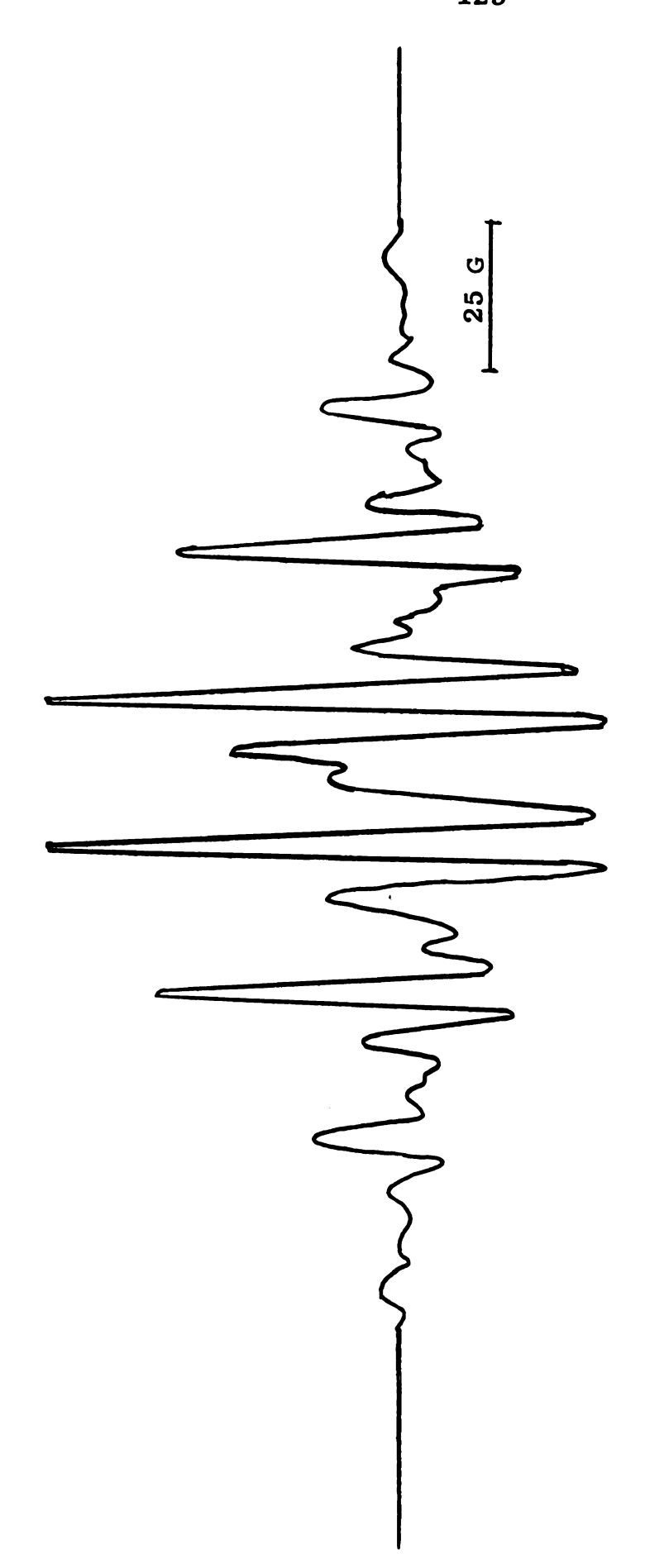
The single crystal of trimethylacetamide which had been  $\gamma$ -irradiated for 3 hours was first warmed to  $-80^{\circ}$  in a dry ice-acetone slush bath. The crystal was allowed to warm for ten minutes at  $-80^{\circ}$  and then remounted in the crystal holder.

The spectrum of Figure 34 was recorded at  $77^0 K$  after warming. The magnetic field is parallel to the c axis in the a\*c plane. As can be seen from Figure 34 the tenline pattern attributed to  $\underline{t}$ -butyl radical is still present

while the three-line pattern attributed to 
$$CH_3$$
- $C$ - $C$ - $NH_2$ 

Table XV. Hyperfine splittings for radicals in irradiated trimethylacetamide

Radical	Hyperfine Splitting (gauss)
CH <sub>3</sub>	$A_{H} = 22.9$
CH <sub>3</sub> -C· CH <sub>3</sub>	$A_{z}^{(13}C) = 92.0$
$ \begin{array}{ccc} \dot{\text{CH}}_2 & \text{O} \\ \dot{\text{CH}}_3 - \dot{\text{C}} & - \ddot{\text{C}} - \text{NH}_2 \end{array} $	
CH <sub>3</sub> -C - C-NH <sub>2</sub> CH <sub>3</sub>	$A_{H} = -22.4$



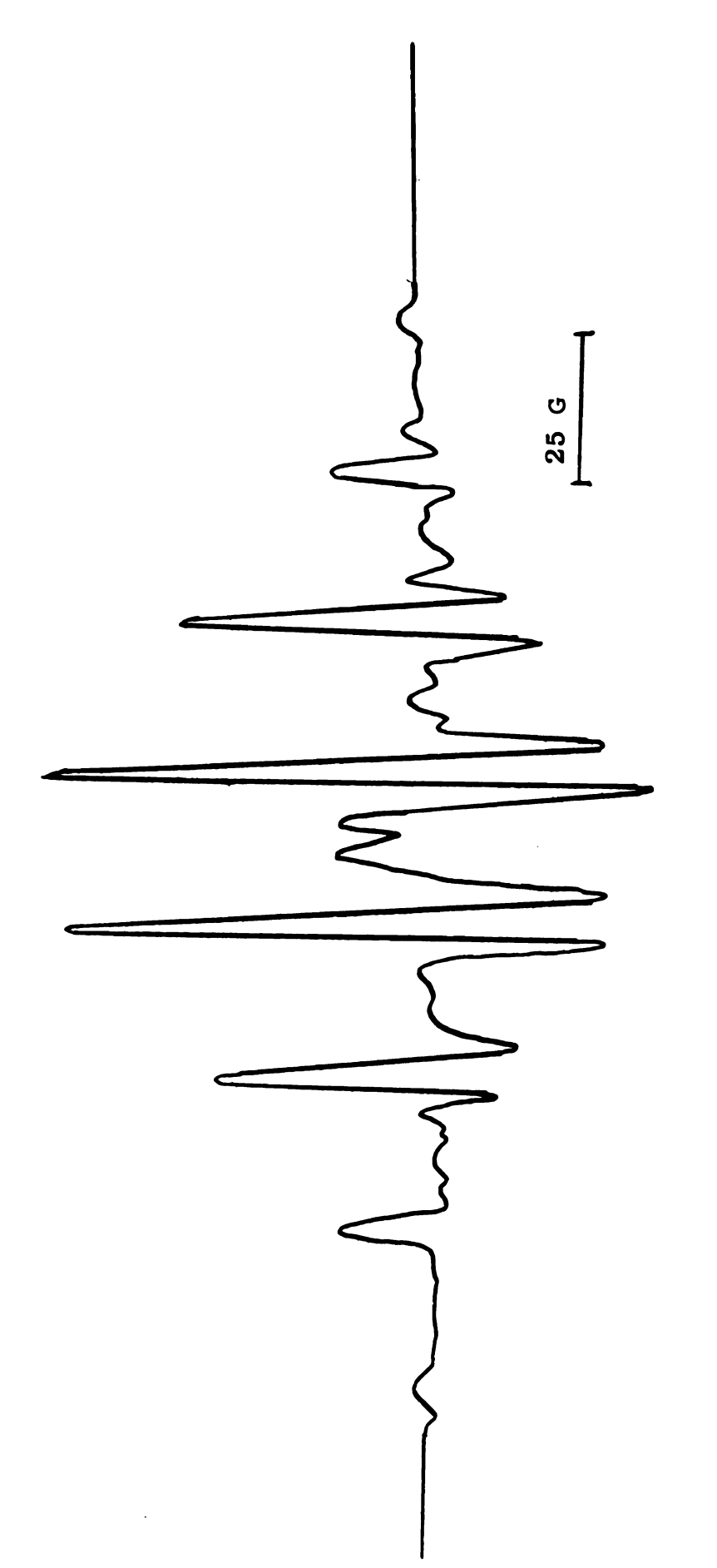
ESR spectrum of an irradiated trimethylacetamide crystal warmed to -800. H  $^{>}|$  c in the a\*c plane. Figure 34.

radical has decreased in intensity. Figure 35 shows the spectrum obtained  $40^{\circ}$  from c in the a\*c plane. Only eight lines of the expected ten-line pattern are evident and the hyperfine splitting is 23 gauss. Spectra in the other two planes also show the pattern attributed to  $\underline{t}$ -butyl radical and resemble those obtained at  $-80^{\circ}$  with slightly less intensity.

# D. 13C Splitting for t-Butyl Radical

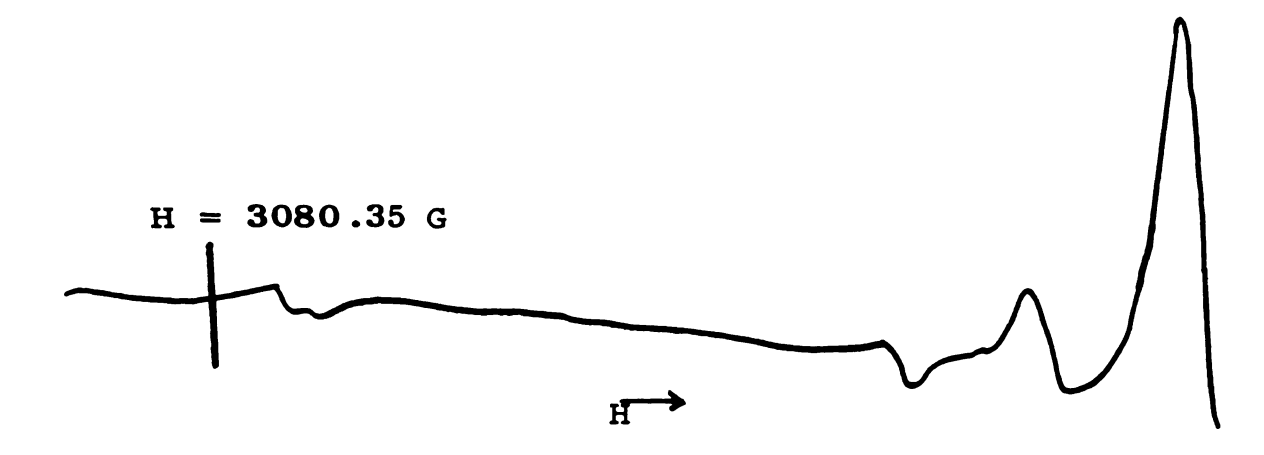
A search was undertaken to attempt to detect the hyperfine splittings from 1.1% naturally abundant \$^{13}\$C in irradiated trimethylacetamide crystals at 770K. The crystal was rotated in each of the three crystallographic planes and first-derivative presentation of the spectra was used so that the weak resonance from \$^{13}\$C could be detected. It was found that when the magnetic field was \$10^0\$ from b in the a\*b plane, a weak line was observed 92 gauss from the high field line of the t-butyl radical spectrum. This line was also observed 92 gauss from the low field line when \$H\_{ext}\$ was \$10^0\$ from b in the a\*b plane. This line is attributed to the maximum \$^{13}\$C hyperfine splitting in t-butyl radical. The position of this line in relation to the spectrum from t-butyl radical is shown in Figure 36.

Attempts to follow the <sup>13</sup>C hyperfine splitting as the crystal was rotated proved fruitless so that the complete tensor could not be evaluated. The results obtained are presented in Table XV.



ESR spectrum of an irradiated trimethylacetamide crystal warmed to -800.  $\overline{\rm H}^2$  is  $40^0$  from c in the a\*c plane. Figure 35.





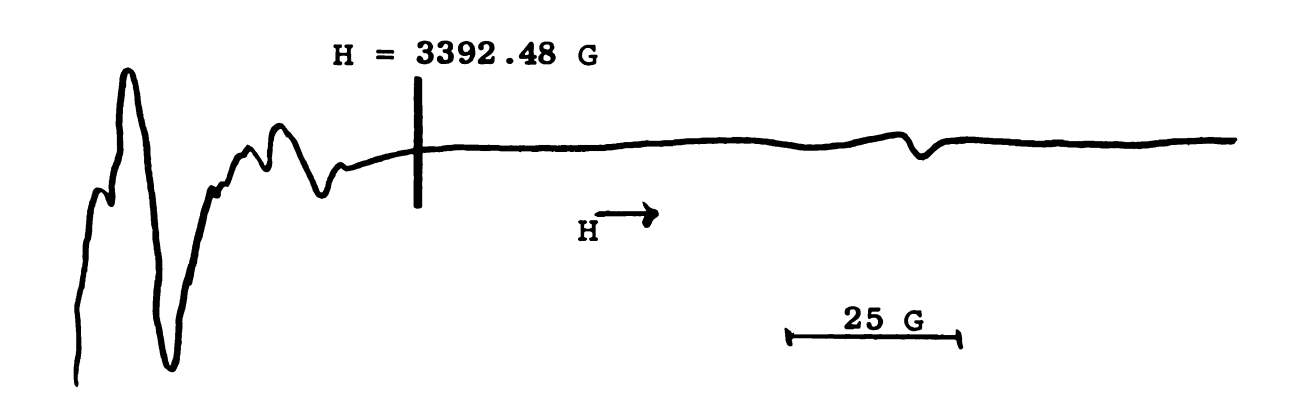


Figure 36. ESR first-derivative spectrum of irradiated trimethylacetamide crystal at  $77^{\circ}K$  showing  $^{13}C$  lines. H is  $10^{\circ}$  from b in the a\*b plane.

# III. Irradiated Isobutyramide Single Crystal

### A. Crystal Structure

Hamrick et al. (17) have reported that the unit cell of isobutyramide is monoclinic with a = 9.69  $\pm$  0.02 Å, b = 5.97  $\pm$  0.01 Å, c = 10.11  $\pm$  0.01 Å and  $\beta$  = 107.1° and that the space group is P2<sub>1</sub>/a with four molecules per unit cell.

Rectangular plates grew easily from a saturated aqueous solution. It was found that the large rectangular face was perpendicular to the c\* axis while the long edge of the plate was parallel to the b crystallographic axis. The crystals were easily mounted using the a, b, and c\* axes as rotation axes. A drawing of the crystal is given in Figure 37.

Single crystals of isobutyramide were  $\gamma$ -irradiated for 5 hours at  $77^{\circ}K$ . The crystals were then mounted without warm-up in the usual manner. Spectra were recorded for every  $10^{\circ}$  rotation in each of the three crystallographic planes ab, bc\* and ac\*.

When the crystal was rotated in the ab plane, the spectrum in Figure 38 was obtained for the magnetic field  $10^{0}$  from b. The spectrum consists of two sets of lines, the first a four-line spectrum with relative intensity ratios

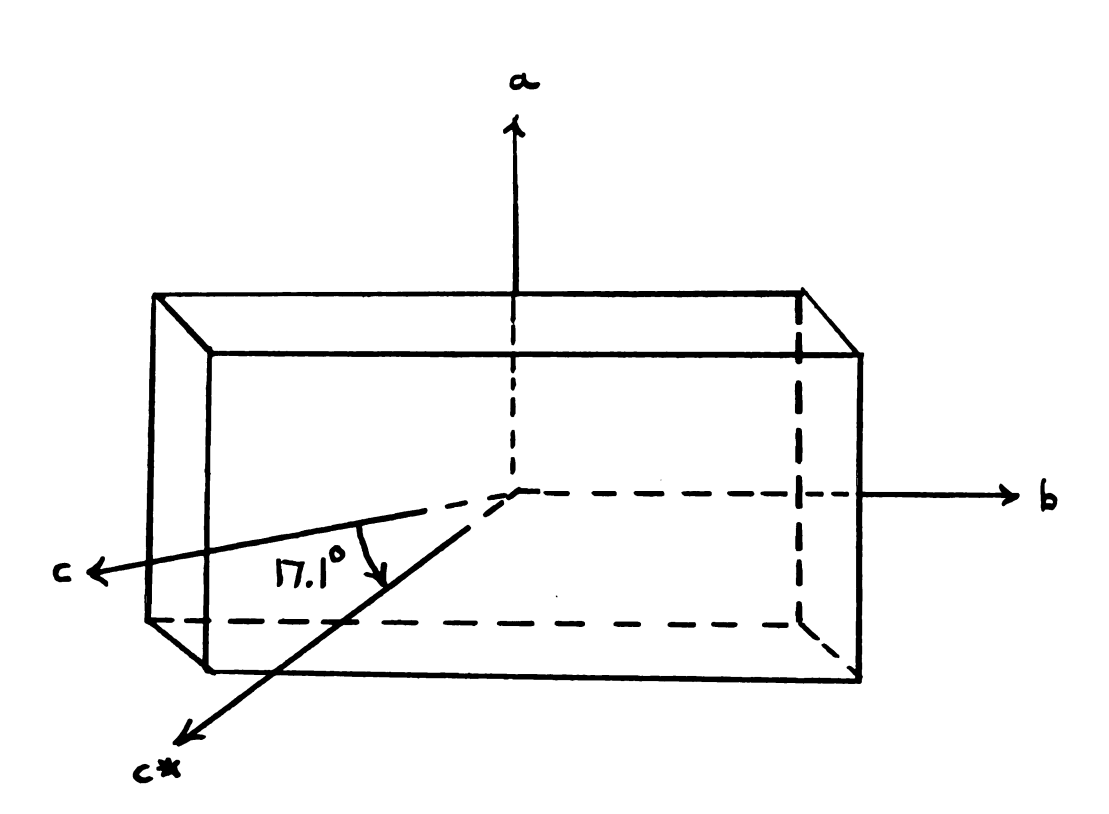
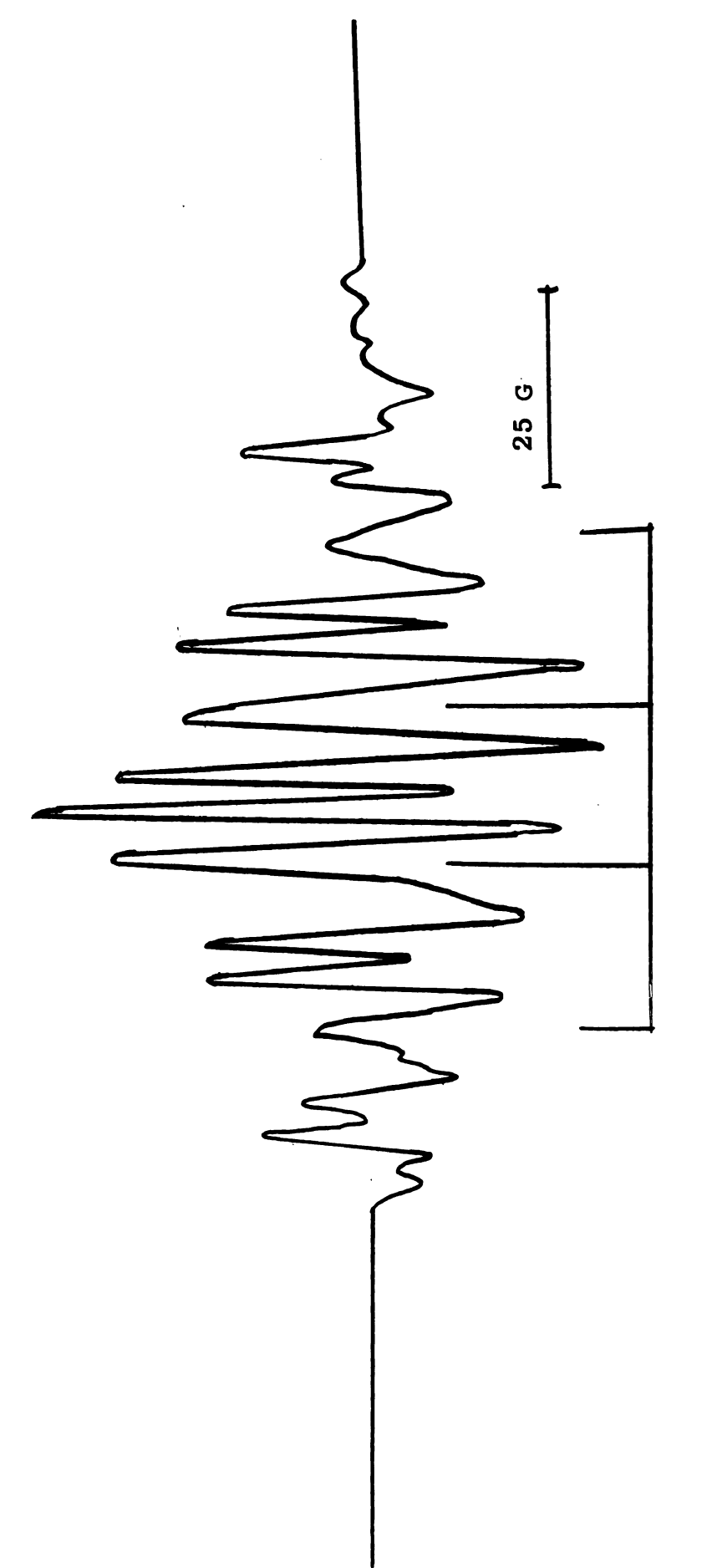


Figure 37. Crystallographic axes for isobutyramide.



ESR spectrum of irradiated isobutyramide crystal at  $77^0 \mathrm{K.}$   $\overline{\mathrm{H}}^{>}$  100 from b in the ab plane. Figure 38.

of 1.1:3.3:3.2:1 as denoted in Figure 38 and with a hyperfine splitting of 24.0 gauss. The remaining lines in the

spectrum are due to the radical  $CH_3$   $CH_3$   $CH_C-NH_2$  which has

been reported previously (17). The four-line spectrum has

been assigned to the radical  $CH_2$   $CH_2$   $CH-C-NH_2$  in which an  $CH_3$ 

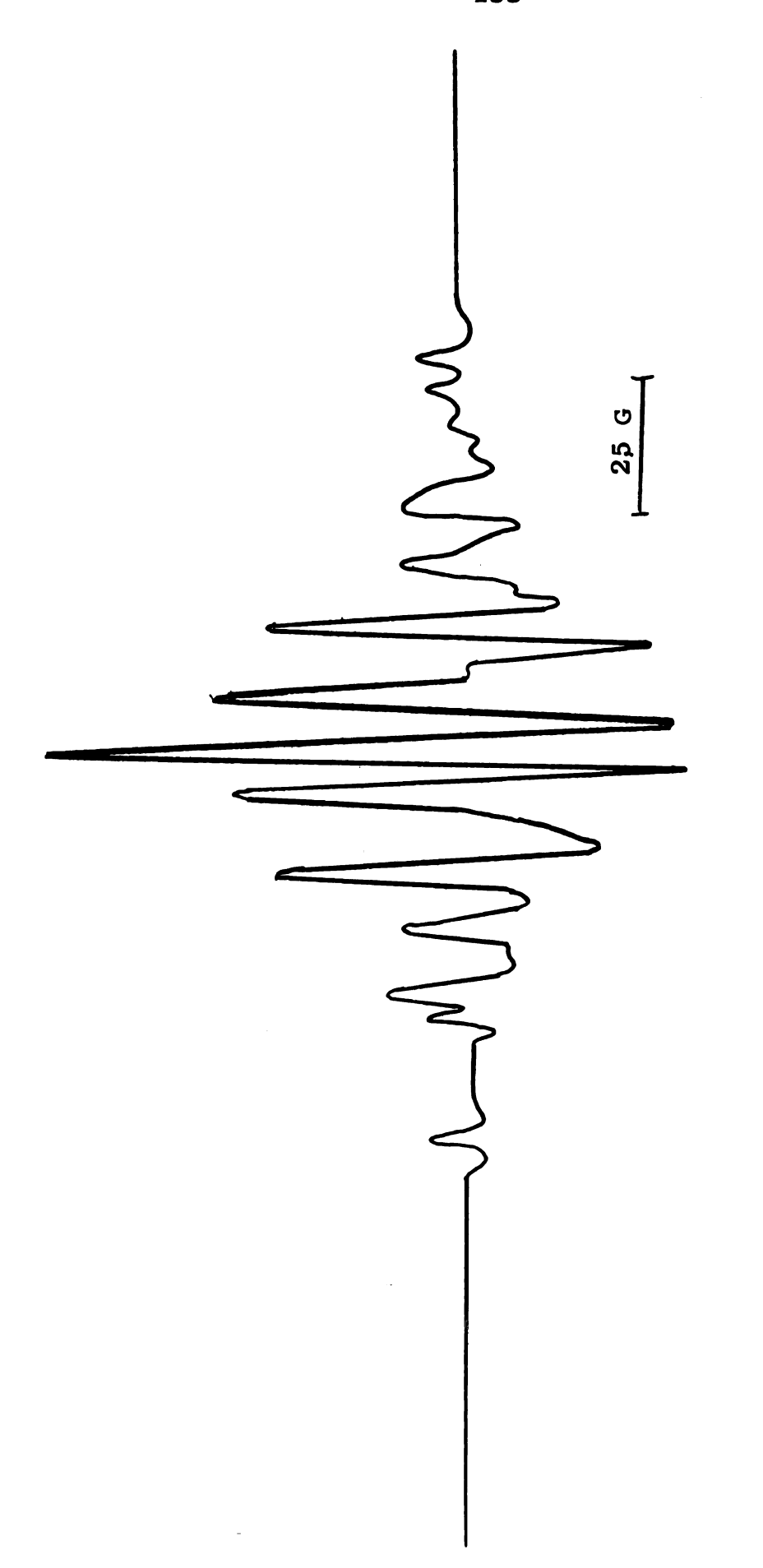
 $\alpha$  proton has been abstracted from the methyl group. The experimental intensity ratio agrees well with the predicted 1:3:3:1 ratio for the equivalent splitting by three protons. The orientation in Figure 38 would thus correspond to equivalent hyperfine splitting by two  $\alpha$  protons and one  $\beta$  proton.

The four-line spectrum can be more easily seen in the case of deuterated crystals in which deuterium has replaced hydrogen in the  $-NH_2$  group. This can be seen from Figure 39 which is  $10^0$  from b in the ab plane. The spectrum now has been simplified so that the doublet splitting in

CH<sub>3</sub> C-C-NH<sub>2</sub> radical has been eliminated. The doublet split-CH<sub>3</sub> ting therefore presumably arose as a result of one of the -NH<sub>2</sub> protons giving a larger hyperfine splitting than the

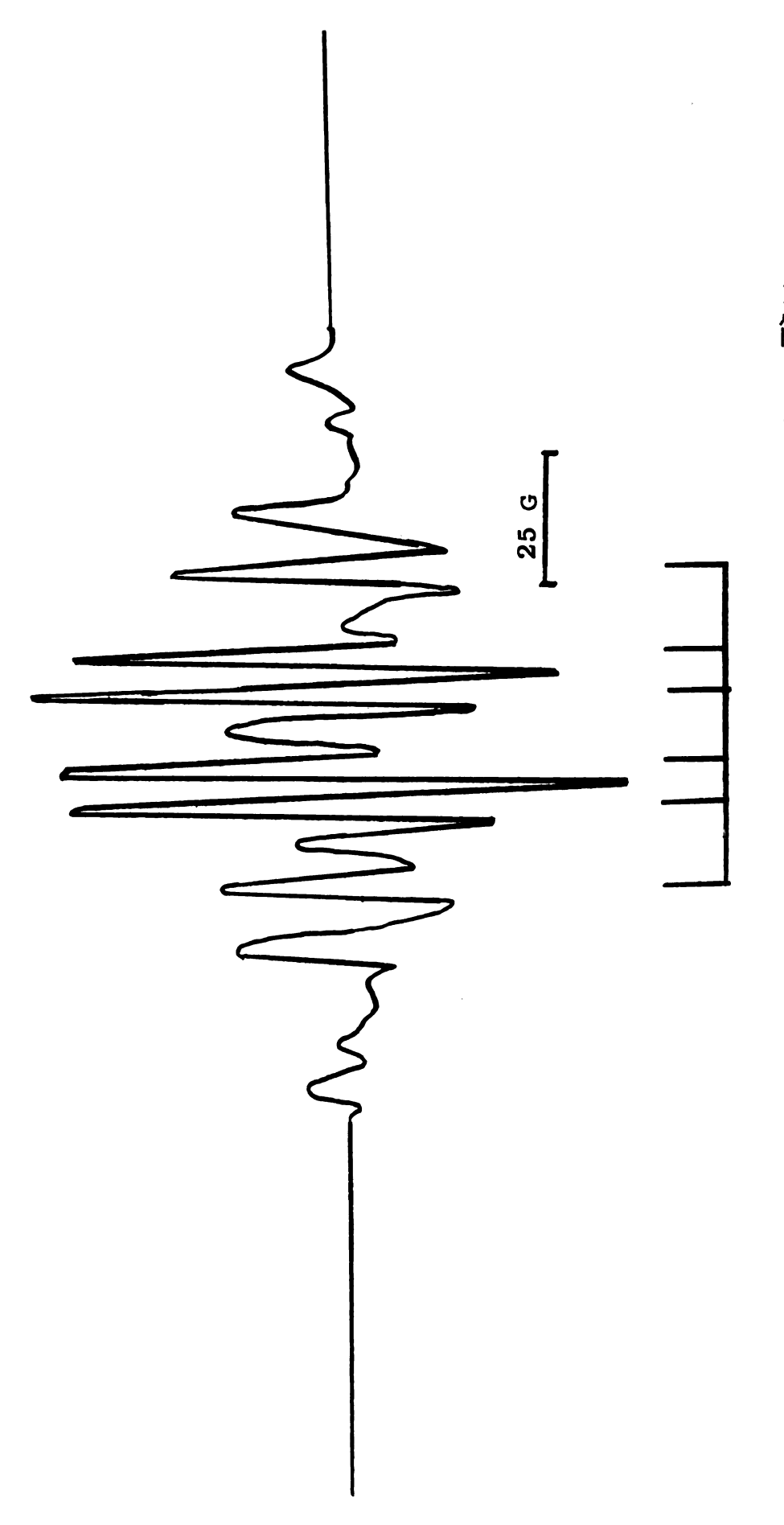
When the crystal was rotated in the bc\* plane, the spectrum of Figure 40 was obtained when H | | | c\*. Disregarding for the moment the lines belonging to

other -NH2 proton, the smaller being unobservable.



ESR spectrum of irradiated deuterated isobutyramide crystal at  $77^0 {\rm K}$ . H is  $10^0$  from b in the ab plane. Figure 39.

be a second seco



ESR spectrum of irradiated isobutyramide crystal at  $77^0 K$  .  $\overline{H}^{>} \big| \, \big| \, c^*$  in the bc\* plane. Figure 40.

 $CH_3$   $CH_3$   $CH_2$  radical, it can be seen that a six-line spec-

trum remains as denoted in Figure 40. In the case of the deuterated crystal the resultant spectrum is the same for H | | | c\* in the bc\* plane. A similar spectrum is obtained for H | | | c\* in the ac\* plane. The six-line spectrum can be interpreted as the equivalent coupling of two  $\alpha$  protons and a further, but nonequivalent, splitting by a  $\beta$  proton. The hyperfine splittings in this case would be  $A_{\alpha_1} = A_{\alpha_2} = 20.5$  gauss and  $A_{\beta} = 13.6$  gauss.

In the ab crystallographic plane it was found that a four-line spectrum resulted for all orientations of the crystal in the magnetic field. This was demonstrated when

the plot of the line positions was made for  $CH_3$   $CH-C-NH_2$   $CH_3$ 

radical in a deuterated crystal as is seen in Figure 41.

The lines for  $CH_3$   $C-C-NH_2$  radical have been left out for  $CH_3$ 

simplification. The slight anisotropy of the outer lines is thought to result from a slight misalignment of the crystal in the magnetic field. It was also found that the spectra were more easily resolved using deuterated crystals than undeuterated ones because the hyperfine splitting from -NH<sub>2</sub> protons is removed in the deuterated crystals; the deuterium hyperfine splittings are much smaller and are lost in the line width.

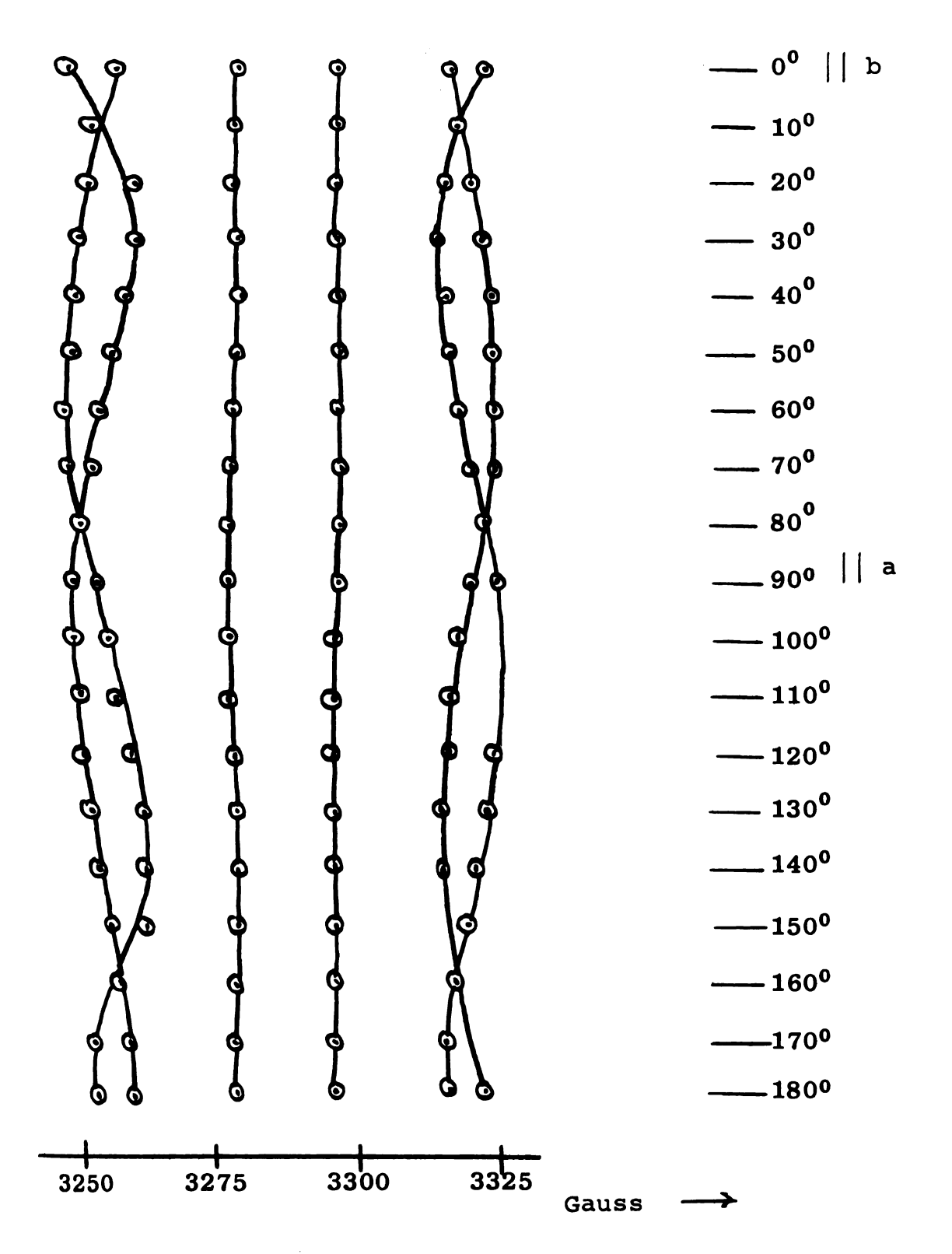


Figure 41. Angular plot of line positions for the CH<sub>2</sub> O CH-C-NH<sub>2</sub> radical in the ab plane.

Additional evidence for the equivalence of the  $\,\alpha\,$  and  $\,\beta\,$  protons in the  $\,ab\,$  plane was provided from variable temperature studies using the Varian V-4557 variable temperature accessory. The crystal was mounted along both the  $\,aa\,$ 

and b crystallographic axes; the decay of  $CH_2$   $CH_2$   $CH_3$   $CH_3$   $CH_3$ 

lines was followed as a function of temperature as shown in Figures 42 and 43. It was found that only four lines decayed at the same rate along either a or b indicating that the  $\alpha$  and  $\beta$  protons must be equivalent in the ab plane.

When the decay of lines belong to  $CH_2$   $CH-C-NH_2$  radical was studied as a function of temperature for H || c\*, it was found that six lines could be attributed to the

CH<sub>2</sub> O CH-C-NH<sub>2</sub> radical as shown in Figure 44. In all cases

where variable temperature studies were done the lines be-

longing to  $\dot{C}H_2$  "CH-C-NH<sub>2</sub> radical have disappeared at -80°C CH<sub>3</sub>  $\dot{C}H_3$   $\dot{C}H_3$   $\dot{C}H_3$   $\dot{C}H_3$   $\dot{C}H_3$   $\dot{C}H_3$   $\dot{C}H_3$  radical.

The line positions found for the spectrum of the  $\dot{C}H_2$   $\ddot{C}H$  CH CH radical were plotted versus angle of orientation  $\dot{C}H_3$ 

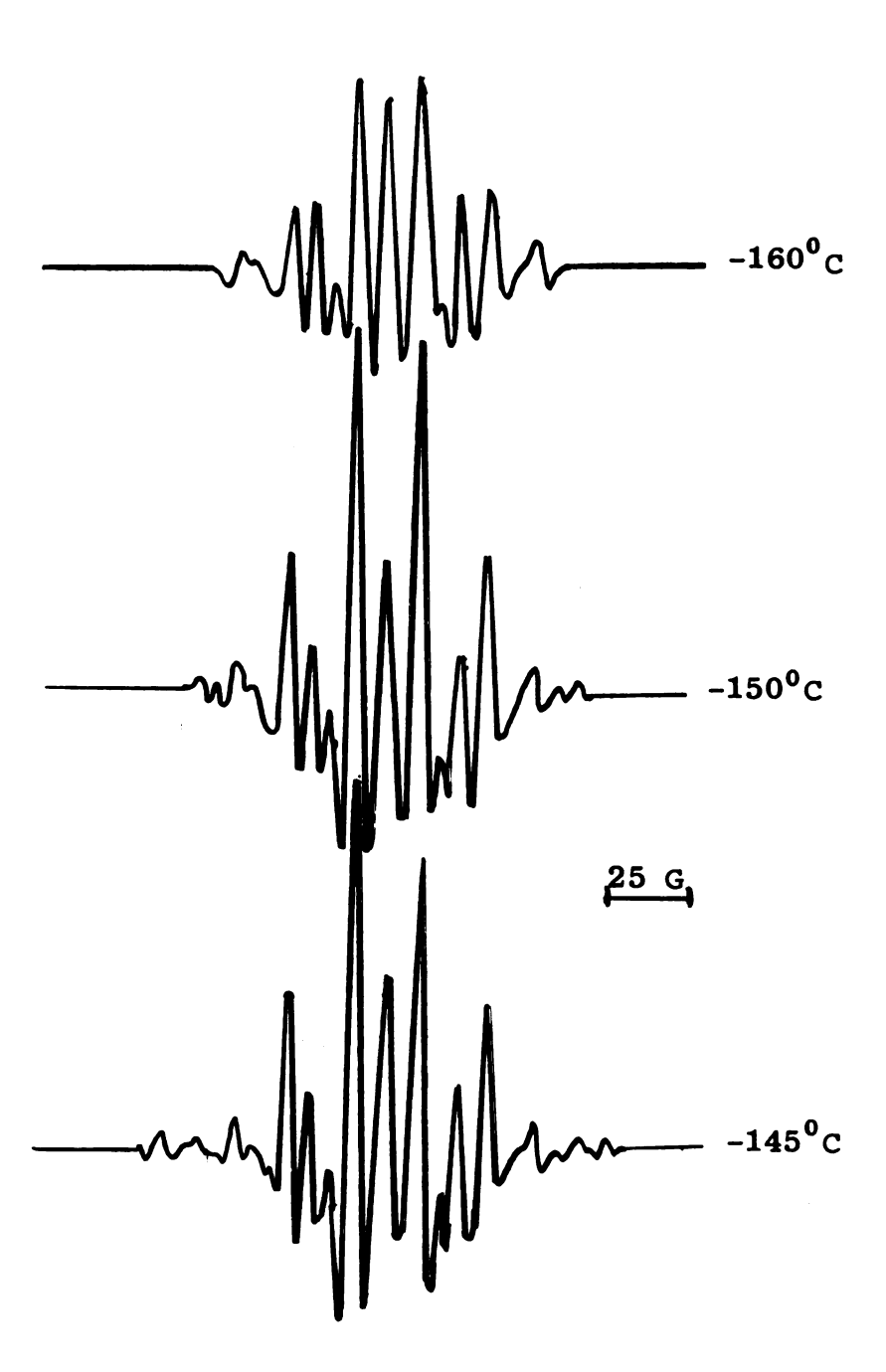
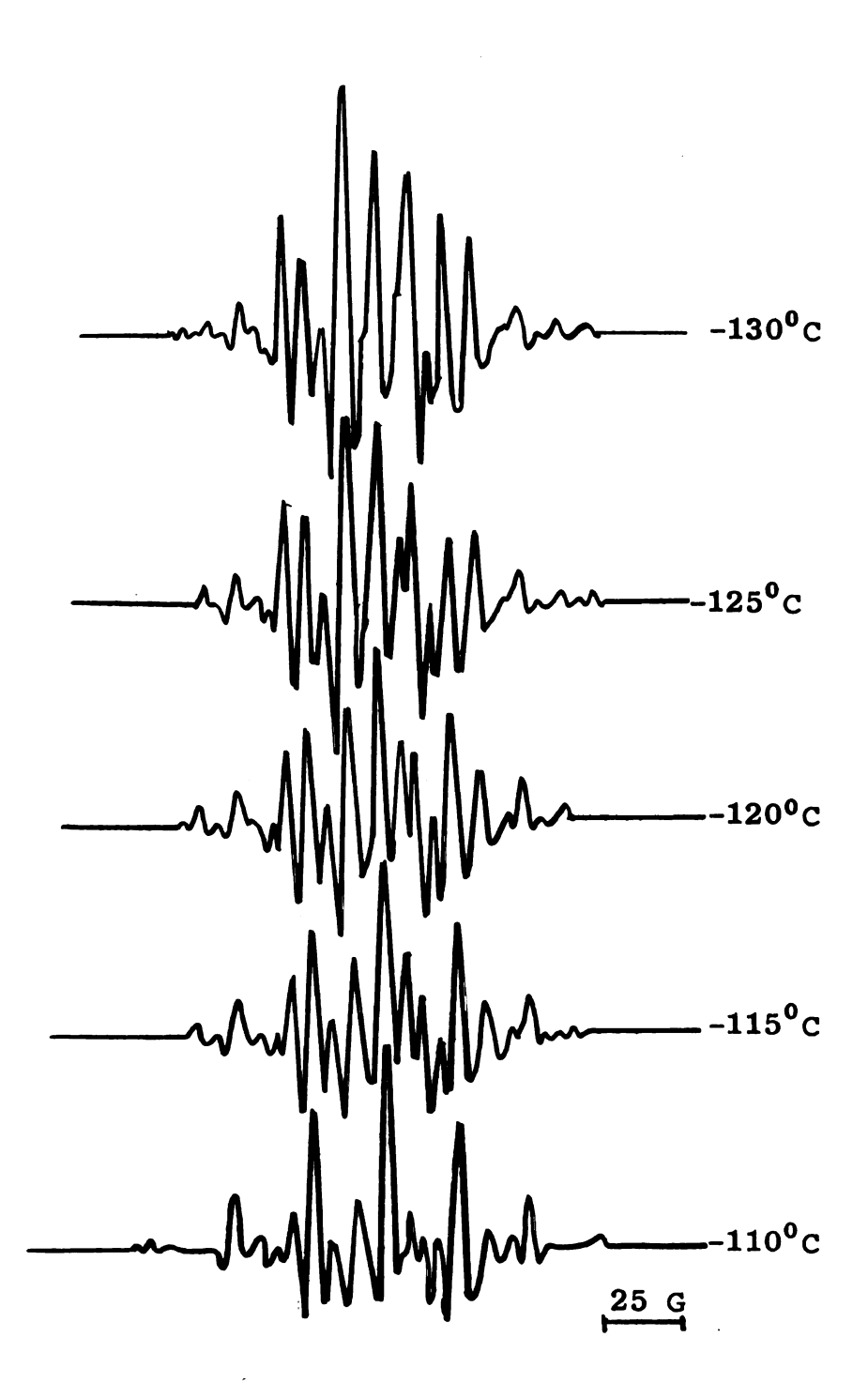
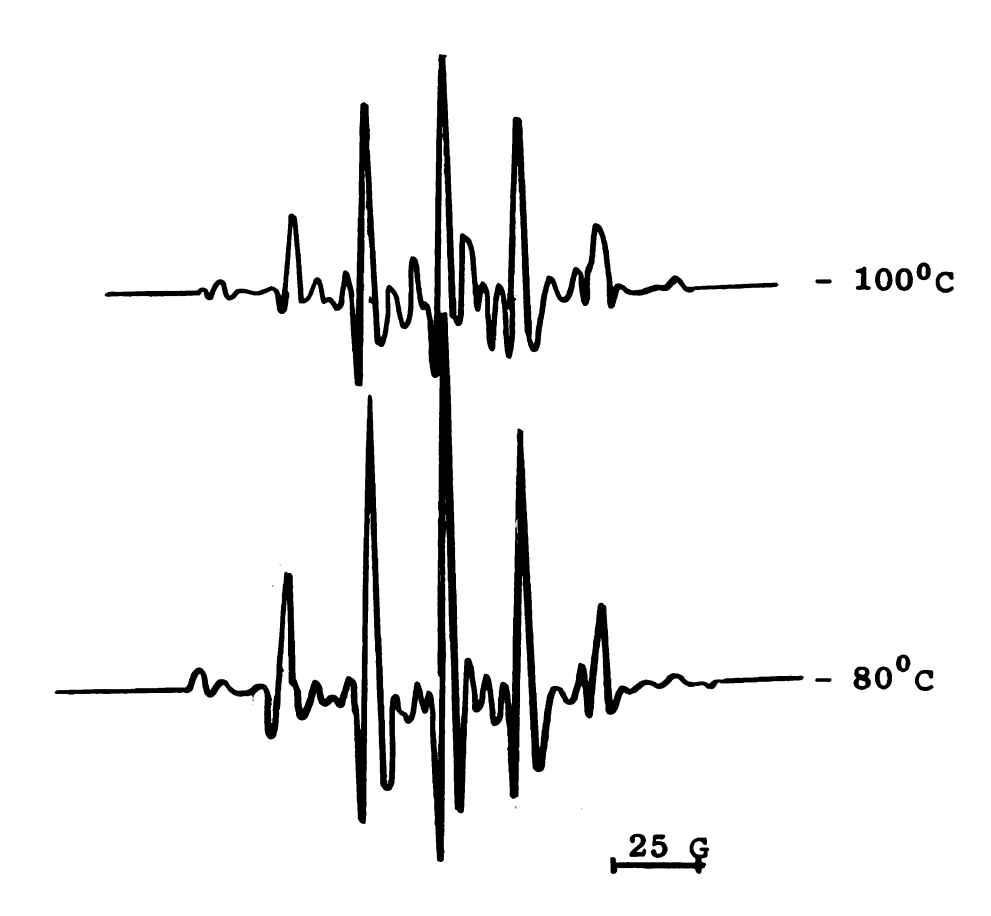


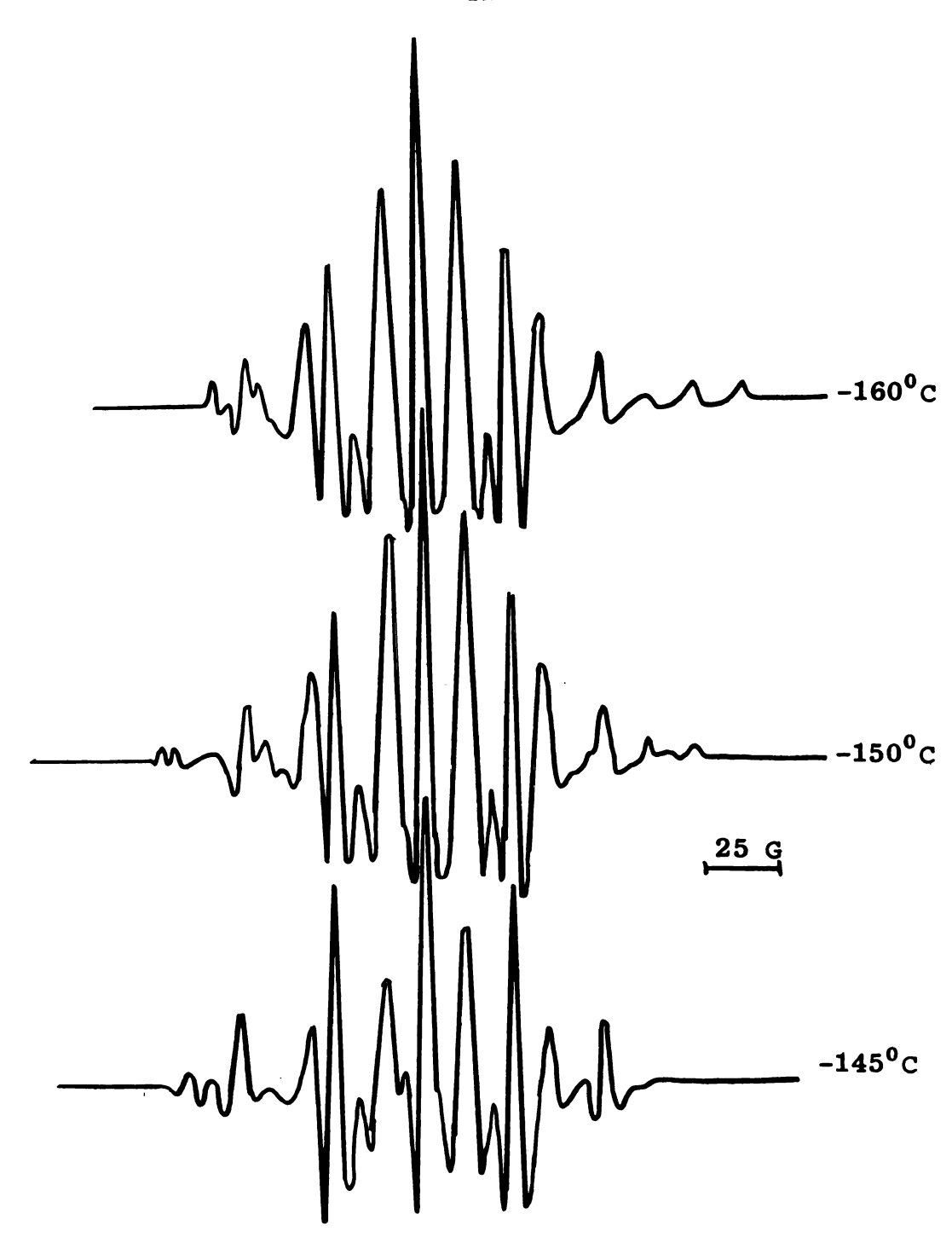
Figure 42. Variable temperature study of the spectrum of the  $\dot{C}H_2$   $\ddot{C}H_2$   $\ddot{C}H_2$   $CH_3$   $CH_3$  radical with  $\ddot{H}$  | | a.



igure 42. (Continued)



gure 42. (Continued).



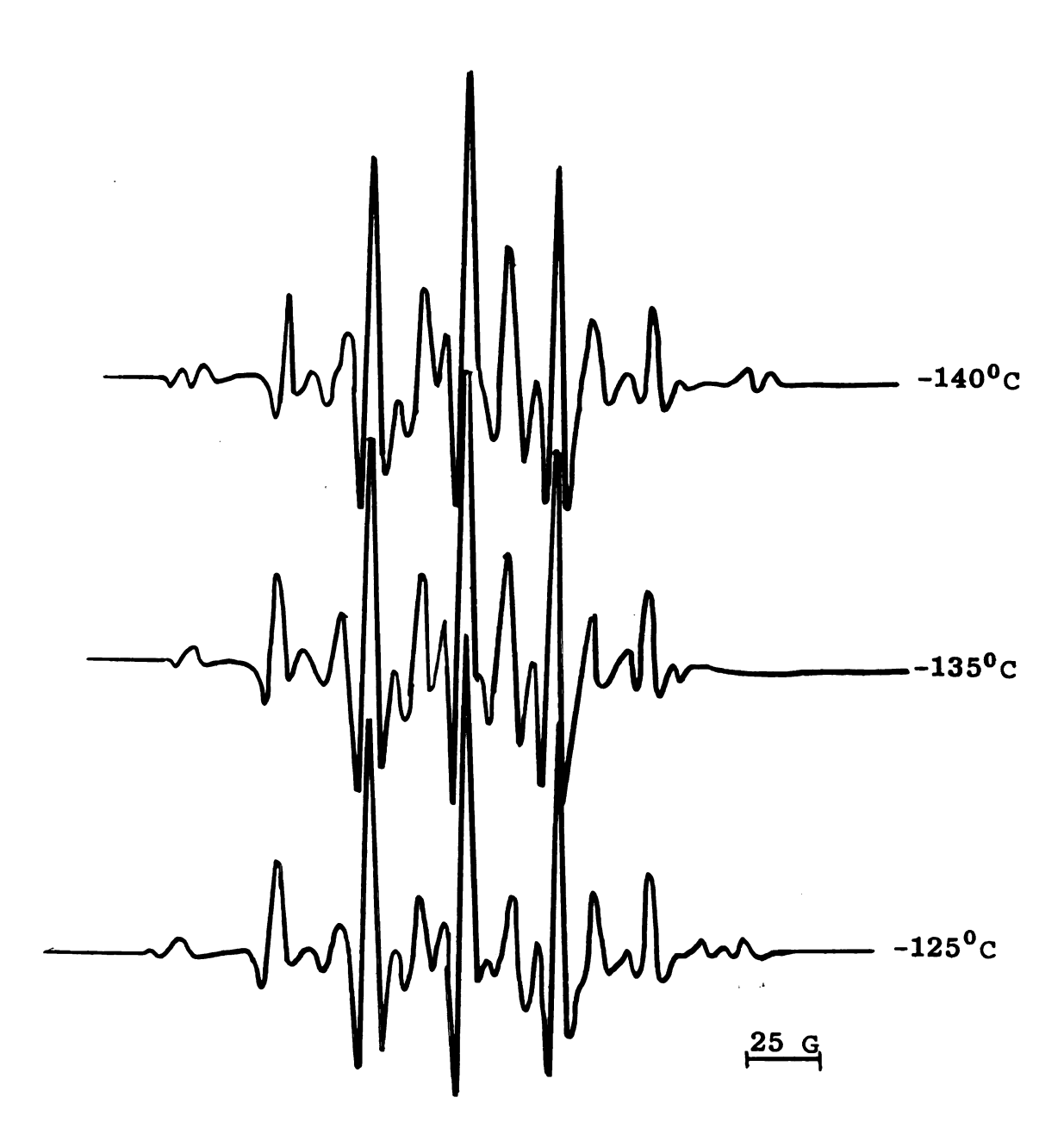


Figure 43. (Continued).

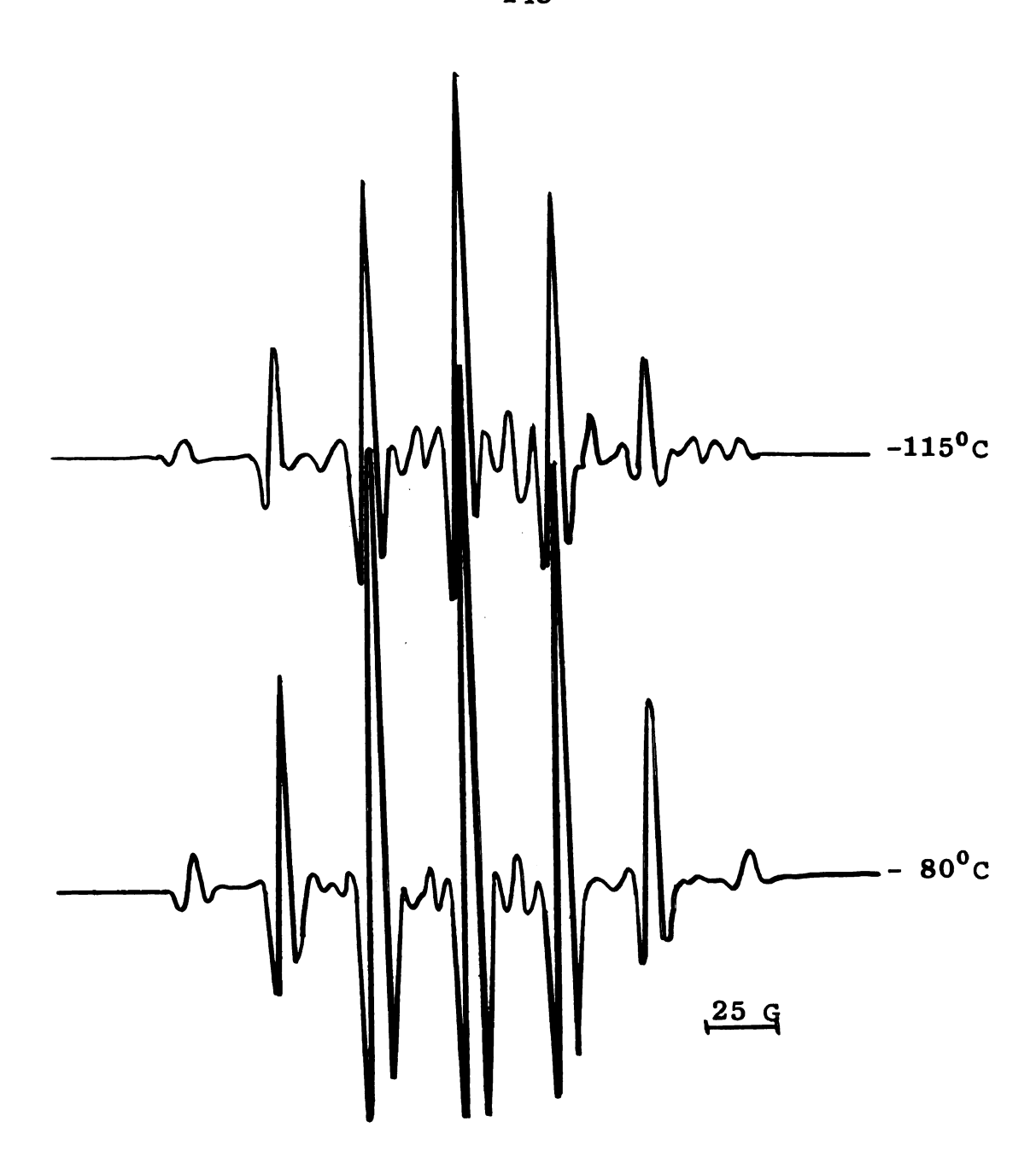


Figure 43. (Continued).

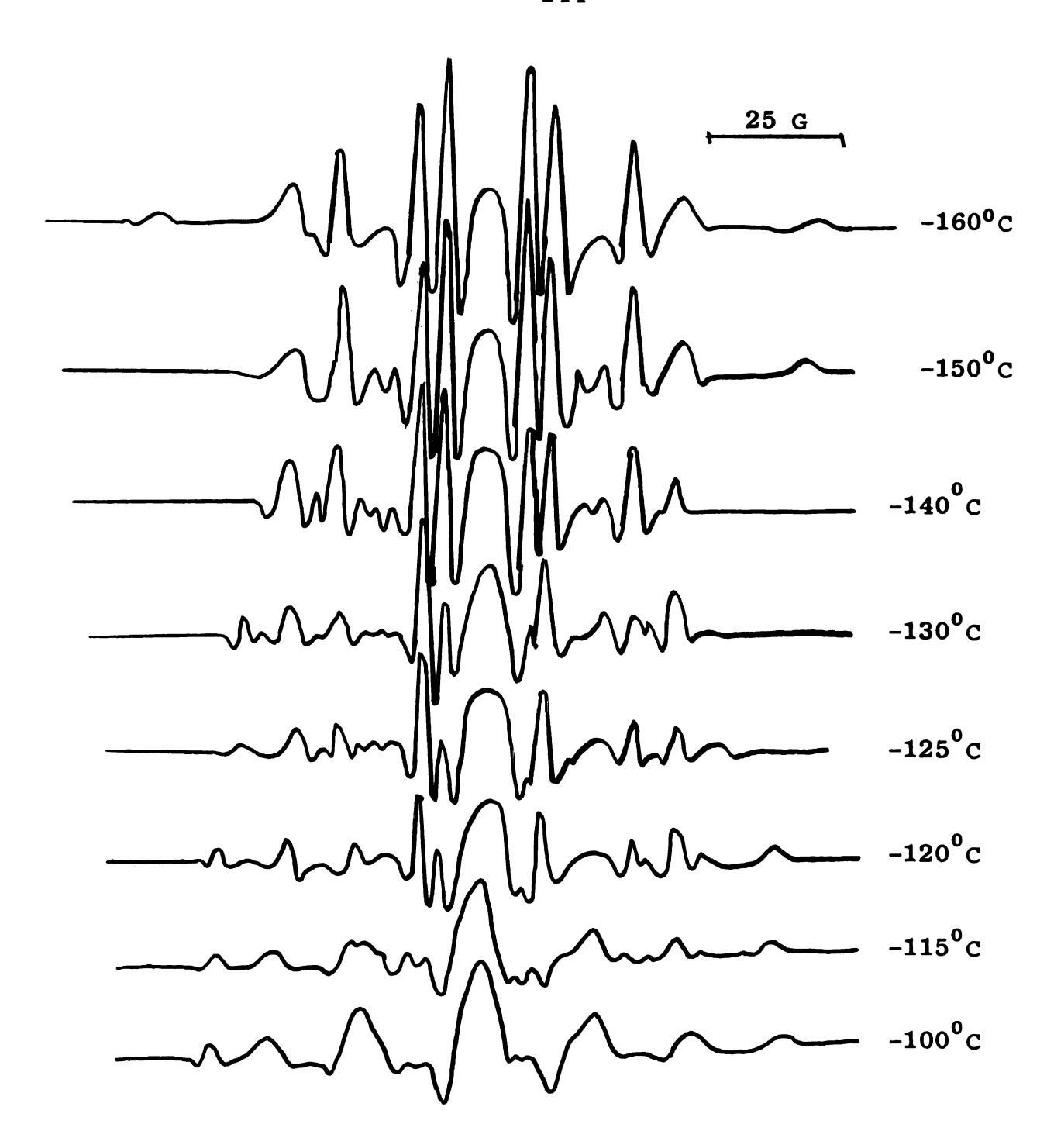


Figure 44. Variable temperature study of the spectrum of the  $\dot{c}_{H_2}$   $\ddot{c}_{H^-C^-NH_2}$  radical with  $\overline{H}^>||c^*|$ .

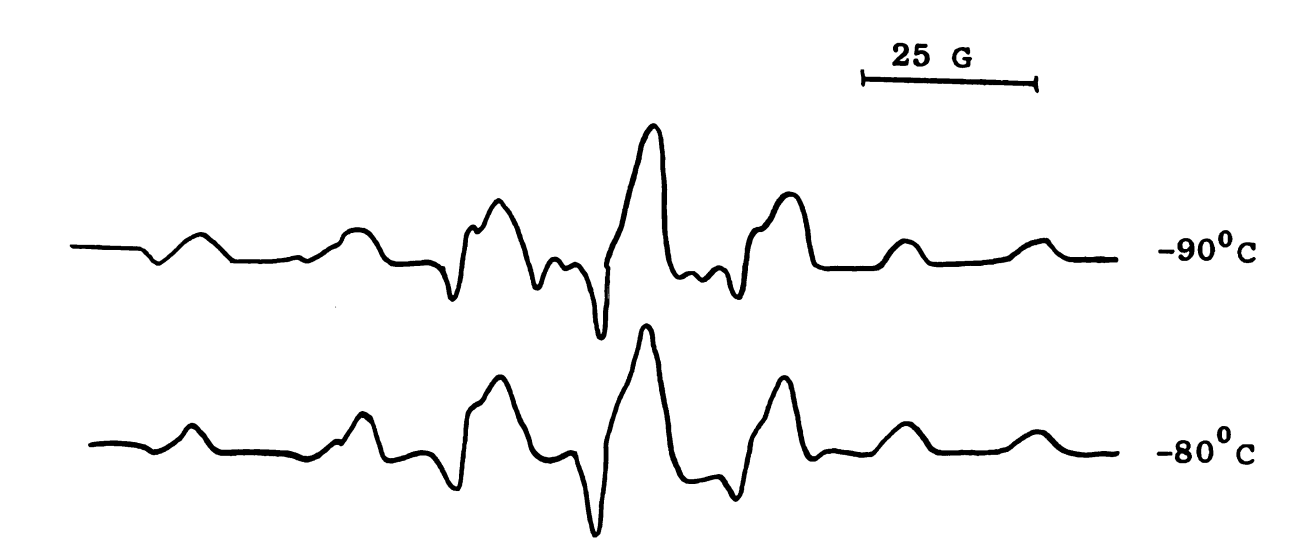


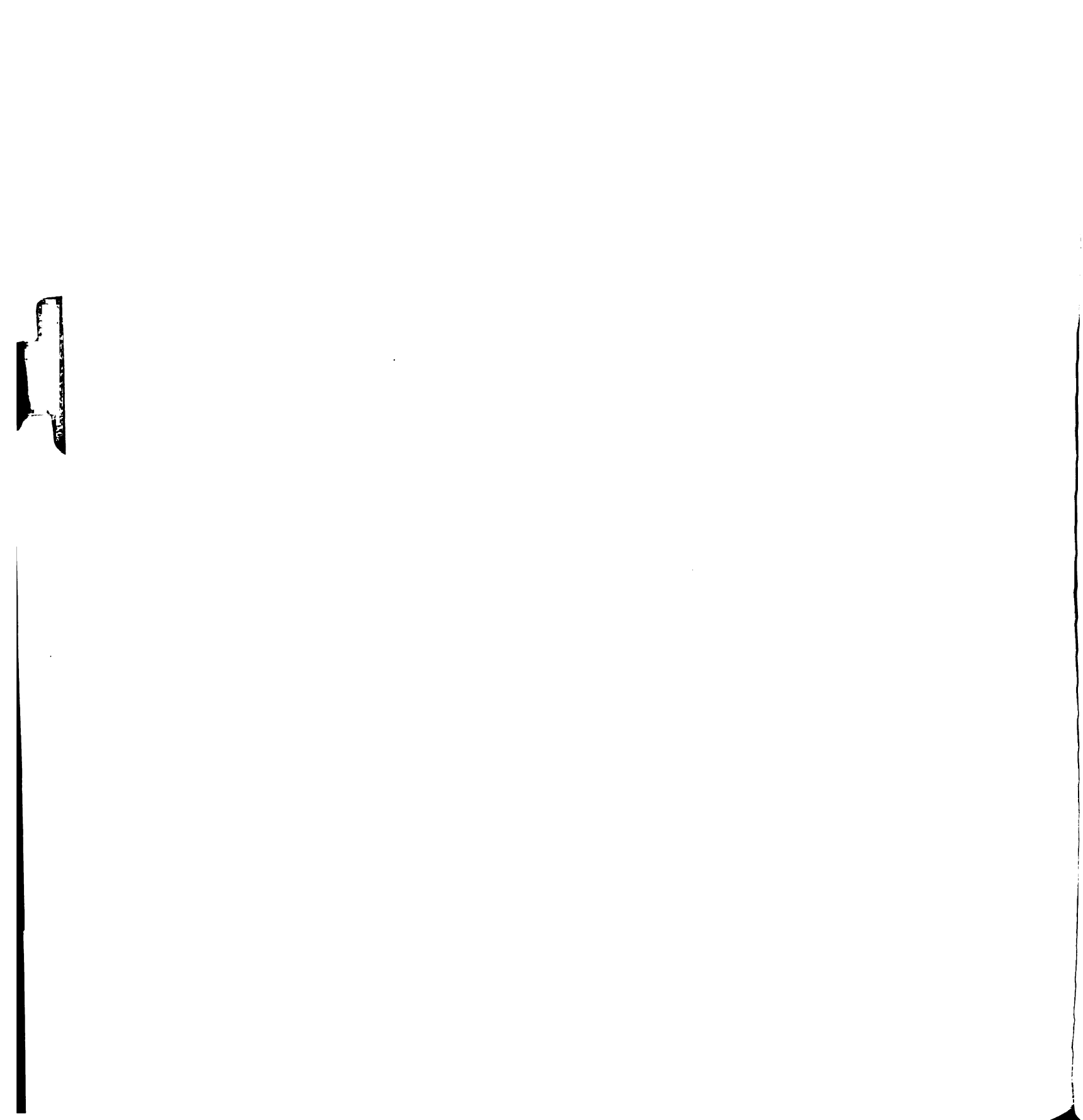
Figure 44. (Continued).

 $\theta$  in the bc\* and ac\* planes also; these plots are given in Figures 45 and 46. In both the bc\* and ac\* planes only six lines were observed for most orientations. The only exception to this was for H || b in the bc\* plane as mentioned previously. This is consistent with equivalent splitting by the two  $\alpha$  protons with an additional different splitting by the  $\beta$  proton. At no orientation were eight lines present as would be true if the  $\alpha$  protons had become non-equivalent. All measurements were done on the spectra of deuterated crystals for these plots.

There is a certain amount of anisotropy in the case of the hyperfine splitting in any of the three crystallographic planes. It was assumed that  $\alpha_1=\alpha_2=\beta$  in the abplane; and  $\alpha_1=\alpha_2\neq\beta$  in the bc\* and ac\* planes. Since the amount of anisotropy was small, the hyperfine splitting tensors were constructed according to Schonland's method (Equation 48); the results are presented in Table XVI. The reason for the apparent equivalence of  $\alpha$  and  $\beta$  protons in the bc\* and ac\* planes and their equivalence in the ab plane is not obvious but will be commented on in the Conclusions. The signs have been chosen to agree with the values found for  $\alpha$  and  $\beta$  proton splittings in previous investigations (Tables I and II).

C. Radical Stable at Higher Temperatures CH<sub>3</sub> ... C-C-NH<sub>2</sub>

When the crystal was warmed to  $-80^{\circ}$ , as shown in the variable temperature spectra (Figures 42 to 44), a seven-line



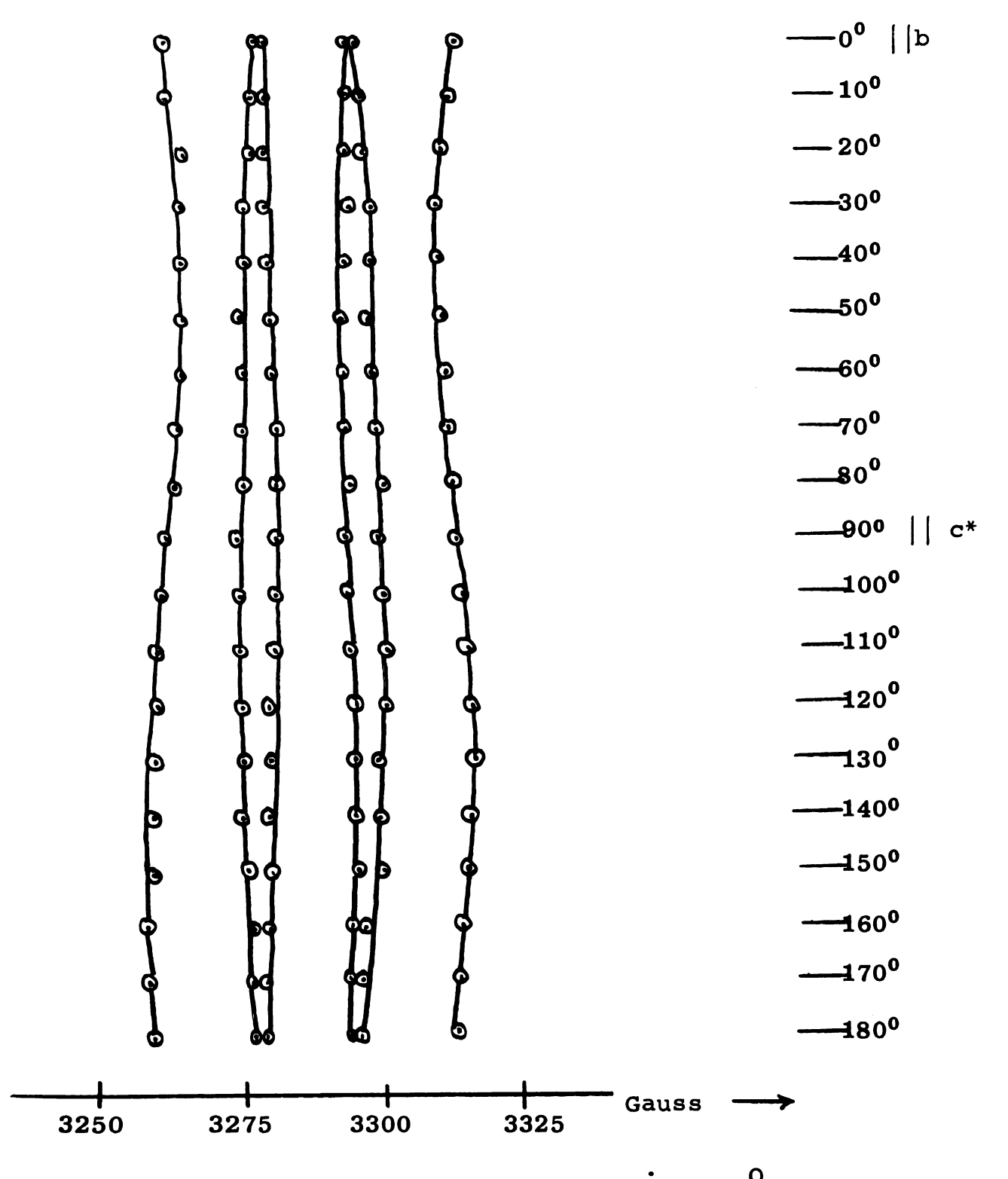


Figure 45. Plot of line positions for CH<sub>2</sub> CH-C-NH<sub>2</sub>

radical as a function of field orientation in the bc\* plane.

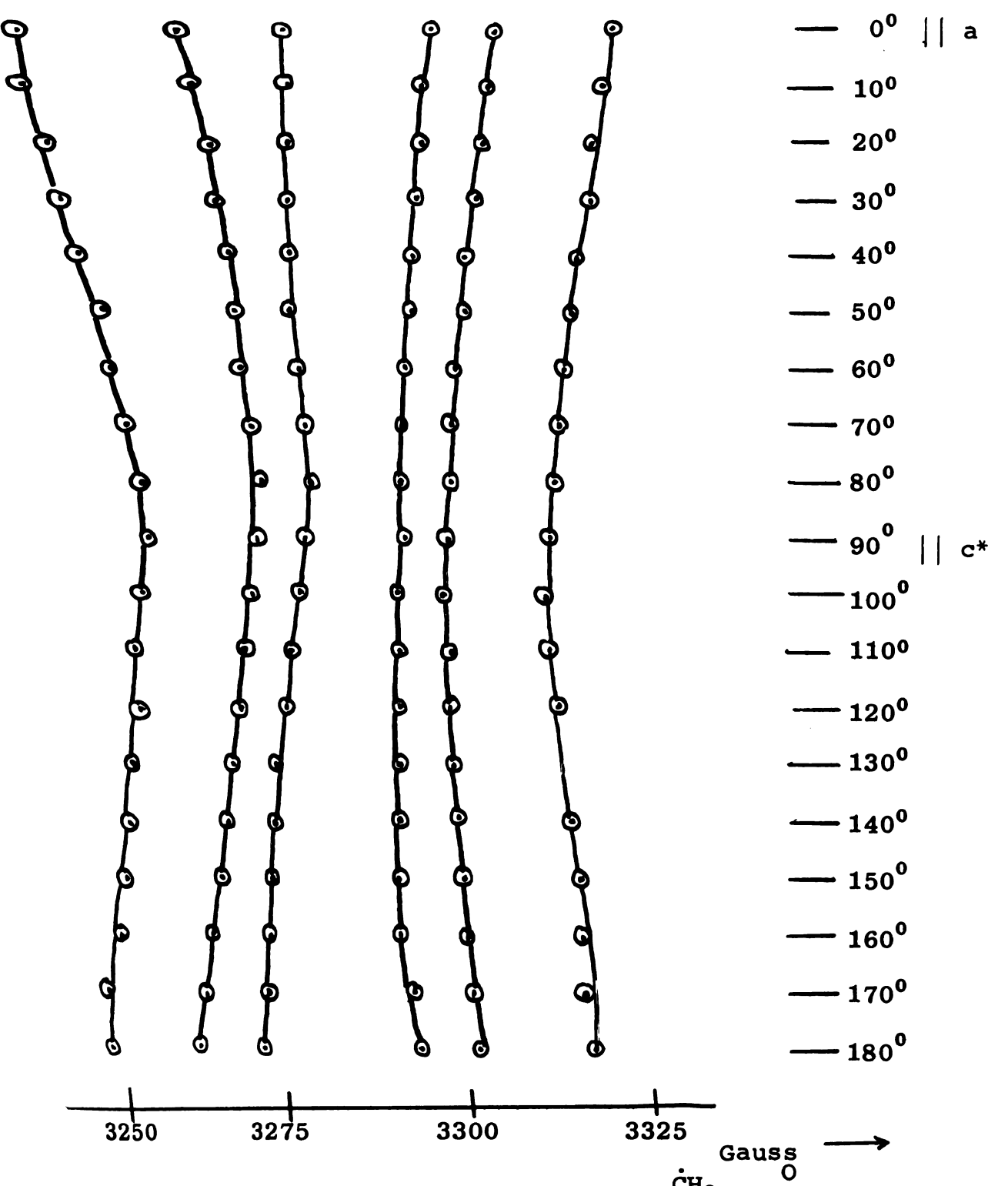


Figure 46. Plot of line positions for CH-C-NH<sub>2</sub>

radical as a function of field orientation in the ac\* plane.

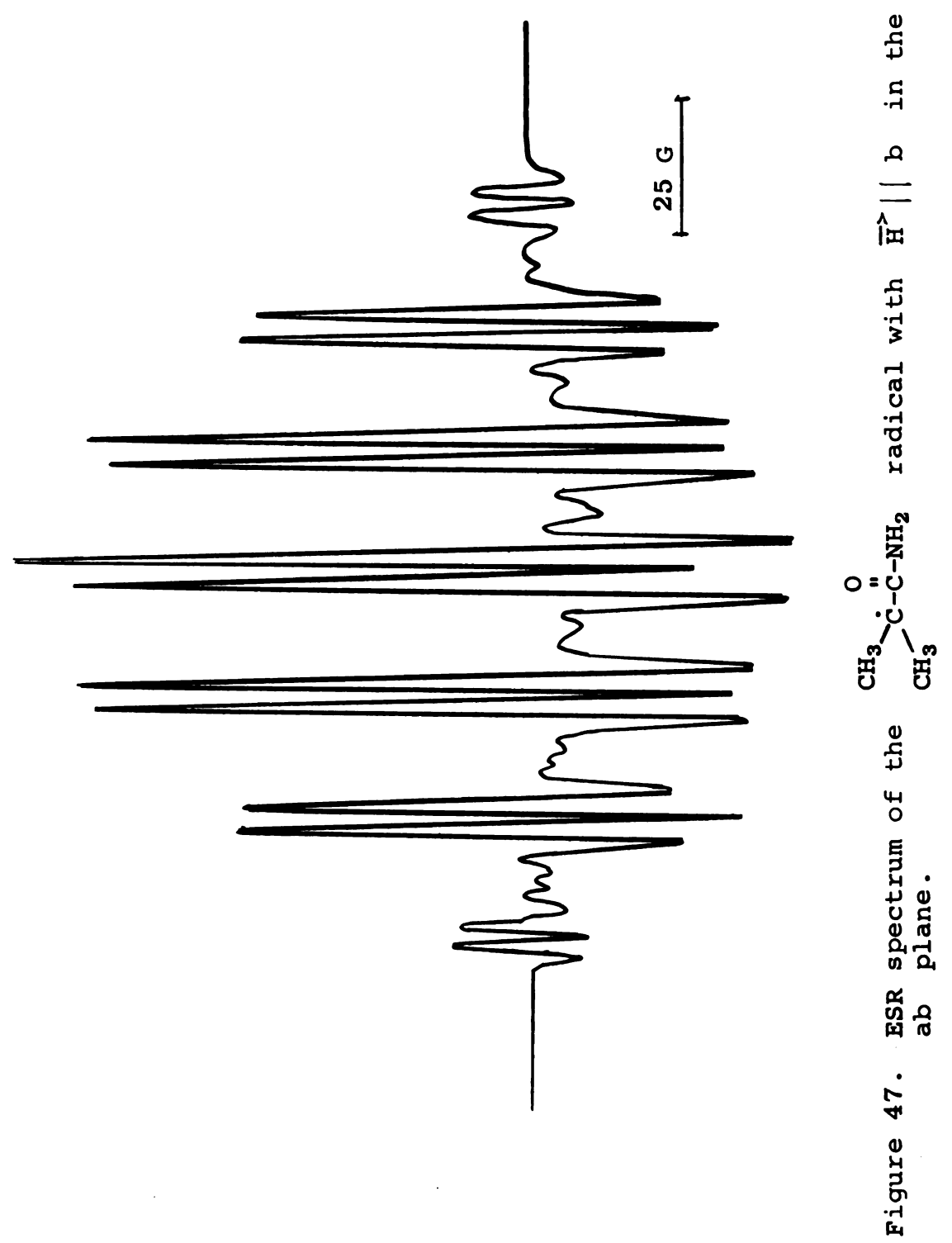
Table XVI. Hyperfine splitting tensors for protons of the H<sub>2</sub> $\dot{c}$   $\overset{O}{\text{H}_{3}}\text{CH-C-NH}_{2}$  radical

Proton $\alpha_1 = \alpha_2$	Principal Values (gauss)		Direction Cosines		
	-24.2		0.99	-0.11	≅ 0
	-20.3	≅	0.0	≃ 0.0	1
	-17.8		-0.11	-0.99	≃ 0
	A <sub>iso</sub> = -20.8				
β	22.8		0.98	-0.19	<b>≅</b> 0
	18.9		0.19	0.98	≃ 0
	12.2	~	0.0	<b>≅</b> 0.0	1
	$A_{iso} = 18.0$				

pattern attributed to  $CH_3$  ...  $C-C-NH_2$  radical results. This  $CH_3$ 

radical has previously been reported by Hamrick et al. (17) in X-irradiated isobutyramide single crystals.

The basic seven-line pattern was observed for all orientations of the crystal in the magnetic field except where H | b in the bc\* and ab planes as is seen in Figure 47. The measured splitting when H | | b was 4.6 gauss for the additional doublet fine structure which agrees well with the 4.2 gauss splitting reported previously (17) for one of the protons of the -NH2 group. The quintet pattern for H | c\* , which arises from equivalent splitting by the -NH2 protons and the amine group nitrogen, was also observed and agrees with previous work (17). The measured hyperfine splitting for H | c\* was 2.5 gauss for the quintet splitting and the spectrum obtained when H | c\* in ac\* plane is shown in Figure 48. The  $\bar{\bar{A}}$ ' tensor for the six-equivalent  $\beta$ -methyl protons was constructed using Schonland's method and the principal values obtained by the usual procedure. Principal values for the hyperfine splitting tensor and the associated direction cosines are given in Table XVII.



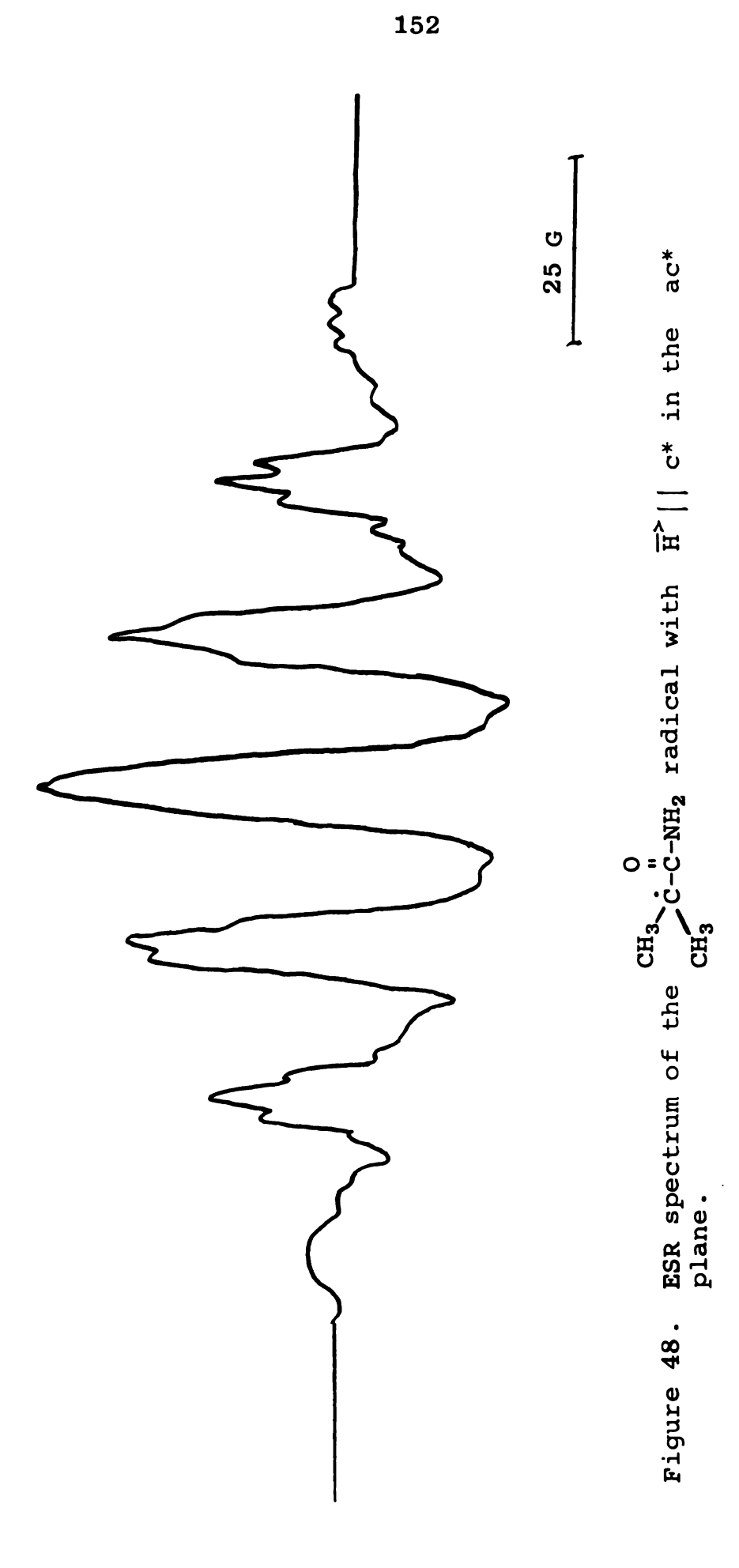


Table XVII. Hyperfine splitting tensor for methyl protons in the  $CH_3$  . ...  $C-C-NH_2$  Radical.

Principal Values (gauss)	Direction Cosines		
23.0	0.00	0.91	0.40
21.7	0.00	-0.40	0.91
21.7	1.00	0.00	0.00

### IV. Irradiated Single Crystals of Hydrazinium Dichloride

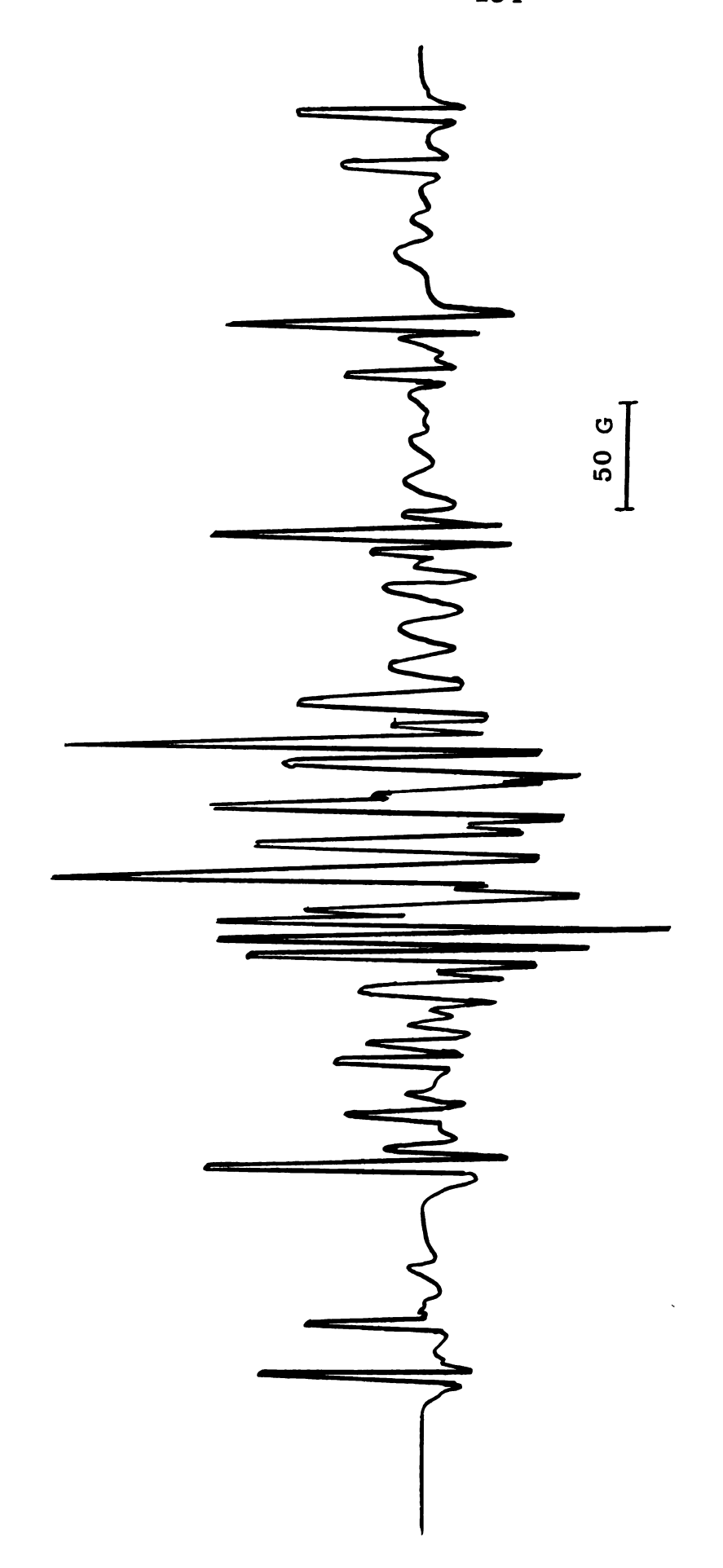
### A. Crystal Structure

The crystal structure of hydrazinium dichloride has been previously reported (14). The unit cell is cubic with a = 7.89 Å. The space group is  $T_h^6$  - Pa3 with four molecules per unit cell.

Crystals grew easily from aqueous solution and were mounted along cubic axes with relative ease.

# B. Presence of Cl<sub>2</sub> at 770K

Single crystals of hydrazinium dichloride were  $\gamma$ -irradiated for 3 hours at  $77^0 K$  and then mounted without warm-up. The crystal was rotated in the aa' plane. When  $\overline{H}_{\rm ext}^{>}$  was  $45^0$  from the a axis in the aa' plane, the spectrum of Figure 49 was obtained. Although the spectrum is complicated, it was possible from the outermost low and high-field



is ESR spectrum of irradiated hydrazinium dichloride at  $77^{0}\mathrm{K}$ .  $45^{0}$  from a in the aa' plane. Figure 49.

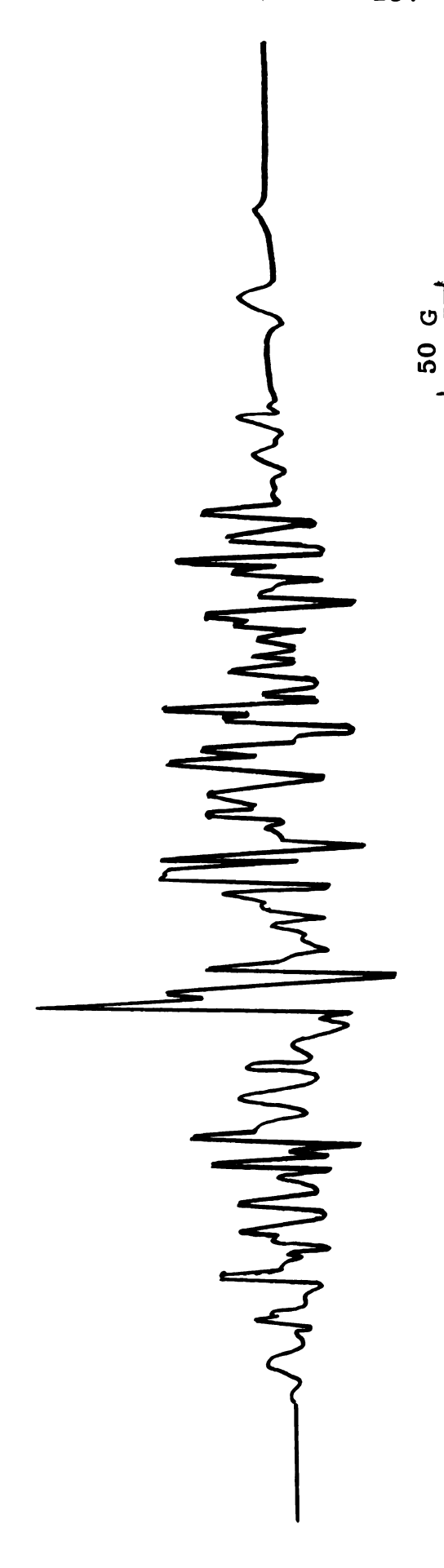
lines to confirm the presence of  $\operatorname{Cl}_2$ . The hyperfine splitting at this orientation is 97.3 gauss which is in reasonable agreement with reported maximum hyperfine splittings for  $\operatorname{Cl}_2$ . The measured g value was 2.0035 which is slightly larger than the expected g value at this position (where A is a maximum). Rotation in the aa' plane again shows a maximum hyperfine splitting of 96.4 gauss 135° from a or 90° from the above orientation as shown in Figure 50.

ent and is oriented along (110) directions in the crystal. It was not possible to analyze completely the hyperfine splitting tensor for  $\operatorname{Cl}_2$  because the presence of a second unidentified radical made the spectra complex and a complete analysis impossible. This complexity is illustrated in Figure 51 which shows the spectrum obtained when the crystal is rotated 45° from the position in Figure 49.

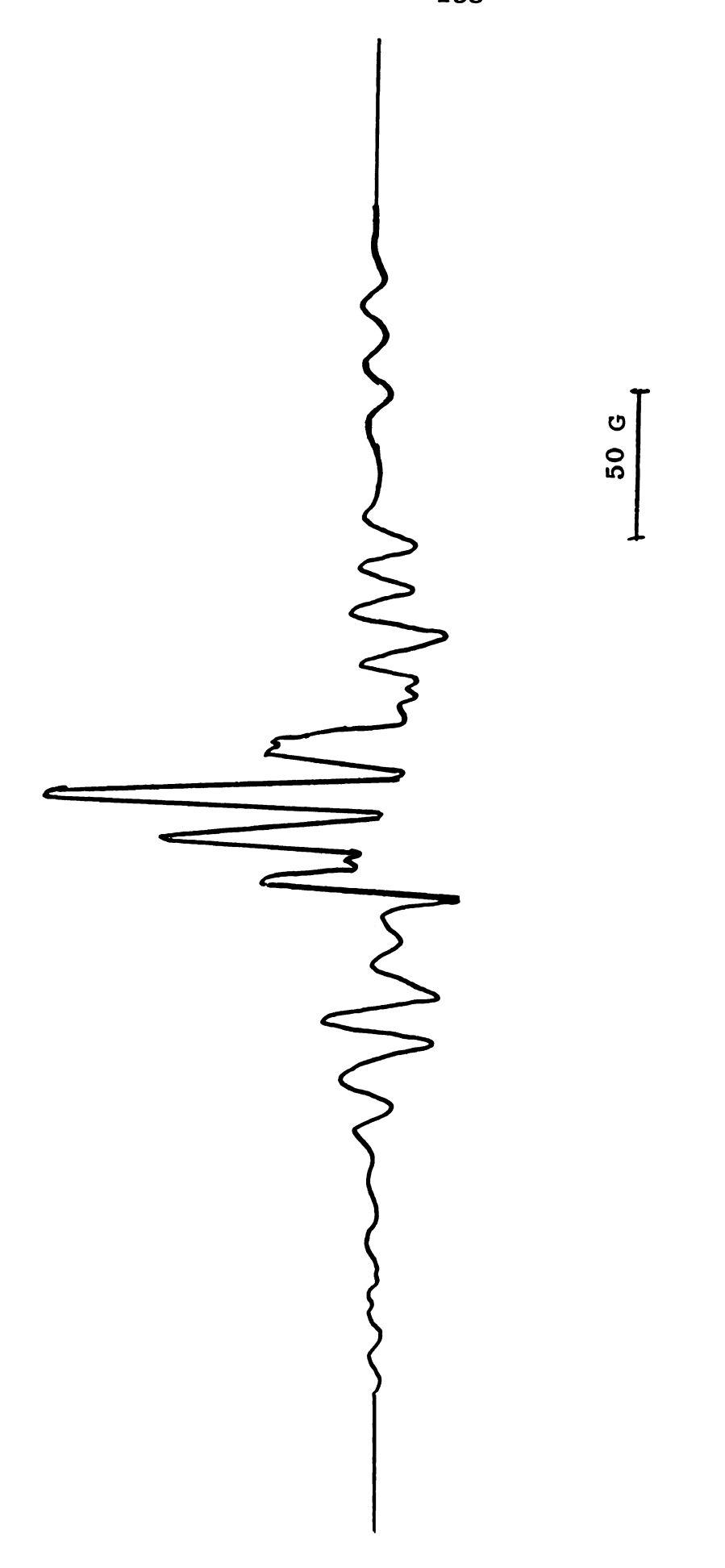
When the crystal was warmed, it was found that Cl<sub>2</sub> lines had almost disappeared by -80° and the spectrum of a second radical predominated. Analysis of this second radical was not possible due to the large number of molecules per unit cell and the complexity of the spectra. Figure 52 shows the spectrum of the second radical at 45° from H || a. in the aa' plane. The second radical, previously discovered by Whiffen (142), remained even at room temperatures.



ESR spectrum of irradiated hydrazinium dichloride at  $77^0 K$ .  $\overline{H}^>$  is 135° from a in the aa' plane. Figure 50.



ESR spectrum of irradiated hydrazinium dichloride at  $77^0 K. \ \overline{H}^{>} \ is \ 90^0$  from a in the aa' plane. Figure 51.



 $\overline{ESR}$  spectrum of irradiated hydrazinium dichloride after warming to -800.  $\overline{H}^{>}$  is  $45^{0}$  from a in the aa' plane. Figure 52.

## V. Irradiated Single Crystals of Hydrazinium Dibromide

#### A. Crystal Structure

No crystallographic data for hydrazinium dibromide have been previously reported. The space group and unit cell dimensions were determined using the usual Weissenberg and Precession method. X-ray photos showed the unit cell to be monoclinic with dimensions a = 3.86 Å, b = 7.53 Å, c = 10.28 Å, and  $\beta = 94^{\circ}$ . Systematic absences occur only for 001; 1 = 2n, consistent with space groups  $P2_1$  or  $P2_1/m$ . The measured density in a mixture of methylene bromide  $(\rho = 2.495 \text{ g/ml})$  and carbon tetrachloride  $(\rho = 1.589 \text{ g/ml})$  gave 2.144 g/ml. This yields a theoretical 1.98 molecules per unit cell consistent with the space group  $P2_1$ . The observation that the crystal was attracted to the walls of a silvered dewar flask containing liquid nitrogen is further evidence for the space group  $P2_1$ .

A drawing of the crystal showing the location of the a\*, b and c crystal axes is given in Figure 53. The crystal grew so that the long edge was parallel to b.

# B. Br<sub>2</sub> Radical in Crystals Irradiated at 770K

Single crystals of hydrazinium dibromide were put in glass vials and  $\gamma$ -irradiated for periods of 5 to 10 hours at  $77^{0}K$ . The crystals were then mounted, without warm-up, in the single-crystal holder described previously.

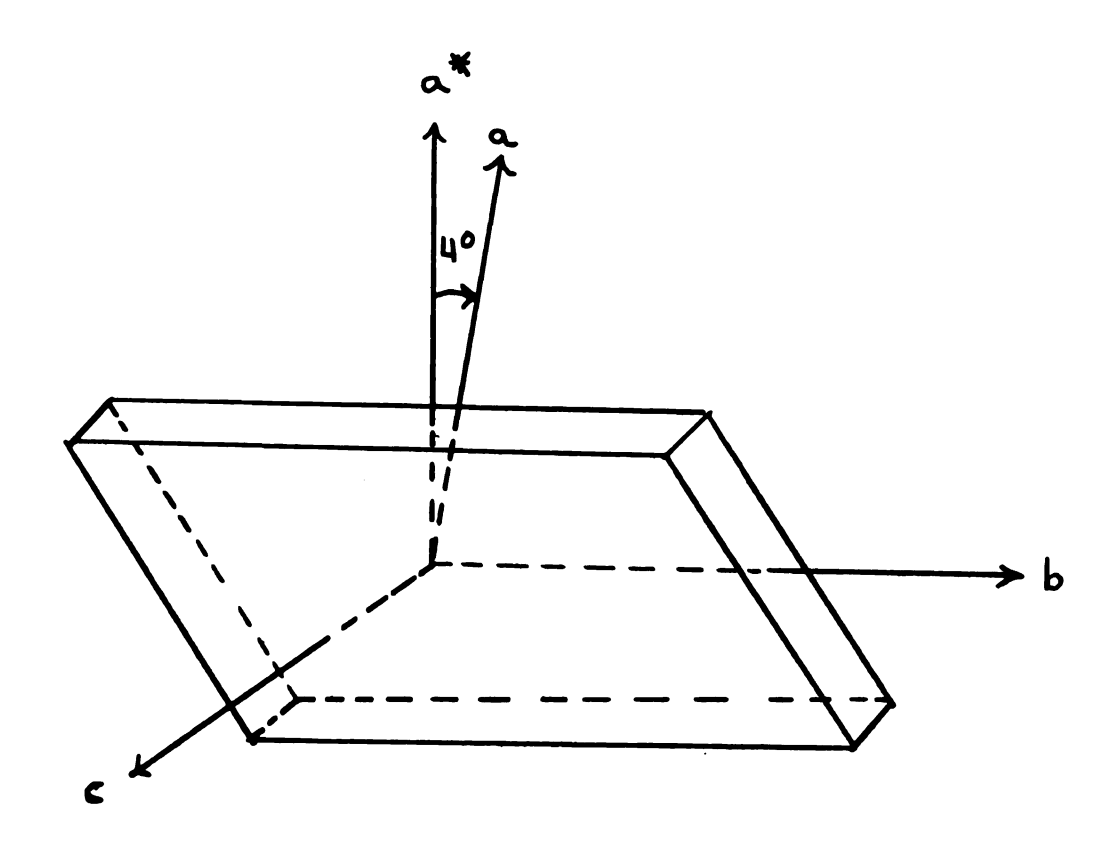
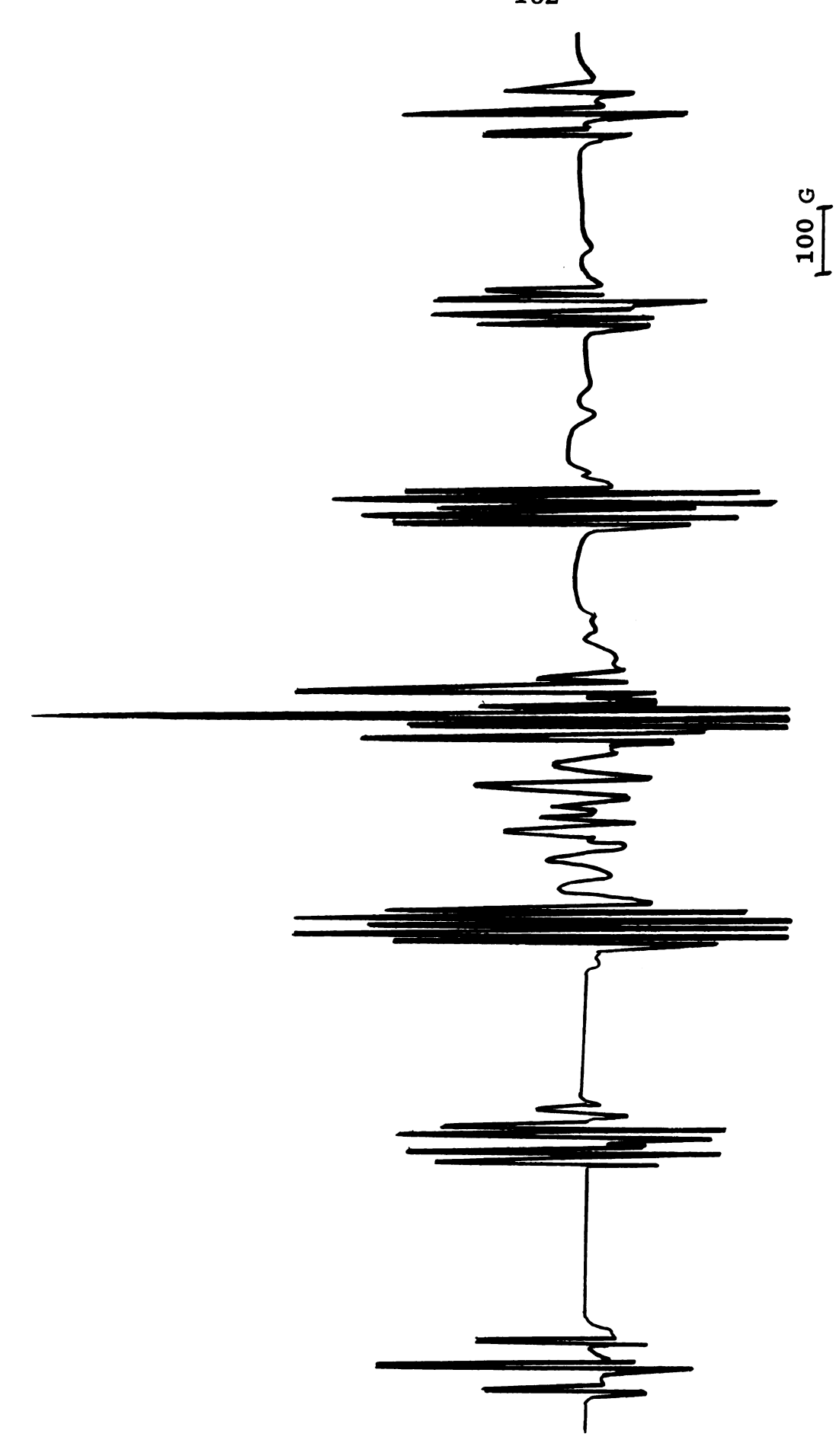


Figure 53. Crystal axes for hydrazinium dibromide.

It was found that the spectrum of  $\gamma$ -irradiated hydrazinium dibromide single crystals at  $77^{\circ}K$  consisted of seven basic groups of lines forming a septet with superhyperfine structure on each line. The main lines of the septet had relative intensity ratios nearly 1:2:3:4:3:2:1. Figure 54 shows the spectrum obtained after 5 hours of  $\gamma$ -irradiation;  $\overrightarrow{H}_{\text{ext}}^{>}$  is  $30^{\circ}$  from b in the bc plane and the measured hyperfine splitting at this orientation is 366 gauss.

Each line of the septet is further split and it should be noted that the outer lines are 1:2:1 triplets. The spectrum of Figure 54 was assigned to the radical anion Br<sub>2</sub> in which the odd electron interacts equally with the two Br (I = 3/2) nuclei which couple together to give an effective nuclear spin of three and hence the basic seven-line pattern observed. The 1:2:1 triplet structure of the outermost lines results from the presence of two isotopes of bromine. The outermost line of the triplet belongs to the radical (8¹Br - 8¹Br) formed from two bromine nuclei of mass 81 (49.43% natural abundance). The next innermost line, which is twice as intense, belongs to (7ºBr - 8¹Br) and (8¹Br - 7ºBr). Finally the last line of the triplet pattern can be assigned to the radical anion (7ºBr - 7ºBr) formed with two 7ºBr nuclei (50.57% natural abundance).

These anion radicals have been observed previously and are well characterized. For the space group  $P2_1$  one would expect two nonequivalent radicals per unit cell; this was found to be the case for  $Br_2$  in  $N_2H_6Br_2$ . The two radicals



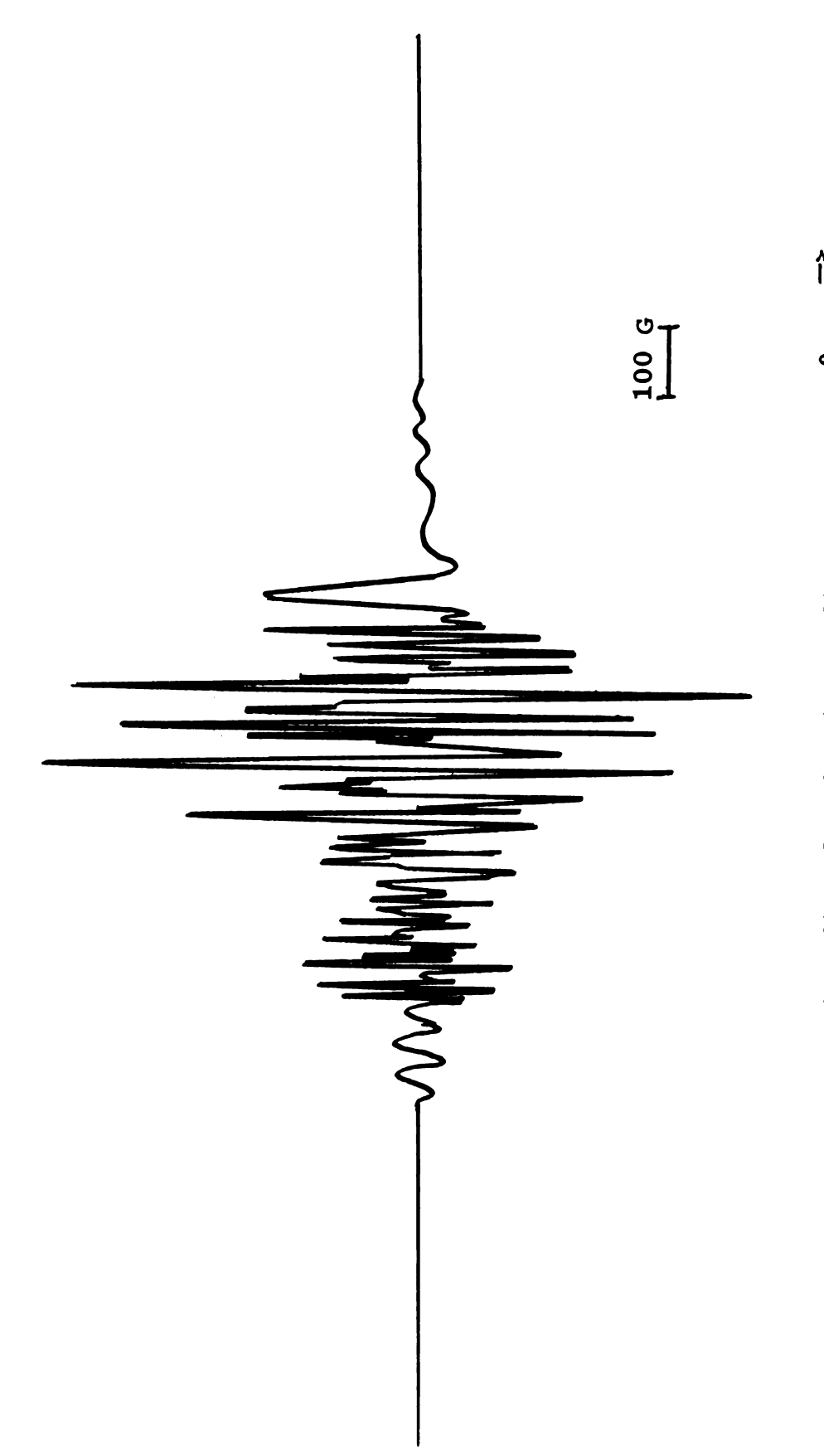
ESR spectrum of irradiated hydrazinium dibromide at  $77^{0}\mathrm{K}.$   $30^{0}$  from b in the bc plane. Figure 54.

become equivalent at certain positions as the crystal is rotated in the magnetic field. Figure 55 shows the spectrum at the orientation where the minimum hyperfine splitting is encountered;  $\overline{H}_{\rm ext}^{>}$  is 30° from c in the a\*c plane and the hyperfine splitting at this position is 128 gauss.

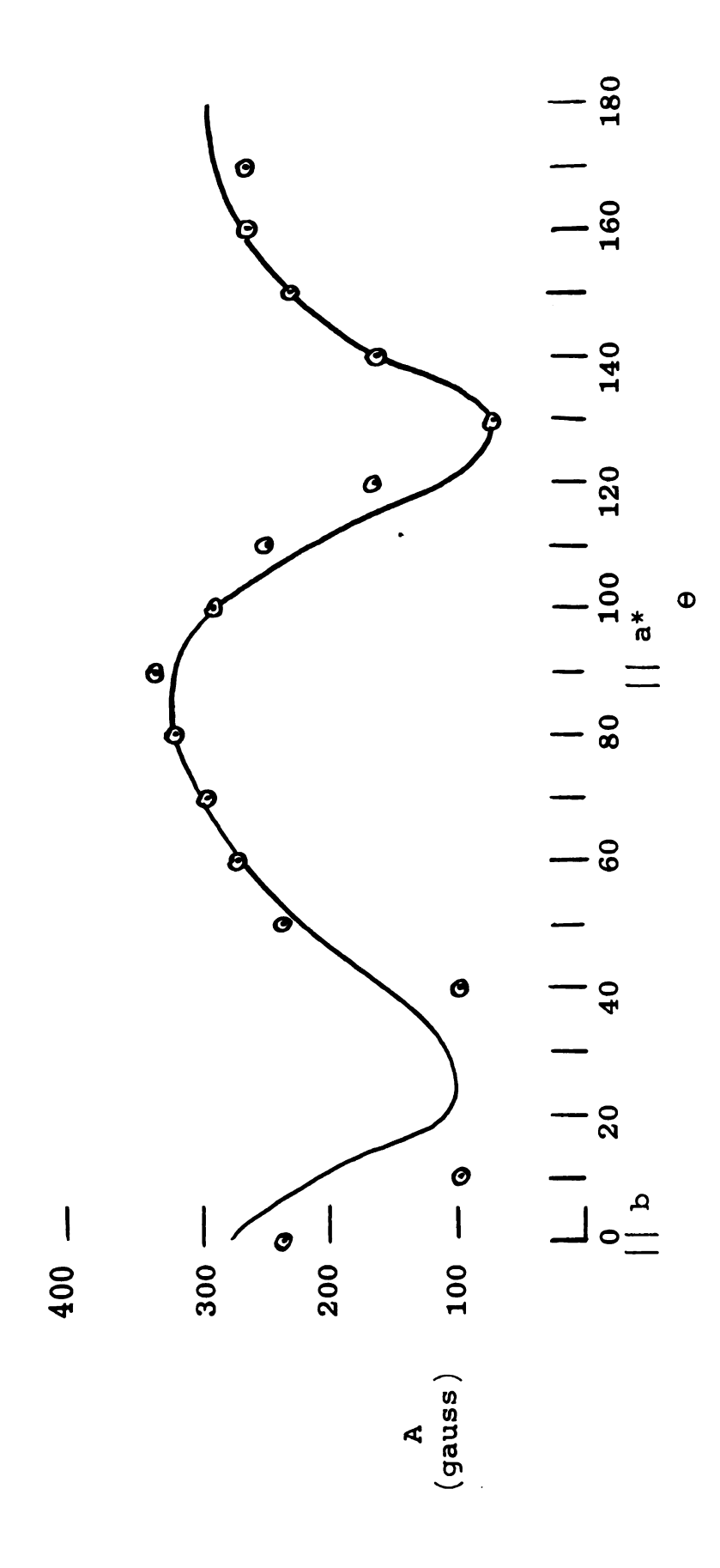
Principal values for the  $\overline{\mathbb{A}}$ ' and  $\overline{\mathbb{g}}$ ' tensors were computed using Schonland's method. The anisotropy was large enough that the conventional curve fitting technique failed to apply. The plots of hyperfine splitting versus angle of rotation are given in Figures 56 to 58; the plots of  $\overline{\mathbb{G}}$  versus angle of rotation are given in Figures 59 to 61. A compilation of the principal values for each tensor and their associated direction cosines is given in Table XVIII.

Table XVIII. Principal values of the hyperfine splitting tensor and g tensor for  $\text{Br}_2$  in  $\gamma$ -irradiated hydrazinium dibromide.

Tensor	Principal Values (gauss)	Direction Cosines		
Ā'	415.6	0.75	0.64	0.16
	243.5	-0.61	0.57	0.55
	79.7	0.26	-0.51	0.82
≣'	2.0635	0.40	0.08	-0.91
	2.0471	-0.59	0.78	-0.19
	1.9809	0.70	0.61	0.36



ESR spectrum of irradiated hydrazinium dibromide at  $77^0 \rm K$ .  $\overline{\rm H}^>$  is  $30^0$  from c in the a\*c plane. Figure 55.



plane. a\*b Figure 56. Hyperfine splitting of Br<sub>2</sub> versus angle of rotation in the

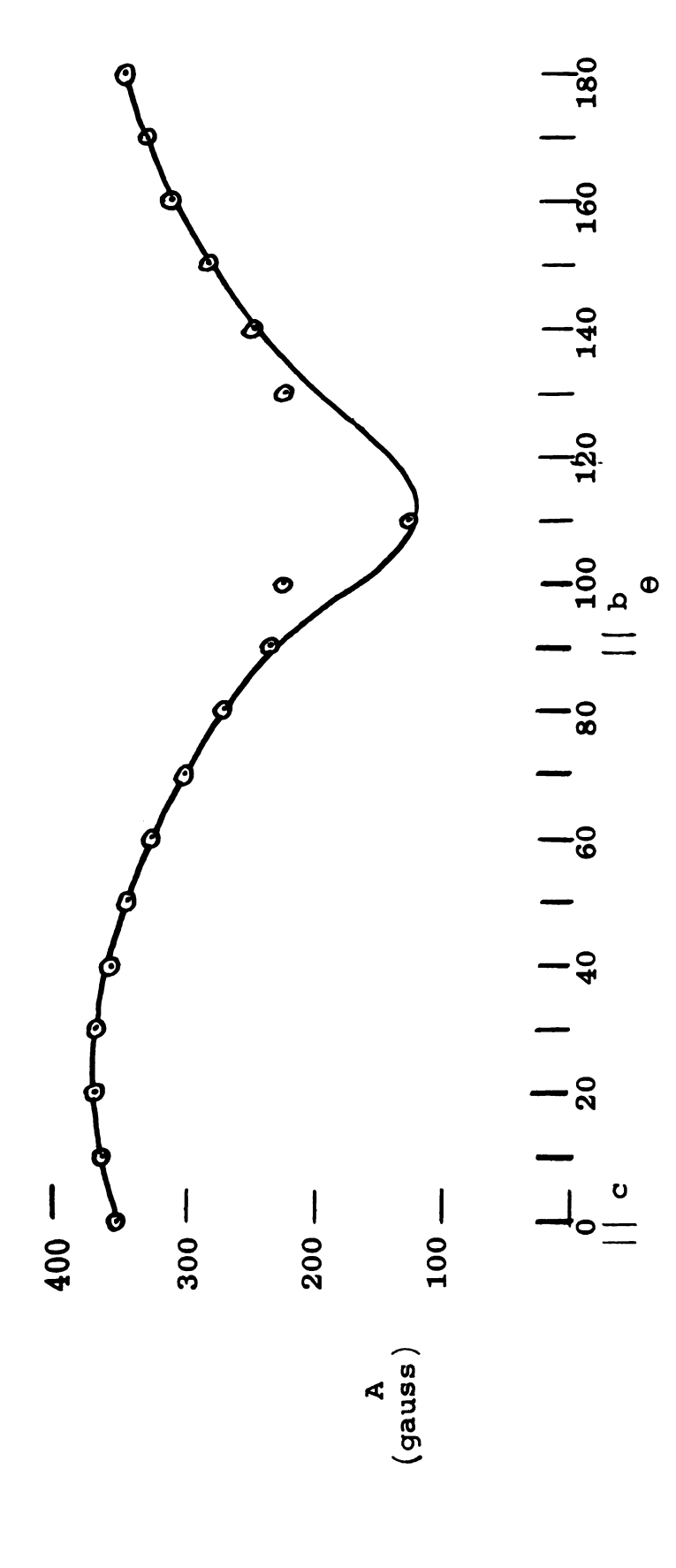
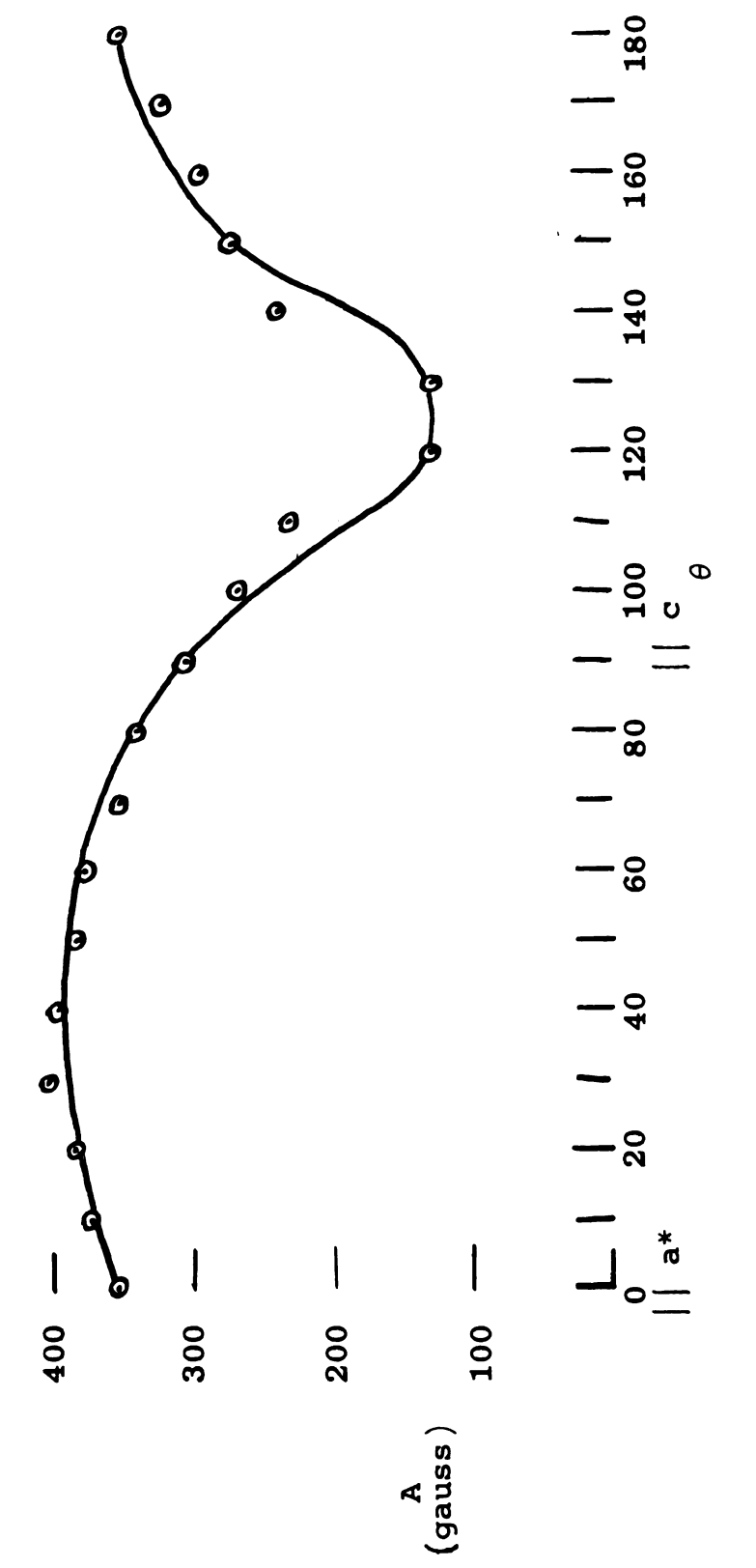
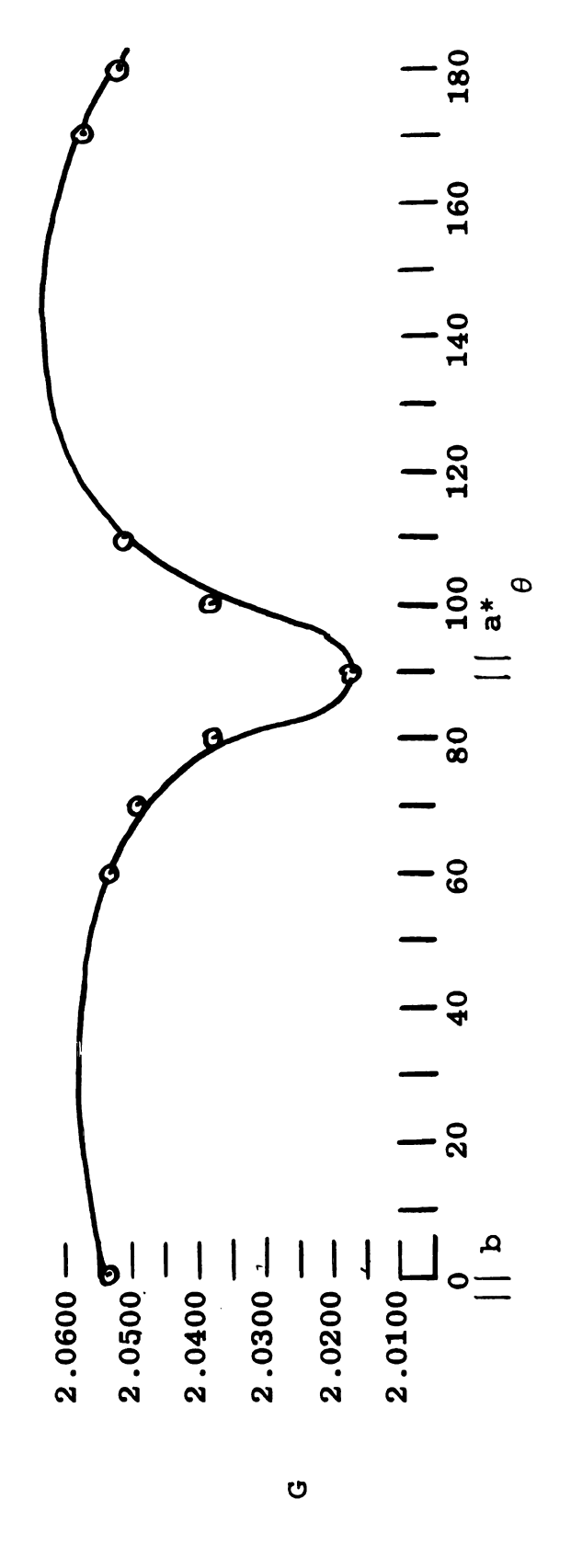


Figure 57. Hyperfine splitting of Br2 versus angle of rotation in the bc plane.



ນ \*ຜ Hyperfine splitting of  $\mathrm{Br}_2^-$  versus angle of rotation in the plane. Figure 58.



Br<sub>2</sub> in the a\*b plane. Figure 59. Plot of g versus angle of rotation for

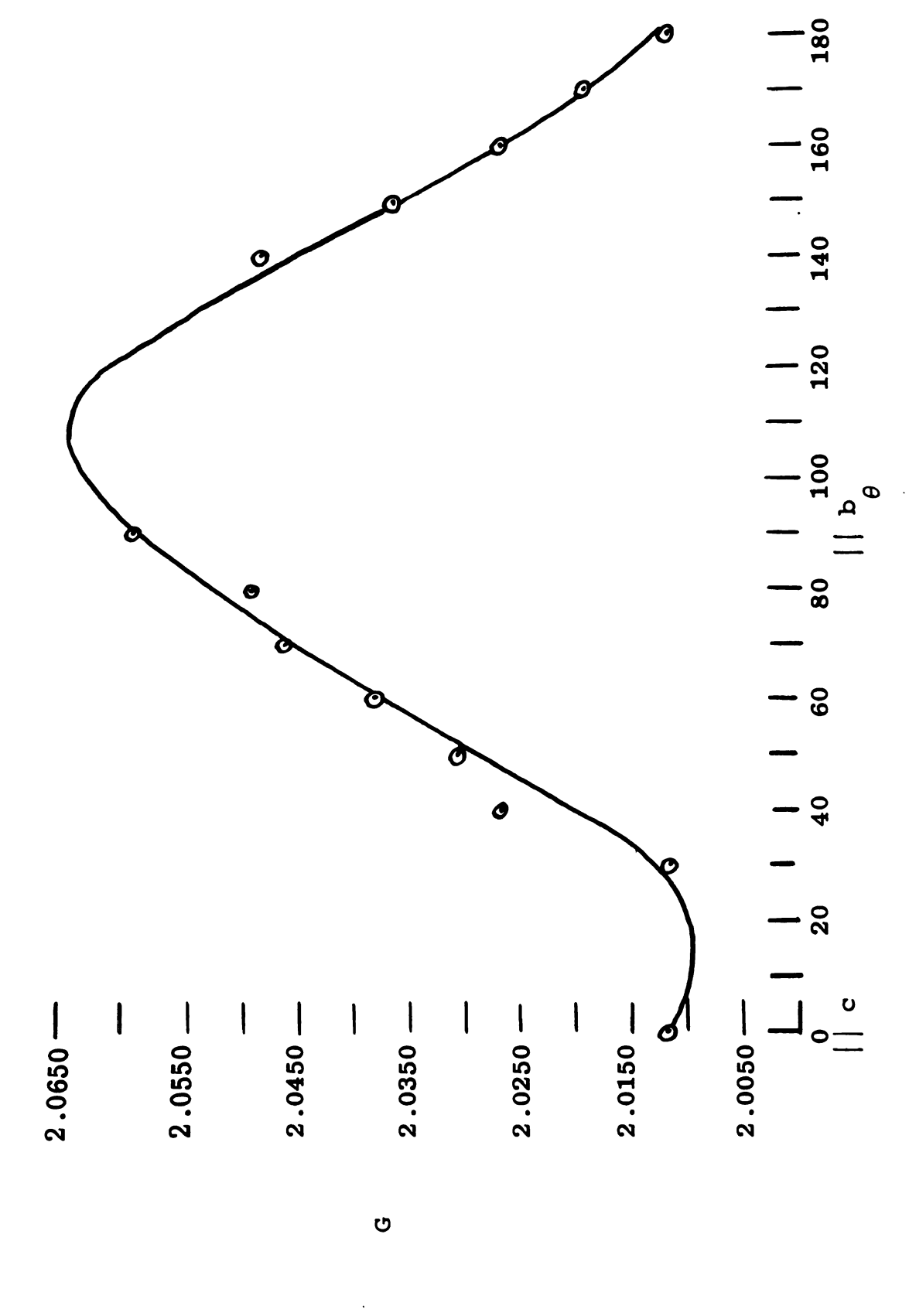
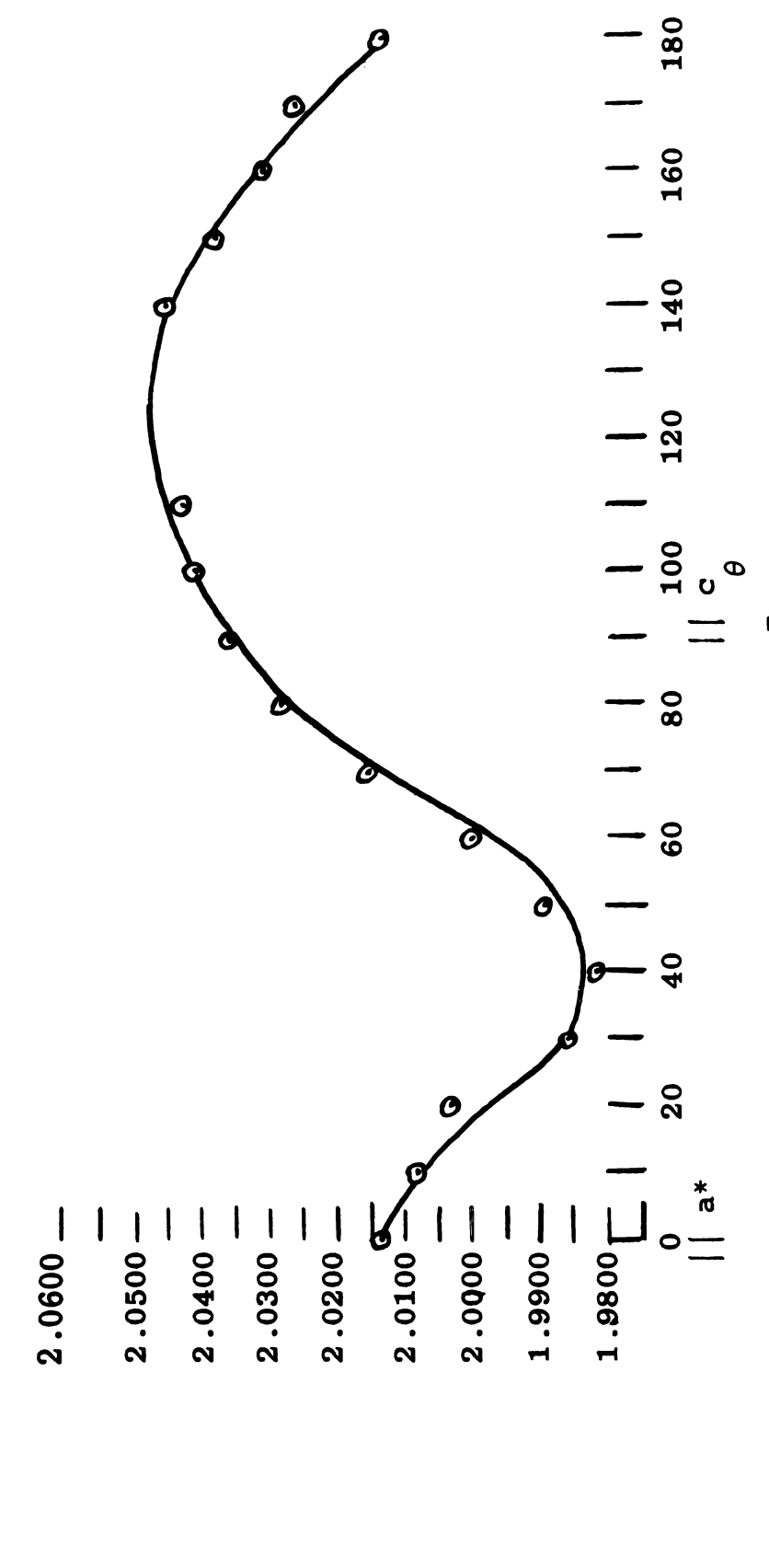


Figure 60. Plot of g versus angle of rotation for Br<sub>2</sub> in the bc plane.



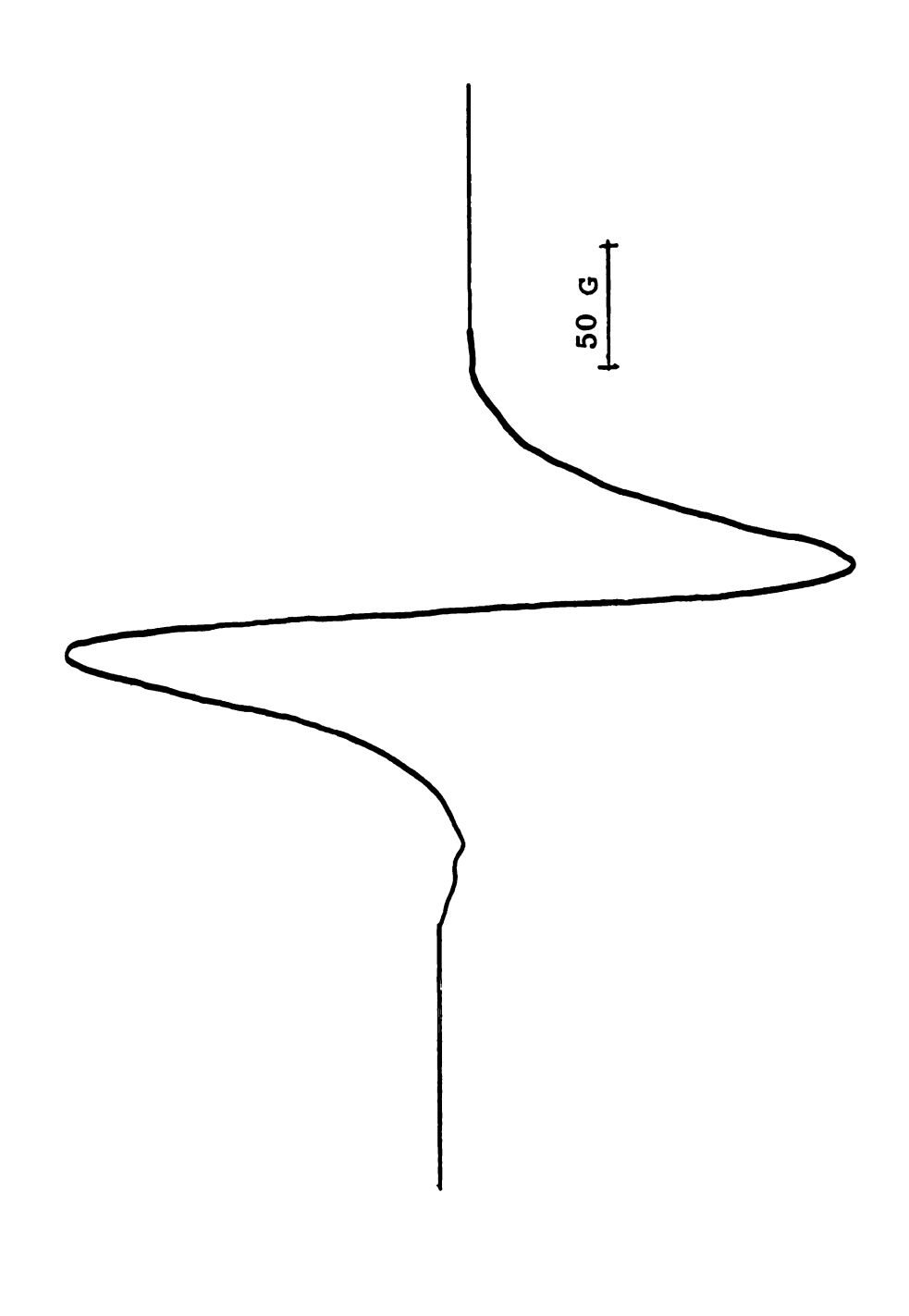
g versus angle of rotation for Br2 in the a\*c plane. Plot of Figure 61.

#### C. Temperature Studies

When a crystal of  $\gamma$ -irradiated hydrazinium dibromide was allowed to warm to  $-160^{\circ}$  it was found that the spectrum due to  $\text{Br}_2$  had disappeared. The measurements were done using the Varian V-4557 variable temperature dewar insert, although essentially the same results could be obtained by allowing the crystal to warm in an isopentaneliquid nitrogen slush bath at  $-155^{\circ}$ .

The spectrum obtained consisted of a single line with g=2.0043 which ultimately disappeared as the temperature was raised to  $-60^{\circ}$ . No structure was noted on this line which would indicate any interaction with other magnetic nuclei. In the absence of any other information this line can be attributed to the formation of a peroxide radical at  $-160^{\circ}$  after  $Br_2^-$  has disappeared. Figure 62 shows the first-derivative spectrum obtained with  $H \mid \mid$  c in the a\*c plane. First-derivative presentation was necessary since the concentration of radical was too low to obtain second-derivative spectra.

No other radical was observed after the decay of the peroxide radical indicating that and radicals produced from its decay are very unstalbe. No radicals stable at room temperature are produced.



First derivative ESR spectrum of irradiated hydrazinium dibromide warmed to  $-160^\circ;~H~\mid\mid c~$  in the a\*c plane. Figure 62.

#### VI. Irradiated Hydrazinium Difluoride

#### A. Crystal Structure

Kronberg and Harker (136) report that hydrazinium diffuoride is hexagonal with unit cell dimensions  $a_0 = 4.43 \pm 0.01$  Å and  $c_0 = 14.37 \pm 0.02$  Å and space group  $D_{3d}^5 - R$   $\overline{3m}$ ; the measured density of 1.46 g/ml gives three molecules per unit cell.

Truncated hexahedra grew easily from a 1:2 molar mixture of hydrazine hydrate and hydrofluoric acid. The large hexagonal face was found to be perpendicular to the c crystallographic axis in some cases. A drawing of the crystal is given in Figure 63 showing the more frequently encountered case where the c axis is perpendicular to one of the side faces. Because of the unique axis system encountered in hexagonal crystals, the reference axes chosen were the c crystallographic axis and two others perpendicular to c as defined in Figure 63.

# B. Hydrogen Atoms Formed at 770K

A single crystal of hydrazinium difluoride was electron irradiated with the G.E. Resonant Transformer for eight minutes at 77°K according to the procedure outlined in the Experimental section. The crystal was then mounted and the ESR spectrum observed at 77°K.

When the crystal was mounted with H | c, a doublet appeared as shown in Figure 64. The separation between

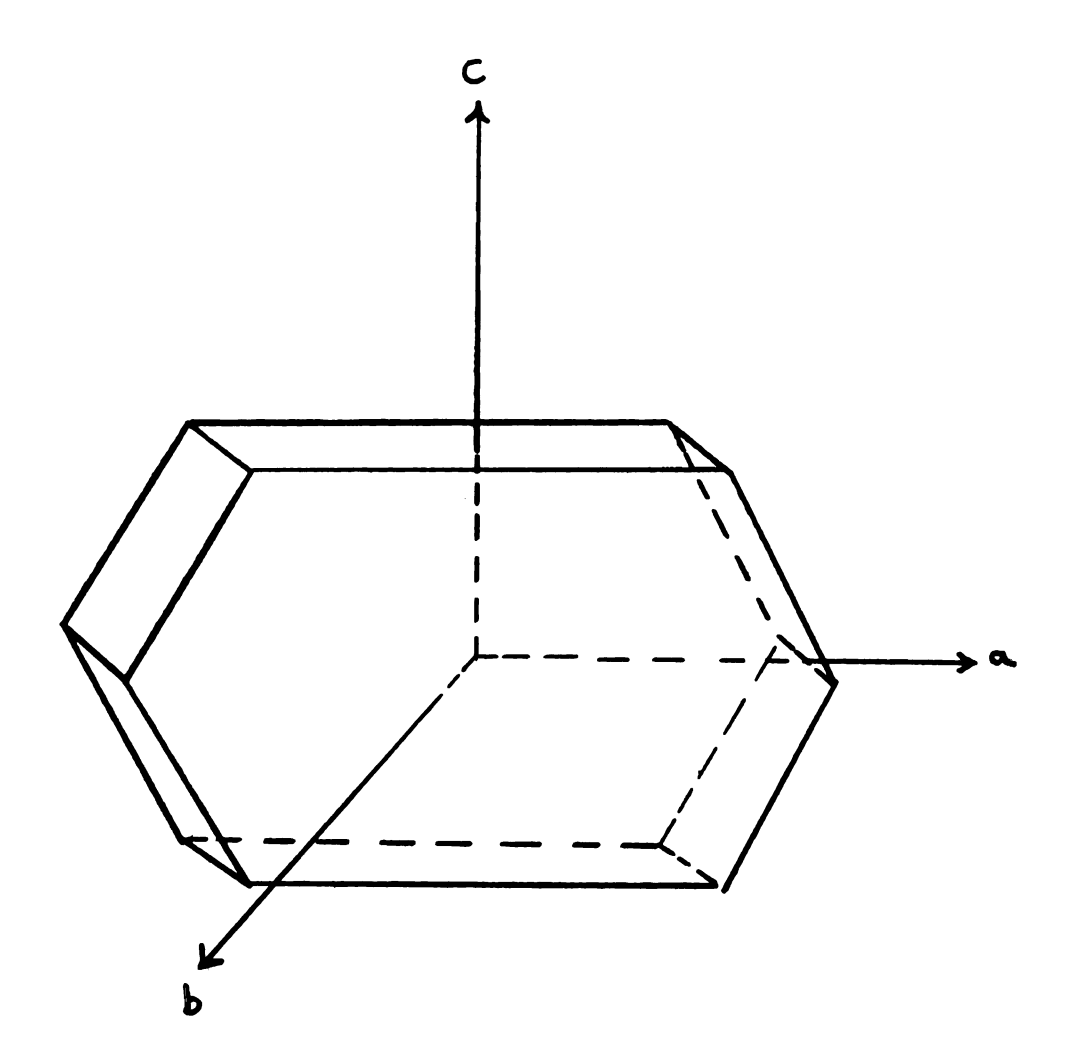
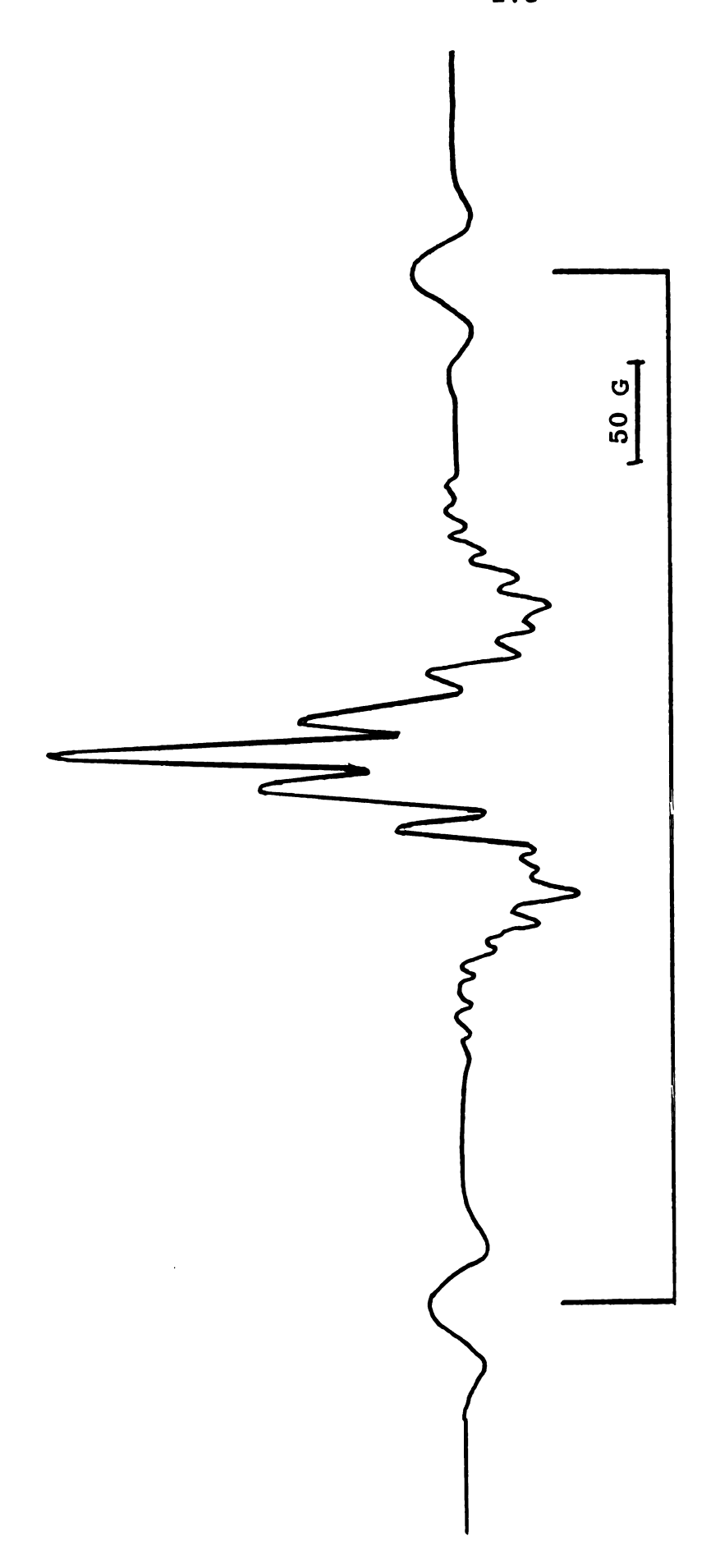


Figure 63. Crystal reference axes for hydrazinium difluoride; c is the threefold axis.

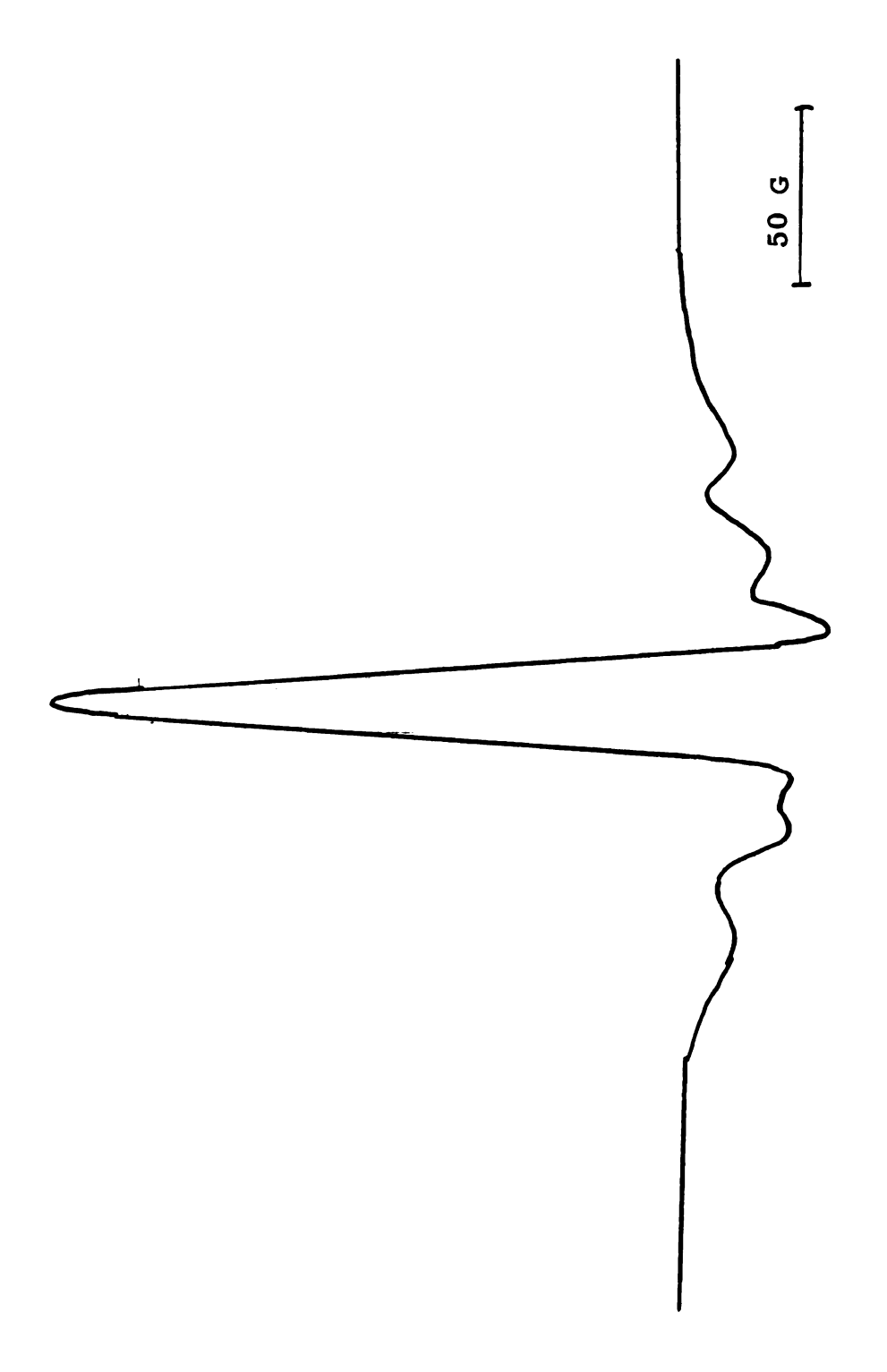


ESR spectrum of electron irradiated hydrazinium difluoride at  $770 \rm K$  showing the spectrum of the hydrogen atom (outer doublet).  $\overline{\rm H}^> \mid \mid \; c$  in the bc plane. Figure 64.

these lines was found to be 508 gauss. As the crystal was rotated in the plane perpendicular to c, it was found that the doublet hyperfine splitting remained essentially constant and equal to 508 gauss. This splitting is attributed to the presence of hydrogen atoms trapped in the crystal. In order to prove the existence of hydrogen atoms the hydrazinium difluoride was exchanged three times with D20. Since the magnetic moment of deuterium is 0.32 times the magnetic moment of a proton, the hyperfine splitting for deuterium atoms is only 15.4% of that for protons or about 78 gauss. Figure 65 shows the ESR spectrum of a crystal of N<sub>2</sub>D<sub>6</sub>F<sub>2</sub> which had been y-irradiated for ten hours with H | c in the bc plane. The spectrum consists of a broad central peak with a line spaced equally on either side of the central peak by 61 gauss. As the crystal is rotated in each of the three reference planes ab, bc, and ac, the splitting changes from a maximum of 61 gauss to a minimum of 55 gauss, and thus remains fairly isotropic. This splitting is probably due to deuterium atoms; however, the reason for the perturbation from the theoretical value of 85 gauss is not understood. This effect was not noted in the case of hydrogen atoms where the isotropic splitting was always 508 gauss.

# C. Radical Pairs at 770K

Single crystals of hydrazinium difluoride were  $\gamma$ -ir-radiated for ten hours at  $77^0K$  and were mounted without warm-up in the usual manner. The spectrum was found to be



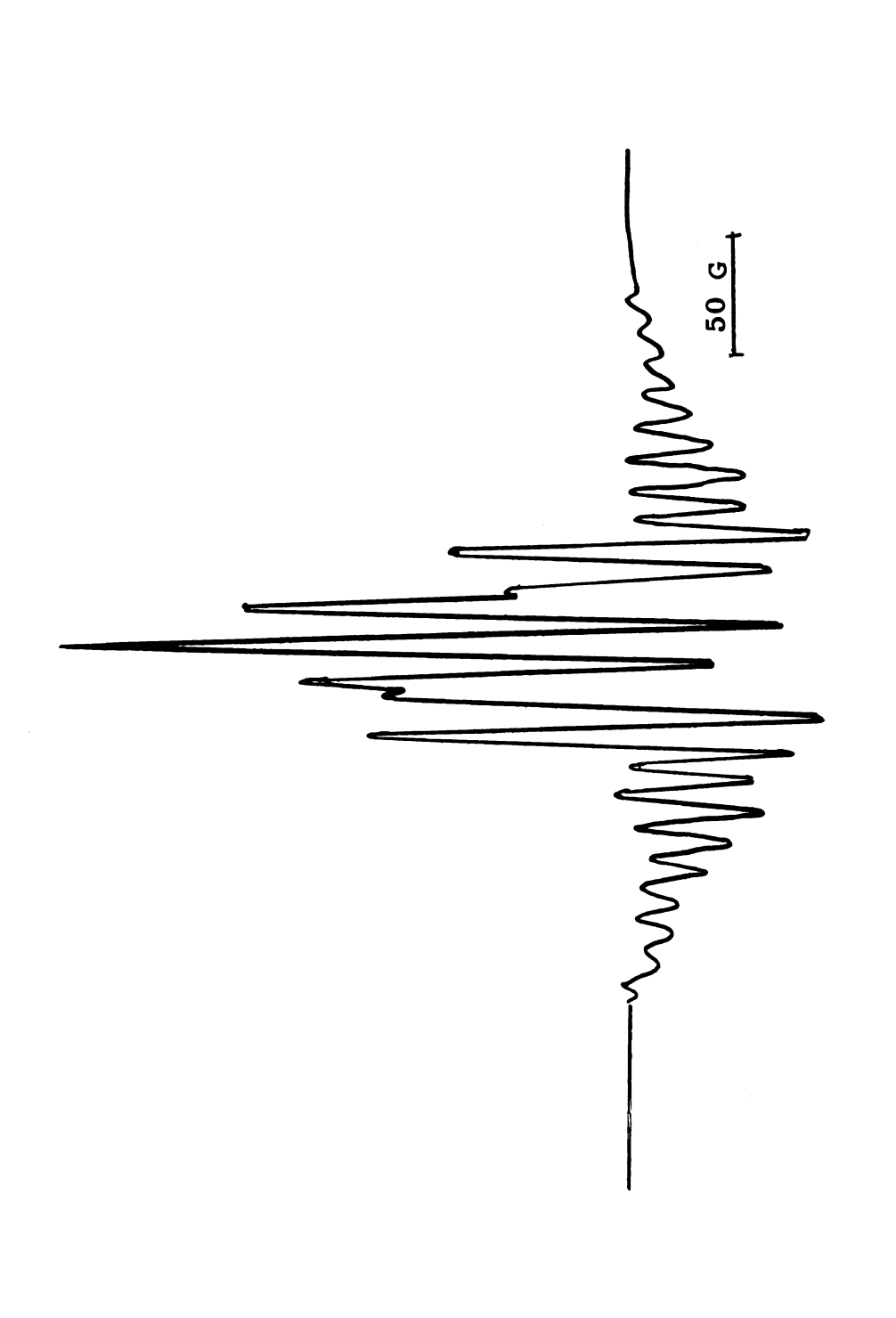
ESR spectrum at 770K of  $\gamma$ -irradjated hydrazinium difluoride which has been exchanged with D20. H  $\mid$  c in the bc plane. Figure 65.

very sensitive to the amount of microwave power used; it was necessary to use 30 db attenuation of the high power arm of the Varian microwave bridge to avoid saturation. When the crystal was mounted in the bc plane with  $H \mid \mid c$  the spectrum of Figure 66 was obtained. As can be seen from the spectrum, the pattern observed is quite complicated but the outer lines in the central portion can be attributed to the presence of a radical pair. This was confirmed by the observation of a complex group of lines at  $g \cong 4$  (Fig. 67). The spectra are not well enough resolved even with  $H \mid \mid c$  to permit identification of the species forming the pair; when the field is rotated from  $H \mid \mid c$  the signals from the pair rapidly become unobservable.

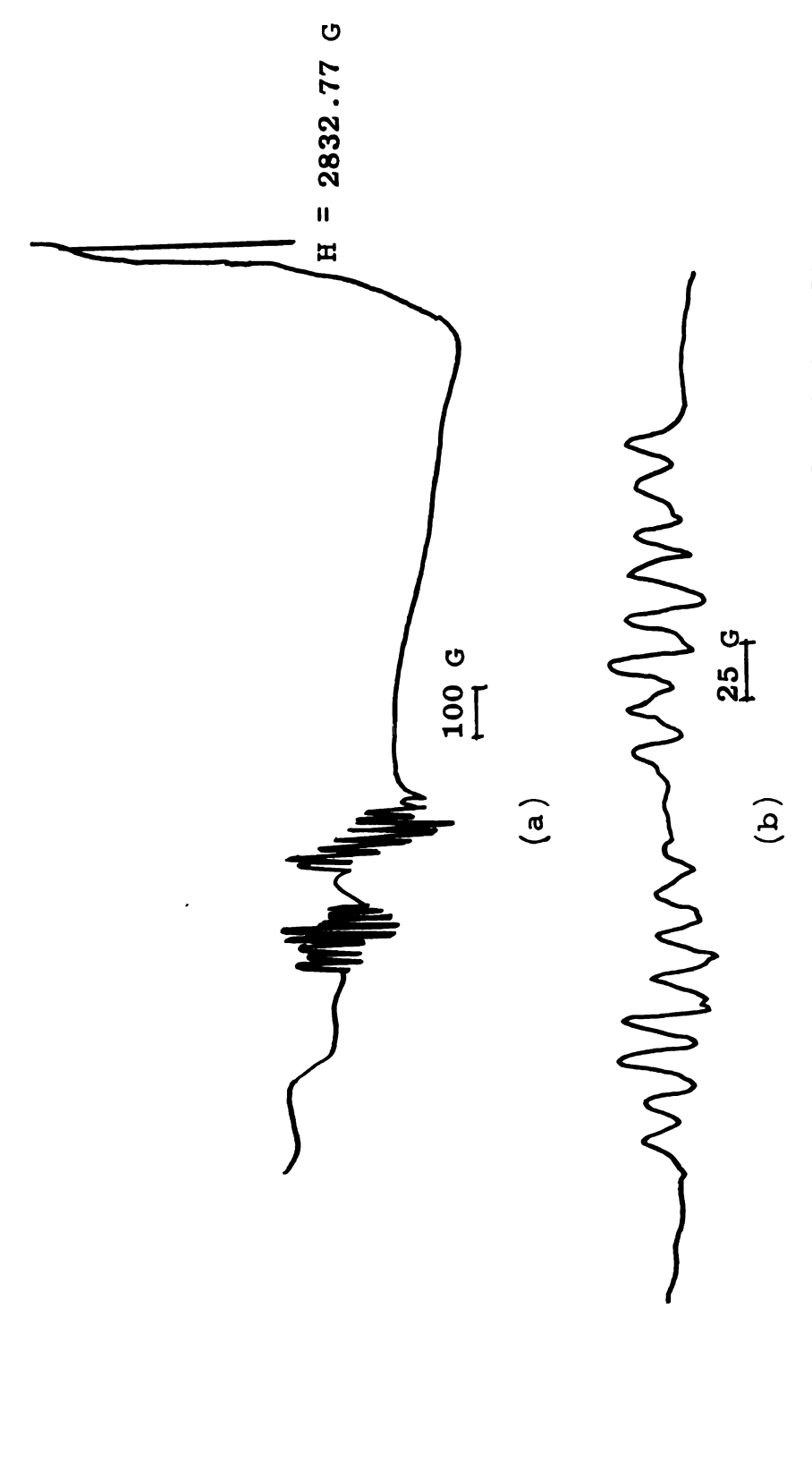
The strong lines in the center of the spectrum of Figure 66 are from a radical which is stable at higher temperatures. By warming to  $-70^{\circ}$  the radical pairs may be destroyed and well-resolved spectra of the new radical obtained as discussed below.

## D. The Radical at -700

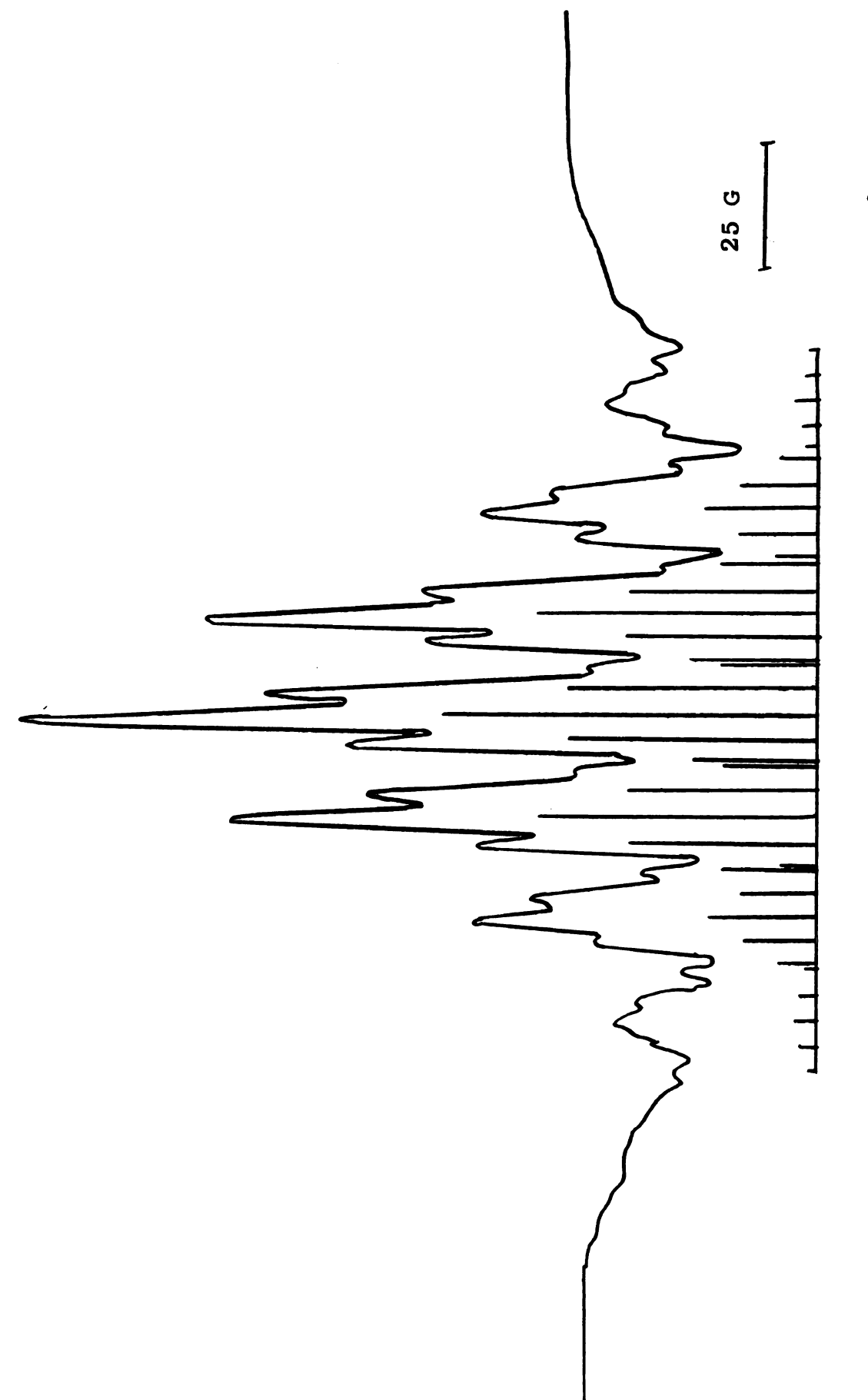
A single crystal of hydrazinium difluoride, which had been  $\gamma$ -irradiated for ten hours, was allowed to warm to  $-70^{\circ}$  in a liquid nitrogen-acrylonitrile slush bath for three minutes. It was found that the radical-pair spectrum had disappeared after this treatment; a much simpler spectrum was observed. Figure 68 shows the spectrum with  $H \mid \mid c$  in the bc plane. The pattern is a septet of quintets with



บ ESR spectrum of  $\gamma\text{-irradiated}$  hydrazinium difluoride at  $77^0K$  with  $\overline{H}^>\big|\,\big|$  in the bc plane. The outer seven lines on each side are attributed to a radical pair. Figure 66.



First derivative ESR spectrum of  $\gamma$ -irradiated hydrazinium difluoride at 770K with  $H^>||c;a\rangle$  position of the g=4 lines relative to the resonance at g=2, b) the g=4 lines with better resolution. Figure 67.

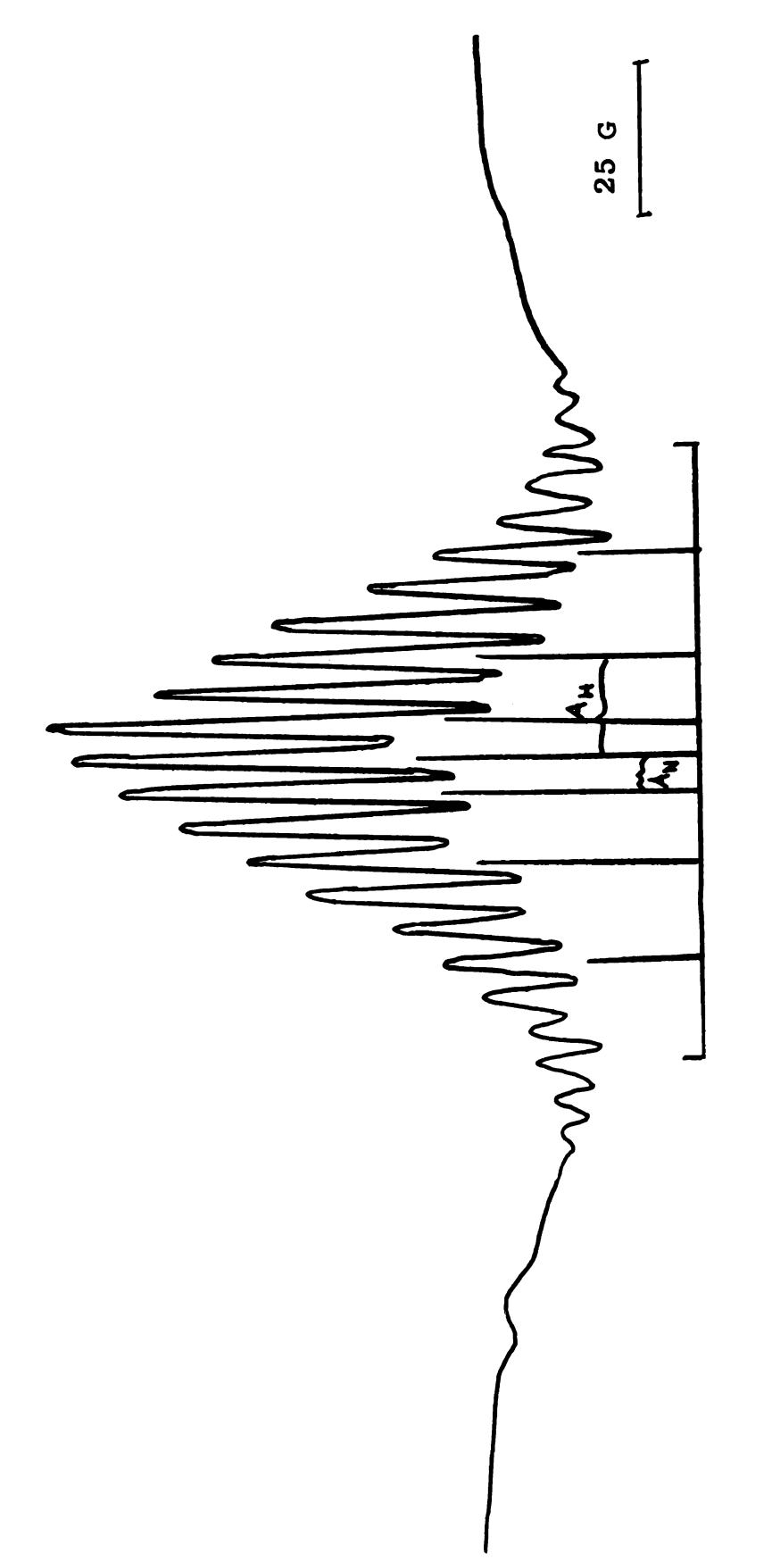


<u>ESR</u> spectrum of  $\gamma$ -irradiated hydrazinium difluoride warmed to -700. H  $\mid \mid$  c in the bc plane. Figure 68.

intensity ratios for the septet being nearly the binomial values 1:6:15:20:15:6:1, while those for the quintet hyperfine are approximately in the ratio 1:2:3:2:1. The outer lines of the quintet pattern are not visible on all the lines of the septet due to overlap. This is indicated in Figure 68.

The spectrum of Figure 68 has been attributed to a radical with coupling to six equivalent protons resulting in the septet pattern. The quintet fine structure on each line of the septet is attributed to equivalent coupling by two nitrogen nuclei  $(I_{total} = 2)$ . The proton hyperfine splitting for H | c (Figure 68) is 19.3 gauss and the nitrogen splitting is 6.0 gauss. As the crystal is rotated in the bc plane toward the b-axis, the spectrum of Figure 69 is observed when  $\overline{H}_{\text{ext}}^{>}$  is 40° from c. This pattern can be again assigned to equivalent splitting by six protons with a smaller splitting by two equivalent nitrogen nuclei. The proton splitting at this orientation is 15.1 gauss; the nitrogen splitting is 5.5 gauss as indicated in Figure 69. As the crystal is rotated further in the bc plane, the nitrogen and proton splittings decrease. The spectrum of Figure 69 appears again at  $135^{\circ}$  and that of Figure 68 reappears for  $\theta = 180^{\circ} (H \mid c)$ .

In the ab plane (H  $\downarrow$  c) the nitrogen splitting is unobservable for all orientations. The maximum proton splitting occurs 30° from the a-axis and is 19.3 gauss. This orientation is shown in Figure 70. The minimum proton splitting occurs when  $\overline{H}_{\rm ext}^{>}$  is 120° from the a axis in the



ESR spectrum of  $\gamma-irradiated$  hydrazinium difluoride warmed to -700. H is 400 from c in the bc plane. Figure 69.

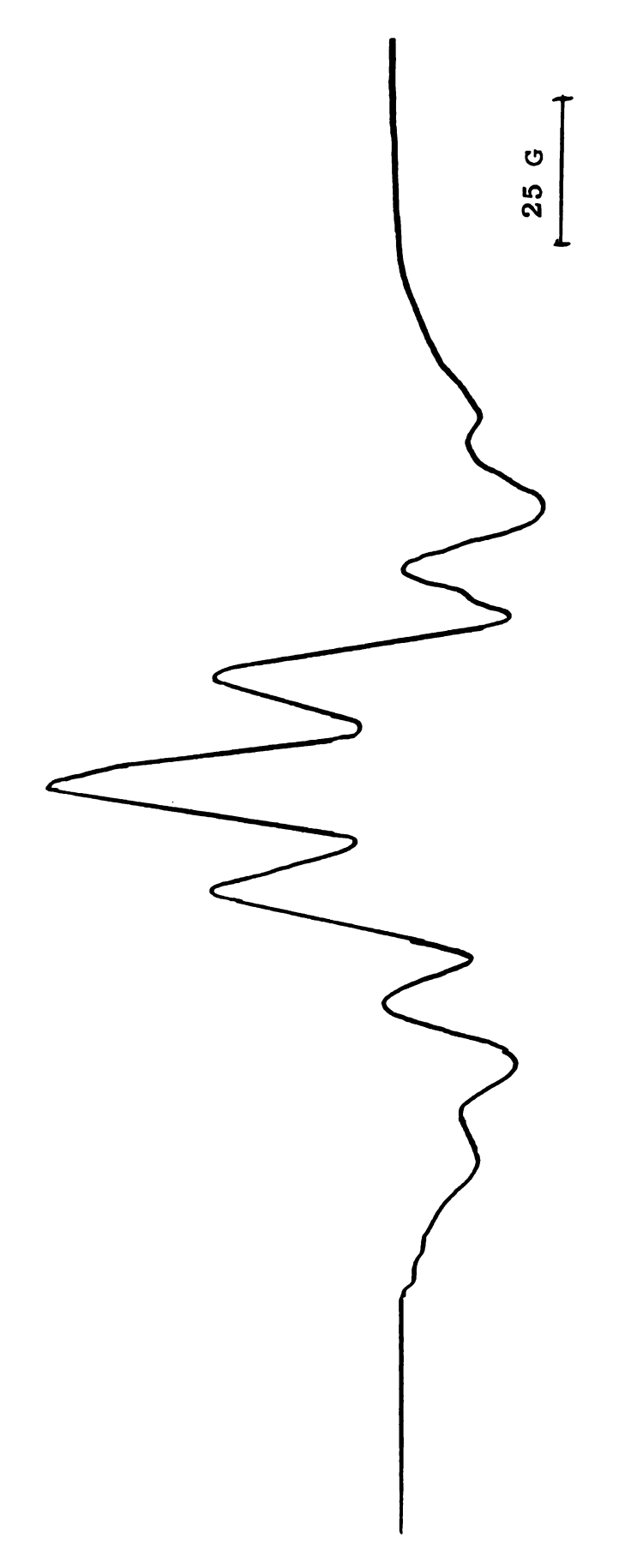


Figure 70. ESR spectrum of  $\gamma$ -irradiated hydrazinium difluoride warmed to -700 H is 300 from the a axis in the ab plane (plane  $\downarrow$  to c axis).

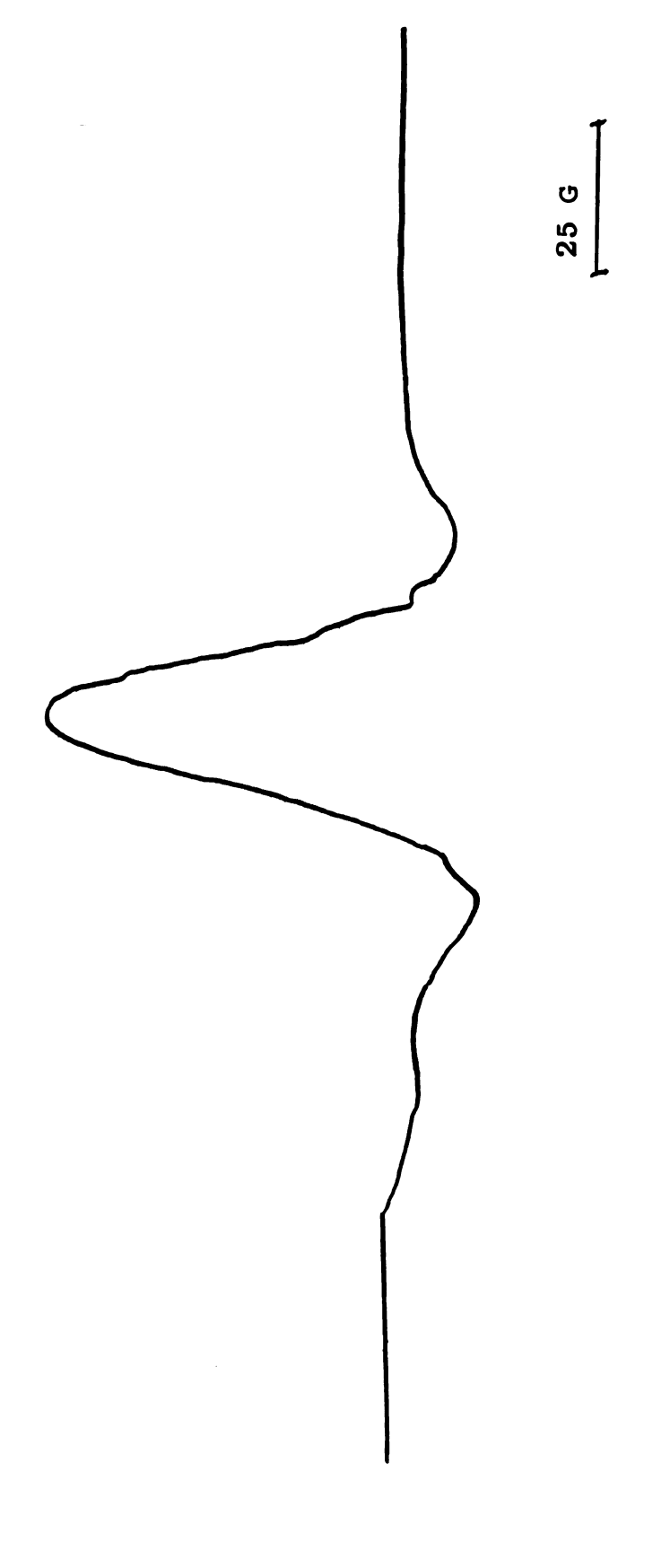
ab plane and is estimated from the line width to be 12.6 gauss. This orientation is shown in Figure 71.

In the ac plane the spectrum of Figure 71 is shown when H  $\mid \mid$  c, while that of Figure 69 appears when  $\overrightarrow{H}_{\text{ext}}^{\rightarrow}$  is 50° from the a axis. Further rotation gives the septet of quintets again at 90° from a in the ac plane (H  $\mid \mid$  C). Further rotation in the ac plane gives the spectrum of Figure 69 when  $H_{\text{ext}}$  is 109° from a in the ac plane resulting ultimately in the spectrum of Figure 71 for H  $\mid \mid$  a.

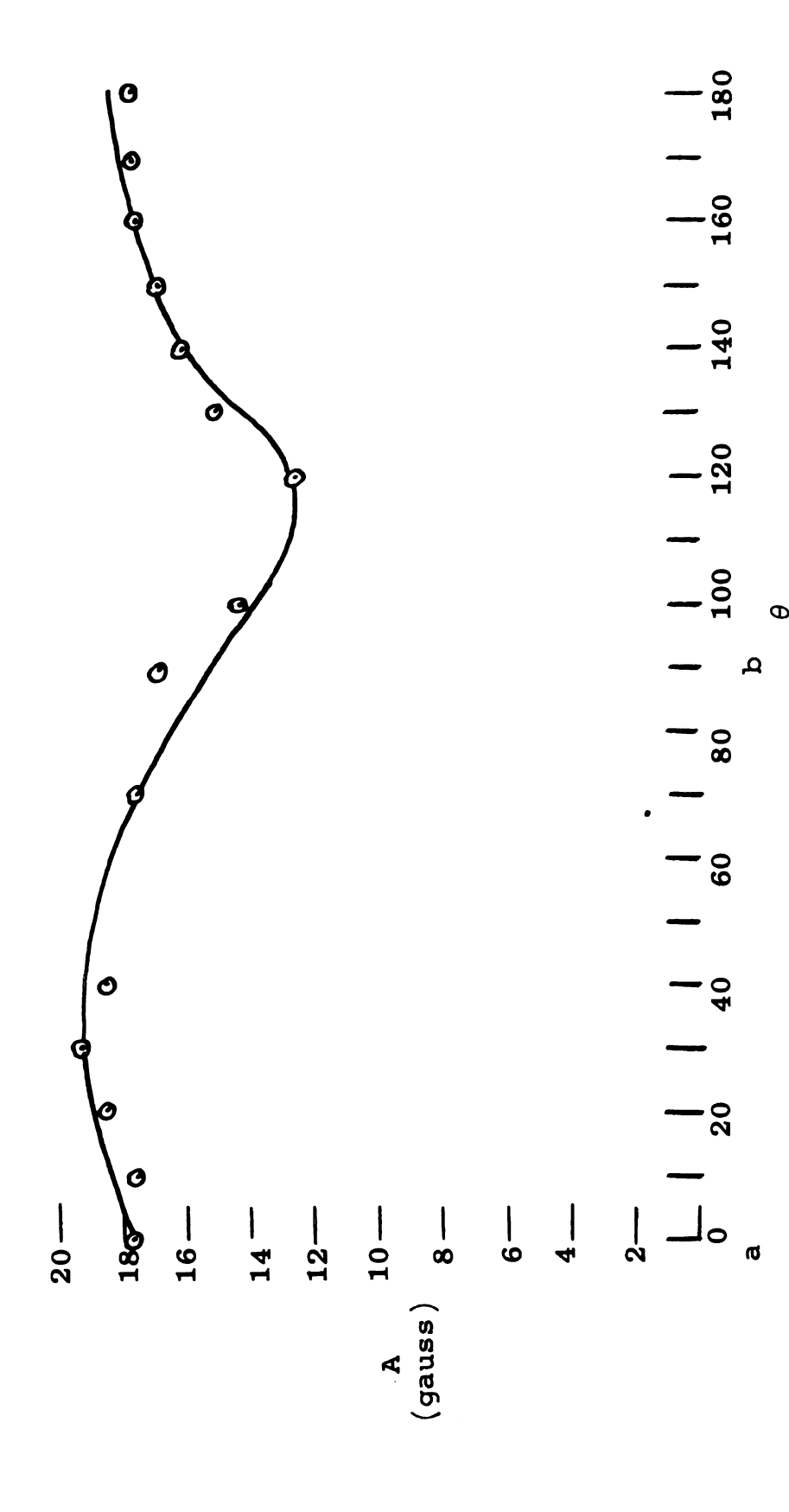
were followed as the crystal was rotated in each of the three reference planes. The angular variation was most pronounced in the bc and ab planes in the case of the proton hyperfine splitting. The nitrogen splitting in the ab plane (H \( \price \) c) was assumed to be rather constant and equal to 1.7 gauss for all crystal orientations. These plots are given in Figures 72 to 74. The principal values of the nitrogen tensor were obtained by Schonland's method. Enough points were available to permit a curve fit (Equation 46) for the proton hyperfine values. The results of these calculations are given in Table XIX.

The g value for the radical was found to change very little and was  $2.0035 \pm 0.0005$  for all orientations in the ab, bc and ac reference planes.

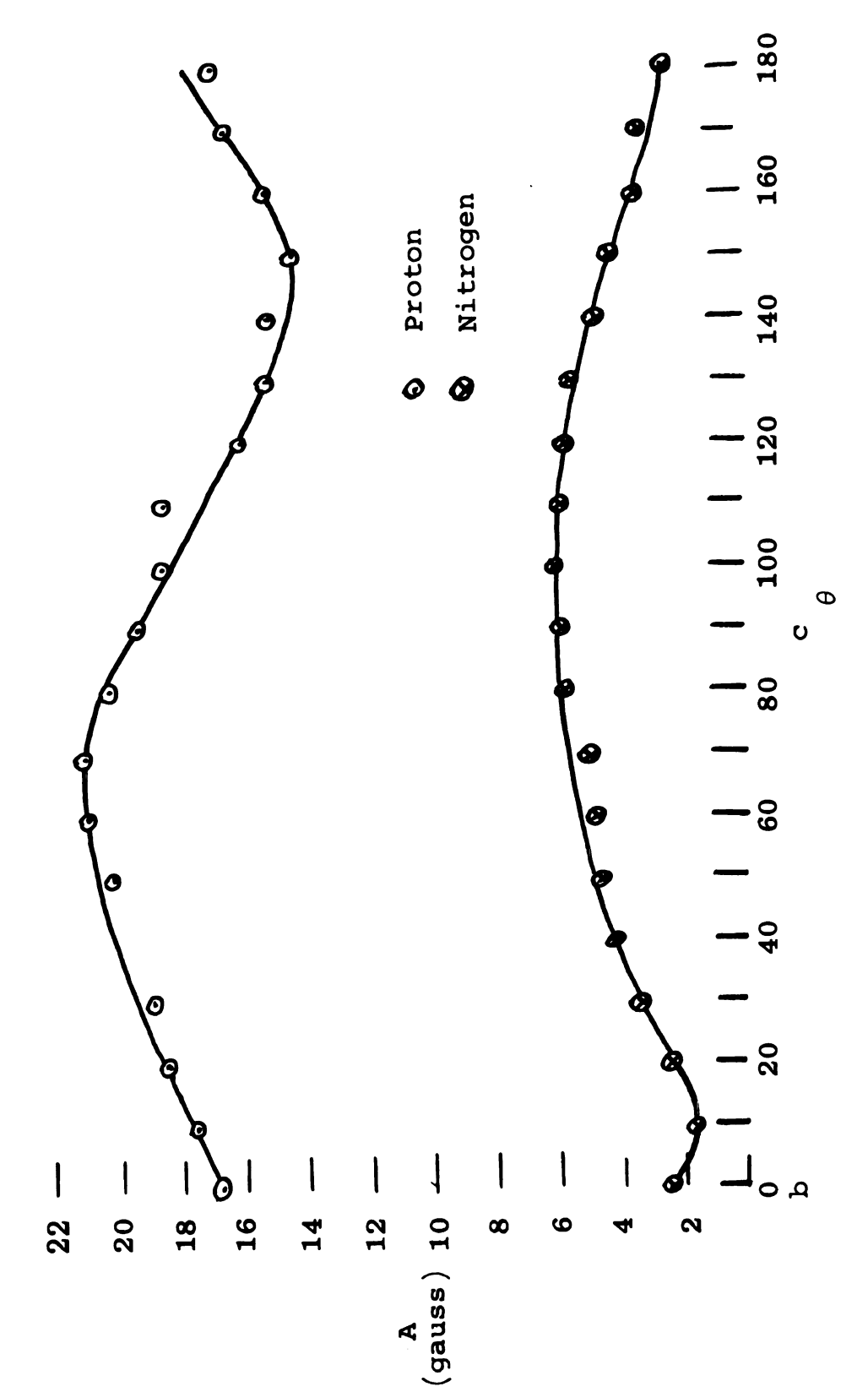
Upon warming no other radical appeared, but it was noted the  $-70^{\circ}$  radical was stable after being brought to room



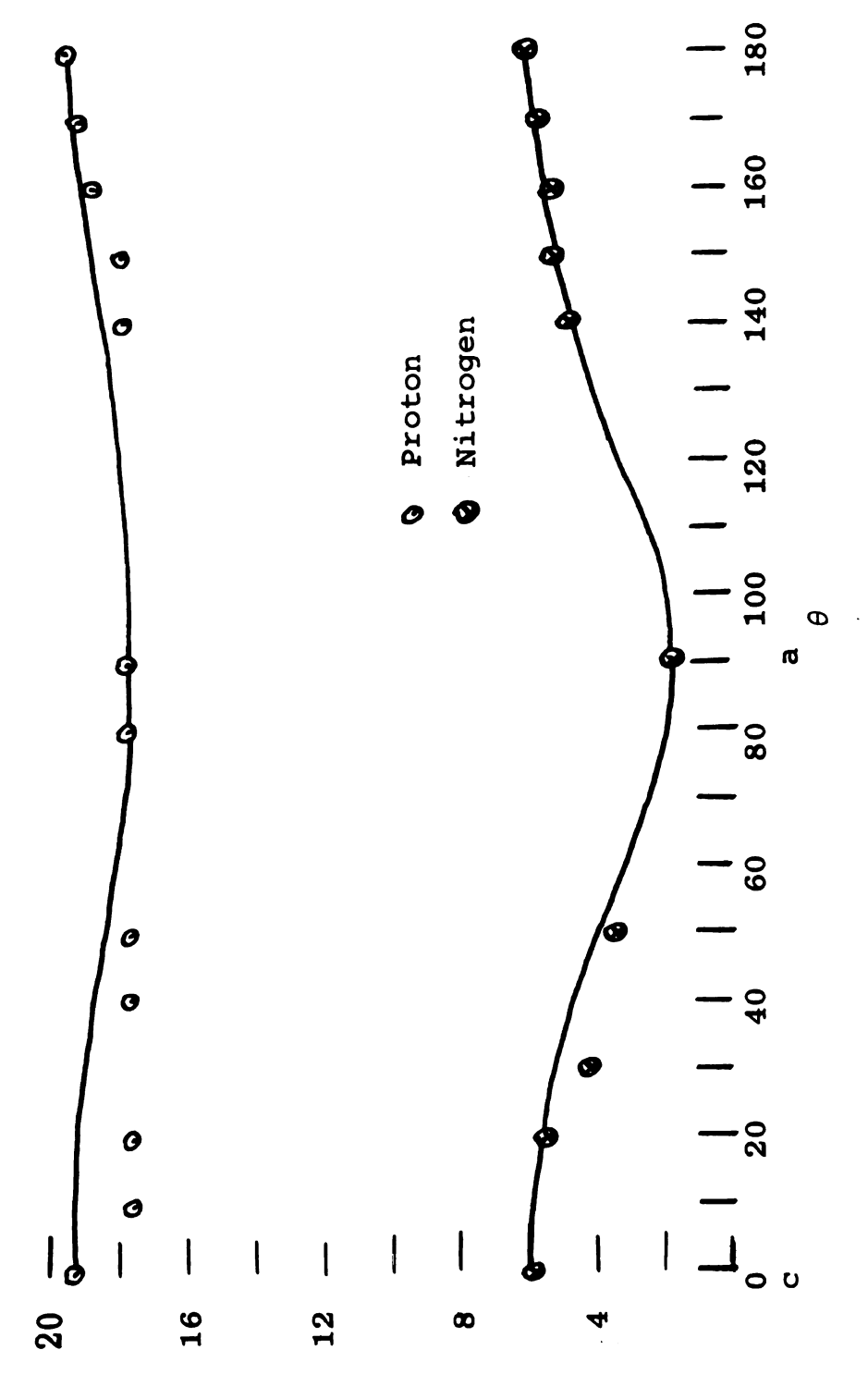
ESR spectrum of  $\gamma\text{-irradiated}$  hydrazinium difluoride warmed to -700.  $\overline{H}^>$  is  $120^0$  from the a axis in the ab plane. Figure 71.



plane Angular variation of the hydrogen hyperfine splitting in the abfor the  $-70^{0}$  radical. Figure 72.



Angular variation of the nitrogen and hydrogen hyperfine splitting in the bc  $\,$  plane for the -700 radical. Figure 73.



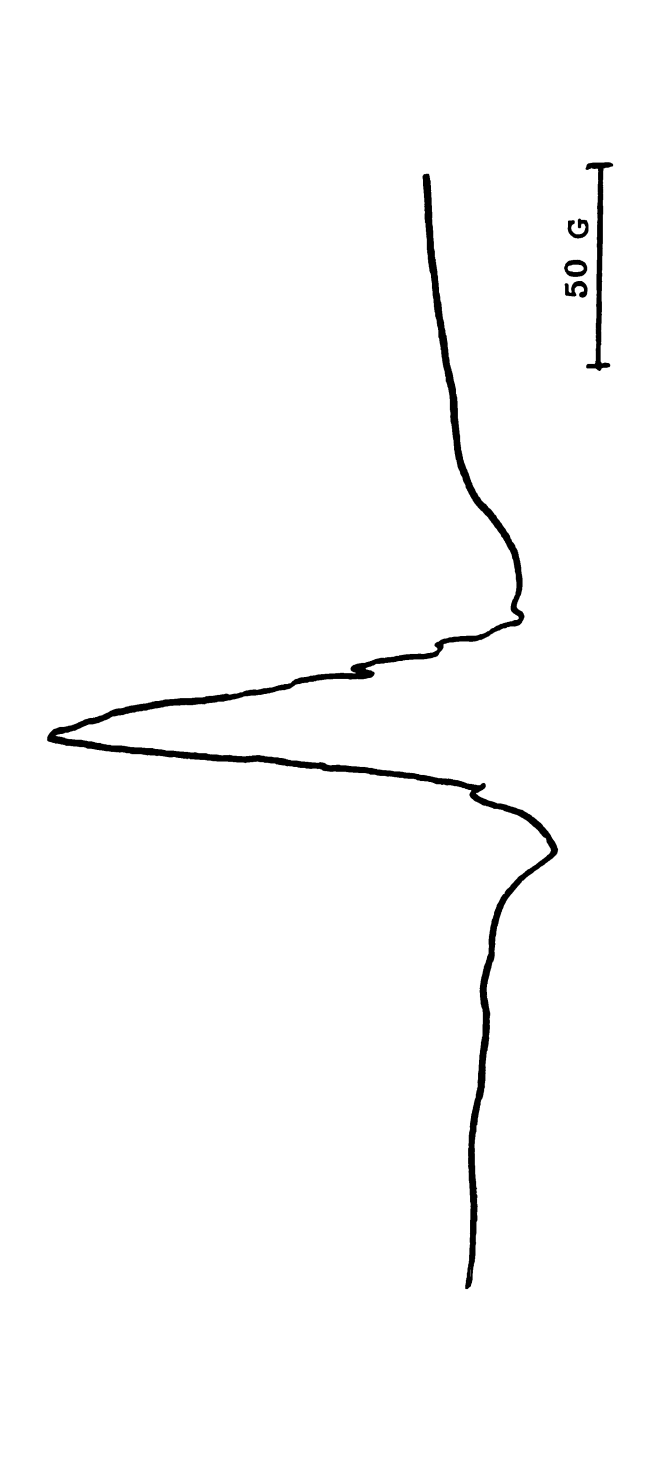
Angular variation of the nitrogen and hydrogen hyperfine splitting in the  $\mbox{ac}$  plane for the  $-70^{0}$  radical. Figure 74.

Table XIX. Hyperfine splitting tensors for nitrogen and hydrogen in the  $-70^{\circ}$  radical.

Tensor	Principal Values (gauss)	Dire	ection Co	osines
A <sub>H</sub>	-21.2	0.37	0.53	0.76
	-18.4	-0.82	-0.21	0.54
	-12.0	0.44	-0.82	0.36
	A <sub>iso</sub> = -17.2			
A <sub>N</sub>	1.7	1.00	0.00	0.00
	6.0	0.00	0.17	-0.98
	1.5	0.00	0.98	0.17
	A <sub>iso</sub> = 3.1			

temperature. No trace of the spectrum from hydrogen atoms was found above  $-80^{\circ}$ .

When the deuterated hydrazinium difluoride crystal was examined the spectra were, as expected, relatively unresolved. Since the nitrogen splitting is small all resolution was lost. The spectrum of Figure 75 is the only exception and was obtained when the magnetic field was -100 from the caxis in the ac plane. At this position the nitrogen splitting is large enough to permit the resolution of some of the deuterium lines. The separation of the lines on the high-field side of the central peak is 3.1 gauss. This is



ESR spectrum of  $\gamma$ -irradiated deuterated hydrazinium difluoride at 770K. H is -100 from the c axis in the ac plane. Figure 75.

close to the expected value of 3.5 gauss for the maximum deuterium splitting which should be about 0.153  $\rm A_H$  or 21.2  $\times$  1/6.5= 3.3 gauss at this orientation.

#### CONCLUSIONS

### I. Radicals in Irradiated Acetamidine Hydrochloride

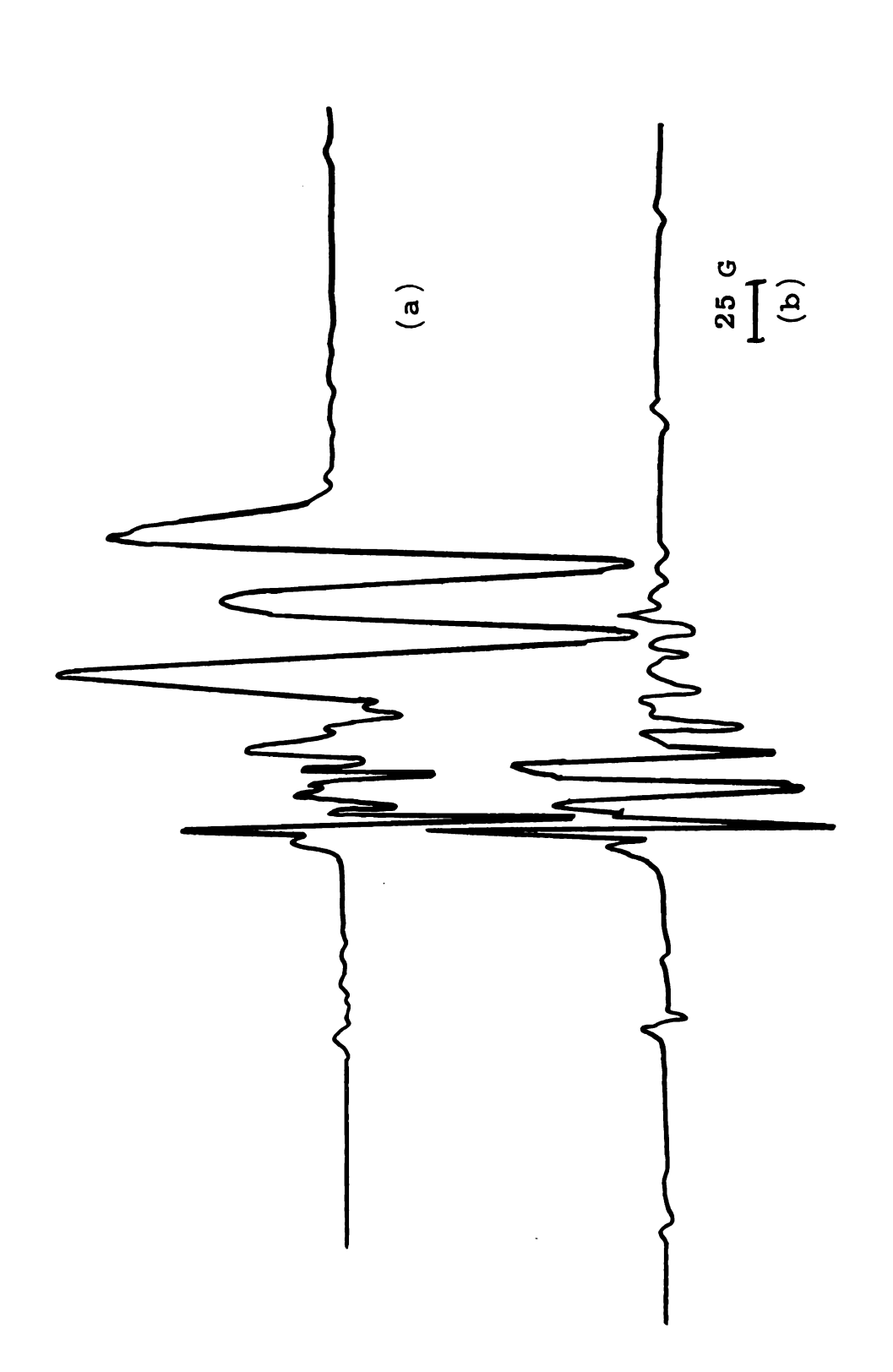
## A. Cl<sub>2</sub> Radical in Irradiated Acetamidine Hydrochloride

Radical anions of the type  $X_2^-$ , where X is a halogen species have been known for some time among the products of irradiated alkali halides (80,81). Their appearance in irradiated organic crystals was not reported until recently when Box et al. (86) observed Cl<sub>2</sub> in X-irradiated monoclinic glycine hydrochloride. The principal values of the chlorine hyperfine splitting tensor which he reports are 110.7 gauss, 42.5 gauss and 24.3 gauss, slightly higher than the principal values of 103.1 gauss, 29.8 gauss, and 10.0 gauss observed in the present case. The values reported by Ueda (85) (103.9, 32.1 and 12.1 gauss) in irradiated hydroxylamine hydrochloride are in better agreement with those found here. The crystal environment of  $Cl_2$  in  $\gamma$ -irradiated NH3OHCl is such that each chlorine has three nearest neighbor chlorines. The Cl-Cl distances calculated from the crystal structure of NH3OHCl are Cl1-Cl2  $(3.92 \ \text{\AA})$ ,  $\text{Cl}_1\text{-Cl}_4$   $(4.90 \ \text{\AA})$ ,  $\text{Cl}_1\text{-Cl}_3$   $(4.17 \ \text{\AA})$ , while the distances from chlorine to other nuclei are much closer, e.g.  $Cl_1-N$  (3.16 Å). These neighboring N, O and H atoms

could cause the distortion of the hyperfine tensor of  $\operatorname{Cl}_2$  from the expected axial symmetry. Although a detailed X-ray analysis has not been done for acetamidine hydrochloride, a distortion of the hyperfine tensor from axial symmetry might be expected, depending on the relative positions of the chlorine nuclei with respect to the neighboring nitrogen and carbon nuclei, because of the low (monoclinic) symmetry. The space group of acetamidine hydrochloride (P2<sub>1</sub>) does make such a distortion seem reasonable in light of the results of Box (86) on glycine hydrochloride which is also monoclinic (space group  $\operatorname{P2}_1/\operatorname{c}$ ).

Additional evidence for the asymmetry of the  $\operatorname{Cl}_2^-$  hyperfine tensor is supplied by a computer simulation of  $\operatorname{Cl}_2^-$  assuming axial symmetry. The program, which was written for the CDC 3600 computer, assumed axial symmetry for both the  $\overline{\mathbb{A}}'$  and  $\overline{\mathbb{g}}'$  tensors with  $\mathbb{A}_{||} = 103.1$  gauss,  $\mathbb{A}_{||} = 10.0$  gauss,  $\mathbb{G}_{||} = 2.0437$ , and  $\mathbb{G}_{||} = 2.0011$  as determined by the diagonalization procedure. The program was designed to simulate a powder pattern using Bleaney's equation (107) (Equation 34). To obtain a spectrum to compare with this computed one a sample of acetamidine hydrochloride which had been  $\gamma$ -irradiated for three hours at  $77^0\mathrm{K}$  was examined. The comparison is shown in Figure 76. It is quite evident that the agreement is poor and that the hyperfine splitting tensor for  $\mathrm{Cl}_2^-$  is not axially symmetric.

It is evident from the direction cosines that the largest principal value, 103.1 gauss, lies nearly along the b axis



spectrum of  $\gamma$ -irradiated acetamidine hydrochloride powder at 770K, Observed spectrum. b) Computed spectrum. ESR a) Figure 76.

which also corresponds to the minimum g value of 2.0011. In glycine hydrochloride the maximum hyperfine splitting of 110.7 gauss lies nearly along the coaxis which also corresponds to the direction of minimum g, g = 1.999.

There have been other examples of irradiated hydrochloride salts of organic compounds reported in which no trace of Cl<sub>2</sub> was found, including irradiated guanine hydrochloride dihydrate (51), L-leucine hydrochloride (143) and L-lysine monohydrochloride dihydrate (31).

The radical formed by the abstraction of an  $\alpha$  proton from acetamidine hydrochloride probably arises by the following scheme:

The Cl<sub>2</sub> fragment formed at 77°K might be expected to lose its extra electron, which is in a  $\sigma$  antibonding orbital, but it seems reasonable to assume that the Cl-Cl bond should remain intact, since it requires 57.1 kcal/mole to break this bond. The energy for the decomposition of Cl<sub>2</sub> to Cl<sub>2</sub> and an electron would then go to break a CH bond. The C-H bond energy of 98.2 kcal/mole is large but could be overcome by the ability of H to abstract an

TNH<sub>2</sub>

 $\alpha$  hydrogen atom from a neighboring  $CH_3-C-NH_2$  molecule to form stable  $H_2$ . The gain in enthalpy of 103.2 kcal/mole for  $H_2$  formation could account for the C-H bond breakage

 $^{+\rm NH}_2$  in the second step. The process for forming  ${\rm CH_2-C-NH_2}$  radical appears therefore to involve a secondary radiative attack by H\*.

The principal values of the  $\alpha$  proton hyperfine split-  $^+_{\rm NH_2}$  ting tensor indicate that  $^+_{\rm CH_2-C-NH_2}$  radical is a  $\pi-$ 

electron radical with the odd electron in a  $p_{\pi}$  orbital on carbon; these are (-35.9, -23.1, -7.5 gauss) for  $H_1$  and (-36.2, -19.0, -5.8 gauss) for  $H_2$ , which are characteristic of the values obtained for  $\alpha$  protons. The isotropic values for  $H_1$  (-22.2 gauss) and for  $H_2$  (-20.3 gauss) are characteristic of isotropic splittings in which carbon has induced a spin polarization of about -0.05 in the hydrogen 1s orbital.

The anisotropic parts of the hyperfine tensor are -13.7 gauss, -0.9 gauss and +14.7 gauss for proton  $H_1$  and -15.9 gauss, +1.3 gauss, and +14.5 gauss for proton  $H_2$  in agreement with the anticipated axial symmetry of the anisotropic components.

The amount of s character in the molecular orbital containing the odd electron may be estimated by comparing the isotropic proton splitting with the theoretical value

of 508 gauss for a pure 1s orbital on hydrogen and is found to be from 4.0 to 4.4%, in good agreement with the 5% delocalization predicted from spin polarization.

McConnell (144) proposed a relationship between isotropic splitting and the spin density on carbon p:

$$a_{\alpha}^{H} = QP_{C} \tag{72}$$

where Q is -22.4 gauss, assuming spin polarization of -0.05. Using McConnell's relation and the Q value above the spin density on carbon in the radical from acetamidine is 0.91. The odd electron density is therefore localized on a 2p orbital on carbon to the extent of 91% and is only 4.0 to 4.4% on each proton.

In agreement with the results for other  $\pi$ -electron radicals, the most positive principal value is associated with the direction parallel to the C-H bond. For this direction the corresponding anisotropic values are 14.7 gauss for proton  $H_1$  and 14.5 gauss for proton  $H_2$ . The most negative principal values of the proton tensors are associated with the directions perpendicular to the C-H bond in the plane of the radical and these are -13.7 gauss and -15.9 gauss for protons  $H_1$  and  $H_2$ , respectively. The other values are associated with the directions parallel to the  $p_{\pi}$  orbital.

Using the direction cosines for the principal values in the plane of the radical and along the C-H bonds it is found that the angle between the two protons is 1110 36',

which is not far from the normal tetrahedral angle for  ${\rm sp^3}$  hybridized bonds. Thus, it seems as if not much distortion of this bond angle has resulted from the formation of the  $\pi$  radical. It would be necessary to obtain the  ${}^{13}{\rm C}$  hyperfine splitting in order to estimate the deviation from planarity, if any, for the radical but the necessary hyperfine lines could not be observed.

The principal values of the hyperfine splitting tensor for the -NH<sub>2</sub> protons are, as stated before in good agreement with the values reported by Kashiwagi (139) for the radical H<sub>2</sub>NOCCH<sub>2</sub>CHCONH<sub>2</sub> in irradiated single crystals of succinamide. The anisotropic contributions to the principal values are -2.3 gauss, 0.0 gauss and 2.4 gauss. Since the principal values were the same for both protons, the protons are equivalent. The reason for the absence of any nitrogen hyperfine splitting is probably that the interaction, which is a long-range one, is very small. Kashiwagi (139) observed a nitrogen splitting with principal values of 5.3 gauss, 0.4 gauss and 0.2 gauss in the case of

O O ...
H<sub>2</sub>N-C-CH<sub>2</sub>-CH-C-NH<sub>2</sub> radical. Such an interaction would surely be evident in the deuterated form but was not found.

### II. Radicals in Irradiated Trimethylacetamide

## A. <u>t</u>-Butyl Radical

The primary product of  $\gamma$ -irradiation of trimethyl-acetamide single crystals is the <u>t</u>-butyl radical; this has

been previously detected in irradiated powders (140,142) and in several liquids (48,147). The binomial intensity distribution of 1:9:36:84:126:126:84:36:9:1 observed is characteristic of equivalent hyperfine splitting by 9 protons. The  $\beta$ -proton splittings are isotropic as expected from previous studies of this radical (Table II). The proton hyperfine splitting, 22.9 gauss, is a reasonable value for  $\beta$ -methyl protons (17,18,29,37,43). The equivalence of the methyl protons implies rotation about the C-CH<sub>3</sub> bonds at 770K. The tunnelling rate for the methyl groups must be faster than 107 sec-1. Horsfield et al. (36) explain the nonequivalence of the three -CH<sub>3</sub> protons in the CH3-CH-COOH radical (from y-irradiated  $1-\alpha$ -alanine) as arising from lifting of the three-fold degeneracy of the torsional energy levels. This could result from a tunnel effect if the barrier to rotation is small or from the hyperfine coupling itself. This implies, in the case of CH3-CH-COOH, that the tunnelling rate is slower than  $10^7 \text{ sec}^{-1}$  if the methyl protons are nonequivalent.

No noticeable effect occurs upon raising the temperature except that the lines sharpen somewhat, probably as a result of decreased broadening from the lines of the

$$\overset{\circ}{C}H_2 \circ \\
H_3C-\overset{\circ}{C}-\overset{\circ}{C}-NH_2 \quad \text{radical.}$$

The positive sign attributed to the  $\beta$ -proton splitting in the <u>t</u>-butyl radical is in accord with the convention (61) for such an assignment based on theoretical considerations which allow mixing of the  $2p_z$  orbital on the  $\alpha$  carbon with a pseudo  $\pi$  system on the methyl group. Both molecular orbital (145) and valence bond (146) calculations predict positive spin density on the methyl protons resulting in the positive sign for  $\beta$ -proton splittings.

The maximum splitting from  $^{13}$ C for <u>t</u>-butyl radical was observed at  $10^{0}$  from b in the ab plane and was 92 gauss. Since the complete tensor could not be obtained for  $^{13}$ C it was not possible to measure the large anisotropy usually associated with  $^{13}$ C splittings (Table 7).

It was possible to obtain an estimate of the deviation from planarity of the radical by using the equation of Karplus and Fraenkel (120) (Equation 67) along with the anisotropic and isotropic carbon hyperfine splittings previously reported for methyl radical (24). The <sup>13</sup>C tensor is assumed to be axially symmetric and the isotropic splitting for <sup>13</sup>C may then be written

$$A_{iso}^{(13C)} = A_{max}^{(13C)} - 2B_0$$
 (73)

where  $2B_0 = 45$  gauss (24). Using these values  $A_{iso}$  (13C) = 47 gauss and  $\theta$ , the deviation from planarity, is found

to be  $\theta$  = 3° 31°. This means that the radical has been distorted from the planar arrangement of the methyl radical to a conformation in which the C-C bonds are bent 3.5° out of the plane. More drastic changes are noted in the cases of 'CX<sub>3</sub> where X is a halogen atom (Table XI) since these substituents have more tendency to be repelled by the electron spin density in the odd electron p-orbital on carbon.

Molecular orbital calculations (148,149) have been previously done on some substituted methyl radicals. The list, however, does not include  $\underline{t}$ -butyl radical. An interesting method has been proposed recently by Pauling (150) who uses electronegativities of groups attached to the methyl carbon to calculate bond angles. Since the electronegativity of -CH<sub>3</sub> is essentially the same as that of hydrogen the method would predict a planar radical.

The presence of another radical which gives a threeline spectrum with relative intensities 1:2:1 was also observed at 770K. This has been attributed to the presence

CH<sub>2</sub> O
of H<sub>3</sub>C-C-C-NH<sub>2</sub> radical. The radical is apparently reCH<sub>3</sub>

orienting more rapidly than  $10^7 \, \text{sec}^{-1}$  since anisotropy would be detected in the hyperfine splitting otherwise (36).

The barrier to reorientation is probably less than 4-5 kcal but it was not possible to measure the potential energy barrier since no line broadening was noted.

The hyperfine splittings for the radical are consistent with those observed for other  $\pi$ -electron radicals with the electron primarily localized in a 2p orbital on carbon. The amount of spin density on carbon using McConnell's relation(144),  $A_H = Q\rho_C$ , and the measured isotropic splitting of -22.4 gauss gives  $\rho_C = 1.00$ . The actual spin density is obviously somewhat less than this since there must be some spin polarization for the proton hyperfine interactions to be observed.

### III. Radicals in $\gamma$ -Irradiated Isobutyramide

A. 
$$CH_2$$
  $CH_2$   $CH_2$   $CH_2$  Radical at  $77^0K$   $CH_3$   $CH_2$   $CH_2$   $CH_2$   $CH_3$   $CH_4$   $CH_5$   $CH_6$   $CH_7$   $CH_8$   $CH_8$ 

cate that the proton hyperfine splittings for two  $\alpha$  protons and a single  $\beta$  proton are approximately equal. Any interaction with the -NH<sub>2</sub> protons was ruled out by the spectra from the deuterated crystal. In the case of the  $\alpha$  protons the anisotropy observed is small, -17.8 gauss to -24.2 gauss. The apparent equivalence of the  $\alpha$  proton splittings must be a result of restricted motion about the  $\dot{\text{CH}}_2$ -CH bond which could be of the order of  $10^7~\text{sec}^{-1}$ . If it happened that the frequency of the reorientation coincided nearly

with this value then a detectable amount of anisotropy, but not the full anisotropy, might be observed. This contrasts with a somewhat less restricted reorientation which was

observed in the case of the  $CH_3$ -C-C- $NH_2$  radical found  $CH_3$ 

in  $\gamma$ -irradiated trimethylacetamide.

The isotropic proton splitting for the  $\alpha$  protons is in the range usually found for such splittings (Table I). Using McConnell's relation (144),  $A_{\rm H} = Q\rho_{\rm C}$ , the calculated spin density on the  $\alpha$  carbon is 0.93 with probable equal spin densities on the  $\alpha$  protons accounting for the remaining spin density. The direction cosines indicate that the principal values are oriented close to the crystallographic axes. The proton anisotropic splitting of -3.4 gauss is directed nearly along the a axis, the splitting of +0.5 gauss nearly along the c\* axis, and the splitting +3.0 gauss nearly along the b axis.

The expected cylindrical symmetry is present in the anisotropic hyperfine splitting values as expected for  $\alpha$  protons. The magnitudes are slightly larger than those reported for  $\dot{CH}_3$  radical by Rogers and Kispert (24) where rotation is occurring about the threefold symmetry axis. The apparent equivalence of both  $\alpha$ - and  $\beta$ -proton splittings in the ab-plane is undoubtedly accidental.

The  $\beta$  proton splitting is somewhat more anisotropic than the  $\alpha$  splittings. Although this is usually not the

case when both  $\alpha$  and  $\beta$  protons are present (Tables I and II) the magnitude of the anisotropy for the  $\beta$  proton is reasonable. Rowlands and Whiffen (151) observed a fairly large anisotropy in the case of HOOC-CH-C-COOH, which had OH OH

anisotropic splittings of 7.8 gauss, 0.3 gauss, and -2.1 CH<sub>2</sub> O gauss. In the case of CH<sub>3</sub>-CH - C-NH<sub>2</sub> the anisotropic splittings are 4.8 gauss, 0.9 gauss and -5.8 gauss. The isotropic value of 18.0 gauss is larger than the 10 gauss splitting observed by Rowlands and Whiffen (151). Other examples of large β-proton anisotropy are reported for the (DO)<sub>2</sub>-CH-CH-CH<sub>2</sub>OD radical by Rao and Gordy (152) and for NH<sub>2</sub> p

the HOOC-CH-CH-COOH radical by Cook et al. (39).

The  $\beta$ -proton principal values are also oriented close to crystal axes with the 22.8 gauss splitting lying nearly along the a-axis, the 18.9 gauss splitting lying nearly along the b-axis, and the 12.2 gauss splitting lying nearly along the c\*-axis. The configuration of the  $\beta$  proton is apparently fixed by the interaction of the  $\mathring{C}H_2-$ , H- and

O -C-NH<sub>2</sub> groups which are attached to the  $\beta$  carbon. A similar fixed configuration could also explain the large anisotropy of the  $\beta$ -proton hyperfine splitting in HOOC-CH-C-COOH radical. OH OH

The orientation of the  $\beta$  proton with respect to the orbital of the odd electron can be calculated using Equation 59, which relates the isotropic  $\beta$ -proton splitting to

the dihedral angle  $\theta$  and the constants  $B_0$ ,  $B_2$  by the equation  $A_{1SO} = B_0 + B_2 \cos \theta$ . Values of  $B_0$  and  $B_2$  have been reported by Whiffen (153); for C-CH these are  $B_0 = 3.6$  gauss and  $B_2 = 51.4$  gauss. The measured isotropic splitting of 18 gauss gives  $\theta = 93^{\circ}$  which means that the  $\beta$ -proton is oriented  $93^{\circ}$  from the plane containing the two carbon atoms and the  $p_{\pi}$  orbital on the  $\alpha$  carbon. This could explain the relatively high anisotropy of the  $\beta$ -proton splitting since the other groups have to be oriented at definite angles with respect to the odd-electron orbital.

The <u>sec</u>-butyl radical, which appears when  $\gamma$ -irradiated isobutyramide single crystals are warmed, has already been previously investigated (17). When the crystal containing

CH<sub>2</sub> CH-C-NH<sub>2</sub> radical was warmed to -80°, a spectrum of 7 CH<sub>3</sub>

lines with relative intensity ratios of 1:6:15:20:15:6:1 appeared indicating that the new radical contains six equivalent protons; the pattern and the observed hyperfine splittings (Table XVII) are in reasonable agreement with the reported values (17) for CH<sub>3</sub> C-C-NH<sub>2</sub> radical (Table CH<sub>3</sub> C-C-NH<sub>2</sub> radical (Table

The mechanism for formation of the high temperature radical probably involves abstraction of a proton from a neutral isobutyramide molecule by the low temperature radical. This can be represented by the following scheme:

## IV. V centers in $\gamma$ -Irradiated Hydrazinium Dihalides

# A. Cl<sub>2</sub> Radical Anion in γ-Irradiated Hydrazinium Dichloride

When a single crystal of hydrazinium dichloride was  $\gamma$ -irradiated at  $77^0 K$  an extremely complicated spectrum resulted for a general orientation in the aa' plane. It was possible at certain orientations to observe a much simpler spectrum and so confirm the presence of the  $Cl_2$  radical anion previously identified in  $\gamma$ -irradiated acetamidine hydrochloride. The outermost group of three lines on either the high or low-field side of the spectrum is associated with the three outer lines anticipated from the istopic species  $(^{35}\text{Cl}-^{35}\text{Cl})^-$ ,  $(^{35}\text{Cl}-^{37}\text{Cl})^-$ , and  $(^{37}\text{Cl}-^{37}\text{Cl})^-$ .

The maximum hyperfine splitting of 97.3 gauss is in good agreement with previous reported maximum splittings for  $\text{Cl}_2^-$  in irradiated alkali halides (Table VIII). It

might be expected that the environment would be similar since the hydrazinium dichloride crystal structure has also been reported to be cubic (141). The agreement for  $g_{\min}$  is not as good, perhaps because the crystal was aligned slightly off a crystal axis. It must be remembered that the principal axes of the  $\overline{g}$ ' and  $\overline{A}$ ' tensors must be coincidental if principal values are to be measured directly from the spectra.

The positions of maximum hyperfine splitting for  $Cl_2$  are  $45^0$  from the crystal axes indicating that the  $Cl_2$  radical anions are oriented along face diagonals, (110), of the unit cube. This is similar to the situation reported in X-irradiated KCl crystals by Hayes and Nichols (154). The reported  $g_{\min} = 2.0010$  value in the case of irradiated KCl (154) is also closer to the g = 2.0035 observed in  $\gamma$ -irradiated hydrazinium dichloride than the  $g_{\min}$  value for crystals where  $Cl_2$  is oriented parallel to a cube face.

## B. Br<sub>2</sub> Radical Anion in γ-Irradiated Hydrazinium Dibromide

When hydrazinium dibromide single crystal was  $\gamma$ -irradiated at  $77^{\circ}K$  the spectrum of Br<sub>2</sub> was detected. There have been no reports of Br<sub>2</sub> in irradiated single crystals belonging to the monoclinic system other than the present case. Nevertheless, it is possible to rationalize the deviation from axial symmetry of the  $\overline{g}$  and  $\overline{A}$  tensor principal values on the same basis as was done for Cl<sub>2</sub> in

a monoclinic crystal (86). The environment of the Br<sub>2</sub> fragment is such that anisotropic interactions with nitrogen may tend to distort the symmetry of the g and hyperfine tensors from that observed in a cubic crystal.

A more plausible explanation is used to account for the  $\bar{g}^i$  anisotropy. The g value, it will be recalled, is perturbed from the free spin value of g=2.0023 primarily by spin-orbit coupling. The spin-orbit coupling is directly related to the electric fields in the crystal and is determined by the spin-orbit coupling parameter,  $\lambda$ . Since the electric field environment in a monoclinic crystal depends on direction, whereas it doesn't in a cubic crystal, it should be expected that the g values would be correspondingly affected. They are altered as shown by the unusually small maximum g value, g=2.0635, found here; the minimum g value, g=1.9809, is in considerably better agreement with the reported  $g_{\min}$  values for cubic crystals given in Table VIII.

The principal values of the hyperfine tensors lie close to crystallographic axes with the largest value of 415.6 gauss lying nearly along the a\* axis and the minimum value of 79.7 gauss lying nearly along the c axis. Likewise the minimum g value of g = 1.9809 lies along the a\* axis and the maximum g value (2.0635) lies nearly along the c axis.

### V. Radicals in $\gamma$ -Irradiated Hydrazinium Difluoride

### A. Trapped Hydrogen Atoms

When a  $\gamma$ -irradiated crystal of hydrazinium difluoride was examined at  $77^0 \mathrm{K}$  a doublet with 508 gauss splitting was observed. The g value for the doublet was g=2.0023. These values are consistent with the formation of hydrogen atoms in the irradiated crystal. It was observed that the 508 gauss doublet was stable up to  $-80^\circ$ .

Although hydrogen atoms have been detected in numerous irradiated liquids (Table IX) the number of instances of its presence in an irradiated crystal is small. Recently it was reported in  $\gamma$ -irradiated N<sub>2</sub>H<sub>4</sub>·HCl single crystal (99) and it has been reported (as an impurity) in single crystals of CaF<sub>2</sub> (97) and in KCl crystals (155).

In hydrazinium difluoride the hydrogen atoms may be trapped in the crystal lattice in the tetrahedral holes adjacent to each nitrogen atom resulting from the cubic closest packing (136) of the molecular layers. Normally these holes are partially filled by fluoride ions from neighboring layers of molecules, but it has been reported by Kronberg and Harker (136) that the distance from a fluoride ion in the hole to the surrounding fluoride ions forming the hole is 25% larger than is normally associated with the F-F contact distance. Thus, a small hydrogen atom could be trapped in these tetrahedral holes.

The linewidth of the hydrogen atom resonance is about 40 gauss which is large compared with the narrow linewidth associated with hydrogen atom resonances in liquids or in other crystals. This broadening could be caused by interactions with the adjacent nitrogen or fluorine nuclei or both. Thus the observed peak is probably an envelope of lines rather than a single absorption. However, it would be necessary to do ENDOR experiments (electron-nuclear double resonance) to prove this. Irradiated crystals of N<sub>2</sub>D<sub>6</sub>Cl<sub>2</sub> should give, by analogy, deuterium atoms and their spectrum would be a triplet with hyperfine splitting about 508 / 6.5 or 78 gauss. Actually the outer lines in the spectrum of N<sub>2</sub>D<sub>6</sub>Cl<sub>2</sub> are separated by only 110-120 gauss and if these arise from deuterium atoms there has been a very large perturbation from the expected splitting; the reason for this is not known.

### B. Radical Pairs at 770K

The nature of the radical pairs has not been determined since it was not possible to obtain sufficiently well-resolved spectra over a range of orientations of the magnetic field. A variety of radical pairs has been observed in irradiated nitrogen compounds (Table XX).

## C. The Radical at -700

When the  $\gamma$ -irradiated crystal of hydrazinium difluoride was warmed to  $-70^{\circ}$  for 3 minutes it was found that the

Table XX. Radical Pairs

Compounds	Radical Pa	Pairs	Distance (A)	Reference
Dimethylglyoxime	HON(CH3)C-C(CH3)NO.	• ON( 1	. c c	157
Glyoxime	HONCH-CHNO		8. <del>8</del> . 9	158
Methylglyoxime	HONCH-C(CH <sub>3</sub> )NO·		5.2	158
p-Chlorobenzaldoxime	Cl-C6H4-CHNO.	(sym) (anti)	6.1	159
Sodium 1-0xyimino- propionate	_00C-C(CH <sub>3</sub> )NO·		7.2	160
Hydroquinone-acetonitrile clathrate	HO-C <sub>6</sub> H <sub>4</sub> -0·		5.1	161
Oxalic Acid	HOOC-COO.	<pre>(dihydrate) (anhydrous)</pre>	6.33 9.93	162
Monofluoroacetamide	$CH_2CONH_2$ $CHFCONH_2$	(dissimilar .pair)	7.03	34
Methane	H· ·CH3		92.9	163

Table XX. (Continued)

Compounds	Radical Pairs	Distance (A)	Reference
Azobis(isobutyronitrile)	·c(CH <sub>3</sub> ) <sub>2</sub> CN	. <b>'</b>	164
Tetraphenylhydrazine	$\cdot N(C_6H_5)_2$	5.9	165
Diphenylcarbonate	·0-C <sub>6</sub> H <sub>5</sub>	o. c	166
Potassium persulfate	.00S00	15.8	167
Maleic anhydride	C=C C=O and O=C C=O	5.39	168
Hydroxyurea	NH2 CONHO ·	6.38	169

spectrum attributed to the radical pairs had vanished and a much simpler spectrum now was observed. This spectrum for H | c is a septet of quintets, the relative intensities of the septet being nearly 1:6:15:20:15:6:1 while the quintet intensity ratios are 1:2:3:2:1 (Figure 67). This suggests that in the radical the odd electron interacts with six equivalent protons and two equivalent nitrogen atoms. The nitrogen anisotropic hyperfine tensor is nearly axially symmetric if the signs of the principal values are all positive; the principal components of the anisotropic hyperfine tensor would then be +2.9 gauss along the c axis, -1.4 gauss along the a axis and -1.6 gauss along the b axis.

The proton hyperfine values are in reasonable agreement with those reported previously for protons attached to nitrogen (Table IV). The value of -4.0 gauss is primarily directed along the caxis, the value of -1.2 gauss is associated with axis a and the value of +5.2 gauss is associated with the baxis.

The spin density of the odd electron in the 2s orbital on nitrogen may be computed using the observed nitrogen isotropic splitting and the theoretical spin density (60,61) (550 gauss) for an electron in a 2s orbital, assuming that the contribution from the 1s orbital is negligible. Since the measured nitrogen isotropic splitting is 3.1 gauss the s spin density is 3.1/550 = 0.0056 or only 0.56%.

The nearly isotropic g tensor with  $g=2.0035\pm0.0005$  is similar to the results for NH<sub>3</sub><sup>+</sup> previously reported (56); NH<sub>3</sub><sup>+</sup> was found to be rotating in the crystal with principal g values of  $g_{aa}=2.0034\pm0.0003$ ,  $g_{bb}=2.0034\pm0.0003$ , and  $g_{cc}=2.0032\pm0.0003$ .

Three possible radicals which would lead to the odd electron interacting with six equivalent protons and two equivalent nitrogen atoms may be suggested but none provide completely satisfactory explanations of all the data. (a) Removing an electron from the hydrazinium ion N2H6 ++ would give a radical cation  $N_2H_6^{3+}$  with some of the properties However, the isotropic nitrogen hyperfine splitobserved. ting for such a radical should be rather larger than observed since the odd electron would be partly in a nitrogen orbital with 25% s character. Also, it is rare to find species in irradiated crystals formed by removing electrons from stable cations. (b) An electron could be added to N<sub>2</sub>H<sub>6</sub> ++ which would then have an electron over and above the number required to fill the stable orbitals. This could be accommodated to form a three-electron bond between the nitrogen atoms, probably utilizing a 2p orbital on each nitrogen with each set of protons then tending to become coplanar with the nitrogen to which they are attached. This species would have a nearly isotropic proton splitting, as observed, but should have either a somewhat larger anisotropic nitrogen splitting than found here (if the NH3 groups are planar) or a much larger anisotropic nitrogen

splitting (if the  $NH_3$  groups remain pyramidal). (c) A third possibility is that an electron trapped in a fluoride ion vacancy interacts with three protons and a nitrogen atom from each of two  $N_2H_6^{++}$  ions in the lattice. Such F-centers are well known but are not often stable to room temperature, as is this radical, and are usually associated with absorption bands in the visible region of the spectrum. Also, it is difficult to locate an electron such that it would interact only with six equivalent protons and two equivalent nitrogen atoms since the holes it might be expected to occupy would generally have larger coordination numbers.

### VI. Summary

The ESR spectra of the radicals produced in six single crystals by irradiation with X-rays and  $\gamma$ -rays have been obtained and analyzed. The spectra have made it possible to identify the radicals produced and, in several cases, to discuss their structures. The systems studied and the radicals found are:

(1) The radicals  $Cl_2$  and  ${}^{\circ}CH_2 - C - NH_2$  in acetamidine hydrochloride.

CH<sub>3</sub> CH<sub>2</sub> O (2) The radicals CH<sub>3</sub>-C and CH<sub>3</sub>-C - C-NH<sub>2</sub> in trimethylacetamide.

(3) The radicals 
$$CH_2$$
  $CH_2$   $CH_3$   $CH_3$   $CH_3$   $CH_3$   $CH_3$   $CH_3$   $CH_3$ 

in isobutyramide.

- (4) The radical Cl<sub>2</sub> in hydrazinium dichloride.
- (5) The radical Br<sub>2</sub> in hydrazinium dibromide.
- (6) A radical pair and another radical, possibly  $N_2H_6^+$ , showing coupling with two nitrogens and six protons in hydrazinium difluoride.

These results show the unusual stability at low temperatures of the  $\rm X_2^-$  radical ion in irradiated organic ionic halides. The reactions of the radicals on warming from  $77^0\rm K$  to room temperature have also been studied and the various stable radical species identified.

REFERENCES

## REFERENCES

- 1. H. M. McConnell and R. W. Fessenden, J. Chem. Phys., 31, 1688 (1959).
- 2. C. Heller and H. M. McConnell, J. Chem. Phys., 32, 1535 (1960).
- 3. D. Pooley and D. H. Whiffen, Mol. Phys., 4, 81 (1961).
- 4. A. Horsfield, J. R. Morton and D. H. Whiffen, Nature, 189, 481 (1961).
- H. M. McConnell, C. Heller, T. Cole and R. W. Fessenden, J. Am. Chem. Soc., 82, 766 (1960).
- 6. J. R. Rowlands, J. Chem. Soc., 4264 (1961).
- 7. A. Horsfield, J. R. Morton and D. H. Whiffen, Mol. Phys., 4, 169 (1961).
- 8. J. R. Morton and A. Horsfield, Mol. Phys., 4, 219 (1961).
- 9. N. M. Atherton and D. H. Whiffen, Mol. Phys., 3, 1 (1960).
- 10. N. M. Atherton and D. H. Whiffen, Mol. Phys., <u>3</u>, 103 (1960).
- 11. D. Pooley and D. H. Whiffen, Trans. Faraday Soc., <u>57</u>, 1445 (1961).
- 12. I. Miyagawa and W. Gordy, J. Chem. Phys., 32, 255 (1960).
- 13. J. R. Morton and A. Horsfield, J. Chem. Phys., <u>35</u>, 1142 (1961).
- 14. D. H. Whiffen, "Free Radicals in Biological Systems," Academic Press, New York, 1961.
- 15. D. K. Ghosh and D. H. Whiffen, Mol. Phys., 2, 285 (1959).
- I. Miyagawa, Y. Kurita and W. Gordy, J. Chem. Phys., 33, 1599 (1960).

- 17. P. J. Hamrick, Jr., H. W. Shields and S. H. Parkey, J. Am. Chem. Soc., 90, 5371 (1968).
- Y. Shioji, S. K. Ohnishi and K. Nitta, J. Polymer Sci., Pt. A., <u>1</u>, 3373 (1963).
- 19. R. J. Cook, J. R. Rowlands and D. H. Whiffen, Mol. Phys., 7, 31 (1963).
- 20. A. Horsfield and J. R. Morton, Trans. Faraday Soc., 58, 470 (1962).
- 21. Y. Kurita, J. Chem. Phys., 36, 560 (1962).
- 22. D. V. G. L. N. Rao and M. Katayama, J. Chem. Phys., 37, 382 (1962).
- 23. H. N. Rexroad, Y. K. Hahn and W. J. Temple, J. Chem. Phys., 42, 324 (1965).
- 24. M. T. Rogers and L. D. Kispert, J. Chem. Phys., <u>46</u>, 221 (1967).
- 25. R. E. Bellis and S. Clough, Mol. Phys., 10, 33 (1965).
- 26. P. B. Ayscough and A. K. Roy, Trans. Faraday Soc., <u>64</u>, 582 (1968).
- 27. H. Ohigashi and Y. Kurita, Bull. Chem. Soc. Japan, <u>41</u>, 275 (1968).
- 28. M. Kashiwagi, Nippon Kagaku Zasshi, 87, 1298 (1966).
- 29. P. B. Ayscough and A. K. Roy, Trans. Faraday Soc., 63, 1106 (1967).
- 30. J. B. Cook, J. P. Elliott and S. J. Wyard, Mol. Phys., 12, 185 (1967).
- 31. M. Fujimoto, W. A. Seddon, and D. R. Smith, J. Chem. Phys., 48, 3345 (1968).
- 32. D. G. Cadena and J. R. Rowlands, J. Chem. Soc., 488 (1968).
- 33. W. Bernhard and W. Snipes, Proc. Natl. Acad. Sci. U.S., 59, 1038 (1968).
- 34. M. Iwasaki and K. Toriyama, J. Chem. Phys., <u>46</u>, 4693 (1967).
- 35. H. C. Box, H. G. Freund, and K. T. Lilga, J. Chem. Phys., 42, 1471 (1965).

- 36. A. Horsfield, J. R. Morton and D. H. Whiffen, Mol. Phys., 4, 425 (1961).
- 37. A. Horsfield, J. R. Morton and D. H. Whiffen, Trans. Faraday Soc., <u>57</u>, 1657 (1961).
- 38. H. Shields and P. Hamrick, J. Chem. Phys., <u>37</u>, 202 (1962).
- 39. R. J. Cook, J. R. Rowlands, and D. H. Whiffen, J. Chem. Soc., 3520 (1963).
- 40. Y. D. Tsvetkov, R. J. Cook, J. R. Rowlands and D. H. Whiffen, Trans. Faraday Soc., <u>59</u>, <u>2213</u> (1963).
- 41. M. Kashiwagi, and Y. Kurita, J. Chem. Phys., <u>40</u>, 1780 (1964).
- 42. Y. D. Tsvetkov, J. R. Rowlands, and D. H. Whiffen, J. Chem. Soc., 810 (1964).
- 43. M. Fujimoto, J. Chem. Phys., 39, 846 (1963).
- 44. J. R. Rowlands and D. H. Whiffen, Mol. Phys.,  $\underline{4}$ , 349 (1961).
- 45. Y. Kurita, Bull. Chem. Soc. Japan, <u>40</u>, 94 (1967).
- 46. H. Shields, P. Hamrick, and D. DeLaigle, J. Chem. Phys., 46, 3649 (1967).
- 47. D. H. Whiffen, Pure Appl. Chem., 4, 185 (1962).
- 48. R. W. Fessenden and R. H. Schuler, J. Chem. Phys., 39, 2147 (1963).
- 49. J. P. M. Bailey and R. M. Golding, Mol. Phys., <u>12</u>, 49 (1967).
- 50. G. R. Underwood and R. S. Givens, J. Am. Chem. Soc., 90, 3713 (1968).
- 51. C. Alexander and W. Gordy, Proc. Natl. Acad. Sci. U.S., 58, 1279 (1967).
- 52. O. Edlund, A. Lund and A. Nilsson, J. Chem. Phys., <u>49</u>, 749 (1968).
- 53. M. A. Collins and D. H. Whiffen, Mol. Phys., <u>10</u>, 317 (1966).
- 54. K. N. Shrivastava and R. S. Anderson, J. Chem. Phys., 48, 4599 (1968).

- 55. J. R. Morton, J. Phys. Chem. Solids, 24, 209 (1963).
- 56. T. Cole, J. Chem. Phys., 35, 1169 (1961).
- 57. J. R. Rowlands and D. H. Whiffen, Nature, 193, 61 (1962).
- 58. J. R. Rowlands, Mol. Phys., 5, 565 (1962).
- 59. H. W. Shields, P. J. Hamrick and W. Redwine, J. Chem. Phys., <u>46</u>, 2510 (1967).
- 60. E. Clementi, C. C. J. Roothaan and M. Yoshimine, Phys. Rev., <u>127</u>, 1618 (1962).
- 61. J. R. Morton, Chem. Rev., 64, 453 (1964).
- 62. J. N. Herab and V. Galogaza, J. Chem. Phys., <u>50</u>, 3101 (1969).
- 63. D. Cordischi and R. DiBlasi, Can. J. Chem., <u>47</u>, 2601 (1969).
- 64. A. Horsfield, J. R. Morton, J. R. Rowlands and D. H. Whiffen, Mol. Phys., 5, 241 (1962).
- 65. J. H. Hadley, Bull. Am. Phys. Soc., 11, 315 (1966).
- 66. C. Chacaty and C. Rosilio, J. Chim. Phys., 64, 777 (1967).
- 67. R. Blinc, M. Schara and S. Poberaj, J. Phys. Chem. Solids, <u>24</u>, 559 (1963).
- 68. J. R. Brailsford, J. R. Morton and L. E. Vannotti, J. Chem. Phys., <u>50</u>, 1051 (1969).
- 69. E. Gelerinter and R. H. Silsbee, J. Chem. Phys., <u>45</u>, 1703 (1966).
- 70. P. L. Marinkas and R. H. Bartram, J. Chem. Phys., <u>48</u>, 927 (1968).
- 71. T. Cole and C. Heller, J. Chem. Phys., 34, 1085 (1961).
- 72. H. M. McConnell and R. W. Fessenden, J. Chem. Phys., 31, 1688 (1959).
- 73. J. R. Morton, J. Am. Chem. Soc., <u>86</u>, 2325 (1964).
- 74. M. T. Rogers and L. D. Kispert, J. Chem. Phys., <u>46</u>, 3193 (1967).
- 75. J. E. Bennett, B. Mile and A. Thomas, Trans. Faraday Soc., 63, 263 (1967).
- 76. C. Corvaja, Trans. Faraday Soc., 63, 26 (1967).

- 77. J. E. Bennett and L. H. Gale, Trans. Faraday Soc., <u>64</u>, 1174 (1968).
- 78. D. W. Ovenall and D. H. Whiffen, Mol. Phys., 4, 135 (1961).
- 79. J. Sinclair and M. W. Hanna, J. Chem. Phys., <u>50</u>, 2125 (1969).
- 80. W. Känzig, Phys. Rev., 99, 1890 (1955).
- 81. T. G. Castner and W. Känzig, J. Phys. Chem. Solids, 3, 178 (1957).
- 82. C. P. Slichter, "Principles of Magnetic Resonance," Harper and Row, New York, 1963.
- 83. H. R. Zeller, L. Vannotti, and W. Känzig, Phys. Kondens. Materie, 2, 133 (1964).
- 84. F. W. Patten and M. J. Marrone, Phys. Rev., <u>142</u>, 513 (1966).
- 85. H. J. Ueda, J. Chem. Phys., 41, 285 (1964).
- 86. H. C. Box, E. E. Budzinski, and H. C. Freund, J. Chem. Phys., 50, 2880 (1969).
- 87. E. Boesman and D. Schoemaker, J. Chem. Phys., <u>37</u>, 671 (1962).
- 88. C. L. Marquardt, J. Chem. Phys., 48, 994 (1968).
- 89. J. W. Wilkins and J. R. Gabriel, Phys. Rev., <u>132</u>, 1950 (1963).
- 90. D. Schoemaker, Phys. Rev., <u>149</u>, 693 (1966).
- 91. L. S. Goldberg and M. L. Meistrich, Phys. Rev., <u>172</u>, 877 (1968).
- 92. C. E. Bailey, Phys. Rev., 136, 1311 (1964).
- 93. J. Sierro, Phys. Rev., <u>138</u>, 648 (1965).
- 94. C. K. Jen, S. N. Foner, E. L. Cochran and V. A. Bowers, Phys. Rev., <u>112</u>, 1169 (1958).
- 95. T. Cole and J. T. Harding, J. Chem. Phys., 28, 993 (1958).
- 96. C. K. Jen, S. N. Foner, E. L. Cochran and V. A. Bowers, Phys. Rev., 104, 846 (1956).
- 97. J. L. Hall and R. T. Schumacher, Phys. Rev., <u>127</u>, 1892 (1962).

- 98. R. Livingston, H. Zeldes, and E. H. Taylor, Discussions Faraday Soc., 19, 166 (1955).
- 99. A. G. Kotov and S. Y. Pshezhetskii, Zh. Fiz. Khim., 38, 1920 (1964).
- 100. S. N. Foner, C. K. Jen, E. L. Cochran and V. A. Bowers, J. Chem. Phys., 28, 351 (1958).
- 101. E. B. Rawson and R. Beringer, Phys. Rev., <u>88</u>, 677 (1952).
- 102. C. L. Gardner, J. Chem. Phys., 46, 2991 (1967).
- 103. C. L. Gardner, J. Chem. Phys., 49, 5558 (1968).
- 104. N. Vanderkooi and J. S. Mac Kenzie, Advan. Chem. Ser., 36, 98 (1962).
- 105. H. Eyring, J. Walter and G. E. Kimball, "Quantum Chemistry," John Wiley and Sons, New York, 1944.
- 106. A. Carrington and A. D. Mc Lachlan, "Introduction to Magnetic Resonance," Harper and Row, New York, 1967.
- 107. B. Bleaney, Phil. Mag., 42, 441 (1951).
- 108. G. Breit and I. I. Rabi, Phys. Rev., 38, 2082 (1931).
- 109. R. W. Fessenden and R. H. Schuler, J. Chem. Phys., <u>43</u>, 2704 (1965).
- 110. J. Maruani, C. A. McDowell, H. Nakajima, and P. Raghunathan, Mol. Phys., 14, 349 (1968).
- 111. D. S. Schonland, Proc. Phys. Soc. (London), <u>73</u>, 788 (1959).
- 112. J. E. Nafe and E. B. Nelson, Phys. Rev., <u>73</u>, 718 (1948).
- 113. H. M. McConnell and H. H. Dearman, J. Chem. Phys., <u>28</u>, 51 (1958).
- 114. J. E. Bennett, B. Mile, and A. Thomas, Trans. Faraday Soc., 61, 2357 (1965).
- 115. G. W. Chantry, A. Horsfield, J. R. Morton and D. H. Whiffen, Mol. Phys., 5, 589 (1962).
- 116. J. G. Hyde and E. S. Freeman, J. Chem. Phys., <u>65</u>, 1636 (1961).
- 117. G. Schoffa, J. Chem. Phys., 40, 908 (1964).

- 118. R. W. Fessenden, J. Mag. Res., 1, 277 (1969).
- 119. H. C. Heller, J. Chem. Phys., 42, 2611 (1965).
- 120. M. Karplus and G. K. Fraenkel, J. Chem. Phys., <u>35</u>, 1312, (1961).
- 121. T. Cole, H. O Pritchard, N. R. Davidson and H. M. Mc-Connell, Mol. Phys., 1, 406 (1958).
- 122. Unpublished data by M. T. Rogers and L. D. Kispert.
- 123. M. Bersohn and J. C. Baird, "An Introduction to Electron Parmagnetic Resonance," W. A. Benjamin, New York, 1962.
- 124. G. E. Pake, "Paramagnetic Resonance," W. A. Benjamin New York, 1962.
- 125. W. Low, "Paramagnetic Resonance in Solids," Academic Press, New York, 1960.
- 126. C. P. Poole, "Electron Spin Resonance," John Wiley and Sons, New York, 1967.
- 127. "V-4502 EPR Spectrometer System Manual," Varian Associates, Palo Alto, California.
- 128. "V-4503 EPR Spectrometer System Manual," Varian Associates, Palo Alto, California.
- 129. G. H. Stout and L. H. Jensen, "X-ray Structure Determination," Macmillan Co., New York, 1968.
- 130. F. C. Phillips, "An Introduction to Crystallography," John Wiley and Sons, New York, 1963.
- 131. N. H. Hartshorne and A. Stuart, "Practical Optical Crystallography," American Elsevier Co., New York, 1964.
- 132. P. Groth, "Chemische Krystallographie," Vol. 3, Verlag von Wilhelm Engelmann, Leipzig, 1910.
- 133. L. Buss and L. Bogart, Rev. Sci. Instr., 31, 204 (1960).
- 134. M. J. Buerger, "X-ray Crystallography," John Wiley and Sons, New York, 1942.
- 135. M. J. Buerger, "The Precession Method in X-ray Crystallography," John Wiley and Sons, New York, 1964.
- 136. M. L. Kronberg and D. Harker, J. Chem. Phys., <u>10</u>, 309 (1942).

- 137. C. M. Deeley and R. E. Richards, Trans. Faraday Soc., 50, 560 (1954).
- 138. R. E. Rondeau, J. Chem. Eng. Data, <u>11</u>, 94 (1966).
- 139. M. Kashiwagi, J. Chem. Phys., 44, 2823 (1966).
- 140. M. T. Rogers, S. J. Bolte and P. S. Rao, J. Am. Chem. Soc., <u>87</u>, 1875 (1965).
- 141. J. Donohue and W. N. Lipscomb, J. Chem. Phys., <u>15</u>, 115 (1947).
- 142. D. H. Whiffen. Unpublished data communicated by M. T. Rogers.
- 143. G. Lassmann and W. Damerau, Biophysik, 5, 14 (1968).
- 144. H. M. McConnell and D. B. Chesnut, J. Chem. Phys., 26, 107 (1958).
- 145. D. B. Chesnut, J. Chem. Phys., 29, 43 (1958).
- 146. A. D. Mc Lachlan, Mol. Phys., 1, 233 (1958).
- 147. P. B. Ayscough and C. Thomson, Trans. Faraday Soc., 58, 1477 (1962).
- 148. J. A. Pople and G. A. Segal, J. Chem. Phys., <u>44</u>, 3289 (1966).
- 149. J. A. Pople, D. L. Beveridge and P. A. Dobosh, J. Chem. Phys., <u>47</u>, 2026 (1967).
- 150. L. Pauling, J. Chem. Phys., <u>51</u>, 2767 (1969).
- 151. J. R. Rowlands and D. H. Whiffen, "Hyperfine Couplings," National Physical Laboratory, Teddington, 1961.
- 152. N. D. V. G. L. Rao and W. Gordy, J. Chem. Phys., <u>35</u>, 764 (1961).
- 153. D. H. Whiffen, Colloq. Int. Centre Nat. Rech. Sci., No. <u>164</u>, 169-175 (1967).
- 154. W. Hayes and G. M. Nichols, Phys. Rev., <u>117</u>, 993 (1960).
- 155. J. M. Spaeth, J. Phys. Radium, 28, 146 (1967).
- 156. I. Barber, Phys. Stat. Sol., 34, 711 (1969).
- 157. (a) Y. Kurita, J. Chem. Phys., <u>41</u>, 3926 (1964); (b) Nippon Kagaku Zasshi, <u>85</u>, 833 (1964).

- 158. Y. Kurita and M. Kashiwagi, J. Chem. Phys., <u>44</u>, 1727 (1966).
- 159. M. Kashiwagi and Y. Kurita, J. Phys. Soc. Japan, <u>21</u>, 558 (1966).
- 160. H. Hayashi, K. Itoh, and S. Nagakura, Bull. Chem. Soc., Japan, 40, 284 (1967).
- 161. H. Ohigashi and Y. Kurita, Bull. Chem. Soc. Japan, <u>40</u>, 704 (1967).
- 162. G. C. Moulton, M. P. Cernansky and D. C. Straw, J. Chem. Phys., 46, 4292 (1967).
- 163. W. Gordy and R. Morehouse, Phys. Rev., 151, 207 (1966).

a m

- 164. (a) P. D. Bartlett, Chem. Eng. News, 44, 106 (1966); (b) Y. S. Lebedev, Dokl. Akad. Nauk SSSR, 171, 378; (1966); (c) M. C. R. Symons, Nature, 213, 1226 (1967).
- 165. D. A. Wiersma and J. Kommandeur, Mol. Phys., <u>13</u>, 241 (1967).
- 166. (a) A. Davis, J. H. Golden, J. A. McRae and M. C. R. Symons, Chem. Commun., 398 (1967); (b) J. A. Mc Rae and M. C. R. Symons, J. Chem. Soc., 428 (1968).
- 167. (a) P. W. Atkins, M. C. R. Symons and P. A. Trevalion, Proc. Chem. Soc., 222 (1963); (b) S. B. Barnes and M. C. R. Symons, J. Chem. Soc., 66 (1966).
- 168. M. Iwasaki and B. Eda, Chem. Phys. Letters, 2, 210 (1968).
- 169. K. Reiss and H. Shields, J. Chem. Phys., <u>50</u>, 4368 (1969).
- 170. H. M. Mc Connell and J. Strathdee, Mol. Phys.,  $\underline{2}$ , 129 (1959).
- 171. P. B. Ayscough, "Electron Spin Resonance in Chemistry," Methuen and Co. Ltd., London, 1967.

**APPENDIX** 



## **APPENDIX**

The following is a listing of the diagonalization program used to obtain principal values and direction cosines for the  $\bar{g}'$  or  $\bar{A}'$  tensors:

PROGRAM DIAGON
DIMENSION A2(50), THETA(50), AX(4), SINT(50),Q(3,3),V(3,3), 1DQ(3), AXY(14,4),Z(50,5),BB(3,3),SSC(3)
600 READ 610,IG,IB,N,JVEC,MM

```
610
       FORMAT ($12)
       IF(IG) 1007,1007,1001
1001
       IG = IG - 1
       READ 4010, (SSC(J), J=1,3)
4010
       FORMAT (3F10.4)
       DO 1004 i=1.3
       READ 1003, GPL, THP, GMIN, MA, MB
1003
       FORMAT
                (3F10.5,212)
       PRINT 1000, MA, MB, GPL, THP, GMIN
1000
       FORMAT (212,6H PLANE,4HGPL=,E12.5,4HTHP=,E12.5,5HGMIN
      1 = .E12.5
       THP=0.0349065*THP
       GPL2=GPL*GPL*SSC(MA)*SSC(MA)
       ALP= (GPL2+GMIN2)/2.0
       BET = COSF(THP)*(GPL2-GMIN2)/2.0
       GAM= SINF(THP)*(GPL2-GMIN2)/2.0
       Q(MA,MA) = ALP+BET
       BB(MB,MB) = ALP-BET
       Q(MA, MB) = GAM
       PRINT 1005,Q(MA,MA),BB(MB,MB),Q(MA,MB)
1004
       FORMAT (//,5HGAA2=,E15.5,3x,5HGBB2=,E15.5,3x,5HGAB2
1005
      1 = , E15.5//)
      Q(1,1) = (Q(1,1) + BB(1,1))/2.0
Q(2,2) = (Q(2,2) + BB(2,2))/2.0
Q(3,3) = (Q(3,3) + BB(3,3))/2.0
       Q(1,3) = Q(3,1)
       GO TO 1023
       READ 1009, (AX(J), J=1,3)
1007
       FORMAT (3F10.0)
1009
       DO 1022 I=1,3
       READ 1008, SCAL, NP
       FORMAT (F10.4, I2)
1008
       READ 1010, (A2(IK), IK=1, NP)
       FORMAT (8F10.0)
1010
```

READ 1011, (THETA(NK), NK=1, NP)

```
1011 FORMAT (16F5.0)
       B=0.0
       A=0.0
       AX(4)=AX(1)
       XX = (AX(I) + AX(I+1))/2.0
       YY = (AX(I) - AX(I+1))/2.0
       DO 1020 J=1,NP
      A2(J)=A2(J)*A2(J)*SCAL*SCAL
       THETA (J)=0.0349065*THETA (J)
 1015
      SINT(J)=SINF(THETA)(J)
       Z(J,I)=A2(J)-XX-COSF(THETA(J))*YY
       B=B+Z(J,I)*SINT(J)
1020
      A=A+SINT(J)*SINT(J)
1022
      AXY(I,I+1)=B/A
       IB=IB-1
       Q(1,1) = AX(1)
       Q(2,2) = AX(2)
       Q(3,3) = Ax(3)
       Q(1,2) = AXY(1,2)
       Q(2,3) = AXY(2,3)
       Q(1,3) = AXY(3,4)
1023
      Q(2,1) = Q(1,2)
       Q(3,2) = Q(2,3)
       Q(3,1) = Q(1,3)
       PRINT 1024, IG, IB
      FORMAT (21HUNDIAGONALIZED MATRIX, /, 10HA RADICAL=, 12,
      14H G =, I2, ///
      PRINT1026, ((Q(I,J)'J=1,3),I=1,3)
      FORMAT (5x,3(E14.5,2x),/)
       CALL DIAG (Q,N,JVEC,V,DQ,MM)
       PRINT 2100, (IB, (DQ(I), I=1,3))
     FORMAT (//,31HDIAGONALIZED MATRIX RADICAL A =,12,
      12HG=, I2,///)
      PRINT 2190, (IB, (DQ(I), I=1,3))
                                             EIGVAL(2)
      FORMAT (5HRADI=, 12,48HEIGVAL(1)
                           ,/,6x,3(E14.5))
          EIGVAL(3)
       DQ(1) = ABSF(DQ(1))
       DQ(2) = ABSF(DQ(2)
       DQ(3) = ABSF(DQ(3))
       V1 = SQRTF\{DQ(1)
       V2 = SQRTF(DQ(2))
       V3 = SQRTF(DQ(3))
       PRINT 2191, (V1, V2, V3)
       FORMAT (3HV1=,E14.5,2x,3HV2=,E14.5,2x,3HV3=,E14.5)
2191
       PRINT 2195
      FORMAT (//,34HNORMALIZED EIGENVECTORS OF RADICAL,/////
2195
       PRINT 2196, ((V(I,J),I=1,3),J=1,3)
      FORMAT (3(E14.5,5X),//)
2196
       IF(IG) 4000,4000,1001
4000
       CONTINUE
       IF(IB) 5000,5000,1007
5000
       CONTINUE
       END
```

```
SUBROUTINE DIAG(Q,N,JVEC,V,DQ,MM)
             DIMENSION Q(MM,MM),V(MM,MM),DQ(MM)
             DIMENSION X(100), IH(100)
              IF (JVEC) 15, 10, 15
   10
             DO 14 I=1,N
             DO 14 J=1,N
              IF(I-J)12,11,12
   11
             V(I,J)=1.0
             GO TO 14
  12
             V(I,J)=0.0
  14
             CONTINUE
  15
             M=0
  17
             MI=N-1
             DO 30 I=1,MI
             X(I) = 0.0
             MJ=I+1)
             DO 30 J = MJ, N
             IF(X(I)-ABSF(Q(I,J)))20,20,30
  20
             X(I)=ABSF(Q(I,J))
             IH(I)=J
  30
             CONTINUE
  40
             DO 70 I=1,MI
             IF(I-1)60,60,45
  45
             IF(XMAX-X(I))60,70,70
  60
             XMAX=X(I)
             IP=I
             JP=IH(I)
  70 CONTINUE
             EPSI=1.0E-8
             IF (XMAX-EPSI)1000,1000,148
148 M=M+1
              IF(_1(IP,IP)-Q(JP,JP))150,151,151
             TANG=-2.0*Q(IP,JP)/(ABSF(Q(IP,IP)-Q(JP,JP))+SQRTF((Q(IP,IP)-Q(JP,JP))+SQRTF((Q(IP,IP)-Q(JP,JP))+SQRTF((Q(IP,IP)-Q(JP,JP))+SQRTF((Q(IP,IP)-Q(JP,JP))+SQRTF((Q(IP,IP)-Q(JP,JP))+SQRTF((Q(IP,IP)-Q(JP,JP))+SQRTF((Q(IP,IP)-Q(JP,JP))+SQRTF((Q(IP,IP)-Q(JP,JP))+SQRTF((Q(IP,IP)-Q(JP,JP))+SQRTF((Q(IP,IP)-Q(JP,JP))+SQRTF((Q(IP,IP)-Q(JP,JP))+SQRTF((Q(IP,IP)-Q(JP,IP)-Q(JP,JP))+SQRTF((Q(IP,IP)-Q(JP,IP)-Q(JP,IP)-Q(JP,IP)-Q(JP,IP)-Q(JP,IP)-Q(JP,IP)-Q(JP,IP)-Q(JP,IP)-Q(JP,IP)-Q(JP,IP)-Q(JP,IP)-Q(JP,IP)-Q(JP,IP)-Q(JP,IP)-Q(JP,IP)-Q(JP,IP)-Q(JP,IP)-Q(JP,IP)-Q(JP,IP)-Q(JP,IP)-Q(JP,IP)-Q(JP,IP)-Q(JP,IP)-Q(JP,IP)-Q(JP,IP)-Q(JP,IP)-Q(JP,IP)-Q(JP,IP)-Q(JP,IP)-Q(JP,IP)-Q(JP,IP)-Q(JP,IP)-Q(JP,IP)-Q(JP,IP)-Q(JP,IP)-Q(JP,IP)-Q(JP,IP)-Q(JP,IP)-Q(JP,IP)-Q(JP,IP)-Q(JP,IP)-Q(JP,IP)-Q(JP,IP)-Q(JP,IP)-Q(JP,IP)-Q(JP,IP)-Q(JP,IP)-Q(JP,IP)-Q(JP,IP)-Q(JP,IP)-Q(JP,IP)-Q(JP,IP)-Q(JP,IP)-Q(JP,IP)-Q(JP,IP)-Q(JP,IP)-Q(JP,IP)-Q(JP,IP)-Q(JP,IP)-Q(JP,IP)-Q(JP,IP)-Q(JP,IP)-Q(JP,IP)-Q(JP,IP)-Q(JP,IP)-Q(JP,IP)-Q(JP,IP)-Q(JP,IP)-Q(JP,IP)-Q(JP,IP)-Q(JP,IP)-Q(JP,IP)-Q(JP,IP)-Q(JP,IP)-Q(JP,IP)-Q(JP,IP)-Q(JP,IP)-Q(JP,IP)-Q(JP,IP)-Q(JP,IP)-Q(JP,IP)-Q(JP,IP)-Q(JP,IP)-Q(JP,IP)-Q(JP,IP)-Q(JP,IP)-Q(JP,IP)-Q(JP,IP)-Q(JP,IP)-Q(JP,IP)-Q(JP,IP)-Q(JP,IP)-Q(JP,IP)-Q(JP,IP)-Q(JP,IP)-Q(JP,IP)-Q(JP,IP)-Q(JP,IP)-Q(JP,IP)-Q(JP,IP)-Q(JP,IP)-Q(JP,IP)-Q(JP,IP)-Q(JP,IP)-Q(JP,IP)-Q(JP,IP)-Q(JP,IP)-Q(JP,IP)-Q(JP,IP)-Q(JP,IP)-Q(JP,IP)-Q(JP,IP)-Q(JP,IP)-Q(JP,IP)-Q(JP,IP)-Q(JP,IP)-Q(JP,IP)-Q(JP,IP)-Q(JP,IP)-Q(JP,IP)-Q(JP,IP)-Q(JP,IP)-Q(JP,IP)-Q(JP,IP)-Q(JP,IP)-Q(JP,IP)-Q(JP,IP)-Q(JP,IP)-Q(JP,IP)-Q(JP,IP)-Q(JP,IP)-Q(JP,IP)-Q(JP,IP)-Q(JP,IP)-Q(JP,IP)-Q(JP,IP)-Q(JP,IP)-Q(JP,IP)-Q(JP,IP)-Q(JP,IP)-Q(JP,IP)-Q(JP,IP)-Q(JP,IP)-Q(JP,IP)-Q(JP,IP)-Q(JP,IP)-Q(JP,IP)-Q(JP,IP)-Q(JP,IP)-Q(JP,IP)-Q(JP,IP)-Q(JP,IP)-Q(JP,IP)-Q(JP,IP)-Q(JP,IP)-Q(JP,IP)-Q(JP,IP)-Q(JP,IP)-Q(JP,IP)-Q(JP,IP)-Q(JP,IP)-Q(JP,IP)-Q(JP,IP)-Q(JP,IP)-Q(JP,IP)-Q(JP,IP)-Q(JP,IP)-Q(JP,IP)-Q(JP,IP)-Q(JP,IP)-Q(JP,IP)-Q(JP,IP)-Q(JP,IP)-Q(JP,IP)-Q(JP,IP)-Q(JP,IP)-Q(JP,IP)-Q(JP,IP)-Q(JP,IP)-Q(JP,IP)-Q(JP,IP)-Q(JP,IP)-Q(JP,IP)-Q(JP,IP)-Q(JP,IP
           1IP)-Q(JP,JP))**2+4.0*Q(IP,JP)**2)
             GO TO 160
             TANG= 2.0*Q(IP,JP)/(ABSF(Q(IP,IP)-Q(JP,JP))+SQRTF((Q)
           1(IP,IP)-Q(JP,JP))**2+4.0*Q(IP,JP)**2)
             COSN=1.0/SQRTF(1.0+TANG**2)
             SINE=TANG*COSN
             QII=Q(IP,IP)
             Q(IP,IP)=COSN**2*(QII+TANG*(2.0*Q(IP,JP)+TANG*Q(JP,JP)))
             Q(JP,JP)=COSN**2*(Q(JP,JP)=TANG*(2.0*Q(IP,JP)-TANG*QII))
             Q(IP,JP)=0.0
              IF(Q(IP,IP)-Q(JP,JP))152,153,153
             TEMP=Q(IP, IP)
152
             Q(IP,IP)=Q(JP,JP)
             Q(JP,JP)=TEMP
              IF (SINE) 154, 155, 155
154
             TEMP=COSN
             GO TO 170
155
             TEMP=-COSN
170
             COSN=ABSF(SINE)
             SINE=TEMP
153
             DO 350 I=1,MI
              IF(I-IP)210,350,200
              IF(I-JP)210,350,210
200
```

100

```
IF(IH(I)-IP)230,240,230
 210
 230
      IF(IH(I)-JP)350,240,350
 240
      K=IH(I)
 250
      TEMP=Q(I,K)
      Q(I,K)=0.0
      MJ=I+1
      x(i)=0.0
      DO 320 J=MJ,N
      IF(XI)-ABSF(Q(I,J)))300,300,320
      X(I)=ABSF(Q(I,J))
 300
      IH(I)=J
 320
      CONTINUE
      O(I,K) = TEMP
 350
      CONTINUE
      X(IP)=0.0
      X(JP)=0.0
      DO 530 I=1,N
      IF(I-IP)370,530,420
 370
      TEMP=Q(I,IP)
      Q(I,IP)=COSN*TEMP+SINE*Q(I,JP)
      IF(X(I)-ABSF(Q(I,IP)))380,390,390
 380
      X(I) = ABSF(Q(I,IP))
      IH(I)=IP
 390
      Q(I,JP) = -SINE*TEMP+COSN*Q(I,JP)
      IF(X(I)-ABSF(Q(I,JP)))400,530,530
 400
      X(I)=ABSF(Q(I,JP))
      IH(I)=JP
      GO TO 530
 420
      IF(I-JP)430,530,480
 430
      TEMP=Q(IP,I)
      Q(IP,I)=COSN*TEMP+SINE*Q(I,JP)
      IF(X(IP)-ABSF(Q(IP,I)))440,450,450
 440
      X(IP)=ABSF(Q(IP,I))
      IH(IP)=I
      Q(I,JP) = -SINE*TEMP+COSN*Q(I,JP)
 450
      IF(X(I)-ABSF(Q(I,JP)))400,530,530
 480
      TEMP=Q(IP,I)
      Q(IP,I) = COSN*TEMP+SINE*Q(JP,I)
      IF(X(IP)-ABSF(Q(IP,I)))490,500,500
 490
      X(IP)=ABSF(Q(IP,I))
      IH(IP)=I
 500
      Q(JP,I) = -SINE*TEMP+COSN*Q(JP,I)
      IF(X(JP)-ABSF(Q(JP,I)))510,530,530
      X(JP)=ABSF(Q(JP,I))
 510
      IH(JP)=I
 530
      CONTINUE
      IF (JVEC)40,540,40
 540
      DO 550 I=1,N
      TEMP=V(I,IP)
      V(I,IP) = COSN*TEMP+SINE)V(I,JP)
      V(I,JP) = -SINE*TEMP+COSN*V(I,JP)
 550
      GO TO 40
1000
      DO 1002 I=1,N
1002
      DQ(I)=Q(I,I)
      END
```

The input for PROGRAM DIAGON is as follows:

- 1. IG Integer number of  $\bar{g}$  or  $\bar{\bar{A}}$  tensors to be diagonalized by Schonland's method.
- 2. IB Integer number of  $\bar{\bar{g}}$ ' or  $\bar{\bar{A}}$ ' tensors to be diagonalized by curve fitting technique.
- 3. N Dimension of the matrix to be diagonalized (equals 3 in this case).
- 4. JVEC Must be set equal to 0 if the eigenvectors are to be printed out, or set equal to 1 if the eigenvectors are not to be printed out.
- 5. MM A variable which must have the same dimensions as N(equals 3).
- 6. SSC(J) Scale factors for Schonland's method to convert g or A values.
- 7. GLP Maximum g or A value in each plane
- 8. THP Angle where maximum g or A value occurs (in degrees).
- 9. GMIN Minimum g or A value in a plane.
- 10. MA Dummy variables to identify reference planes, <u>e.g.</u> for 1-2 plane MA = 1, MB = 2.
- 11. AX(J) Squares of the hyperfine splittings along the reference axes (in gauss<sup>2</sup>).
- 12. SCAL Scale factor for converting mm or inches to gauss.
- 13. NP Number of points to be used in the curve fit.
- 14. A2(IK) Hyperfine splittings measured in mm or inches.
- 15. THETA(NK) Angle corresponding to each A2(IK) in degrees.

The output for PROGRAM DIAGON is as follows:

- 1. V1, V2, V3-Eigenvalues of radical in gauss or eigenvalues of  $\bar{q}$ ' tensor.
- 2. V(I,J) Eigenvector elements.

This program was written in FORTRAN IV for use on a CDC 3600 computer.

